6. Lasers

The LASER light source, whose name is based on "*L*ight *A*mplification by *S*timulated *E*mission of *R*adiation", is the most important device in almost all photonic applications. First built in 1960 [6.1–6.5] it allows the generation of light with properties not available from natural light sources. Modern commercially available laser systems allow output powers of up to 10^{20} W for short times with good beam quality and of several kW in continuos operation, usually with less good beam quality. Very short pulses with durations smaller than $5 \cdot 10^{-15}$ s, wavelengths from a few nm in the XUV to the far IR with several 10 µm, pulse energies of up to 10^4 J and frequency stability's and resolutions of better 10^{-13} can be generated. The laser prices range from $1 to many millions of dollars and their size from less than a cubic mm to the dimensions of large buildings.

The good coherence and beam quality of laser light in combination with high powers and short pulses are the basis for many nonlinear interactions, but the laser is a highly nonlinear optical device itself, using nonlinear properties of materials as described in the previous chapters. Therefore, the fundamental laws treated in Chap. 2 for the description of light as well as the description of linear and nonlinear interactions of light with matter in Chaps. 3, 4 and 5 are the basis for the analysis of laser operation and its light properties.

Therefore, the theoretical description of laser devices represents an application of these laws and can be presented in this chapter in a compact form. For details the related sections of the previous chapters should be consulted. The different lasers and their constructions, as well as the resulting relevant light and operation parameters, are described and the consequences for photonic applications are discussed. Finally, possible classifications are given and safety aspects are mentioned. For further reading see [M6, M16, M17, M23–M25, M27, M28, M30, M33, M43, M44, M49, M50, M58–M65].

6.1 Principle

Lasers are based on the stimulated emission of light in an active material which has been pre-excited by a pump mechanism. The stimulated emission can be carried out in laser oscillators which are always the primary source of laser light. In addition this light can be amplified via stimulated emission

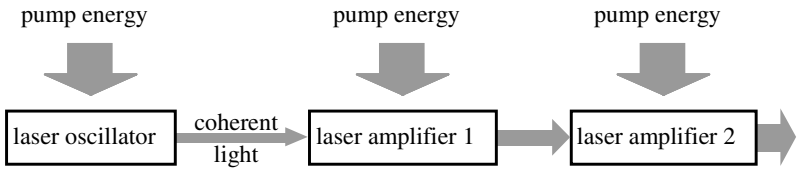

Fig. 6.1. Laser setup consisting of a laser oscillator (master oscillator) and two amplifiers (MOPA scheme)

in light amplifiers as shown in Fig. 6.1 where a master oscillator is combined with, e.g. two amplifiers in a MOPA (*M*aster *O*scillator *P*ower *A*mplifier) setup. In combination with these amplifier and/or other nonlinear converter systems the light can be modified regarding almost all parameters such as, e.g., for shorter or longer pulses, different wavelengths, polarization or geometry.

In any case the coherent laser light has to be originally generated in a laser oscillator. This laser oscillator as nothing else but a special light source consists of *three basic parts* as shown in Fig. 6.2.

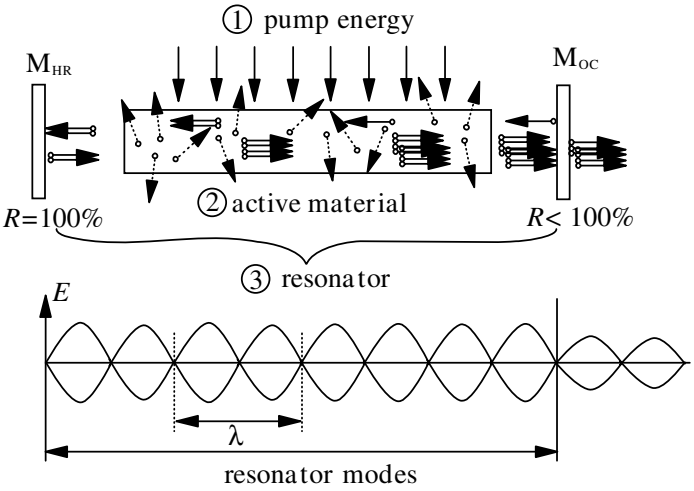

Fig. 6.2. The three basic parts of a laser oscillator: pump source ①, active material ② and resonator ③

The fundamental function of these three components is described in Table 6.1 (p. 361).

The laser operates in the following way:

- The pump mechanism provides enough energy in the active material and produces an *inversion* of the population density resulting in the higher

Table 6.1. Function and examples for the three components of lasers

Component	Function	Examples
Pump	energy/power provider	electric current electrical discharge flash or arc lamp other laser chemical reaction
Active material	possible laser light properties	semiconductor structures (GaAs) atoms in gases (Ne, Ar, Kr) ions in crystals (Nd, Cr, Yb, Ti) molecules in gases (XeCl, CO_2) molecules in solution (dyes)
Resonator	selection of the laser light properties	simple two-mirror resonator resonator with frequency selection resonator with internal frequency conversion resonator with Q switch resonator with mode locking unstable resonator folded resonators phase conjugating resonator

population of the upper laser level compared to the lower laser level in the laser material (in fundamental contrast to a thermal population, for an exception see Sect. 5.4.10, p. 320).

- *Spontaneous emission* produces incoherent photons in all directions, possibly with different polarizations and in a wide spectral range as a function of the active material.
- The resonator mirrors reflect some of these photons back into the active material selectively for their propagation direction, their polarization, their wavelength and perhaps as a function of time (*laser mode selection, short pulse generation*).
- These reflected photons are "cloned" by the stimulated emission in the active material (*amplification*) and thus a large number of equal and coherent photons are produced by sequential selective reflection and amplification forming the high-brightness laser beam.
- Part of this laser beam is coupled out of the resonator, e.g. by a partly transparent mirror at one side of the resonator (*outcoupling*).

The function of these steps will be described in detail in the following sections.

6.2 Active Materials: Three- and Four-Level Schemes – Gain

Almost all materials (except, e.g. solid metals) can be used as the active material in lasers. Even single atom lasers were realized [see, for example, 6.6]. The efficiency and the possible laser properties are very different and therefore the number of practically used laser materials is more limited but still quite large. Therefore we can distinguish gas, liquid and solid-state lasers on one hand, and on the other, the active material can be built by molecules (CO_2, CO, N_2, excimers such as XeCl or KrF, dyes), atoms in gases (HeNe, Cu vapor), ions in gases (Ar^+, Kr^+), atoms and ions in solids (Nd, Cr, Ti, Yb, Er, Pr ...), color centers or semiconductors (GaAs, ZnSe, PbSnSe, ...). Solid-state host materials can be crystals, glasses and organic matter. Crystals can be fluoride or oxide. Typical crystals are YAG ($Y_3Al_5O_{12}$) and sapphire. The different constructions will be described in Sect. 6.13.

In any case the laser action (stimulated emission) takes place between at least two energy levels (or bands) of the matter, the upper and the lower laser level (see Fig. 6.3).

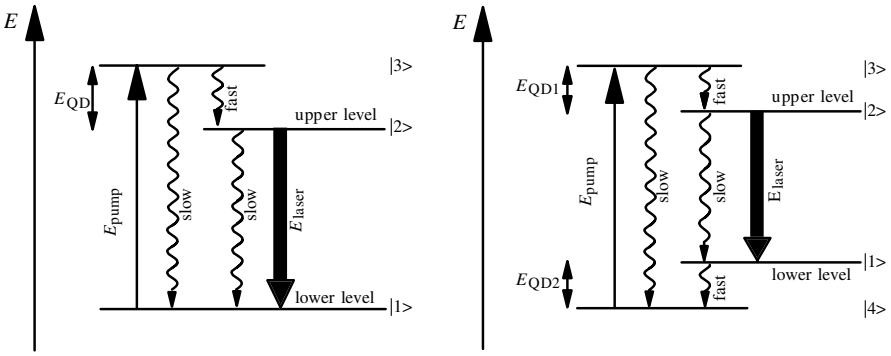

Fig. 6.3. Three (left side) and four (right side) level scheme of an active material. The laser works between levels 2 and 1 via stimulated emission as a consequence of inversion (level 2 is more highly populated than level 1). The upper laser level is populated by the pump mechanism via level 3

But for achieving inversion more than two energy levels are necessary, because the two-level scheme allows at best only equal populations of the upper and lower levels and thus transparency but no amplification.

In the *three-level scheme* (see Fig. 6.3, left side) the upper laser level (2) is populated via the higher level (3). This pump level can be a collection of several levels which can even form a pump band. If in the laser material the radiationless population channel (3) → (2) is fast compared to the possible radiationless deactivation channels (3) → (1) and (2) → (1) the upper laser level can be almost 100% populated. But the laser action populates the lower

laser level (1) which will stop operation if the pump is not strong enough. Thus laser materials with a three-level scheme may have the advantage of a possibly small quantum defect (see next chapter) and therefore higher efficiency. But the strong pump demands can be difficult especially in cw operation. Furthermore high pumping can also favor excited state absorption from the upper levels which will decrease the laser efficiency.

In the *four-level scheme* (see Fig. 6.3, p. 362, right side) the upper laser level (2) is again populated via the higher level (3) but in addition the lower laser level (1) is not identical with the ground state of the system (4). Therefore if thermal population of the lower laser level (1) can be neglected each pumped particle will produce inversion. The thermal equilibrium population density N_1 of level 1 compared to the population density N_4 in level 4 is a function of the energy difference E_1–E_4 between levels 4 and 1 and can be calculated from Boltzman equation: $N_1 = N_4 \exp -(E_1 - E_4)/k_\mathrm{B}T$ with the Boltzman constant k_B (compare Eq. (3.183). If in addition as usual the radiationless transition (1) $\rightarrow$ (4) is fast the lower laser level will stay empty even during strong laser action. Therefore four-level lasers can be very easily pumped. However, their efficiency may be lower compared to three level schemes because of the often higher quantum defect energy which is $(E_3 - E_2) + (E_1 - E_4)$ compared to $(E_3 - E_2)$ for the three level system.

However, finally all important laser material parameters have to be considered in detail for the desired application for the most suitable material independent of its three or four level character.

The amplification of the laser light in the active material can be calculated with rate equations. The gain coefficient g (negative absorption coefficient) is proportional to the cross section for stimulated emission σ and the inversion population density $N_2 - N_1$:

$$\textbf{gain coefficient} \quad g(z,t,\lambda) = \sigma(\lambda)\{N_2(z,t) - N_1(z,t)\} \tag{6.1}$$

which is a function of the wavelength λ, the position in the propagation direction z and the time t. Its influence on the laser properties will be discussed in Sect. 6.8.

Some common and some newer laser materials and their parameters are described in [6.7–6.105]. For effective pumping energy transfer mechanisms can be used to separate the pump energy absorption and the laser operation in two different materials as, for example, in the Helium–Neon laser [6.74–6.79]. Of increasing interest are upconversion lasers which allow laser operation at shorter wavelengths as the absorption [6.80–6.105], and, thus, the generation of blue light from red diode pumping. More details are given in Sect. 6.13.

6.3 Pump Mechanism: Quantum Defect and Efficiency

The pump mechanism of the active material and its efficiency are important for the output parameters, the handling and the price of a laser system.

Almost all active materials can be *pumped by another laser* beam of suitable wavelength. The resulting opto-optical efficiency can reach high values limited by the quantum defect, radiationless transitions and excited state absorption (see Fig. 6.3, p. 362).

The quantum defect energies E_{QD} in Fig. 6.3 (p. 362) result from:

quantum defect energy

$$E_{\mathrm{QD}} = E_{\mathrm{pump}} - E_{\mathrm{laser}} = hc\left(\frac{1}{\lambda_{\mathrm{pump}}} - \frac{1}{\lambda_{\mathrm{laser}}}\right) \tag{6.2}$$

with the wavelengths λ_i of the pump and laser light, Planck's constant h and the velocity of light c.

The quantum efficiency η_{Q} is the ratio between the number of emitted laser photons and the number of absorbed pump photons independent of their photon energy (see Sect. 6.3.6, p. 379).

In the case of 100% quantum efficiency, i.e. each absorbed photon will generate a laser photon, the quantum defect will reduce the opto-optical efficiency to values of usual less than 90%. But in the case of Yb:YAG laser crystals emitting at 1030 nm and pumped with diode lasers at 940 nm the quantum defect is as small as 9% (see Table 6.2).

Table 6.2. Quantum defects of some lasers for their strongest laser transitions

Laser material	λ_{laser} (nm)	λ_{pump} (nm)	$E_{\mathrm{QD}}/E_{\mathrm{pump}}$ (%)
Yb:YAG	1030	940	8.7
Nd:YAG	1064	808	24
Er:YAG	2940	532	82
Rhodamin 6G	e.g. 580	308	47
Ti:Sapphire	e.g. 800	532	34

Because of the possible choice of the pump and the emission wavelengths the quantum defect for a given material can vary drastically. As an example the absorption spectrum of Nd:YAG is given in Fig. 6.4 (p. 365).

This material can be pumped with flash lamps over a wide spectral range containing all the visible light. If laser diodes are applied usually the strongest absorption around 808 nm is used for pumping. However, in some cases longer wavelengths are applied. The efficiency and thus all secondary effects like heating are then very different.

For simplicity in a laser system, direct pumping of the active material with electrical current is attempted. In *diode lasers* the resulting electro-optical efficiency can be as high as 40%. Therefore these lasers may become even more important in the very near future in high-power applications with

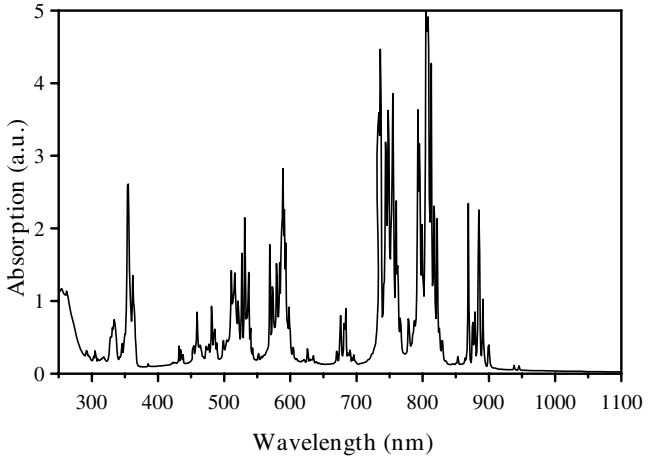

Fig. 6.4. Absorption spectrum of a Nd:YAG laser crystal

average output powers of hundreds of watts or kilowatts. The disadvantage of diode lasers with output powers of more than ten watts is today their poor beam quality with M^2 factors of more than 10^4, which prevent these lasers being used in high-precision applications or nonlinear optics. Nevertheless, in addition to applications in surface treatment they are progressively being used for pumping of solid-state lasers. This results in a reduced thermal load by optimal adaptation of the pump wavelength to the absorption of the active matter and in high overall efficiencies of up to 20%.

6.3.1 Pumping by Other Lasers

This type of pump scheme is used to transform the wavelength or spectral width of the laser radiation or to increase the beam quality or coherence of the laser light. In the first case, as, e.g. in dye or Ti:sapphire lasers, the large spectral emission band width of the pumped laser allows the generation of very short pulses in the ps or fs range.

Pulsed and continuously (cw) operating systems have been built and thus the pump laser can be pulsed or cw, too. A typical scheme for pumping a pulsed dye laser is a transversal geometry as shown in Fig. 6.5.

Because of the possible population of the triplet system in the dye, which would take these dye molecules out of the laser process, a slow or fast flow of the dye solution is usually applied depending on the average output power.

A much better excitation profile across the active material can be achieved using a Berthune cell for pumping as depicted in Fig. 6.6.

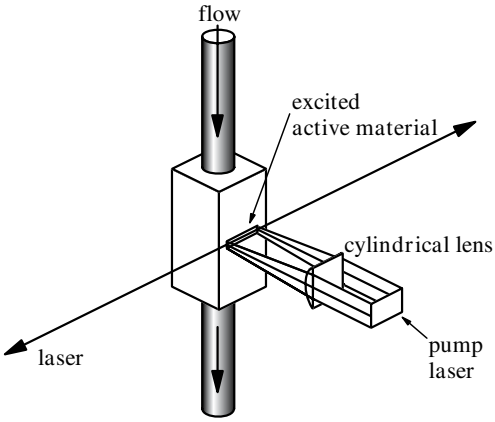

Fig. 6.5. Transversal pump laser geometry as applied in pulsed dye lasers

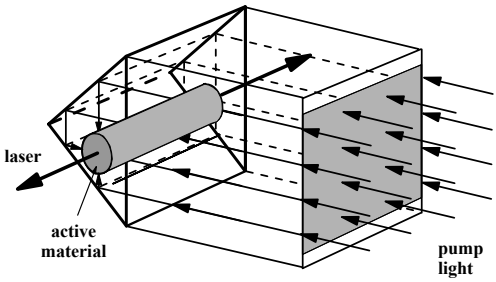

Fig. 6.6. Berthune cell for uniform transverse pumping of the active material

The totally reflecting 90° prism allows the laser material, e.g. the dye solution, to be excited from all sides in the same way. Thus power amplifier fs laser pulses pumped with ns pulses can be obtained.

Dyes in a polymer matrix are usually moved across the excitation spot to achieve average output powers in the range of a few 10 mW. This cools the active material, which was warmed up by the quantum defect energy via radiationless transitions and avoids the triplet accumulation. Typically excimer lasers (e.g. XeCl at 308 nm) or frequency doubled Nd:YAG lasers (532 nm) are used with pulse widths of 10–20 ns as pulsed pump lasers. Nitrogen lasers (337 nm) can be used both with pulse widths of a few ns (3–4 ns) or a few 100 ps (e.g. 500 ps).

If dye lasers run continuously the problems of triplet population and heating are increased and thus a strong flow is necessary. For this, dye jets are produced by injection nozzles having a very stable shape with good optical (interferometric) quality without windows as shown in Fig. 6.7 (p. 367).

The jet has a typical thickness of 0.3 mm and a width of 5 mm. The flow speed is more than $10^2\,\mathrm{m\,s^{-1}}$. The excitation spot has a diameter of, e.g. 50 µm. Argon (or krypton) ion lasers were first used as the pump, but diode pumped and frequency doubled solid-state lasers have been increasingly applied recently. In these cases the dye has to absorb in the green region, as

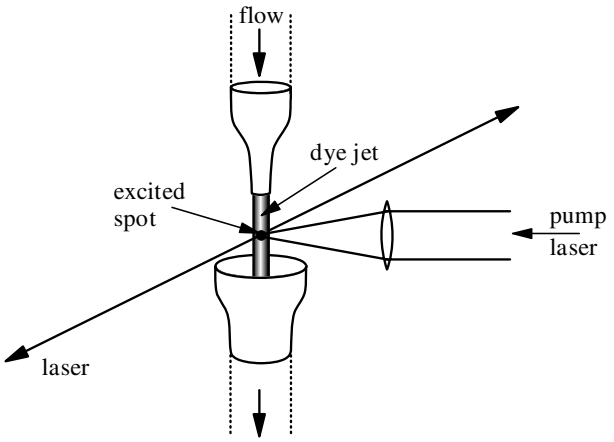

Fig. 6.7. Cw laser pumping of a dye jet

e.g. rhodamine 6G does. The solvent has to be of suitable viscosity, as e.g. ethylene-glycol. A concentration of e.g. $1.4\,\mathrm{mmol\,l^{-1}}$ can be used. The excitation power is in the range of 5–10 W. Dye lasers have the advantage of large band width especially in the visible range and thus the potential of tuneability and short pulses. The dye material can be produced in large sizes. However, solid state laser materials such as, e.g., Ti:sapphire or Presodym doped crystals and frequency conversion techniques such as optical parametric converters are successfully competing.

Thus in a similar way the Titan sapphire laser can be pumped by e.g. the frequency doubled radiation of a Nd:YAG laser (see Fig. 6.8).

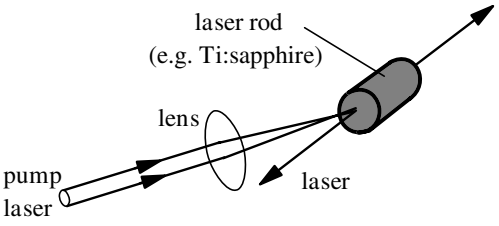

Fig. 6.8. Laser pumping of a solid-state laser (as, e.g. Ti:sapphire)

Solid-state lasers pumped by diode lasers are becoming more and more important, especially in industrial application such as welding, cutting, drilling and marking. In this case the good efficiency of the diode lasers and their high reliability is combined with the good coherence and beam quality of the solid-state lasers. Several schemes have been developed to meet the different needs in power and construction.

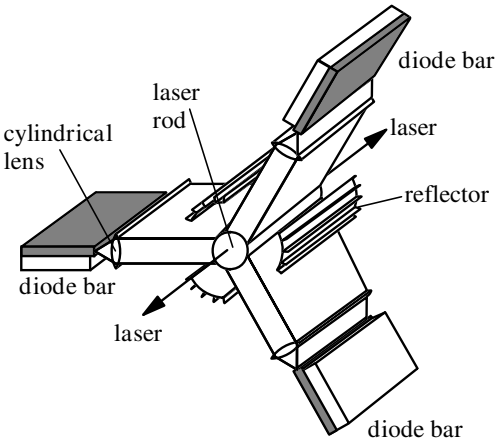

Fig. 6.9. Side-pumping of a solid-state laser rod with bars of diode lasers

Solid-state rod lasers can be side-pumped and end-pumped [6.106–6.139]. A common scheme for side-pumping is shown in Fig. 6.9.

The diode lasers are arranged in stripes of 10–25 diode lasers (bars) which emit about 50 W or in some systems even above 100 W average power each at wavelengths typically above 800 nm (e.g. 808 nm for pumping of Nd:YAG and 940 nm for Yb:YAG). Because of the long rod length of some mm to more than 10 cm and the resulting high gain, as well as the large possible rod diameter of more than 10 mm resulting in a possible large stored inversion energy, this type of laser is well suited for pulsed operation such as Q-switching.

Cylindrical aspherical lenses are often applied to collimate the highly divergent diode laser beam of about 90° in the axis vertical to the stripe (fast axis) before the solid-state laser rod is illuminated. Opposite to the bar on the other side of the rod a reflector usually collects the unabsorbed pump light. For uniform excitation usually three, five or seven bars are symmetrically mounted. The geometrical parameters are the important design criteria and determine to a large extent the possible quality of the laser beam.

For higher powers more than one star of diode bars can be used along the rod axis resulting in rod lengths of several cm. The efficiency of diode pumping the laser rods is higher than with lamp pumping, as a consequence of the better match of the pump laser spectrum to the absorption spectrum of the active material. Despite this reduced heat load, in high-power systems with average output powers of more than 10 W the laser rod is usually water cooled. The electro-optical efficiency can reach values of 20%.

The side-pumping of solid-state slabs [e.g. 6.131–6.137] has been applied as shown in Fig. 6.10, reaching very high average output powers of several kilowatts (see Sect. 6.13.2, p. 498). In one example [6.133] the slab was e.g. 170 mm long, 36 mm high and 5 mm wide.

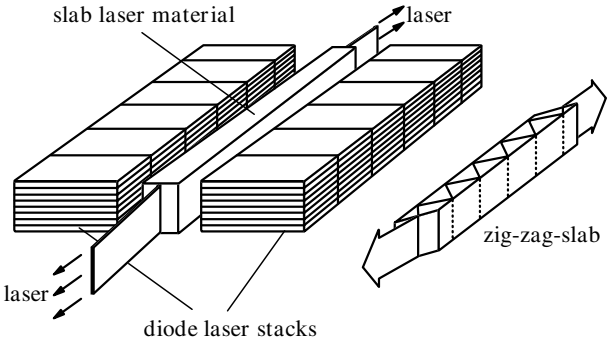

Fig. 6.10. Side-pumping of a solid-state laser slab with a stack of laser diode bars for reaching several kW average output power with good beam quality. The slab can be used as a zig-zag slab as shown on the right, decreasing thermal problems

For achieving high pump powers from diode lasers the bars were combined in arrays of 16 bars vertically resulting in a 1 cm wide and 2 cm high package. Fifteen of theses arrays were mounted in stacks along the laser axis at each side. Thus each stack contains 240 bars. Each bar consists of 20 diode lasers and has a nominal peak power of 50 W with a duty cycle of 20%. Thus the total pump average power of the 9600 laser diodes was 4.8 kW. The pulse duration could be varied from 100 µs to 1 ms. With one of the described laser heads an average output power of 1.1 kW could be obtained with a beam quality of 2.4 times the diffraction limit. Two modules allowed 2.6 kW with $M^2 = 3.2$ and three modules resulted in 3.6 kW with $M^2 = 3.5$. The maximum average output power of the three-module system in multimode operation was 5 kW.

The slab material can be used in a zig-zag geometry to overcome to a large extent thermally-induced lensing and birefringence. The laser beam is totally reflected by the polished sides of the slab and in this way crosses the temperature profile in the slab which occurs between the exciting diode stacks if the slab is side-cooled. Nevertheless, carefully designed cooling has to be applied so as not to crack the strongly pumped laser material and the deformation of the end surfaces needs to be considered (see Sect. 6.4 and references there).

Solid-state lasers with output powers of less than about 100 W can be end-pumped [e.g. 6.110–6.119] as shown in Fig. 6.11 (p. 370).

The pump radiation excites the active material concentric to the laser beam and therefore radial symmetric inversion profiles can be achieved. The diode laser radiation is often coupled into fibers especially for average pump powers above 10 W for easier handling and for achieving a homogeneous spot with a certain beam quality. If in addition the laser material is cooled at the end-faces the temperature profile occurs along the axis of the laser. In this case almost no thermally induced lensing or birefringence is obtained

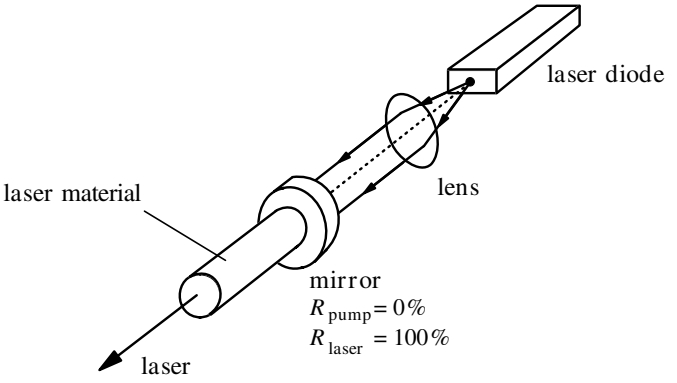

Fig. 6.11. Scheme of end-pumping a solid-state laser with laser diodes

for the laser radiation. Thus with this simple scheme good beam quality can be achieved. The diode laser fiber-coupling results in easy maintenance (but higher prices). Because of the longitudinal temperature gradient and the cooling limitations of this pump scheme the maximum average output power is limited by the damage of the active material. For small pump spots at the active material using diode laser bars or stacks for pumping lens ducts were developed to change the beam shape of the pump light with its bad beam quality [for example, 6.117–6.120]. 40 W of output power from Nd:YVO_4 has been demonstrated (see Sect. 6.13.2, p. 498).

In the power range below 5 W this scheme can be used to build microchip lasers with a close arrangement of the diode, the solid-state laser material and if needed the interactivity SHG crystal or passive Q-switch. Output powers above 0.5 W green light have been observed from a 2 W diode (see Sect. 6.15.1, p. 525).

The pumping scheme of Fig. 6.8 (p. 367) takes advantage of the good inversion profile available by end-pumping and is applied, e.g. in Ti:sapphire pumped by frequency doubled Nd:YAG laser radiation or from ion lasers. Fiber lasers are also mostly end-pumped (see Sect. 6.13.2.10, p. 508).

Longitudinal pumping is also applied in disk lasers containing a thin slice of solid-state laser material with a thickness of, e.g. 0.2 mm and a diameter of a few mm as active matter, as shown in Fig. 6.12 (p. 371).

For the absorption of the diode laser pump light in the thin disk usually several passes are necessary and thus the pump beam has to be back-reflected. Four, 8, 16 or 32 passes are used in practical cases (see Sect. 6.13.2.4 (p. 502) and e.g. [6.138, 6.139]).

The thin disk is cooled longitudinally and thus almost no thermal lensing or birefringence occurs even at high powers. Difficulties may be caused by the mirror coatings at the disk back-side. Good reflectivity and optical quality for both the laser and the pump beams have to be combined with good thermal conductivity. The scaling of the disk laser to very high average output

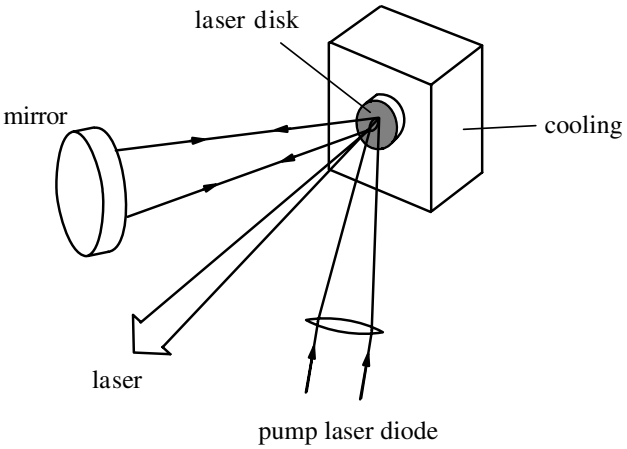

Fig. 6.12. Pumping scheme of a disk laser containing a thin slice of solid-state laser material with a thickness of, e.g. 0.2 mm and a diameter of a few mm longitudinally pumped by diode laser radiation. Because of the small absorption in the thin disk the pump beam has to be back-reflected by external mirrors

powers may be limited by the high gain perpendicular to the laser emission in the plane of the disk which may cause super-radiation and thus high losses on one hand and residual thermally induced phase distortions on the other [e.g. 6.140]. Nevertheless, average output powers of several 100 W have been achieved with a Yb:YAG laser with very good beam quality and electro-optical efficiencies of more than 10% (see Sect. 6.13.2.4, p. 502). Commercial systems with several kW average output power and moderate beam quality are available.

Most prominent optically pumped fiber lasers were developed in the last time (see Sect. 6.13.2.10 and 6.13.2.11 and references there). The fiber design of the active material has the advantage of almost no thermally induced problems as lensing or birefringence because cooling of the thin material of only a few 100 µm radius is easily possible. Using new low mode fibers with large core diameter very high average output powers in the kW-range became possible. If mono-mode fibers are applied the resulting beam quality is perfect. In all other cases the beam quality is usually much better than from all other laser concepts if the average output power is the same.

These fiber lasers are mostly end pumped often from both sides. Side-pumped methods are developed. The diode laser radiation can usually not coupled into the core directly because of their bad beam quality. Thus several fiber designs are developed to transfer the pump radiation from the larger cladding into the core with high efficiency. Thus, e.g., double cladding fibers with a d-shaped pump cladding were developed (see Fig. 6.13, p. 372).

As active material in the fiber core many known laser materials are already proven and others may be possible (see Sect. 6.13.2 and references there).

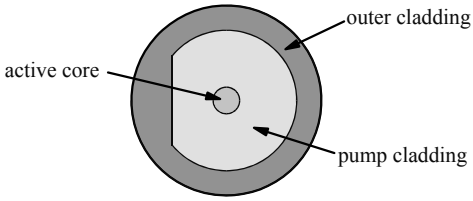

Fig. 6.13. Fiber design (d-shape) for optimal pump laser coupling to the core. With the d-shape rotating modes in the pump cladding were suppressed

Especially Er, Yb, and Nd ions are used. Because of the long gain length new materials and techniques as up-conversion lasers can be applied and thus new wavelengths are available.

Because of the high gain, good stability and excellent beam quality, the fiber lasers are also useful for short pulse generation with impressing parameters. Thus ps anf fs pulse trains with repetition rates in the MHz range were generated with average output powers above 100 W (see Sect. 6.13.2.10 and 6.14 and references there).

Therefore fiber lasers may overtake all applications where good beam quality in combination with good stability and no high pulse energies are required. Average output powers in the kW-range are feasible for these lasers and only the high diode laser price is limiting an even larger distribution in these cw and quasi-cw applications. Only in Q-switched applications the fiber lasers are very limited. The maximum pulse energy is in the range of a few mJ because of the small active volume and the possible damage of the front facets. In these applications the rod (or slab) geometry of the active material is unbeaten. Several J can be generated with these large volume devices with good beam quality, narrow bandwidth and average output powers of several 100 W. In special cases hundreds of kJ are possible. However, simple flash lamp pumped rod lasers (see Sect. 6.3.4, p. 377) may also have a longer future at least as long as diode prices are not decreasing drastically. However, in long term perspectives completely new laser concepts may be developed with even higher efficiencies and very low prices.

6.3.2 Electrical Pumping in Diode Lasers

Diode lasers [6.141–6.146] are pumped directly by an electrical current of 10–20 mA with a voltage of about 2 V per single stripe of the laser diode as shown in Fig. 6.14 (p. 373). The active zone is built between a p-n junction and has a typical height of about 1 µm. In commercial diode lasers typically 10–20 stripes are arranged closely spaced resulting in a driving current of about 2 A for the whole structure (see Sect. 6.13.1, p. 492).

In the p-doped material (with less electrons than positively charged holes) the high lying conduction band is empty and the valence band is only partly occupied with electrons. In the n-doped material the valence band is complete

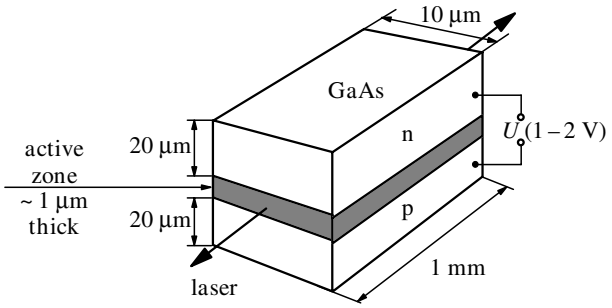

Fig. 6.14. Schematic structure of a diode laser consisting of a p-n junction of, e.g. GaAs with an active laser zone in between. Commercial diode lasers have a more complicated structure including cladding layers and waveguide channels for improved laser parameters. One diode laser consists typically of 10–20 stripes (see Sect. 6.13.1, p. 492). The length of the structure here given as 1 mm can be varied between < 0.5 mm and > 2 mm. As longer the laser as higher the output power

and the conduction band is partly filled with electrons. Under the influence of the electric field across the p-n transition (produced by the external voltage U) some electrons from the upper (conduction) band of the n-doped material will move to the p-doped side. There they can recombine with the positive holes under the emission of a photon. Radiationless processes depopulate the upper laser band within about 1 ns. Nevertheless, the electro-optical efficiency of diode lasers is up to 50%.

Commercial diode lasers have a much more complicated structure. This includes, e.g. cladding layers resulting in double heterostructure lasers for improved efficiencies and waveguide channels for better laser light parameters.

The beam quality is diffraction limited in the vertical axis of Fig. 6.14 which is called the fast axis and shows a full divergence angle of about 90°. In the horizontal axis (slow axis) the beam quality depends on the size of the gain guided structure of the electrodes. The slow axis full divergence angle is typically close to 10°. It can be almost diffraction limited for a single emitter producing an average output power of some mW. In diode lasers, as described in Sect. 6.13.1 (p. 492), several of these single channels are combined and the emitted radiation of these single emitters is not coherent. Thus, the beam quality in the slow axis is usually very poor for these power lasers. New concepts may increase the lateral coherence of these lasers and thus improve their beam quality.

The wavelength of the laser results from the size of the quantum confinement which is about 20 nm wide, and the doping, which is about 10^{-4}. The emission wavelength is temperature dependent. A temperature change of +20 K shifts the emission wavelength by about +6 nm.

The voltage at the single diode $U = U_0 + IR_S$ is a function of the applied current, with $R_S \approx 200$–$400\,\mathrm{m\Omega}$ and $U_0 \approx 1\,\mathrm{V}$. The threshold current is in the range of a few 100 mA and the slope efficiency is about 1 W/A.

The lifetimes of the diode lasers which are specified for more than 80% of the maximum output power reach values of many tens of thousands of hours. The long term decrease in the output power can partially be compensated for by an adequate increase in the current.

Another concept for diode lasers is the vertical cavity surface emitting lasers or VCSELs (see Sect. 6.13.1.3). Their structure is shown schematically in Fig. 6.15.

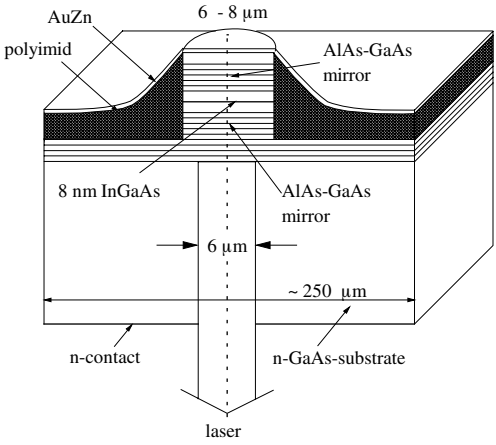

Fig. 6.15. Schematic structure of a vertical cavity surface emitting laser (VCSEL)

In this case the laser radiation is built up in a resonator perpendicular to the p-n layer of the semiconductor structure. Because of the high gain in the active material this short amplification length is sufficient for the laser. As a consequence of the small diameter of the active zone the light is almost diffraction limited. The etalon effect of the short resonator can be used for narrow bandwidth generation.

Instead of inorganic also organic matter can be used as active material in light emitting devices of a similar structure as diode lasers [5.947–5.951]. Although they are not available as lasers, yet, they may become important. Their use is expected for flat-panel displays and efficient illumination devices, probably at large scale in the near future. Displays of more than 0.5 m are demonstrated. Laser action was reached by optical pumping. These organic light emitting diodes (OLEDs) consist of an active material, which can be a light emitting polymer, e.g. poly(p-phenylene-vinylene) or a dye. The active material is usually sandwiched between a transparent anode material; e.g. indium-tin-oxide (ITO), and a metallic cathode, mostly low-work function metals such as Ba, Ca or Al. In order to reduce the hole injection barrier and to smooth the surface, the anode is often covered with a layer of a highly doped polymer, for example polyaniline or polythiophene (PEDOT). An ultrathin layer of LiF or CsF placed between the active material and the metallic cathode can improve device performance. The whole layer structure

is usually less than 1 µm thick and can be produced by vacuum deposition, spincoating or ink jet printing. The applied voltages are in the range of V. The life time and efficiency of these devices is not in all cases sufficient, yet. The active layer is quite small and laser action is not reached by electrical pumping and operation at room temperature, up to now.

6.3.3 Electrical Discharge Pumping

In electrically excited gas lasers (see Fig. 6.16, p. 376), such as e.g. argon or krypton lasers, the wall-plug efficiency can be as low as 0.1% but, e.g. a copper vapor laser or excimer laser shows values as high as 1% and 2%. The argon ion laser is excited with up to 35 eV and the laser emits at 488 nm. The resulting quantum defect is 94%.

In the helium-neon (He-Ne) laser the excitation of He takes place with an electron energy of about 20 eV and the laser transition in Ne has a wavelength of 632.8 nm resulting in a quantum defect of about 92%. The helium-cadmium (He-Cd) laser is excited in the same way but the emission appears at 441.8 nm resulting in a smaller quantum defect of about 89%.

In CO_2 lasers the molecules are excited with 0.28 eV. The wavelength of the CO_2 laser is 10.6 µm which results in a quantum defect of 66%.

The three-level copper and lead lasers are pumped with about 4 eV and emit at 510.5 nm/578.2 nm and 722.9 nm, respectively. The resulting quantum defects are 50%/57% and 70%.

A further reason for the limited efficiencies of these electrically pumped gas lasers is the imperfect adaptation of the velocity distribution of the accelerated electrons in the discharge with the collision cross-section of the active particles [e.g. 6.147–6.149]. The energy distribution F_{electron} of the electrons as a function of their temperature T can be given as:

$$F_{\text{electron}}(E_{\text{electron}}) = 2\sqrt{\frac{E_{\text{electron}}}{\pi(k_{\text{Boltz}}T)^3}}\ \exp\left(-\frac{E_{\text{electron}}}{k_{\text{Boltz}}T}\right). \tag{6.3}$$

As an example the electron speed distribution and the absorption cross-section are shown for the discharge in a nitrogen laser in Fig. 6.16 (p. 376). As can be seen from this figure the distribution of slow electrons with kinetic energies below 10 eV and with fast electrons with more than 35 eV is not optimally adapted to the excitation cross-section of the nitrogen molecules.

Although the velocity distributions of the electrons can be modified with buffer gases of certain pressures and the density of the active matter is chosen for optimal absorption the final excitation efficiency is sometimes smaller than 1%. In addition radiationless deactivation takes place in the gas by collisions between the particles. Better efficiencies are reached with copper (Cu) or gold (Au) vapor lasers. Values of 1% for Cu and 0.2% for Au lasers reported. This is based on a quantum defect of e.g. 40% for the copper vapor laser.

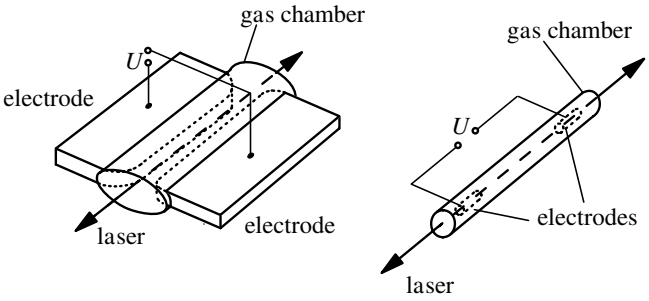

Fig. 6.16. Electrical discharge pumping of gas lasers with transversal (left side) or longitudinal (right side) geometry

The electrical discharge can be arranged transversally or longitudinally to the laser beam (see Fig. 6.16). The transversal pump geometry is more suitable for pulsed electrical excitation and longitudinal for cw operation.

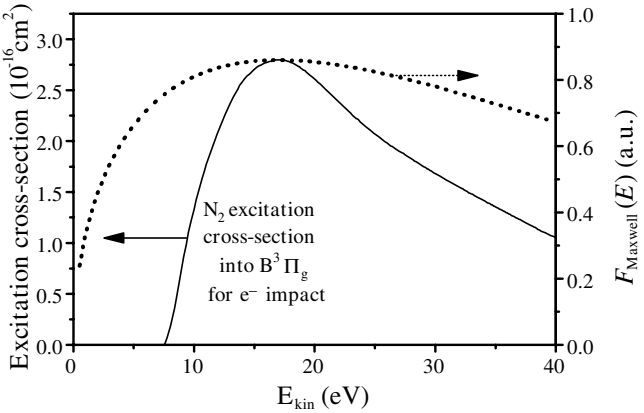

Fig. 6.17. Absorption cross-section and electron velocity distribution as a function of the electron kinetic energy representing the square of the electron velocity for the discharge in a nitrogen laser

In pulsed excimer or nitrogen (N_2) lasers the discharge has to take place within about 10 ns. Therefore the discharge in the gas chamber with pressures of 0.1 bar in the nitrogen laser and a few bars in the excimer laser is spread over the whole length of the electrodes. Electric circuits with very low inductivities have to be applied. Capacities of several nF charged to voltages of 10–30 kV are used as electrical power source. As electrical switches thyratrons are used and in the best cases trigger jitters of a few ns and delays of several 10 ns between the electric trigger and the laser pulse are obtained.

Thus these lasers with ns output pulses can be synchronized electrically. For simple arrangements spark gaps can be used as high-voltage switches. Thus it is possible to built a nitrogen laser (using air as the active material) with a 500 ps pulse width at 337 nm based on a very simple construction (see Sect. 6.13.3.2, p. 511).

The longitudinal discharge is typically used in cw operating He-Ne lasers or Ar and Kr ion lasers. In ion lasers with output powers of several watts the discharge tube is the most expensive part, and costs about 1/3 of the laser and losts typically for only 2 years. If the output power is reduced to less than half of the maximum the lifetime increases drastically.

6.3.4 Lamp Pumping

Flash or arc lamps are very common *for the pumping* of solid-state lasers. Typical arrangements are shown in Fig. 6.18. Also the solid-state slab arrangement of Fig. 6.10 (p. 369) can be pumped using lamps from both sides, instead of the diode laser stacks. Using lamps for pumping, the laser material acts as a light converter producing monochromatic and coherent light with good beam quality and polarization in possibly short pulses.

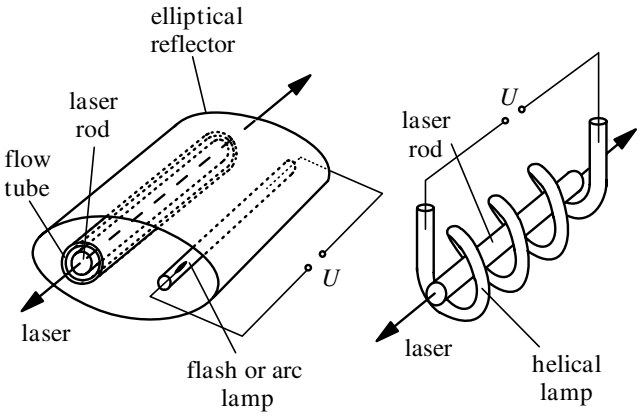

Fig. 6.18. Lamp pumping of solid-state laser rods with linear lamps (left) and helical lamps (right)

Helical lamps were used in pioneer times but may find new applications, and linear lamps are used today. For saving the flash light the laser rod and the lamp(s) are mounted inside a pump chamber which can scatter, diffuse or reflect the light. In the latter case the rod is often mounted in one focal line of an elliptically shaped reflector. If more than one lamp is applied each has its own elliptical reflector combined into a flower-like cross-section. Diffuse pump chambers will show a more equal inversion distribution and reflecting ones

show a maximum in the rod center which is more useful for light extraction with Gaussian beams. It turned out in practice that smaller cross sections of the reflectors and diffusors are more efficient than larger constructions. In any case the absorption of the rod should be adapted to the chamber dimensions by choosing the appropriate diameter and concentration.

Flash lamps are typically filled with Xe or Kr and emit their light for about 100 µs to several ms. The pulse length depends on the construction of the lamp and the design of the electrical circuit. Flash lamp pumping of dye lasers is also sometimes applied to reach high output powers. Because of the possible triplet population the flash pulse has to be as short as a few µs which demands special lamps and drivers which work with more than 10 kV instead of a few 100 V for the solid state lasers. The duration of the laser pulse is about the same as the flash.

Lamp pumping results in an electro-optical efficiency of up to 5%. Thus 95% of the flash lamp energy is converted to heat. This often limits the laser output parameters such as power and brightness. Therefore cooling of the laser material and lamp(s) is essential. Flow tubes around the rod and lamps increase the cooling efficiency. Nevertheless the laser rod will show a temperature profile with highest values in the rod center and the temperature of the cooling liquid at the surface. The refractive index of the active laser rod then shows a quadratic profile and sometimes even higher orders as a function of the rod radius. Thermally induced lensing, birefringence and depolarization occur as a consequence of the refractive index modulation (see Sect. 6.4). The resulting phase shifts cause amplitude distortions after the propagation of the light via interference effects and thus the beam quality of such laser is decreased in the high-power regime. In the worst case thermally induced tension can cause damage to the laser rod.

Flash or arc lamps emit light in a wide spectral range which is absorbed in the active material via several different transitions or bands. Thus different excited states are populated and the quantum defect will be different for them. To increase the efficiency of the pumping process and to avoid the distraction of the laser material by short-wavelength radiation sometimes quantum converters, such as e.g. Ce atoms, are used to transform UV light into the visible and red spectral region which the laser rod can absorb. These materials can be introduced into the flow tubes and the pump efficiency can be increased by 20–50%. Further details are described in [6.106, 6.150–6.185].

6.3.5 Chemical Pumping

Chemical lasers are pumped by the excess energy of a chemical reaction. Typical lasers are based on the reaction of fluorine and hydrogen to HF^* in specially designed flow chambers (see Fig. 6.19).

The reaction takes place as:

$$F + H_2 \rightarrow HF^* + H \tag{6.4}$$

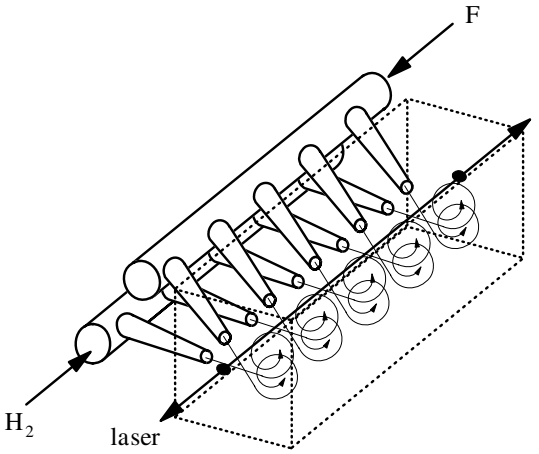

Fig. 6.19. Scheme of pumping an active material by a chemical reaction in a flow chamber

or

$$F_2 + H \rightarrow HF^* + F \tag{6.5}$$

with a reaction heat of about $32\,\mathrm{kcal\,mol^{-1}}$. This allows the excitation of the third vibrational level ($v = 3$) of HF which rapidly decays to the $v = 2$ level. The laser works between the levels with $v = 3$ and $v = 2$ with an efficiency of inversion relative to chemical energy of about 50%. The emission wavelengths of the transitions between the vibrational levels are in the range of 2.7–3.3 µm. Other possible laser molecules are HBr, HCl and DF with emissions in the range 3.5–5 µm (see [6.186–6.189] and Sect. 6.13.5, p. 520 and references there).

Large volumes of the active material can be made in this way and thus large output powers are possible. Pulsed and cw operation is possible. A maximum of more than 2 MW average output power has been obtained from such a chemical laser. Because of the technological and environmental problems of these lasers as a result of the toxic halogens, military applications are mainly intended.

6.3.6 Efficiencies

Several efficiency values are used to characterize the pump process:

- quantum defect efficiency
- quantum efficiency
- opto-optical efficiency
- electro-optical efficiency
- slope efficiency
- total efficiency (or wallplug efficiency).

The quantum defect energy is caused by, as described in the previous section, the difference between the photon energies of the pump E_{pump} and the laser E_{laser} light. Small values result in high quantum defect efficiencies:

$$\textbf{quantum defect efficiency} \quad \eta_{\text{QD}} = \frac{E_{\text{laser}}}{E_{\text{pump}}}. \tag{6.6}$$

The quantum efficiency gives the share of emitted laser photons $N_{\text{photons,laser}}$ relative to the number of absorbed pump photons $N_{\text{photons,pump}}$ independent of the energy of both:

$$\textbf{quantum efficiency} \quad \eta_{\text{Q}} = \frac{N_{\text{photons,laser}}}{N_{\text{photons,pump}}}. \tag{6.7}$$

It accounts for, e.g. the radiationless transitions parallel to the laser transition in the active material. Thus the efficiency of the absorbed photons is the product of both η_{QD} and η_{Q}.

The opto-optical efficiency is the quotient of the laser light power $\text{P}_{\text{laserlight}}$ relative to the light power $\text{P}_{\text{pumplight}}$ of the pump source:

$$\textbf{opto-optical efficiency} \quad \eta_{\text{o-o}} = \frac{P_{\text{laserlight}}}{P_{\text{pumplight}}}. \tag{6.8}$$

It is especially used for characterizing laser pumping, e.g. with diode lasers. If the diode laser is fiber-coupled it should be stated whether the pump light is measured at the output of the diode laser or at the output of the fiber. This difference can be as high as 50%.

The electro-optical efficiency relates the laser light output power $\text{P}_{\text{laserlight}}$ to the electric input power to the pump source $\text{P}_{\text{pump,electric}}$:

$$\textbf{electro-optical efficiency} \quad \eta_{\text{e-o}} = \frac{P_{\text{laserlight}}}{P_{\text{pump,electric}}}. \tag{6.9}$$

In this efficiency the losses in the pump source and in the active material are considered. It is relevant to all lasers with all kinds of pump mechanism. In particular, solid-state lasers with flash lamp or diode laser pumping are characterized with this value and compared to other high-power lasers.

The slope efficiency characterizing the slope of the laser output power curve as a function of the electrical input power $P_{\text{laserlight}} = f(P_{\text{pump,electric}})$ is used especially for solid-state lasers:

$$\textbf{slope efficiency} \quad \eta_{\text{slope}} = \frac{\Delta P_{\text{laserlight}}}{\Delta P_{\text{pump,electric}}}. \tag{6.10}$$

This curve shows, after a threshold of a certain electrical input power (e.g. of the flash lamps), an almost linear increase of the output power. The differences ΔP_i are used from this linear part of the curve.

Finally the *total efficiency* or wallplug efficiency of the pump process and the laser operation has to be calculated for evaluating different laser types for certain applications. The total power of the laser light $P_{\text{laserlight}}$ has to be

compared to the sum of the total electric plug-in powers of the power supply and cooling system $P_{\text{wallplug,total}}$:

$$\textbf{total efficiency} \quad \eta_{\text{e-o,total}} = \frac{P_{\text{laserlight}}}{P_{\text{wallplug,total}}}. \tag{6.11}$$

In addition to the mechanismus already discussed the efficiency of the pump source and the active material is decreased by radiationless transitions, long lifetimes of the lower laser level, population of long-living energy states such as e.g. triplet levels of laser dyes, unwanted chemical reactions, and phase and amplitude distortions. The principle limit of the laser efficiency was discussed in [6.191]. Further special demands such as complicated cooling or control systems may decrease the efficiency of the laser system. A very rough overview of these costs for different laser photons was given in Table 1.1 (p. 9). Finally the total efficiency has to be used to compare lasers with comparable brightness, wavelength and pulse duration with respect to their cost, in addition to purchase, installation and maintenance conditions.

6.4 Side-Effects from the Pumped Active Material

The active material changes the properties of the laser resonator by its refractive index and thus the optical length of the resonator. This has to be taken into account while calculating the transversal and longitudinal mode structure of the laser. In the worst case its refractive index is a complicated function of space and time. Additional amplitude distortions may occur from the inhomogeneous gain in the active material. Thus the resonator properties may change during the laser process.

Especially in solid-state lasers, heating of the active material, which results from the thermal load from the pumping process, can cause serious problems [6.191–6.292]. The laser material can show thermal lensing and induced birefringence, as will be described below. Several concepts have been developed to avoid or minimize these thermally induced problems. Thus, slab, zig-zag-slab or thin disc geometry can be applied to the laser material. Resonator concepts with adaptive mirrors such as, for example, via optical phase conjugation or special polarization treatment, have been developed to compensate for these distortions. Therefore, detailed experimental investigations of the different parameters involved have been done [e.g. 6.191–6.208]. Modeling of the thermal effects in general can be found in [6.209–6.219].

6.4.1 Thermal Lensing

A typical distortion of the desired laser operation from the active material is the thermal lensing of solid-state laser rods [6.220–6.267]. The rod can be cooled at the rod surface, only. Thus a quadratically refractive index profile across the cross-section of the rod can be observed (see Table 2.6 (p. 37) for

the ray matrix). The focal length f_{therm} of the resulting lens can be as short as a few 0.1 m while the rod is pumped with a few kW. The refractive power D_{therm} per pump power P_{pump} is often used for characterization of the active material:

$$\textbf{refractive power} \quad D_{\text{therm}} = \frac{1}{f_{\text{therm}} P_{\text{pump}}} \qquad [D_{\text{therm}}] = \frac{\text{dpt}}{\text{kW}} \tag{6.12}$$

with typical values of 1–4 dpt kW^{-1}.

A typical example is shown in Fig. 6.20 for a flash lamp pumped Nd:YALO laser rod (1.1 at%) with a diameter of 4 mm and a length of 79 mm measured with a He-Ne-laser probe beam.

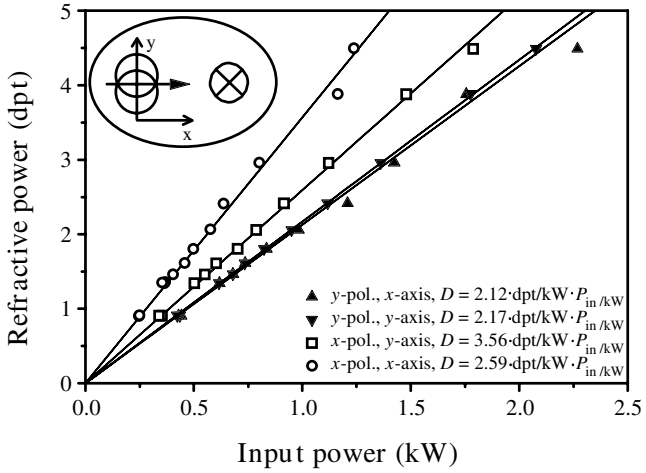

Fig. 6.20. Refractive power of a flash lamp pumped Nd:YALO laser rod (1.1 at%) with a diameter of 4 mm and a length of 79 mm measured with a He-Ne-laser probe beam. The c axis of the crystal was horizontal in the x direction in the elliptical pump chamber. The lensing was measured in the x and y direction for the two polarization directions

Unfortunately, the laser material is also cooled by the laser radiation, and thus the thermal lens can change more than 10% with and without laser operation. Further the refractive power can be different for the different polarization if the material was birefringent or birefringence was thermally induced. Thus for more precise design of the laser resonators the refractive power should be measured under laser conditions, e.g. using the stability limits of the resonator (see Sect. 6.6.15, p. 424).

Thermally steady-state conditions are fulfilled if the laser is continuously operating (cw) or the repetition rate of the laser is larger than the inverse of the thermal relaxation time τ_{therm}:

$$\textbf{thermal relaxation time} \quad \tau_{\text{term}} = \frac{c_{\text{heat}} \gamma_{\text{D}}}{4 K_{\text{cond}}} r_0^2 \tag{6.13}$$

with the specific heat of the laser material c_{heat}, the mass density γ_{D}, the thermal conductivity K_{cond} and the radius of the rod r_0. As an example for Nd:YAG, $c_{\mathrm{heat}} = 0.59\,\mathrm{W\,s\,g^{-1}\,K^{-1}}$, $\gamma_{\mathrm{D}} = 4.56\,\mathrm{g\,cm^{-3}}$, $K_{\mathrm{cond}} = 0.11$–$0.13\,\mathrm{W\,cm^{-1}\,K^{-1}}$ and with a rod radius of 4 mm a thermal relaxation time of 0.83–0.98 s is obtained [6.238].

The calculation of the thermally induced lensing of laser rods can be based on the one-dimensional heat conduction differential equation for the temperature T if these steady state conditions are fulfilled:

$$\frac{\mathrm{d}^2T}{\mathrm{d}r^2} + \frac{1}{r}\frac{\mathrm{d}T}{\mathrm{d}r} + \frac{\eta_{\mathrm{therm}}P_{\mathrm{pump}}}{\pi r_0^2 L_{\mathrm{rod}} K_{\mathrm{cond}}} = 0 \tag{6.14}$$

with the pump power P_{pump}, the rod length L_{rod} and η_{therm} as the fraction of the pump power dissipated as heat in the rod. For this model – neglecting the heat dissipation via the end surfaces – the rod length should be more than 10 times larger than the rod radius. At the surface of the rod with radius $r = r_0$ the temperature is given by $T(r_0)$. The typical thermal time constants are of the order of magnitude of 1 s and thus this equation will hold for lasers with repetition rates larger than a few Hz or in cw operation. Other systems need more complicated analysis as, e.g. given in [6.217–6.219, 6.232]. The solution of this equation is given by:

$$T(r) = T(r_0) + \Delta T\left[1 - \left(\frac{r}{r_0}\right)^2\right] \quad \text{with} \quad r \le r_0 \tag{6.15}$$

This temperature profile is quadratic, as mentioned above, with the highest value $T_{\mathrm{max}} = T(r_0) + \Delta T$ in the rod center using:

$$\Delta T = \frac{\eta_{\mathrm{therm}}P_{\mathrm{pump}}}{4\pi L_{\mathrm{rod}} K_{\mathrm{cond}}} \tag{6.16}$$

which increases linearly with the pump power per length. From this thermal distribution across the rod a distribution of the refractive index $\Delta n(r)$ follows and is given by:

$$\begin{aligned}\Delta n(r) &= [T(r) - T(r_0)]\left(\frac{\mathrm{d}n}{\mathrm{d}T}\right) \\ &= \frac{\eta_{\mathrm{therm}}P_{\mathrm{pump}}}{4\pi L_{\mathrm{rod}} K_{\mathrm{cond}}}\left(\frac{\mathrm{d}n}{\mathrm{d}T}\right)\left[1 - \left(\frac{r}{r_0}\right)^2\right]\end{aligned} \tag{6.17}$$

with the temperature-dependent refractive index change $(\mathrm{d}n/\mathrm{d}T)$. This formula can be written as:

$$\Delta n(r) = n_0 - \frac{1}{2}n_{\mathrm{therm}}r^2 \tag{6.18}$$

with the newly defined n_{therm}:

$$n_{\mathrm{therm}} = \frac{\eta_{\mathrm{therm}}P_{\mathrm{pump}}}{2\pi r_0^2 L_{\mathrm{rod}} K_{\mathrm{cond}}}\left(\frac{\mathrm{d}n}{\mathrm{d}T}\right) \tag{6.19}$$

and can be used in the matrix ray propagation formalism with a quadratic index profile (n_2 in Tab. 2.6).

The focal length f_{rod} of thermally induced focusing in the laser rod can be given as an approximation, especially for cases with long focal lengths compared to the rod length, by:

thermal induced focal length

$$f_{\mathrm{rod}} = \frac{2\pi r_0^2 K_{\mathrm{cond}}}{\eta_{\mathrm{therm}} P_{\mathrm{pump}}} \left(\frac{\mathrm{d}n}{\mathrm{d}T}\right)^{-1} \tag{6.20}$$

which shows the influence of the parameters. The larger the radius of the laser rod the longer the focal length of the rod. The rest are material parameters.

In addition a stress-dependent component will increase the thermal effect by about 20% and the end-face curvature will add a further 5%. For more detailed analysis see [6.209–6.219, 6.260, 6.261].

The temperature-dependent change of the refractive index ($\mathrm{d}n/\mathrm{d}T$) for some solid-state laser materials is given in Table 6.3.

Table 6.3. Temperature-dependent change of the refractive index ($\mathrm{d}n/\mathrm{d}T$) for some solid-state laser materials, their expansion coefficient α_{expan} and their thermal conductivity K_{cond}. The double numbers for Nd:YALO and Nd:YVO_4 are for the a and the c axes of the crystal

Material	λ_{laser} (nm)	n_0	α_{expan} (K^{-1})	$\mathrm{d}n/\mathrm{d}T$ (K)	K_{cond} ($\mathrm{W\,cm^{-1}\,K^{-1}}$)
Ruby	694	1.76	$5.8 \cdot 10^{-6}$	$13 \cdot 10^{-6}$	0.42
Nd:glass	1054	1.54	$8.6 \cdot 10^{-6}$	$8.6 \cdot 10^{-6}$	0.012
Nd:YAG	1064	1.82	$7.5 \cdot 10^{-6}$	$7.3 \cdot 10^{-6}$	0.13
Nd:YALO	1080	1.90	$9\text{–}11 \cdot 10^{-6}$	$10\text{–}14 \cdot 10^{-6}$	0.11
Nd:YVO_4	1064	1.45	$4\text{–}11 \cdot 10^{-6}$	$8.5\text{–}3 \cdot 10^{-6}$	0.5–0.05
Nd:$GdVO_4$	1063	1.97–2.19	$1.5\text{–}7.5 \cdot 10^{-6}$	$4.7 \cdot 10^{-6}$	0.05
Nd:YLF	1047	1.45		$-3 \cdot 10^{-6}$	0.06
Nd:KGW	1067	1.94		$0.4 \cdot 10^{-6}$	0.03
Nd:Cr:GSGG	1060	1.94	$7.4 \cdot 10^{-6}$	$11 \cdot 10^{-6}$	0.06
Er:glass	1540	1.53	$12 \cdot 10^{-6}$	$6.3 \cdot 10^{-6}$	≈ 0.01
Er:YAG	2940	1.79	$7.7\text{–}8.2 \cdot 10^{-6}$	$7.3 \cdot 10^{-6}$	0.14
Yb:YAG	1030	1.82	$7.5 \cdot 10^{-6}$	$7.3 \cdot 10^{-6}$	0.13
Ti:Al_2O_3	e.g. 800	1.76	$8.4 \cdot 10^{-6}$	$\approx 13 \cdot 10^{-6}$	0.52
Cr:LiSAF	846	1.41	$25 \cdot 10^{-6}$	$-4.8, -2.5 \cdot 10^{-6}$	0.03
Cr:LiCAF	763	1.39	$22 \cdot 10^{-6}$	$-4.6, -4.2 \cdot 10^{-6}$	0.05

As can be seen in the table these parameters are mostly determined by the host material. In addition to the described lensing higher-order aberrations can occur which cannot be compensated by simple lenses or mirrors. Phase conjugating mirrors can help to solve this problem (see Sect. 6.6.12, p. 416). Other solutions are described in [6.268–6.273].

6.4.2 Thermally Induced Birefringence

The pump process can also cause thermally induced birefringence [6.271–6.290] in the active material and thus depolarization of the laser radiation can occur. For example, in solid-state laser rods as in Nd:YAG material thermally induced depolarization can be a serious problem for designing high-power lasers with good beam quality. In Fig. 6.21 the measuring method for determining the depolarization is shown.

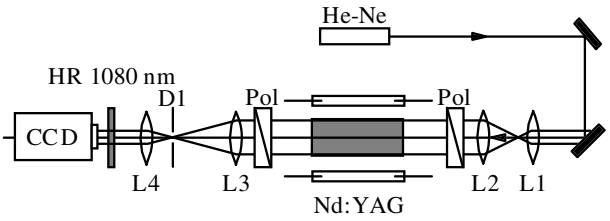

Fig. 6.21. Setup for measuring the depolarization of a flash lamp pumped Nd laser rod using a He-Ne laser probe beam and two crossed polarizer (Pol)

As an example the results for the measurement of a Nd:YAG laser rod with a diameter of 7 mm and a length of 114 mm as a function of the electrical flash lamp pump power measured between crossed polarizers, as in the scheme of Fig. 6.21, are given in Fig. 6.22.

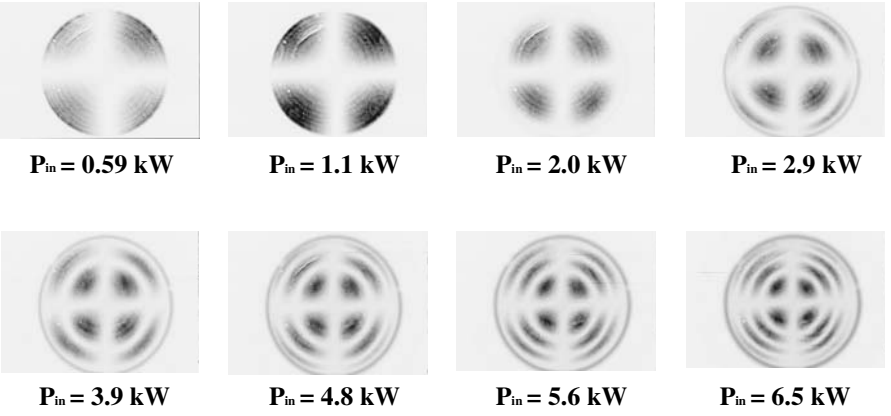

Fig. 6.22. Depolarization in a Nd:YAG laser rod with a diameter of 7 mm and a length of 114 mm as a function of the electrical flash lamp pump power measured between crossed polarizers as in the scheme of Fig. 6.21

Based on the previous Section giving the description of the thermal heating of the laser rods the depolarization can also be calculated as a function of the pump power.

The temperature difference causes mechanical strain in the laser crystal which deforms the lattice. Because of the radial symmetry of the strain the resulting refractive index change Δn will be different for the radial and the tangential components of the light polarization. The difference of the changes of the refractive indices of the radial Δn_{r} and the tangential Δn_{ϕ} polarization is given by:

$$\begin{aligned}\Delta n_{\phi}(r) - \Delta n_r(r) &= -\frac{n_0^3 \alpha_{\mathrm{expan}} C_{\mathrm{bire}}}{\pi K_{\mathrm{cond}} L_{\mathrm{rod}}} \left(\frac{r}{r_0}\right)^2 \eta_{\mathrm{therm}} P_{\mathrm{pump}} \\ &= \frac{\lambda_{\mathrm{laser}} C_T}{2\pi L_{\mathrm{rod}}} \left(\frac{r}{r_0}\right)^2 \eta_{\mathrm{therm}} P_{\mathrm{pump}} \end{aligned} \tag{6.21}$$

with the additional constants α_{expan} as the expansion coefficient and the dimensionless factor C_{bire} accounting for the birefringence. C_{bire} can be calculated from the photoelastic coefficients of the material but it is easier to determine it experimentally from the birefringence measurement and the determination of C_{T} as will be shown below. For Nd:YAG, C_{bire} is about $C_{\mathrm{bire,Nd:YAG}} = -0.0097$ and thus $C_{\mathrm{T,Nd:YAG}} = 67\,\mathrm{kW}^{-1}$.

The difference of the refractive indices for the two polarizations of the laser light leads to a well-defined alteration of the polarization state of the light, often called depolarization. This can easily be measured, as shown in Fig. 6.22 (p. 385). The intensity of the light $I_{\mathrm{out},||}$ polarized parallel to the incident light behind the laser rod at position r, ϕ in polar coordinates is given by:

$$\frac{I_{\mathrm{out},||}(r,\phi)}{I_{\mathrm{out,total}}} = 1 - \sin^2(2\phi)\, \sin^2\left(\frac{\delta_{\mathrm{bire}}}{2}\right) \tag{6.22}$$

with the phase difference δ_{bire}:

$$\begin{aligned}\delta_{\mathrm{bire}} &= \frac{2\pi L_{\mathrm{rod}}}{\lambda_{\mathrm{laser}}} (\Delta n_{\phi} - \Delta n_r) \\ &= C_{\mathrm{T}} \eta_{\mathrm{therm}} P_{\mathrm{pump}} \left(\frac{r}{r_0}\right)^2 . \end{aligned} \tag{6.23}$$

This equation can be integrated over the cross-section of the rod to get the degree of polarization of the transmitted light p_{pol}:

$$\begin{aligned} p_{\mathrm{pol}} &= \frac{I^{\mathrm{all}}_{\mathrm{out},||} - I^{\mathrm{all}}_{\mathrm{out},\perp}}{I^{\mathrm{all}}_{\mathrm{out},||} + I^{\mathrm{all}}_{\mathrm{out},\perp}} \\ &= \frac{1}{2} + \frac{\sin(C_{\mathrm{T}} \eta_{\mathrm{therm}} P_{\mathrm{pump}})}{2 C_{\mathrm{T}} \eta_{\mathrm{therm}} P_{\mathrm{pump}}} \end{aligned} \tag{6.24}$$

which can be measured as a function of the pump power.

As shown in [6.238] the agreement between these experimental and calculated results is quite satisfying.

Anisotropic materials with high natural birefringence such as Nd:YALO or Nd:YLF show only a negligible thermally induced birefringence. Therefore they emit linearly polarized light even at the highest average output powers.

The depolarization caused by thermally induced birefringence in highly pumped isotropic laser crystals can be compensated by the arrangement of two identical active materials in series with a 90° polarization rotator in between [6.276, 6.289, 6.290] as shown in Fig. 6.23.

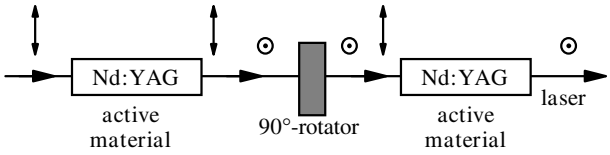

Fig. 6.23. Arrangement of two active isotropic materials, e.g. two Nd:YAG laser rods, with 90° polarization rotation in between for compensation of depolarization from birefringence

The birefringence in the first active material, which can be, e.g. a Nd:YAG rod, causes the generation in general of different elliptically polarized light across the beam. The x and y components of the polarization one interchanged by the 90° rotator (quartz plate). The depolarization is compensated during the pass through the second identical active material. Thus the depolarization loss, e.g. in Nd:YAG lasers can be reduced from the 25% level to theoretically zero and experimentally to less than 5% for pump powers of up to 16 kW [6.289].

For improved compensation a relay imaging telescope can be applied between the two laser rods. Therefore, two lenses with focal length f_{relim} are positioned in front of the rods at the distances z_{L1} and z_{L2} from the end faces. The distance between the two lenses should be $2f_{\mathrm{relim}}$ and the condition $z_{\mathrm{L1}} + z_{\mathrm{L2}} = 2f_{\mathrm{relim}} - L_{\mathrm{rod}}/n_{\mathrm{rod}}$ should be fulfilled [6.289]. A similar scheme can be realized with one laser rod in front of a 100% mirror and a Faraday rotator. With a detailed analysis the stability ranges of a laser oscillator containing two such identical rods with rotator and imaging can be almost perfectly matched for the two polarizations. As a result, high average output powers of 180 W were obtained with diffraction limited beam quality of $M^2 < 1.2$ from a single Nd:YAG laser oscillator which is also useful for Q-switch operation [6.1535].

6.4.3 Thermal Stress Fracture Limit

The maximum output power of solid-state lasers is given by the maximum pump power and related efficiencies and thus the maximum thermally induced stress the active material can bear [e.g. 6.291, 6.292]. From the quadratic tem-

perature profile across the diameter of the laser rods, the maximum surface stress $\sigma_{\max}$ follows as given in [6.292]:

$$\sigma_{\max} = \frac{\alpha_{\text{expan}} E_{\text{young}}}{8\pi K_{\text{cond}}(1-\nu_{\text{poisson}})} \frac{\eta_{\text{therm}} P_{\text{pump}}}{L_{\text{rod}}} \tag{6.25}$$

with Young's modulus E_{young}, Poisson's ratio ν_{poisson} and all other parameters as given above. The damage stress is typically in the range 100–200 MPa for common solid-state laser materials. The maximum power per laser rod length follows from:

$$\frac{P_{\text{pump}}}{L_{\text{rod}}} = 8\pi R_{\text{shock}} \tag{6.26}$$

with the thermal shock parameter R_{shock}:

$$R_{\text{shock}} = \frac{K_{\text{cond}}(1-\nu_{\text{poisson}})\sigma_{\max}}{\alpha_{\text{exp and}} E_{\text{yound}}} \tag{6.27}$$

for which the values in Table 6.4 were given in [M33].

Table 6.4. Shock parameter for different host materials of solid-state lasers

Host material	Glass	GSGG	YAG	Al_2O_3
R ($W\,cm^{-1}$)	1	6.5	7.9	100

It should be noticed that following this consideration the rod diameter does not influence the maximum output power per rod length. An example with YAG as the host laser material involves a maximum optical pump power of about $200\,W\,cm^{-1}$.

6.5 Laser Resonators

The laser resonator determines the laser light characteristics within the frames given by the active material. It consists of at least two mirrors (see Fig. 6.2, p. 360) but it can contain many additional elements:

- apertures, lenses, additional mirrors and diffractive optics may be used for forming special transversal modes;
- gratings, prisms and etalons are applied for frequency selection;
- shutters, modulators, deflectors and nonlinear absorbers are used for generating short pulses;
- polarizing elements are applied for selecting certain polarizations.

Other linear and nonlinear elements are applied as well. For example, phase plates, adaptive mirrors or phase conjugating mirrors can be used for compensating phase distortions.

Because of all these options the design of a resonator with respect to a certain application producing laser light of the required properties in combination with high brightness and efficiency is a difficult task. However, the basic laws as well as the general ideas and strategies will be described in the next sections. Detailed descriptions can be found in, for example, [M24, M33, M49, M50, 6.293–6.299].

6.5.1 Stable Resonators: Resonator Modes

The laser resonator (or cavity) can be designed as a *stable resonator* producing a standing light wave from the interference of the two counterpropagating light beams with a certain transversal and longitudinal distribution of the electric field inside. These distributions are eigensolutions of Maxwell's equations for the standing light wave with the boundary conditions of the curved resonator mirror surfaces and including all further optical elements in the resonator.

The transversal structures of these eigensolutions are called *transversal resonator modes*. The transversal structure can change along the axis of the laser and a certain transversal light pattern will be observed behind the partially transparent resonator mirror, the output coupler (see Fig. 6.24). For many applications a Gaussian beam is required as the transversal mode of the laser.

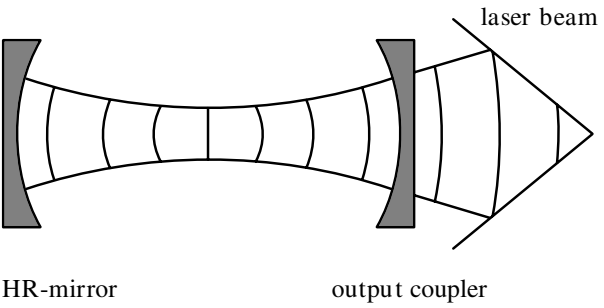

Fig. 6.24. Transversal eigenmode of a stable empty resonator consisting of the high-reflecting HR mirror ($R \simeq 100\%$) and the partially reflecting mirror, the output coupler (with, e.g. $R = 50\%$). The curvatures of the stable transversal modes are the same as the mirror curvatures at the mirror positions

The curvatures of the wave fronts of the resonator modes of the light beam at the position of the mirror surfaces is the same as the curvature of the mirrors. This condition defines the possible transversal modes of a stable resonator.

The axial structures of these eigensolutions are the *longitudinal resonator (or axial) modes* (see Fig. 6.25). The standing light wave is built by the

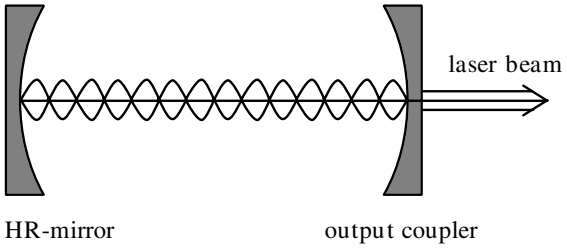

Fig. 6.25. Longitudinal eigenmode of a stable empty resonator as in Fig. 6.24 (p. 389). The electric field of the stable longitudinal modes have knots at the mirror surfaces

interference of the back and forth moving light waves reflected at the mirrors. The electric field has a knot at the mirror surface and thus the longitudinal modes are selected.

6.5.2 Unstable Resonators

In an unstable resonator the light beam diameter grows while the light is reflected back and forth in the resonator as depicted in Fig. 6.26.

In this case the near field of the out-coupled beam has a hole in the middle which has the size of the smaller mirror at its place but will be filled in the far field. With this resonator type large mode diameters in the active material can be achieved but the beam quality is not diffraction limited. Using unstable resonators with a mirror with radially varying reflectivity, near-diffraction-limited beam quality can be achieved with large mode diameters [6.317, 6.326, 6.332–6.334, 6.338]. Diffractive optics used as structured phase plates can be placed inside the unstable resonator for improving the beam quality [6.344]. Some examples of unstable resonators are given in [6.300–6.352]. The theoretical treatment of unstable resonators is discussed in, for example, [6.300–6.315].

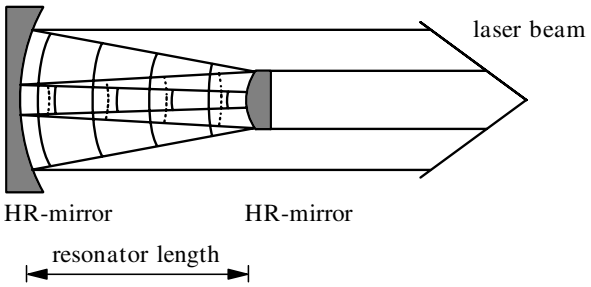

Fig. 6.26. Transversal structure of a light beam in an a unstable empty resonator consisting of two high-reflecting HR mirrors ($R = 99.9\%$) of different size

6.6 Transversal Modes of Laser Resonators

In general the transversal modes of a given resonator design have to be calculated as a solution of Maxwell's equations for the electric field between the two resonator mirrors including all optical elements inside this space. This problem can be solved by calculating the Kirchhoff integral including the dimensions of the resonator mirrors.

The still complicated mathematical problem is often reduced to three types of special cases:

- a fundamental mode describing a Gaussian beam as an eigensolution of a stable resonator including the optical elements in the resonator;
- higher transversal modes for an empty optical resonator with high transversal symmetry;
- simple solutions for unstable resonators.

Some resonators with an active material of very high gain and thus a very small number of round trips such as, e.g. in the excimer or nitrogen lasers, show a mixture of so many modes that the description based on geometrical optics using the geometrical dimensions of the resonator elements with their apertures and determining the possible light rays can be the most efficient.

6.6.1 Fundamental Mode

The fundamental transversal mode, the TEM_{00} mode, has a Gaussian transversal profile and represents a Gaussian beam. Thus it can be derived from Gaussian beam propagation through the resonator under the condition of self-reproduction after one complete round trip. Thus the complex beam parameter of the beam $q(z)$ (see Sect. 2.4) has to be reproduced:

$$\text{eigensolution} \quad q(z_{\mathrm{oc}}) = \frac{a_{\mathrm{roundtrip}} q(z_{\mathrm{oc}}) + b_{\mathrm{roundtrip}}}{c_{\mathrm{roundtrip}} q(z_{\mathrm{oc}}) + d_{\mathrm{roundtrip}}} \tag{6.28}$$

with z_{oc} as a fixed position of observation, e.g. at the output coupler. The elements of the roundtrip matrix $M_{\mathrm{roundtrip}}$:

$$\text{roundtrip matrix} \quad M_{\mathrm{roundtrip}} = \begin{bmatrix} a_{\mathrm{roundtrip}} & b_{\mathrm{roundtrip}} \\ c_{\mathrm{roundtrip}} & d_{\mathrm{roundtrip}} \end{bmatrix} \tag{6.29}$$

have to be derived from the multiplication of all single matrices accounting for all optical elements of the resonator including the free space propagation as described in Sect. 2.5. From the determined value of $q(z_{\mathrm{oc}})$ the beam radius $w(z)$ and wave front curvature $R(z)$ can be calculated at any position inside and outside the resonator by the propagation of the Gaussian beam.

Notice that the beam parameter outside the resonator (laser beam parameter q_{laser}) has to be calculated from $q(z_{\mathrm{OC}})$ by applying the transmission

matrix M_{OC} of the output coupler which may act as a lens:

$$q_{\mathrm{laser}} = \frac{a_{\mathrm{OC}} q(z_{\mathrm{oc}}) + b_{\mathrm{OC}}}{c_{\mathrm{OC}} q(z_{\mathrm{oc}}) + d_{\mathrm{OC}}} \tag{6.30}$$

and thus the divergence angle and beam diameter of the laser can be determined.

In particular, numerical calculations are easily possible using personal computers. Analytical solutions can be hard because of lengthy algebraic complex expressions, but algebraic computer programs can be used for this purpose.

6.6.2 Empty Resonator

As an example the description of an empty resonator (see Fig. 6.27) will be given.

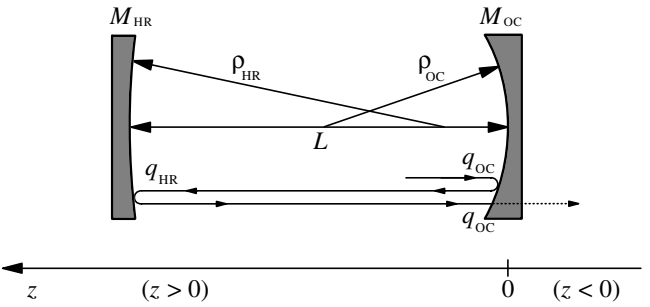

Fig. 6.27. Scheme of an empty resonator with the out-coupling mirror OC and the high-reflecting mirror HR. The curvature radii are positive for concave mirrors. The resonator length is L

This resonator with curvature ρ_{HR} of the high-reflecting mirror and ρ_{OC} of the output coupler placed at a distance L as the resonator length leads to the round trip matrix of the empty resonator:

$$M_{\mathrm{roundtrip}} = \begin{bmatrix} 1 & L \\ 0 & 1 \end{bmatrix} \cdot \begin{bmatrix} 1 & 0 \\ \frac{-2}{\rho_{\mathrm{HR}}} & 1 \end{bmatrix} \cdot \begin{bmatrix} 1 & L \\ 0 & 1 \end{bmatrix} \cdot \begin{bmatrix} 1 & 0 \\ \frac{-2}{\rho_{\mathrm{OC}}} & 1 \end{bmatrix} \tag{6.31}$$

which accounts for the first reflection at the output coupler, the path L, reflection at the high-reflecting mirror and the path L again considered as a positive value because for beam propagation calculations the resonator has to be unfolded. The resulting matrix of the empty resonator is given by:

$$M_{\text{roundtrip}} = \frac{1}{\rho_{\text{OC}}\rho_{\text{HR}}} \cdot \begin{bmatrix} -\rho_{\text{HR}}(4L-\rho_{\text{OC}}) - 2L(2L-\rho_{\text{OC}}) & 2L\rho_{\text{OC}}(\rho_{\text{HR}}-1) \\ -2(\rho_{\text{OC}}+\rho_{\text{HR}}-2L) & \rho_{\text{OC}}(\rho_{\text{HR}}-2L) \end{bmatrix}. \tag{6.32}$$

An algebraic calculation of (6.28) using (6.32) which is easily done with a suitable algebraic computer program shows that the curvatures R_i of the fundamental mode of this empty resonator are equal to the curvature of the mirrors ρ_i:

$$\text{wave curvature radii} \quad \begin{matrix} R(z=z_{\text{OC}}) = \rho_{\text{OC}} \\ R(z=z_{\text{HR}}) = \rho_{\text{HR}} \end{matrix} \tag{6.33}$$

whereas the diameter of the beam $2w_{\text{OC}}$ at the position of the out-coupling mirror follows from:

beam diameter at OC

$$2w_{\text{OC}} = 2\sqrt{\frac{\lambda}{\pi}\rho_{\text{OC}}\sqrt{\frac{L(L-\rho_{\text{HR}})}{(\rho_{\text{OC}}+\rho_{\text{HR}}-L)(L-\rho_{\text{OC}})}}} \tag{6.34}$$

and the diameter at the high-reflecting mirror follows analogously:

beam diameter at HR

$$2w_{\text{HR}} = 2\sqrt{\frac{\lambda}{\pi}\rho_{\text{HR}}\sqrt{\frac{L(L-\rho_{\text{OC}})}{(\rho_{\text{OC}}+\rho_{\text{HR}}-L)(L-\rho_{\text{HR}})}}} \tag{6.35}$$

The position z_{waist} and diameter $2w(z_{\text{waist}})$ of the beam waist can easily be calculated from these solutions by using (2.88) and (2.89):

$$\textbf{waist position} \quad z_{\text{waist}} = \frac{L(L-\rho_{\text{HR}})}{\rho_{\text{OC}}+\rho_{\text{HR}}-2L} \tag{6.36}$$

where the z coordinate is measured positively from the out-coupling mirror to the left in Fig. 6.27 (p. 392) towards the inside of the resonator and negative to the right.

waist diameter

$$2w_{\text{waist}} = 2\sqrt{\frac{\lambda}{\pi}\sqrt{\frac{L(\rho_{\text{OC}}-L)(\rho_{\text{HR}}-L)(\rho_{\text{OC}}+\rho_{\text{HR}}-L)}{(\rho_{\text{OC}}+\rho_{\text{HR}}-2L)^2}}}. \tag{6.37}$$

As can be seen from this equation the diameter can be very large as the curvature of the mirrors is very flat. This case is usually hard to achieve because it is close to the stability limit and the misalignment sensitivity becomes very bad. Thus in this case mixtures of higher-order transversal modes are usually oscillating, resulting in bad beam quality.

Stable eigensolutions of the fundamental mode of the empty resonator are possible for:

$$\text{stability condition} \quad \rho_{\mathrm{OC}} + \rho_{\mathrm{HR}} \geq L \tag{6.38}$$

and further conditions can be evaluated from the condition of a positive expression in the root (see below).

6.6.3 *g* Parameter and *g* Diagram

For a general discussion of the stability ranges the g parameters of the resonator as depicted in Fig. 6.27 (p. 392), can be used. These parameters are defined as:

$$\textbf{g parameter of OC mirror} \quad g_{\mathrm{OC}} = 1 - \frac{L}{\rho_{\mathrm{OC}}} \tag{6.39}$$

and

$$\textbf{g parameter of HR mirror} \quad g_{\mathrm{HR}} = 1 - \frac{L}{\rho_{\mathrm{HR}}}\,. \tag{6.40}$$

The beam waist at the output coupler follows then from:

$$\text{beam at OC} \quad 2w_{\mathrm{OC}} = 2\sqrt{\frac{\lambda}{\pi} L \sqrt{\frac{g_{\mathrm{HR}}}{|g_{\mathrm{OC}}(1 - g_{\mathrm{OC}} g_{\mathrm{HR}})|}}} \tag{6.41}$$

and at the high reflecting mirror:

$$\text{beam at HR} \quad 2w_{\mathrm{HR}} = 2\sqrt{\frac{\lambda}{\pi} L \sqrt{\frac{g_{\mathrm{OC}}}{g_{\mathrm{HR}}(1 - g_{\mathrm{OC}} g_{\mathrm{HR}})}}} \tag{6.42}$$

whereas the beam waist occurs at the position:

$$\text{waist position} \quad z_{\mathrm{waist}} = \frac{L g_{\mathrm{HR}}(L - g_{\mathrm{OC}})}{g_{\mathrm{HR}}(2g_{\mathrm{OC}} - 1) - g_{\mathrm{OC}}} \tag{6.43}$$

with the waist diameter:

$$\text{waist diameter} \quad 2w_{\mathrm{HR}} = 2\sqrt{\frac{\lambda}{\pi} L \frac{\sqrt{g_{\mathrm{OC}} g_{\mathrm{HR}}(1 - g_{\mathrm{OC}} g_{\mathrm{HR}})}}{|g_{\mathrm{HR}}(2g_{\mathrm{OC}} - 1) - g_{\mathrm{OC}}|}}\,. \tag{6.44}$$

With these g parameters the general stability condition for the fundamental mode operation of the resonator can obviously be written as:

$$\textbf{general stability condition} \quad 0 < g_{\mathrm{OC}} g_{\mathrm{HR}} < 1\,. \tag{6.45}$$

This condition can be nicely visualized in the g diagram which is built by one g parameter as one coordinate (e.g. g_{OC}) and the other g parameter as the other coordinate as shown in Fig. 6.28 (p. 395).

At the limits of these stability ranges the Gaussian beam would have an infinite or zero diameter at the mirrors. In Fig. 6.28 (p. 395) some selected resonators, as described below, are marked with letters (a)–(f).

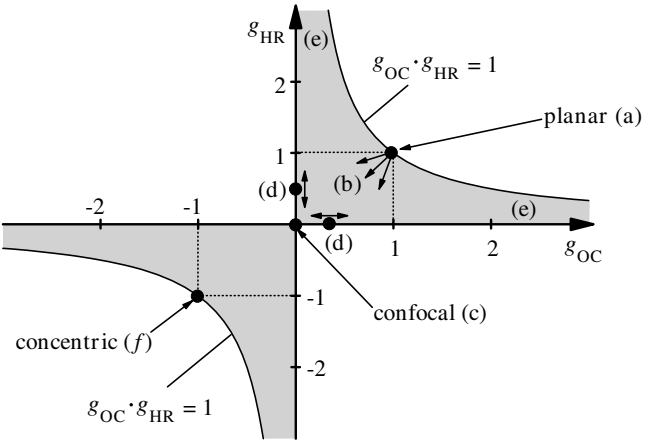

Fig. 6.28. *g* diagram for discussing the stability of an empty resonator. The gray area indicates the stable ranges of operation. Specially named selected resonators are indicated (see next section)

6.6.4 Selected Stable Empty Resonators

Some of the stable empty resonators, e.g. with g_i equal 0, 1 or -1 are named for their special construction.

(a) Planar mirror resonators consist of two planar mirrors at any distance (see Fig. 6.29).

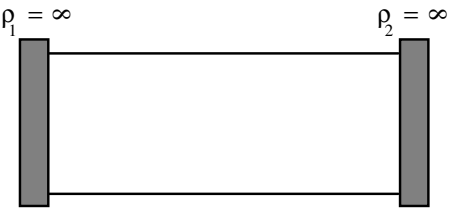

Fig. 6.29. Schematic of a planar resonator (a). The beam radius is theoretically indefinite

This resonator demands unconfined mirrors and would show an infinite beam diameter. It is at the stability limit (see Fig. 6.28) and thus it cannot be built as an empty resonator. As soon as some positive refraction occurs inside the resonator it will become stable. Therefore some times for solid-state lasers plan-plan resonators are used including the refraction of the thermal lensing of the laser rod.

If the lensing is too large the resonator will again become unstable. This effect can be used for measuring the thermal lensing of the active material under high-power pumping by measuring the output power as a function of the input power (see Sect. 6.6.15, p. 424).

(b) Curved mirror resonators with concave radii larger than the resonator length as shown in Fig. 6.30 are very common.

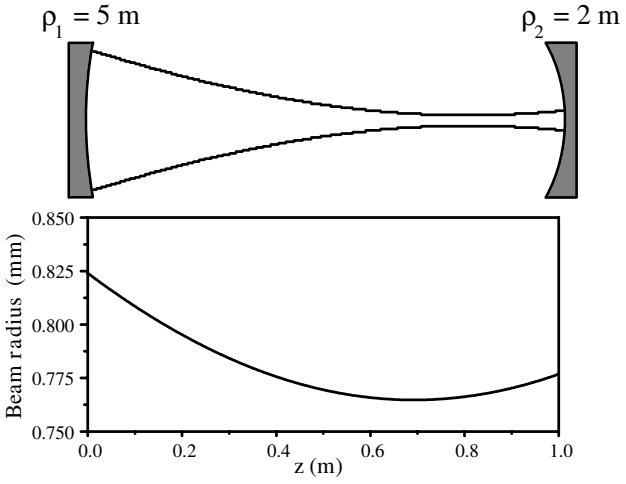

Fig. 6.30. Schematic of a resonator with curved mirrors (b). The beam radius of the fundamental mode was calculated for 1 µm wavelength, 1 m resonator length and the given mirror curvature radii

These resonators are very stable and easy to design and to align. Thus new lasers can be checked with this type of resonator, first. Usually the output coupler can be used as a planar mirror in this type of cavity and different out-coupling reflectivities can easily be obtained.

(c) Confocal resonators are symmetric with the mirror curvature radius equal the resonator length. Thus the beam waist is in the center and has a diameter of $1/\sqrt{2}$ compared to the diameter at the mirrors (see Fig. 6.31).

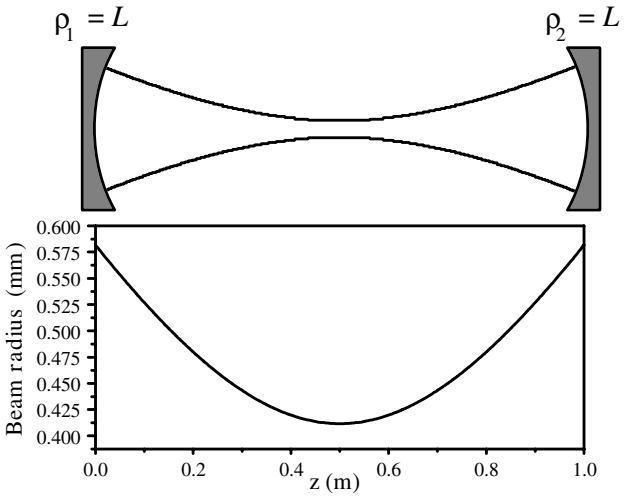

Fig. 6.31. Schematic of a confocal resonator (c). The beam radius of the fundamental mode was calculated for 1 µm wavelength, 1 m resonator length and the given mirror curvature radii

The intensity is twice as high in the resonator center compared to the mirror position. These resonators stay stable if the resonator length is increased as long as the resonator length is not longer than twice the curvature radius of the two equal mirrors (see below).

(d) Semiconfocal resonators have the beam waist at one mirror which is planar. The curvature of the other mirror is $\rho_i = 2L$ (see Fig. 6.32).

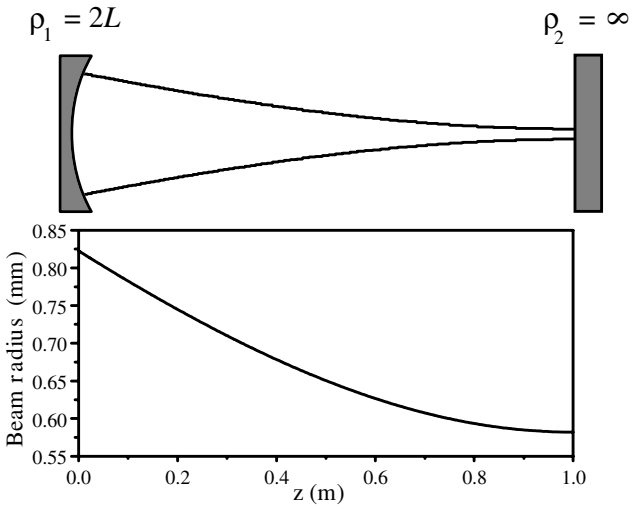

Fig. 6.32. Schematic of a semiconfocal resonator (d). The beam radius of the fundamental mode was calculated for 1 µm wavelength, 1 m resonator length and the given mirror curvature radii

The diameter of the beam is $1/\sqrt{2}$ smaller at the planar mirror compared to the curved one.

(e) Hemispherical resonators have a focus at the planar mirror (see Fig. 6.33, p. 398).

The resulting high intensity at the planar mirror can be used for nonlinear effects in the resonator such as passive Q switching or passive mode locking with dyes. Care has to be taken not to damage this mirror with the resulting high intensities.

A similar transversal beam shape distribution along the resonator axis can be obtained if the two mirrors are curved and have much different radii. If, e.g. mirror 1 has a curvature radius of a few 10 mm while the radius of the other mirror 2, is in the range of m a focus will occur close to mirror 1 independent of whether the short focal length of is positive or negative (see also Fig. 6.35, p. 399). The waist radius close to the mirror with short focal length is smaller if the longer curvature radius approaches the resonator length.

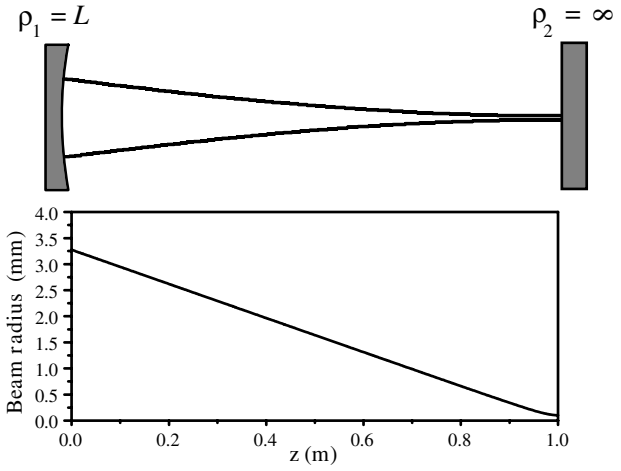

Fig. 6.33. Schematic of a hemispherical resonator (e). The beam radius of the fundamental mode was calculated for 1 μm wavelength, 1 m resonator length and the given mirror curvature radii

(f) Concentric or spherical resonators have their focus in the middle of the cavity. The two mirrors have curvature radii equal to $L/2$ (see Fig. 6.34).

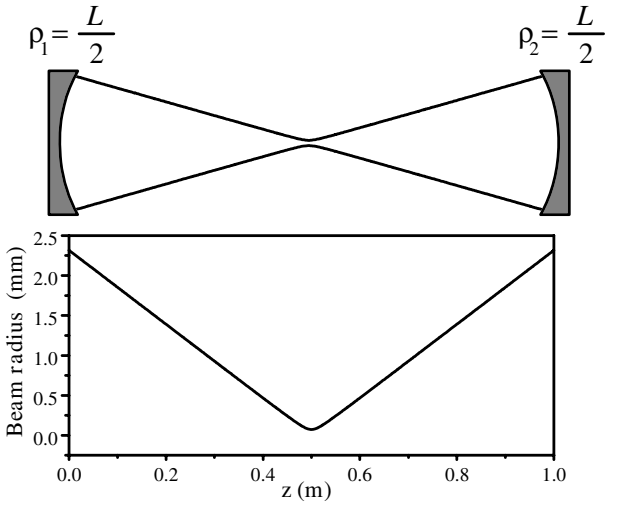

Fig. 6.34. Schematic of a concentric or spherical resonator (f). The beam radius of the fundamental mode was calculated for 1 μm wavelength, 1 m resonator length and the given mirror curvature radii

This sharp focus can cause optical breakdown in air or damage in the active material if this resonator is used in pulsed lasers. On the other hand the focus in the center allows the use of an aperture for selection of the fundamental mode in an effective way.

(g) Concave–convex resonators have a common focal point of the two mirrors outside the resonator. The curvatures radii are $\rho_1 > L$ and $\rho_2 = -(\rho_1 - L)$ as shown in Fig. 6.35.

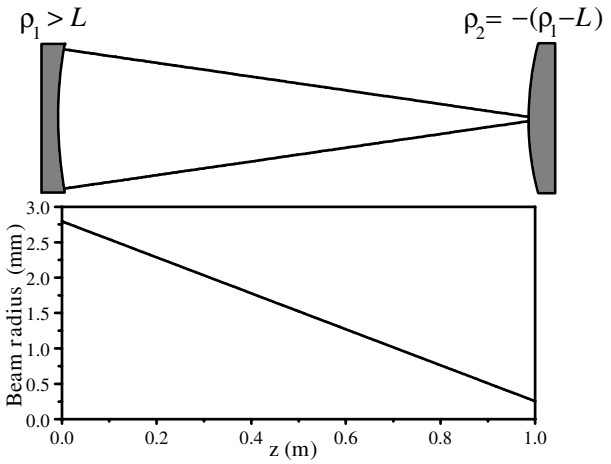

Fig. 6.35. Schematic of a concave–convex resonator (g). The beam radius of the fundamental mode was calculated for 1 µm wavelength, 1 m resonator length and the given mirror curvature radii. The curvatures radii are $\rho_1 = 1.1\,\mathrm{m}$ and $\rho_2 = -0.1\,\mathrm{m}$

If the curvature radii of the two mirrors are very different the beam diameter can be very small at the mirror with the smaller radius. Thus the intensity at this mirror can cause damage similar to that in hemispherical resonators (see above), but for the application of nonlinear effects in the resonator this configuration may be well suited.

6.6.5 Higher Transversal Modes

Transversal modes of lasers with stable optical resonators higher than the fundamental can be determined analytically for empty resonators as the steady state solution for the electric field. The transversal structure of the electrical field of the light beam has to reproduce after each roundtrip. This can be described by the Kirchhoff integral equation as discussed, e.g. in [M24] in the following form:

$$
\begin{aligned}
E_1(x_2, y_2) = -\mathrm{i}\frac{\mathrm{e}^{\mathrm{i}kL}}{2Lg_m\lambda} \cdot \int\int E_m(x_1, y_1) \\
\cdot \exp\left\{\mathrm{i}\frac{\pi}{2Lg_m\lambda}\left[(x_1^2 + y_1^2 + x_2^2 + y_2^2)(2g_1g_2 - 1)\right.\right. \\
\left.\left. -2(x_1x_2 + y_1y_2)\right]\right\} \mathrm{d}x_m\,\mathrm{d}y_m \\
l, m = 1, 2, \quad l \neq m
\end{aligned}
\tag{6.46}
$$

with the g parameters $g_{1,2}$, the resonator length L, the wavelength λ and the wave number $k = 2\pi/\lambda$.

The solutions of this equation are the transversal modes of this empty resonator. They are called *TEM modes* for transverse electromagnetic field vectors and are numbered by indices. If the mirrors are transversally unconfined and no other apertures limit the beam diameter an infinite number of transversal modes with increasing transversal dimension and structure exist. The lowest-order mode is of course the fundamental or Gaussian or TEM_{00} mode as described above.

Eigenmodes of a resonator higher than the fundamental can have a circular or rectangular symmetry. The transversal mode structure of the intensity can be described by analytical formulas as given below.

Examples of higher-order transversal modes as e.g. Gauss–Laguerre-modes, Gauss–Hermite-modes or donut-modes are described in [6.353–6.362, 6.364–6.411]. In addition to the modes described below, flat top modes are of interest for high extraction efficiency and certain applications [6.381–6.394]. Also, mode converters leading to, for example, Bessel modes, which allow a constant intensity over a certain distance and thus good efficiency in some nonlinear optical processes, are of interest [6.395–6.401]. Whispering-gallery modes occur in microlasers with microresonators [6.402–6.411]. These laser resonators may be of interest for use as diode lasers or in communication technology.

6.6.5.1 Circular Eigenmodes or Gauss–Laguerre Modes

These modes are described with Laguerre polynomials. The square of the solution for the electric field leads to the following transversal distribution for the intensity at the position of mirrors 1 and 2:

circular modes

$$I_1^{(m,p)}(r,\varphi) = \frac{I_{\max}}{F_{\max,\mathrm{circ}}} \left(\frac{2r^2}{w_l^2}\right)^p \cdot \left[L^{(m,p)}\left(\frac{2r^2}{w_l^2}\right)\right]^2 \mathrm{e}^{-2r^2/w_l^2} \cos^2(p\varphi) \tag{6.47}$$

with cylindrical coordinates r, φ, beam radius of the Gaussian beam w_l for this resonator calculated for w_OC from (6.34) or (6.41) and for w_HR from (6.35) or (6.42). The Laguerre polynomials $L^{(m,p)}(t)$ are given in mathematical textbooks. The first few are:

Laguerre polynomials:

$$L^{(0,p)}(t) = 1$$
$$L^{(1,p)}(t) = p + 1 - t$$
$$L^{(2,p)}(t) = \frac{1}{2}(p+1)(p+2) - (p+2)t + \frac{1}{2}t^2$$

$$L^{(3,p)}(t) = \frac{1}{6}(p+1)(p+2)(p+3) - \frac{1}{2}(p+2)(p+3)t + \frac{1}{2}(p+3)t^2 - \frac{1}{6}t^3$$

$$L^{(4,p)}(t) = \frac{1}{24}(p+1)(p+2)(p+3)(p+4) - \frac{1}{6}(p+2)(p+3)(p+4)t + \frac{1}{4}(p+3)(p+4)t^2 - \frac{1}{6}(p+4)t^3 + \frac{1}{24}t^4. \quad (6.48)$$

The highest relative maxima of these circular transversal modes $F_{\max,\mathrm{circ}}$ under the condition of equal power or energy content of all modes are given in Table 6.5.

Table 6.5. Maxima of the transversal modes $F_{\max,\mathrm{circ}}$ under the condition of equal power or energy content for all modes as a function of the mode numbers m and p

$m\backslash p$	0	1	2	3	4
0	1.0	0.73	0.54	0.45	0.39
1	1.0	0.65	0.49	0.40	0.34
2	1.0	0.66	0.47	0.38	0.33
3	1.0	0.69	0.47	0.38	0.32
4	1.0	0.67	0.47	0.38	0.32

The intensity distributions of the lowest of these circular modes are shown in Fig. 6.35.

The first index in this nomenclature gives the number of maxima in the radial distribution and the shape has cylindrical symmetry for $p = 0$. The number of maxima around the circumference $\varphi = 0, \ldots, 2\pi$ is given by $2p$. Usually the modes with $p = 0$ are much easier to detect than the modes with $p > 0$. As can be seen from Table 6.5 and Fig. 6.36 (p. 403). the energy is spread over a larger cross section with increasing mode numbers and thus the peak intensity is decreasing.

The electric field vector is polarized antiparallel, with a phase shift of π, in neighboring peaks and their surrounding area up to the minima between them.

6.6.5.2 Rectangular or Gauss–Hermite Modes

These modes are described in Cartesian coordinates x, y using Hermite polynomials $H^{(m)}(t)$. The transversal intensity distribution is given by:

rectangular modes

$$I_1^{(m,p)}(x,y) = \frac{I_{\max}}{F_{\max,\mathrm{rect}}} \left[H^{(m)}\left(\frac{\sqrt{2}x}{w_l} \right) \right]^2 \cdot \left[H^{(p)}\left(\frac{\sqrt{2}y}{w_l} \right) \right]^2 \mathrm{e}^{-2(x^2+y^2)/w_l^2} \quad (6.49)$$

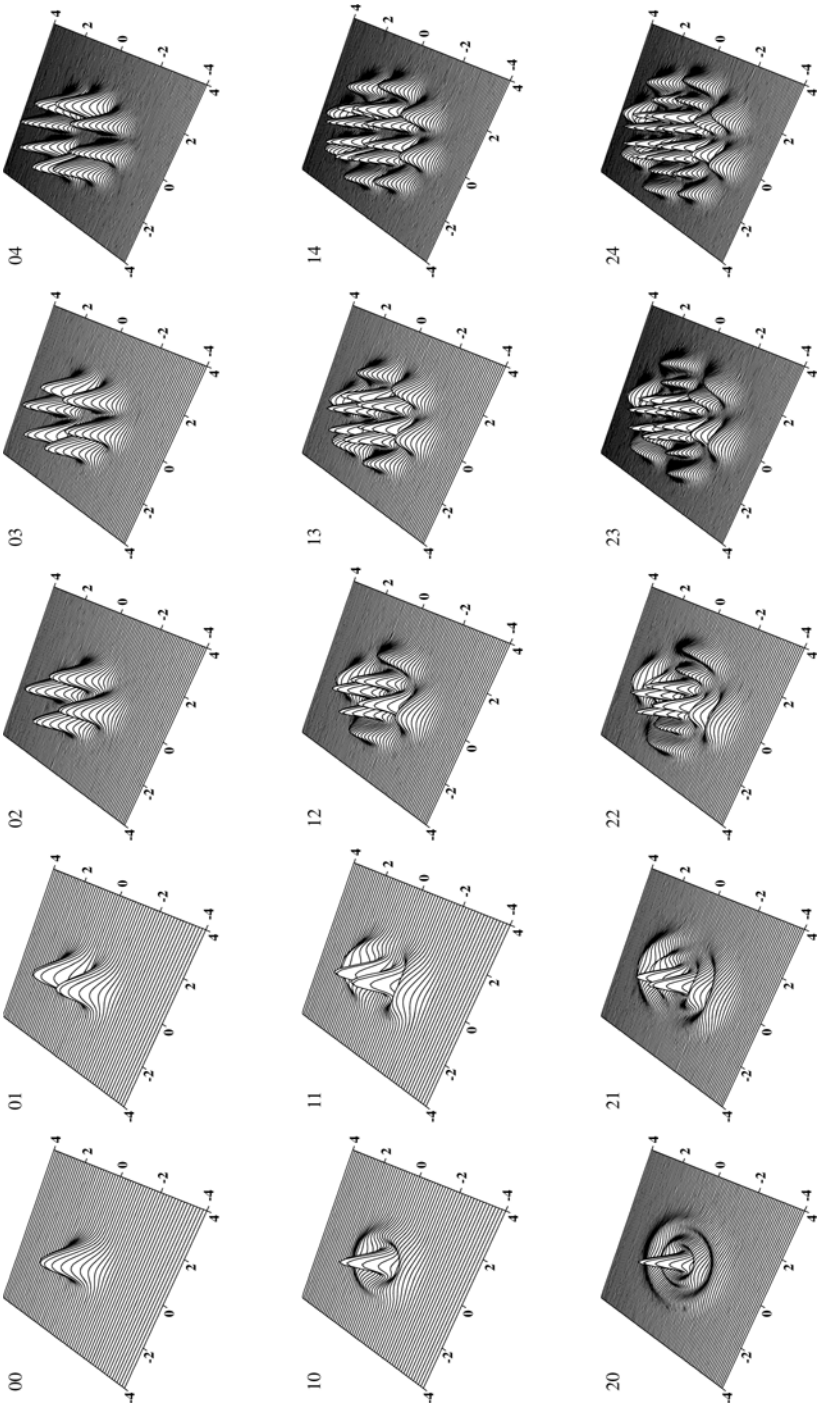
04
14
24
03
13
23
02
12
22
01
11
21
00
10
20

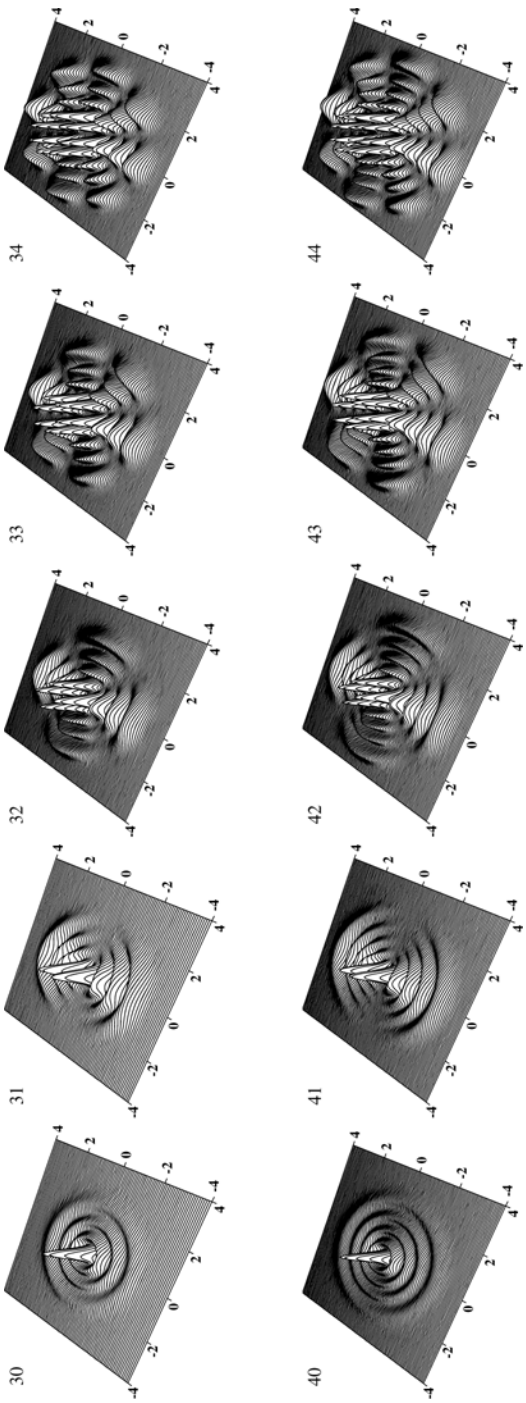

Fig. 6.35. Intensity profile of higher transversal modes of stable laser resonators with circular symmetry. The intensity was normalized for equal heights. Compare values of Tab. 6.5 for absolute intensities.

again with the beam radius of the Gaussian beam w_l for the resonator calculated for w_{OC} from (6.34) or (6.41) and for w_{HR} from (6.35) or (6.42). The Hermite polynomials $H^{(m/p)}(t)$ are also given in mathematical text books. The first few are:

Hermite polynomials:

$$\begin{aligned} H^{(0)}(t) &= 1 \\ H^{(1)}(t) &= 2t \\ H^{(2)}(t) &= 4t^2 - 2 \\ H^{(3)}(t) &= 8t^3 - 12t \\ H^{(4)}(t) &= 16t^4 - 48t^2 + 12. \end{aligned} \tag{6.50}$$

The highest relative maxima of these rectangular transversal modes $F_{\mathrm{max,rect}}$ under the condition of equal power or energy content of all modes are given in Table 6.6.

Table 6.6. Maxima of the transversal modes $F_{\mathrm{max,rect}}$ under the condition of equal power or energy content of all modes as a function of the mode numbers m and p

$m\backslash p$	0	1	2	3	4
0	1	0.73	0.65	0.61	0.58
1	0.73	0.53	0.48	0.45	0.43
2	0.65	0.48	0.42	0.40	0.38
3	0.61	0.45	0.40	0.37	0.35
4	0.58	0.43	0.38	0.35	0.34

The intensity distributions of the lowest rectangular modes are shown in Fig. 6.36.

Again the mode indices account for the number of maxima in the direction of the coordinate, x and y in this case, with $m + 1$ and $p + 1$, and again the electric field vector is polarized antiparallel, with a phase shift of π, in neighboring peaks and their surrounding area up to the minima between them.

Different laser modes can occur at the same time and thus the observed mode pattern of a realistic laser may be a *superposition of several modes*. The transversal field distribution can be written as a sum of eigenmodes because Laguerre and Hermite polynomials are each a complete set of orthogonal functions. Thus the intensity distribution $I(r, \varphi, t)$ of a circular mode can be expressed as:

$$\text{circular modes} \quad I(r, \varphi, t) = \sum_{m=0}^{\infty} \sum_{p=0}^{\infty} c_{m,p}(t) I^{(m,p)}(r, \varphi) \tag{6.51}$$

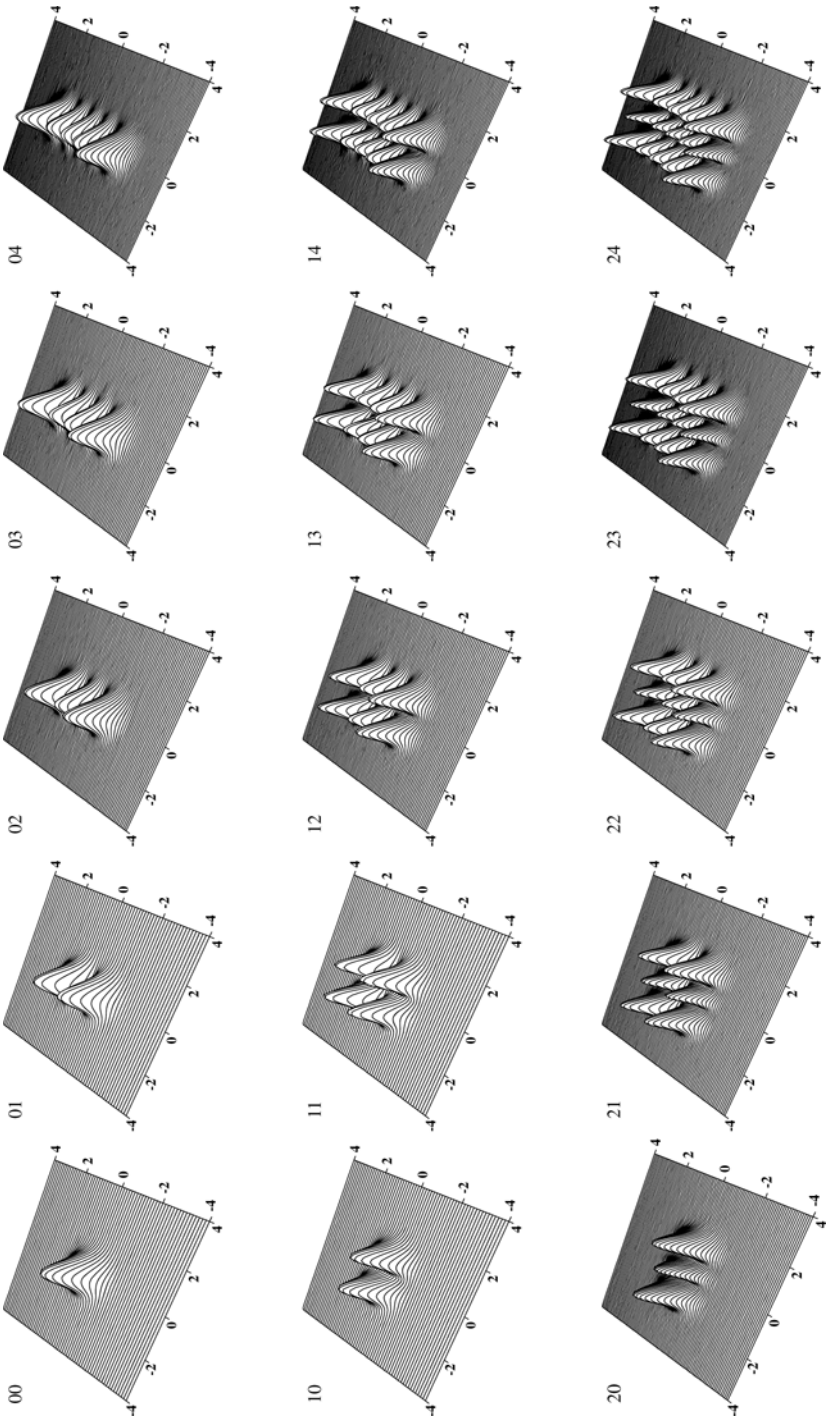
04
14
24
03
13
23
02
12
22
01
11
21
00
10
20

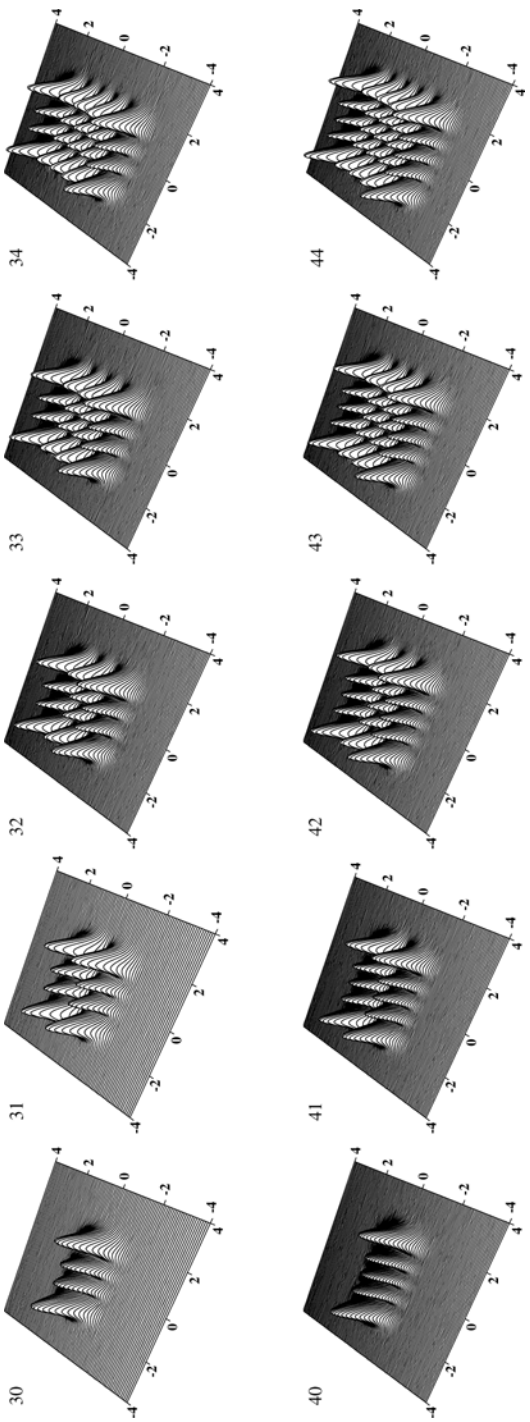

Fig. 6.36. Intensity profiles of higher transversal modes of stable laser resonators with rectangular symmetry (see text Fig. 6.35 or supplements)

with the coefficients $c_{\mathrm{m,p}}(t)$ accounting for the share of the m, p eigenmode. Rectangular modes can be constructed the same way using the rectangular eigenmodes:

$$\text{rectangular modes} \quad I(x/y,t) = \sum_{m=0}^{\infty} c_{x/y,m}(t) I^{(m,p)}(x/y). \tag{6.52}$$

In some cases, e.g., if the laser modes are degenerated, it is necessary to sum over the electric field instead of over the intensity of the different modes.

6.6.5.3 Hybrid or Donut Modes

In solid-state rod lasers, hybrid or donut modes can be obtained (see references in Sect. 6.6.5). These transversal modes are constructed as a superposition of two circular transversal modes of the same order m, p but rotated by 90°. The radial distribution of these modes can be calculated analogous to the circular modes from:

$$\textbf{donut modes} \quad I_1^{(m,p)}(r) = \frac{I_{\max}}{F_{\max,\mathrm{donut}}} \left(\frac{2r^2}{w_l^2}\right)^p \cdot \left[L^{(m,p)}\left(\frac{2r^2}{w_l^2}\right)\right]^2 \mathrm{e}^{-2r^2/w_l^2} \tag{6.53}$$

but they show full circular symmetry in the intensity distribution. These modes are marked with an asterisk at the mode number. The relative maxima $F_{\max,\mathrm{donut}}$ of the first three hybrid modes TEM_{01*}, TEM_{02*} and TEM_{03*} for the same power or energy content as the fundamental mode are 0.37, 0.34 and 0.34. The intensity distributions of these lowest three modes are shown in Fig. 6.38.

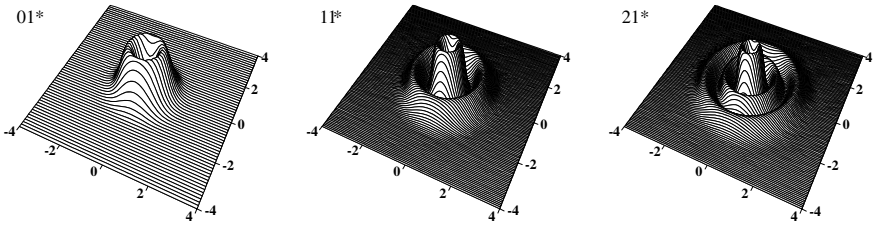

Fig. 6.38. Intensity profiles of higher transversal donut or hybrid modes of laser resonators with circular symmetry

The share of different modes can change in time and thus very complicated mode structures may be obtained with time-dependent coefficients. Mode apertures may be used for emphasizing certain modes required for the application (see Sect. 6.6.10, p. 413).

6.6.5.4 Coherent mode combining

As discussed in Sect. 2.7.7 (p. 65) the coherently generated laser modes can be combined or transformed to new laser modes [e.g. 6.412, 6.413] and even better beam quality can be realized this way. In principle the different coherent laser modes can be transformed to each other, as long as perfect coherence is assumed.

Thus, e.g., two orthogonal oriented TEM_{01} modes can be combined for a TEM_{01*} donut mode. The polarization of this donut mode is a function of the polarization of the two TEM_{01} modes. If they are for example both antiparallel orthogonal polarized each and orthogonal polarized to each other the resulting donut will show an tangential polarization, i.e. an orbital momentum (AOM), as shown in Fig. 6.39.

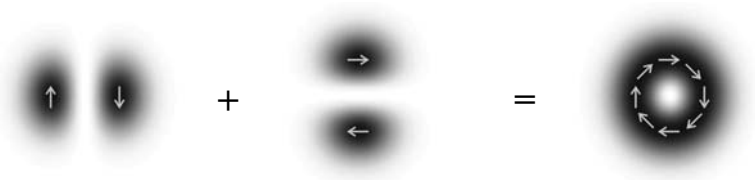

Fig. 6.39. Combining of two orthogonal oriented TEM_{01} modes results in a TEM_{01*} donut mode. If the polarization (arrows in the figure) is as given orthogonal the donut mode is tangentially polarized and it has an orbital momentum (AOM)

If the polarization of the single TEM_{01} modes is antiparallel parallel as shown in Fig. 6.40 the resulting donut mode is radial polarized.

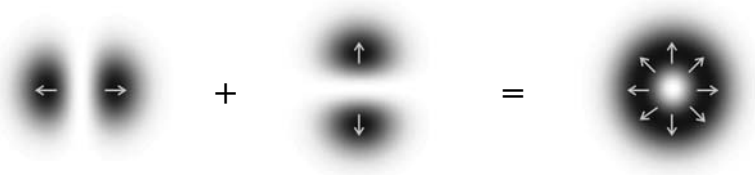

Fig. 6.40. Combining of two orthogonal oriented TEM_{01} modes results in a TEM_{01*} donut mode. If the polarization (arrows in the figure) is as given in the figure parallel the resulting donut mode is radial polarized

Both may have advantages in certain interactions, e.g. in material processing applications. The generation of these two modes out of the same laser is possible with a two branch resonator design generating the two modes, coherently.

The combination of other modes seems to be possible in a similar way. In this case phase plates may be used inside and outside the resonator for producing and combining the beams, coherently.

6.6.6 Beam Radii of Higher Transversal Modes and Power Content

The beam radius of a higher laser mode can be defined differently. As discussed in Sect. 2.7.3 (p. 57) the beam radius is defined using the second intensity moment. For circular modes the beam radius follows from:

$$\text{beam radius} \quad w_r^2 = \frac{2\int r^3 I_{\text{uncal}}(r)\,\mathrm{d}r}{\int r I_{\text{uncal}}(r)\,\mathrm{d}r} \tag{6.54}$$

with the measured, not calibrated and thus relative intensity distribution $I_{\text{uncal}}(r)$ which can be measured with a CCD camera of sufficient dynamic.

For rectangular modes the beam radii may be different in the x and y directions. Therefore they can be determined for symmetric beams separately from:

$$w_x^2 = \frac{4\int x^2 I_{\text{uncal}}(x,y)\,\mathrm{d}x\,\mathrm{d}y}{\iint I_{\text{uncal}}(x,y)\,\mathrm{d}x\,\mathrm{d}y} \tag{6.55}$$

and

$$w_y^2 = \frac{4\int y^2 I_{\text{uncal}}(x,y)\,\mathrm{d}x\,\mathrm{d}y}{\iint I_{\text{uncal}}(x,y)\,\mathrm{d}x\,\mathrm{d}y}. \tag{6.56}$$

These radii are of course larger than the radius of the associated Gaussian mode w_{gauss} as follows:

$$\text{circular modes} \quad w_{r,m,p} = w_{\text{gauss}}\sqrt{(2m+p+1)} \tag{6.57}$$

and

$$\text{rectangular modes} \quad w_{x/y,m} = w_{\text{gauss}}\sqrt{(2m+1)} \tag{6.58}$$

with m and p as the indices of the Laguerre polynomials for circular modes and of the Hermite polynomials for rectangular modes as given above. The values of some circular modes are given in Table 6.7 (p. 410).

The values for the beam width w_{m} of rectangular modes in comparison to the associated Gaussian beam are given in Table 6.8 (p. 411). In this case the values along the two dimensions can be calculated, separately.

The *power content* P_{wr} *and* P_{wm} inside the areas given by the beam radius w_r or the beam width w_m is not the same for the different higher modes. This becomes obvious from Fig. 6.41 (p. 410) in which these radii are shown at the relative intensity $1/\mathrm{e}^2$ for the lowest circular modes in relation to the radial intensity distribution.

Therefore the power contents P_{wr} and P_{wm} relative to the total power of the beam P_{total} is also given in Tables 6.7 (p. 410) and 6.8 (p. 411). For the fundamental mode TEM_{00} the radius defined by the second moment corresponds to the intensity $I = I_{\max}/\mathrm{e}^2$ and the area inside this radius contains 86.5% of the total energy of the beam.

Thus for comparison the beam radii or beam widths $w_{86.5\%}$ for the power content of 86.5% of the higher laser modes are given relative to the radius of the associated Gaussian mode in the Tables 6.7 (p. 410) and 6.8 (p. 411).

Table 6.7. Beam parameters for higher circular Gauss–Laguerre modes

m	p	w_r/w_{gauss}	P_{wr}/P_{total}	$w_{86.5\%}/w_{gauss}$	M^2	$M^2_{86.5\%}$
0	0	1	86.5%	1	1	1
0	1	1.41	90.8%	1.32	2	1.75
0	2	1.73	93.8%	1.56	3	2.44
0	3	2	95.8%	1.76	4	3.10
1	0	1.73	90.8%	1.65	3	2.71
1	1	2	92.2%	1.88	4	3.54
1	2	2.24	93.7%	2.08	5	4.32
1	3	2.45	95.0%	2.25	6	5.06
2	0	2.24	92.3%	2.12	5	4.48
2	1	2.45	93.0%	2.31	6	5.35
2	2	2.65	93.9%	2.48	7	6.17
2	3	2.83	94.9%	2.64	8	6.96
3	0	2.65	93.1%	2.51	7	6.29
3	1	2.83	93.6%	2.68	8	7.17
3	2	3	94.2%	2.83	9	8.02
3	3	3.16	94.9%	2.97	10	8.84
10	0	4.58	95.2%	4.39	21	19.3
0	10	3.32	99.7%	2.71	11	7.34

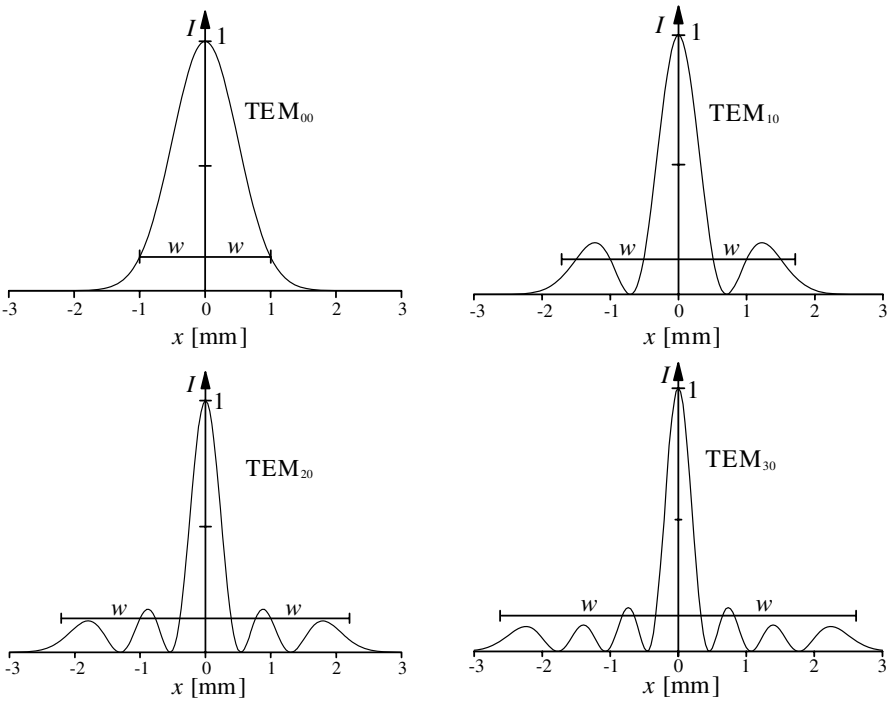

Fig. 6.41. Second-moment beam radii and radial intensity distribution for some circular modes. The intensity was normalized for equal height 1 in all graphs. Compare values of Table 6.5 (p. 401) for absolute intensities

Table 6.8. Beam parameters for higher rectangular Gauss–Hermite modes

m	$w_{\mathrm{m}}/w_{\mathrm{gauss}}$	$P_{\mathrm{wm}}/P_{\mathrm{total}}$	$w_{86.5\%}/w_{\mathrm{gauss}}$	M^2	$M^2_{86.5\%}$
0	1	1	1	1	1
1	1.73	99.3%	1.18	3	1.39
2	2.24	99.8%	1.50	5	2.25
3	2.65	99.7%	1.77	7	3.13
4	3	100.0%	2.01	9	4.02
5	3.32	100.0%	2.22	11	4.92
6	3.61	100.0%	2.41	13	5.83

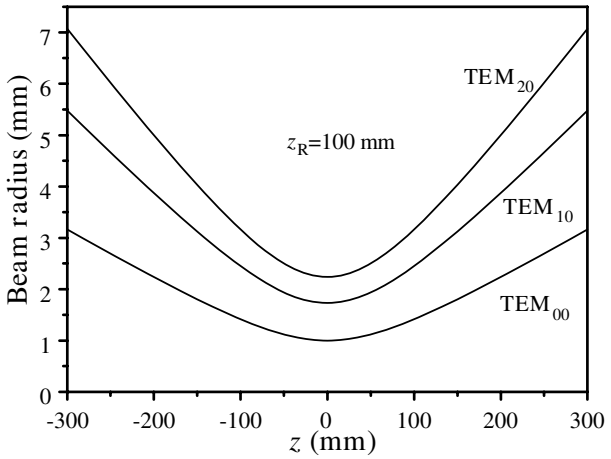

Fig. 6.42. Beam radius defined by second moment for different circular modes around the waist. The Rayleigh length is $z_{\mathrm{R}} = 100\,\mathrm{mm}$ and the wavelength is 500 nm

6.6.7 Beam Divergence of Higher Transversal Modes

Both types of these higher laser modes, circular and rectangular, are also solutions of Maxwell's equation for free space. Using the second moment radii the higher-mode beams can be transferred through optical systems using the matrix formalism.

The simplest procedure can be based on the associated Gaussian mode which has radius w_{gauss} as given relative to the radius or width of the higher mode in Tables 6.7 and 6.8 (see Sect. 6.6.9, p. 412). Both beams which have the same Rayleigh length will propagate "parallel" with a constant ratio of radii as given in Tables 6.7 and 6.8 as shown in the example of Fig. 6.42 (p. 411).

This results in a (far-field) *divergence angle* of the higher circular $\theta_{r,m,p}$ or rectangular $\theta_{x/y,m}$ modes which is larger than the divergence of the associated

Gaussian beam by:

$$\text{circular modes} \quad \theta_{r,m,p} = \theta_{\text{gauss}} \sqrt{(2m + p + 1)} \tag{6.59}$$

and

$$\text{rectangular modes} \quad \theta_{x/y,m} = \theta_{\text{gauss}} \sqrt{(2m + 1)} \tag{6.60}$$

with the mode indices for the Laguerre polynomials m, p and for the Hermite polynomials m as given above. The resulting factors are the same as for the radii or widths and can be taken from Tables 6.7 (p. 410) and 6.8 (p. 411).

6.6.8 Beam Quality of Higher Transversal Modes

Using these values for the beam radius and the divergence angle for the higher laser modes the beam propagation factor M^2 for the higher transversal modes can be given by:

$$\text{circular modes} \quad M^2_{m,p} = 2m + p + 1 \tag{6.61}$$

and

$$\text{rectangular modes} \quad M^2_m = 2m + 1 \tag{6.62}$$

The resulting values are also given in Tables 6.7 (p. 410) and 6.8 (p. 411).

It has to be noticed that this value of the beam propagation factor M^2 is based on the method of second moments and thus the power contents related to this beam propagation factor can be larger for higher modes than the 86.5% which is used for Gaussian beams. Therefore the beam propagation factor $M^2_{86.5\%}$ is also given in Tables 6.7 (p. 410) and 6.8 (p. 411). A further example is given in [6.414].

6.6.9 Propagating Higher Transversal Modes

The propagation of higher transversal modes through an optical system can be calculated using the following steps based on the matrix formalism for the propagation of Gaussian beams:

- determination of the beam radius $w_r(z_i)$ for circular symmetry and the beam widths in x and y directions for rectangular symmetry;
- determination of the beam divergence(s);
- determination of the beam propagation factor M^2;
- determination of the wave front radius $R(z_i)$ from these values;
- determination of the complex beam parameter $q(z_i)$ for the higher-order mode with:

$$\frac{1}{q(z_i)} = \frac{1}{R(z_i)} - \frac{\mathrm{i}\lambda M^2}{\pi n w_r^2(z_i)}; \tag{6.63}$$

- propagation of this beam as described in Sect. 2.4.4 (p. 33) using the ray matrix formalism:
$$q(z) = \frac{aq(z_i) + b}{cq(z_i) + d} \tag{6.64}$$
with the elements a, b, c and d of the propagation matrix;
- determination the searched beam radius $w_r(z)$ and the wave front curvature $R(z)$ of the propagated beam parameter $q(z)$.

The determination of the beam parameters can be based on the theoretical formulas given above or the values given in Tables 6.7 (p. 410) and 6.8 (p. 411) if the transversal mode structure is known. Otherwise it has to be done experimentally as described in Sects. 2.7.3 (p. 57) and 2.7.4 (p. 60).

The resulting beam radius will be at any position M times larger than the radius of the associated Gaussian beam independent of whether M^2 is calculated or measured based on the second-order moment method or on the 86.5% power content of the beam. The beam divergence will also be M times larger than the divergence of the associated Gaussian beam. The Rayleigh length will be the same for all transversal modes for the same wavelength. Other examples are given in [6.415–6.425].

6.6.10 Fundamental Mode Operation: Mode Apertures

Without any restrictions all kinds of mixtures of transversal modes can occur and thus almost any kind of mode pattern can be obtained as the laser output then. Therefore methods for controlling the transversal mode structure have been developed [6.426–6.463]. For photonic applications usually low order modes are preferred in particular, the safe operation of the fundamental mode is of great interest. This TEM_{00}-mode gives the best possible beam quality and thus the highest brightness and best ability to focus the laser radiation.

Because the beam diameter increases with increasing mode number (see Tables 6.7 (p. 410) and 6.8 (p. 411)) mode filtering can be achieved with mode apertures. In the simplest case a suitable mode aperture is applied in the resonator [6.426–6.441], e.g. near to one of the resonator mirrors as shown in Fig. 6.43 (p. 413).

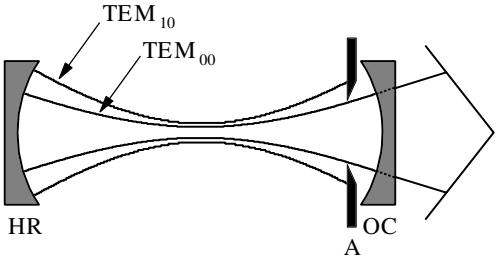

Fig. 6.43. Laser with mode aperture A which causes large losses for transversal modes higher than the fundamental mode as shown for the two lowest circular modes

The losses of the higher-order mode are larger and therefore the low-order mode will be more amplified and become dominant if the laser operates for long enough.

The *diameters of these mode apertures* have to be carefully adapted to the resonator. They have to be large enough not to cause high loss for the lower mode and have to be small enough to depress the higher ones. For pulsed lasers mode aperture radii of 1.5× the beam radius (at $I_{\max}/e^2$) have been successfully tested. For cw lasers even larger values may be used. The best value should be determined experimentally.

But if the higher losses of the higher modes at the mode aperture are compensated by higher amplification in the active material, mode discrimination will not work satisfactorily. This can occur if the inversion at the volume of the lower and active mode is used up whereas the higher and nonoperating mode may occur in other and still inverted areas of the active material. Thus mode selection cannot always be guaranteed by one mode aperture. Even oscillations between different mode patterns are possible. Therefore different concepts have been developed using two or more apertures.

The fundamental mode can almost be guaranteed using two mode apertures in the following scheme [6.426] (see Fig. 6.44).

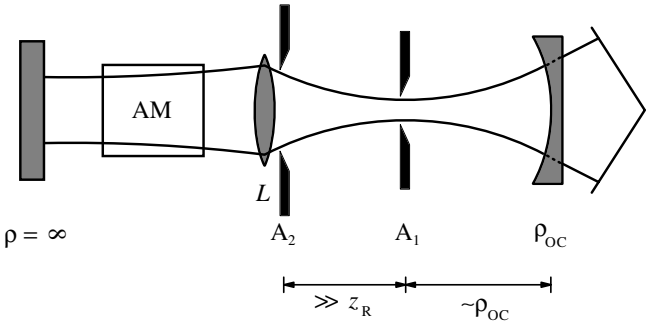

Fig. 6.44. Laser resonator with two apertures for guaranteeing fundamental mode operation

In this resonator one of the apertures A_1 is positioned in the waist position of the fundamental mode inside the cavity which is produced by a curved resonator output mirror. It should be noticed that the distance of this aperture is usually not exactly equal to the curvature ρ_{OC}. The diameter of this aperture is chosen for the desired Gaussian mode of the resonator of, e.g. 1.5 times the beam diameter in pulsed lasers. Then higher order transversal modes with approximately the same diameter at this aperture as the fundamental mode will show much higher divergence. Using a second mode aperture A_2 which is placed sufficiently away from the waist by many Rayleigh lengths z_R the beam divergence can be selected for the fundamental mode. Thus the

combination of these two beams causes very high losses for all higher modes and thus the laser will operate in fundamental mode or it will not work at all [6.426].

Using this concept of the fundamental mode aperture design the potential of different inversion profiles of active materials for fundamental mode emission can be tested. Because of the nonlinear coupling of all laser modes via inversion in the active material this concept allows high efficiencies.

The apertures can be realized partly by the resonator components. For example the smaller aperture A_1 may be obtained from the inversion profile of a laser pumped active material [6.463] positioned in the waist of the beam. In other resonators the aperture A_2 may be obtained by the limited diameter of a solid-state laser rod.

Mode discrimination can also be made outside of the cavity by spatial filtering as shown in Fig. 6.45.

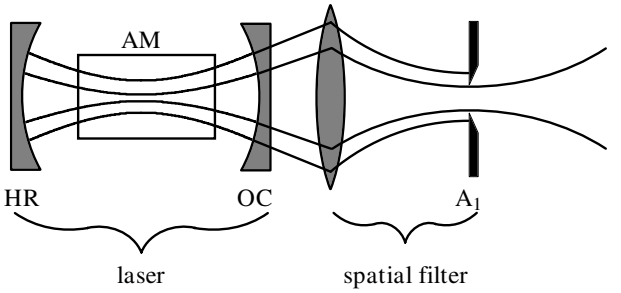

Fig. 6.45. Spatial filter for depressing higher laser modes externally

In this case one small aperture A_1 is placed in the waist of an external lens. The disadvantage of this scheme is poor efficiency. The energy of all higher modes is just wasted. Further the residual intensities from the diffraction of the higher modes may still disturb the application. Thus this scheme should be used, only for beams which already have good beam quality, or in low-power applications.

If the mode diameter is very small (below 100 μm) optical breakdown can occur and the aperture has to be damaged. In the worst case the aperture has to be placed in a vacuum chamber ($<10^{-2}$ bar). Good results can be achieved using small quartz tubes with the required inner diameter as a pin-hole.

Another method for mode discrimination is based on Resonator mirrors with transversally varying reflectivity, such as, for example, Gaussian mirrors [6.442–6.450]. Further waveguides can be used for the suppression of higher-order modes [6.451–6.456]. Phase plates or more complicated diffractive optical elements can be used for mode discrimination [6.457–6.460]. Methods for smoothing the beam have been developed [6.461, 6.462].

6.6.11 Large Mode Volumes: Lenses in the Resonator

For laser wavelengths in the range of 1 µm the beam diameter inside empty laser resonators of 1 m length is roughly in the range of 1 mm (see Sect. 6.6.4, p. 395). High-power lasers demand larger diameters for larger mode volumes in the active material [6.464–6.472]. Thus additional lenses may be applied for increasing the mode diameter. But the larger the mode diameter the more crucial is the alignment of the mirrors and the smaller is the stability range of the high-power lasers. Nevertheless, e.g. a telescope inside the cavity can be used in combination with the fundamental mode aperture design of Fig. 6.44 (p. 414) as shown in Fig. 6.46.

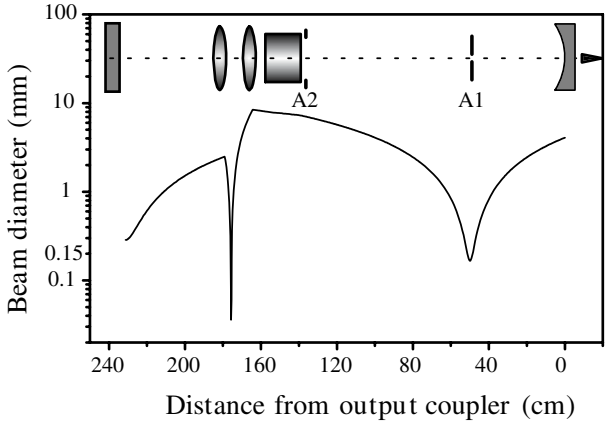

Fig. 6.46. Resonator for high-power solid-state laser with fundamental mode operation and large mode volume

With this type of resonator fundamental mode diameters of 9 mm have been achieved in stable fundamental mode operation [6.426]. The distance between the telescope lenses can be easily adapted for compensation of the thermal lensing of the laser rod. Nevertheless fluctuations of the thermal lens of the active material cause stronger fluctuations in the output power of the laser in cases of larger mode diameters.

6.6.12 Transversal Modes of Lasers with a Phase Conjugating Mirror

An ideal phase conjugating mirror (PCM) used as one of the resonator mirrors, usually the high-reflecting one, will perfectly reflect each incident beam in itself. Thus for an empty resonator with PCM all modes with a curvature equal to the curvature of the output coupler at its place are eigenmodes. In addition double or multiple roundtrip eigenmodes can occur. Therefore an indefinite number of eigenmodes exist without any further restricitions.

With apertures these modes can be discriminated. Thus the fundamental mode aperture design given in the Sect. 6.6.10 (p. 413) is especially useful to provide stable fundamental mode operation in lasers with PCM (see also Sect. 4.5.14 and references there).

For the theoretical description of transversal Gaussian modes an ideal phase conjugating mirror can be described based on the matrix as given in Table 2.6 (p. 37) [6.473]. Real phase conjugating mirrors may decrease the beam diameter of a Gaussian mode. Their nonlinear reflectivity as a function of the intensity can result in lower reflectivity at the wings of the beam compared to the reflectivity at the center.

In particular, for lasers with phase conjugating mirrors [4.630] based on stimulated Brillouin scattering (SBS) [6.474–6.505] it was suggested to calculate the roundtrip in the resonator without the PCM and considering it separately. The calculation of the fundamental mode can be based on the definitions of Fig. 6.47.

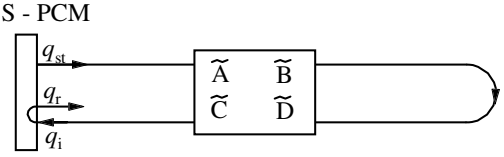

Fig. 6.47. Scheme for calculating transversal fundamental mode of lasers with phase conjugating mirror (PCM) based on stimulated Brillouin scattering (SBS)

The beam propagation matrix $\tilde{M}$ is calculated for the roundtrip through all optical elements towards the other conventional resonator mirror, the reflection there and the way back. Not included is the reflection at the phase conjugating mirror. This is considered with two assumptions about the beam parameter q (see Sect. 2.4.3, p. 30) with $1/q = 1/R - \mathrm{i}\lambda/\pi w^2$ [6.474]:

$$w_r = \beta_{\mathrm{PCM}} w_i \quad \text{with} \quad 0 < \beta_{\mathrm{PCM}} \leq 1 \tag{6.65}$$

and

$$R_r = -R_i \tag{6.66}$$

with the factor β_{PCM} accounting for the different nonlinear reflectivity across the beam.

The eigensolution for the fundamental transversal mode follows from:

$$q_r \stackrel{!}{=} q_{st} \quad \text{and} \quad q_i = \frac{\tilde{A} q_{st} + \tilde{B}}{\tilde{C} q_{st} + \tilde{D}} \tag{6.67}$$

with the matrix elements $\tilde{A}$, $\tilde{B}$, $\tilde{C}$, $\tilde{D}$ of the matrix $\tilde{M}$.

These equations have the solution for the beam radius at the PCM w_{PCM} which is equal to w_{st}, w_r and w_i:

$$\textbf{beam radius at PCM} \quad w_{\mathrm{PCM}} = \sqrt{\frac{\beta_{\mathrm{PCM}} \lambda_{\mathrm{laser}} \tilde{B}}{\pi}} \tag{6.68}$$

and for the curvature of the beam at the PCM moving towards the output coupler:

$$\textbf{curvature at PCM} \quad R_{\mathrm{PCM}} = -\frac{\tilde{B}}{\tilde{A}}. \tag{6.69}$$

With these eigensolutions the further beam propagation of the fundamental mode in the resonator can be done with the matrix formalism.

The phase conjugating SBS mirror can also be considered using its beam propagation matrix M_{PCM} which follows from the combination of the matrix of the ideal PCM with the matrix of a Gaussian aperture resulting in:

$$M_{\mathrm{PCM}} = \begin{pmatrix} 1 & 0 \\ -\dfrac{\mathrm{i}\lambda}{\pi a^2} & -1 \end{pmatrix} \tag{6.70}$$

where the radius of this aperture a is related to the β_{PCM} given above by:

$$a = w_{\mathrm{in}} \sqrt{\frac{\beta_{\mathrm{PCM}}^2}{1 - \beta_{\mathrm{PCM}}^2}}. \tag{6.71}$$

It turns out that β_{PCM} is almost 1 in most practical cases, but the calculation with values slightly smaller than 1 leads to non-diverging useful results.

The optical phase conjugating mirror, e.g. based on SBS, can compensate for phase distortions in resonators as they result from the thermal lensing of solid-state laser rods only if the PCM is located close to the distortion as shown in Fig. 6.48.

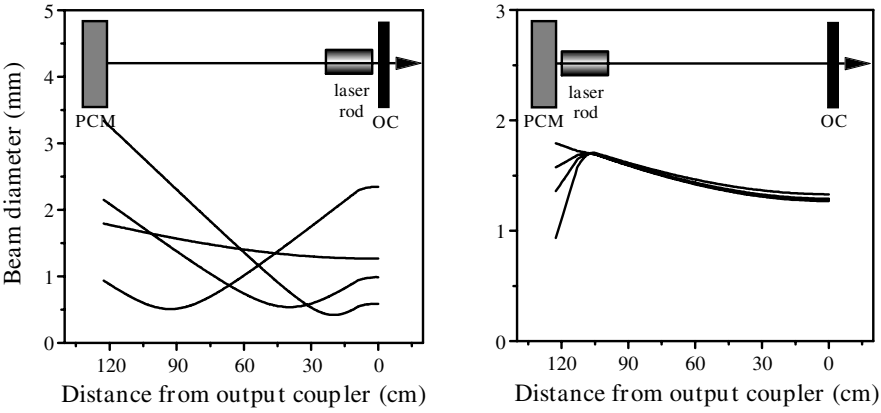

Fig. 6.48. Compensation of phase distortions with optical phase conjugating mirror (PCM) in resonators works only if the PCM is close to the disturbance (see right picture). The beam paths were calculated for an eigenmode

As shown in the right part of this figure the output beam of the laser is almost the same although thermal lensing in the laser rods shows very different values and thus the beam parameters at the PCM are very different.

For using stimulated Brillouin scattering as a self-pumped nonlinear phase conjugating mirror in the resonator a scheme as shown in Fig. 6.49 (p. 419) can be applied [6.475–6.478].

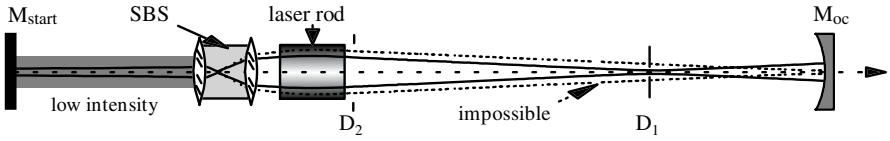

Fig. 6.49. Schematic of a laser resonator with fundamental mode discrimination and phase conjugating SBS mirror for compensation of phase distortions from the laser rod

To provide the start intensity for the nonlinear reflector a start resonator is formed by the mirror M_{start} with low reflectivity R_{start} on the very left of Fig. 6.49 and the output coupler M_{OC} on the right. As soon as the reflectivity of the SBS mirror is larger than R_{start} the laser will operate mostly between the phase conjugating SBS mirror and the output coupler; mirror M_{start} becomes more and more functionless. The mode is determined by the apertures D_1 and D_2.

Using this scheme average output powers of 50 W with diffraction-limited beam quality have been obtained from a single rod flash lamp pumped Nd:YALO laser [6.475].

Besides stimulated scattering processes such as stimulated Brillouin scattering (SBS), also four-wave mixing can be applied for realizing optical phase conjugation in lasers [4.630, 6.506–6.522]. These mirrors can be based on gain gratings in the active material, on absorption gratings or on third-order nonlinearity in transparent crystals. Phase distortions from the active material such as, for example, thermal lensing in solid-state lasers can also be compensated for by actively controlled adaptive mirrors [6.523–6.527].

6.6.13 Misalignment Sensitivity: Stability Ranges

Misalignment of the resonator results from tilting resonator mirrors or by changing the resonator length L. In addition the active material may change the resonator alignment by varying optical parameters. For example, solid-state laser rods can show thermally induced lensing and birefringence as a function of the pumping conditions. These effects may vary and thus may disturb the stable operation of the laser.

The discussion of the misalignment sensitivity and of the stability of any resonator [6.528–6.540] can be based on the equivalent g parameters g_i^* and resonator length L^* which follow from the transfer matrix M_T of the resonator. This transfer matrix is built by calculating a single transfer through the resonator using half of the focusing of the resonator mirrors:

transfer matrix

$$M_\mathrm{T} = \begin{bmatrix} a_\mathrm{T} & b_\mathrm{T} \\ c_\mathrm{T} & d_\mathrm{T} \end{bmatrix} = \begin{bmatrix} 1 & 0 \\ -1/\rho_\mathrm{HR} & 1 \end{bmatrix} \cdot \begin{bmatrix} a_n & b_n \\ c_n & d_n \end{bmatrix} \cdots \begin{bmatrix} a_1 & b_1 \\ c_1 & d_1 \end{bmatrix} \cdot \begin{bmatrix} 1 & 0 \\ -1/\rho_\mathrm{OC} & 1 \end{bmatrix} \tag{6.72}$$

From the elements of this transfer matrix it follows that:

$$\textbf{g*-parameters} \quad g_\mathrm{OC}^* = a_\mathrm{T} \quad \text{and} \quad g_\mathrm{HR}^* = d_\mathrm{T} \tag{6.73}$$

and the equivalent optical resonator length is:

$$\textbf{L*-length} \quad L^* = b_\mathrm{T} \tag{6.74}$$

Using these definitions it follows that:

$$c_\mathrm{T} = \frac{g_\mathrm{OC}^* g_\mathrm{HR}^* - 1}{L^*}. \tag{6.75}$$

The laser resonator is stable as long as:

$$\textbf{stability condition} \quad a_\mathrm{T} b_\mathrm{T} c_\mathrm{T} d_\mathrm{T} < 0 \tag{6.76}$$

with the result of infinite beam diameters at the resonator mirrors as one of these matrix elements is zero (see Table 6.9).

Table 6.9. Beam radii at the two resonator mirrors M_OC and M_HR at the stability limits of the resonator

	w_OC	w_HR
$a_\mathrm{T} = 0$	∞	0
$b_\mathrm{T} = 0$	0	0
$c_\mathrm{T} = 0$	∞	∞
$d_\mathrm{T} = 0$	0	∞

The discussion of the whole stability range of the resonator can be based on the g^* diagram as described above for the g diagram. As an example three solid-state laser resonators with their stability ranges along the lines of operation as a function of the thermal lensing of the active material are shown in Fig. 6.50 (p. 421).

Resonator (a) shows as usual two separated stability ranges, one in the upper right and the other in the lower left part of the diagram. Thus increasing the pump power leads to operation, nonoperation and operation

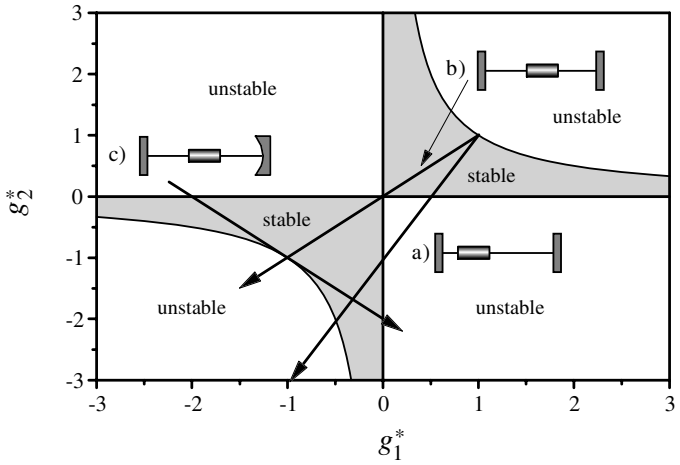

Fig. 6.50. g* diagram with the lines of operation for three resonators as a function of thermal lensing in the laser rod. The arrows indicate increasing pump power and lensing

again. In resonator (b) these two stability ranges are connected at the confocal, (0,0)-point of the diagram and result in one wide stability range. In resonator (c) the two stability ranges are connected at the concentric point with $g^*_{\mathrm{OC}} g^*_{\mathrm{HR}} = 1$ resulting in a wide and uninterrupted stability range. But the misalignment sensitivity of the two last resonators is much different.

Misalignment sensitivity can also be discussed based on the transfer matrix elements. Element $b_{\mathrm{T}} = 0$ results in an imaging of the resonator mirror M_{OC} to M_{HR} and vice versa. Thus the misalignment sensitivity is minimal for this type of resonator.

If the matrix element $c_{\mathrm{T}} = 0$ the misalignment sensitivity is maximal. Figure 6.51 (p. 422) shows at which point of operation inside the stability ranges of the two resonators (b) and (c) this extreme occurs.

Resonator (c) shows the highest misalignment sensitivity in the middle of the stability range and will therefore be difficult to operate. In resonator (b) the maximum of the misalignment sensitivity is at the left side of the stability range. This type of resonator crossing the confocal point should be used if a large stability range and low misalignment sensitivity is demanded.

The detailed discussion of the misalignment sensitivity can be based on the calculation of the resonator including the misalignment vectors for each element:

$$\text{misalignment vector} \quad \begin{pmatrix} x_{\text{element}} \\ \alpha_{\text{element}} \end{pmatrix} \tag{6.77}$$

with the misalignment shift x and the misalignment angle α of the optical element. This vector is multiplied by the resulting beam matrices [M24].

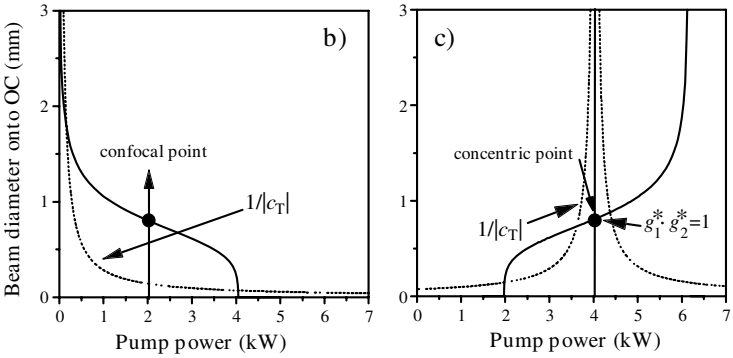

Fig. 6.51. Beam diameter at the output coupler of the resonators (b) and (c) of Fig. 6.50 (p. 421) as a function of the pump power P_{in} of the laser rod inducing thermal lensing. In addition the inverse matrix element $1/c_{\text{T}}$ is shown to describe the maximum misalignment sensitivity

6.6.14 Dynamically Stable Resonators

Resonators designed with their point of operation at the center of the stability range are called dynamically stable resonators [6.541–6.543]. For the analysis the beam radius or diameter is plotted as a function of the pump power, as e.g. shown in Fig. 6.52 (p. 423).

The beam diameter in the rod is in general a symmetric function of the pump power with its axis between the two stability ranges. As can be seen the best choice is the stability range I which has two foci at the two mirrors.

At the center-point the change of the beam radius as a function of e.g. the thermally induced changes of the refractive power of the active material is minimal and thus the fluctuation of the output power can be minimized.

The stability range of the pump power P_{pump} was calculated for dynamically stable resonators of solid-state rod lasers as [6.467, 6.542]:

$$\Delta P_{\text{pump}} = \frac{2\lambda_{\text{laser}}}{C_{\text{material}}} \left(\frac{r_{\text{rod}}}{w_{00,\text{rod}}} \right)^2 \tag{6.78}$$

with the material parameter C_{material}, the wavelength of the laser λ_{laser}, the radius of the laser rod r_{rod} and the radius of the TEM_{00} mode in the rod $w_{00,\text{rod}}$. The parameter C_{material} is of the order of 10^{-5}–$10^{-6}\,\text{m}\,\text{kW}^{-1}$ (see Table 6.10, p. 424).

This would demand small transversal mode diameters in the active material. On the other hand the efficiency and the maximum possible output power demands large mode volumes. Thus values of 1.5–4 have been achieved for the ratio of the rod radius divided by the mode radius.

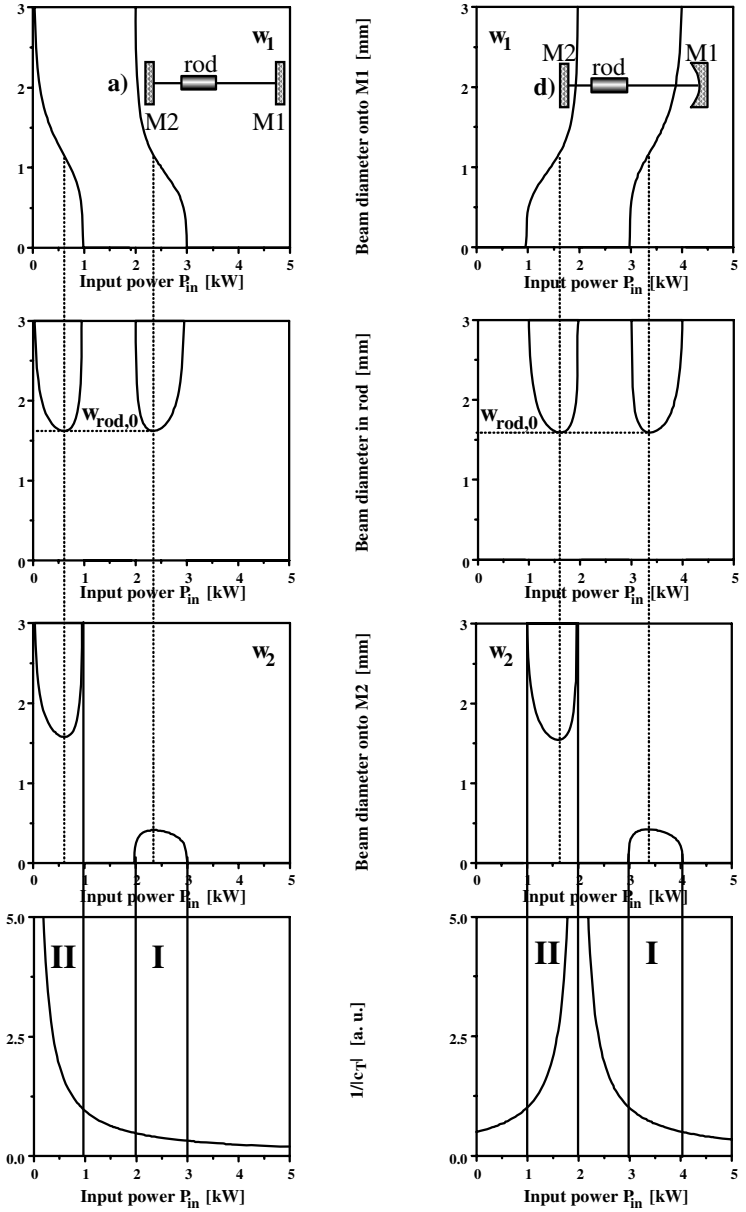

Fig. 6.52. Beam radii at the resonator mirrors M_1 and M_2 and inside the laser rod and misalignment sensitivity as a function of the pump power for two resonators. Left resonator is resonator (a) in Fig. 6.50 (p. 421) and resonator (d) at the right row shows the longer curvature of mirror M_1

Table 6.10. Material constant C_{material} defining the stability range and the TEM_{00}potential for different lasers

Laser	λ_{laser} (nm)	doping (at%)	C_{material} ($\mu\text{m}\,\text{kW}^{-1}$)	$C_{00\text{-pot}}$ ($\%\text{W}\,\mu\text{m}^{-1}$)
Nd:YAG	1064	1.1	16	230–260
Nd:YALO	1080	0.8	36	70–150
Nd:YLF	1047	1.0	−1.3/−4.4	880
	1053	1.0	−0.89/0.72	1280

Finally, the ratio $C_{00\text{-pot}}$ of the efficiency of the laser material η_{material} divided by the material parameter C_{material} is a measure for the TEM_{00} mode potential of the laser material:

$$C_{00\text{-pot}} = \frac{\eta_{\text{material}}}{C_{\text{material}}} \tag{6.79}$$

which is also given for flash lamp pumped Nd lasers in Table 6.10. For diode pumped lasers these values can be higher and, e.g. for Nd:YAG, values of up to $C_{00\text{-pot}} \approx 470\%\text{W}\,\mu\text{m}^{-1}$ were obtained. A similar value to $C_{00-\text{pot}}$ is sometimes used, namely χ_{therm}:

$$\chi_{\text{therm}} = \frac{\eta_{\text{heating}}}{\eta_{\text{excitation}}} \tag{6.80}$$

which is the quotient of the heating efficiency η_{heating} and the excitation efficiency $\eta_{\text{excitation}}$.

6.6.15 Measurement of the Thermally Induced Refractive Power

The refractive index of the active material will modify the transversal and longitudinal modes of the resonator. In high-power systems the refractive index can be a complicated function of the pump conditions and may vary in space and time (see Sect. 6.4).

As an example in rods of solid-state lasers, such as e.g. in the Nd:YAG or Nd:YALO material, thermally induced lensing will occur. The refractive power is dependent on the pump conditions, and the laser operation, e.g. via laser cooling. It may be different for the different polarizations. Thus it should be measured in the operating laser. The measurement of the stability ranges of the laser resonator allows the determination of the refractive power of the active material in an easy way [e.g. 6.544–6.547] as shown in Fig. 6.53 (p. 425).

Therefore the laser output power is measured as a function of the pump power for a given resonator configuration. At the stability limits the output power drops as can be seen in the figure. The thermal lens can be determined from the modeling of these results.

The intensity cross-section pictures from the output coupler taken at the stability limits of the resonator clearly show the natural birefringence of the

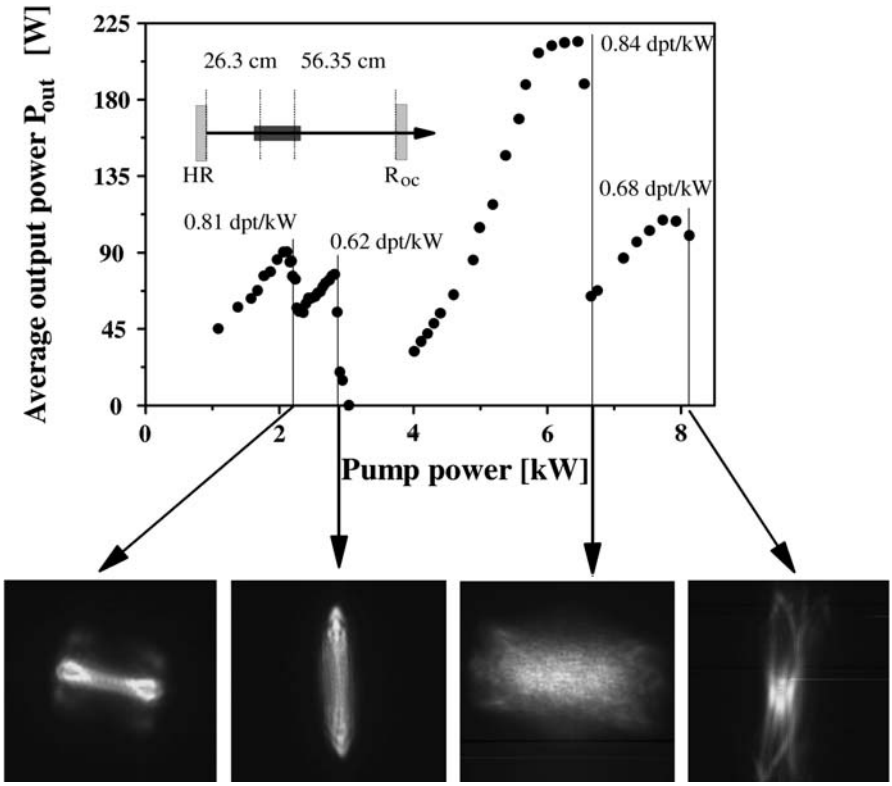

Fig. 6.53. Measurement of the output power as a function of the pump power of a solid-state laser to determine the refractive index profile as a consequence of the heating of the active material from the stability limits of the resonator. The Nd:YALO laser rod had a diameter of 8 mm and a length of 154 mm (1.1 at%). The c axis of the crystal was aligned vertical and the a axis horizontal in the pictures. The connecting line between the two flash lamps was perpendicular to the c axis. The laser light was also vertically polarized in the c direction

material leading to an astigmatic thermal lens. The two refractive powers of 0.81 and 0.84 dpt kW^{-1} in the a axis direction and 0.62 and 0.68 dpt kW^{-1} for the direction of the c axis demonstrate the high accuracy of the method.

6.7 Longitudinal Modes

Longitudinal or axial modes of the resonator are determined by its geometry and the reflectivity of the mirrors. Which of these possible modes are activated in the operating laser depends on the properties of the active material and on possible frequency-selective losses of the resonator.

6.7.1 Mode Spacing

The eigensolution for the standing wave of the electric light field in the laser resonator shows knots at the resonator mirrors (see Fig. 6.54 and compare Fig. 2.3 on page 22).

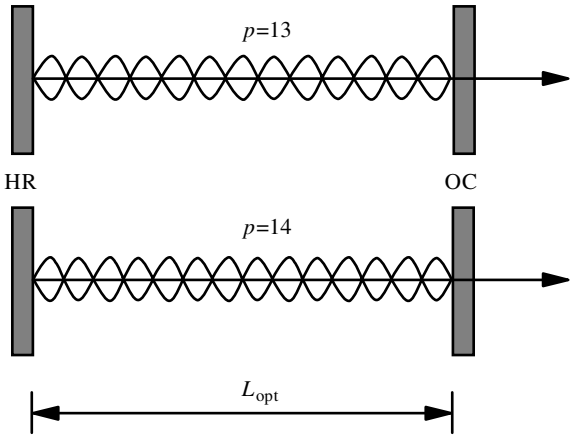

Fig. 6.54. Longitudinal modes of a laser resonator with the optical length L_{opt} which is 6.5 and 7 times as long as the light wavelength

Thus the optical length of the resonator L_{opt} has to be an integer multiple p_{mode} of half the possible wavelengths λ_p of the laser:

$$\lambda_p = \frac{2}{p_{\text{mode}}} L_{\text{opt}} \tag{6.81}$$

with mode number p_{mode}. The optical length of the resonator has to be calculated from the geometrical length $L_{i\text{th part,geom}}$ of all path lengths from one resonator mirror to the other multiplied by the refractive index $n_{i\text{th part}}$ of the components, as e.g. laser rods

$$L_{\text{opt}} = \sum_{\text{all parts}} n_{i\text{th part}} L_{i\text{thpart,geom}}. \tag{6.82}$$

Thus, e.g. a Nd:YAG rod of 0.1 m length increases the optical length of the resonator by 0.082 m ($n = 1.82$).

The related mode frequencies $\nu_{\text{p}} = c_0/\lambda_{\text{p}}$ show a constant difference, the mode spacing frequency $\Delta\nu_{\text{res}}$ of the resonator:

$$\textbf{mode spacing} \quad \Delta\nu_{\text{res}} = \left| \frac{c_0}{\lambda_p} - \frac{c_0}{\lambda_{p\pm1}} \right| = \frac{c_0}{2L_{\text{opt}}} \tag{6.83}$$

and the wavelength spacing is:

$$\Delta\lambda_{\text{res}} = \frac{\lambda^2}{2L_{\text{opt}}} \tag{6.84}$$

with the vacuum speed of light c_0 and the central wavelength λ. The mode numbers are, e.g., for a 1 m empty resonator and a center laser wavelength of 1 µm in the region of 2 million and the mode spacing is 150 MHz in this case. This periodic sequence of axial modes can be generated over the possibly wide spectral range of the amplification bandwidth of the active material as shown in Fig. 6.55.

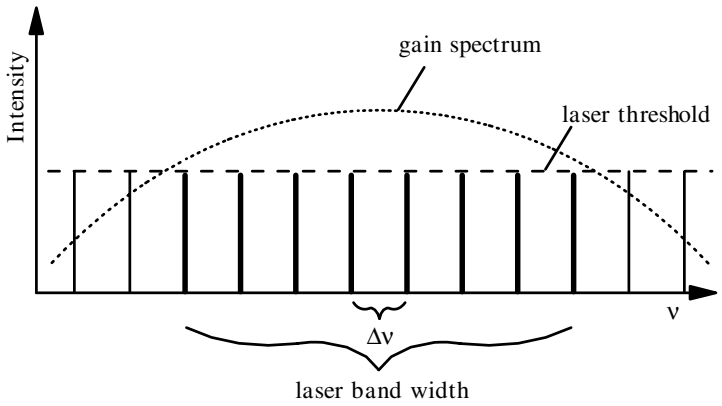

Fig. 6.55. Mode spectrum of a laser with gain spectrum and laser threshold selecting the active longitudinal laser modes

The gain of the active material always shows spectral behavior. The gain region for which the laser operators above threshold defines the potential laser bandwidth and only longitudinal modes inside this laser bandwidth can be obtained.

The mode spacing frequency for a resonator length of 0.5 m is 300 MHz resulting in a wavelength spacing of 0.25 pm at a central laser wavelength of 500 nm. Thus in a 0.5 m resonator of a Nd:YAG laser with a gain bandwidth of 0.5 nm about 2.000 longitudinal modes could oscillate. In practice the number of lasing axial modes is much smaller as a consequence of the nonlinear amplification and of the order of 10–100.

Because of different field distributions resulting in slightly different "optical path lengths" inside the resonator the different transversal modes will have slightly different longitudinal mode frequencies with the changed mode spacing frequency $\Delta\nu_{\mathrm{trans},m,p}$ compared to the TEM_{00}-mode:

$$\Delta\nu^{\mathrm{circ}}_{\mathrm{trans},m,p} = \frac{c_0}{2L_{\mathrm{opt}}}\,\frac{1}{\pi}(2m+p)\,\arccos\left(1-\frac{L_{\mathrm{opt}}}{\rho_{\mathrm{res}}}\right) \tag{6.85}$$

for circular modes and

$$\Delta\nu^{\mathrm{rect}}_{\mathrm{trans},m,p} = \frac{c_0}{2L_{\mathrm{opt}}}\,\frac{1}{\pi}(m+p)\,\arccos\left(1-\frac{L_{\mathrm{opt}}}{\rho_{\mathrm{res}}}\right) \tag{6.86}$$

for rectangular modes both with the transversal mode numbers m, p and the curvature of the resonator mirrors ρ_{res}.

These differences are small compared to the mode spacing $\Delta\nu_{\text{res}}$ as long as the curvature of the resonator mirrors is large compared to the resonator length. In confocal resonators the mode spacing between the transversal modes is equal to or half of the TEM_{00} mode longitudinal mode spacing [M33].

In lasers with a phase conjugating mirror based on stimulated Brillouin scattering the longitudinal mode structure may be much more complicated as at each roundtrip all laser modes will be shifted by the Brillouin frequency shift (see Sect. 4.5.8, p. 222). A rather complicated longitudinal mode pattern was observed and the temporal structure showed strong modulations (see Sect. 6.7.6, p. 435).

6.7.2 Bandwidth of Single Longitudinal Modes

The empty laser resonator represents a Fabry–Perot interferometer (see Sect. 2.9.6 (p. 84) and [6.548]) of optical length L_{opt} formed by two mirrors M_1 and M_2 with reflectivityies R_1 and R_2 with normal incidence as depicted in Fig. 6.56.

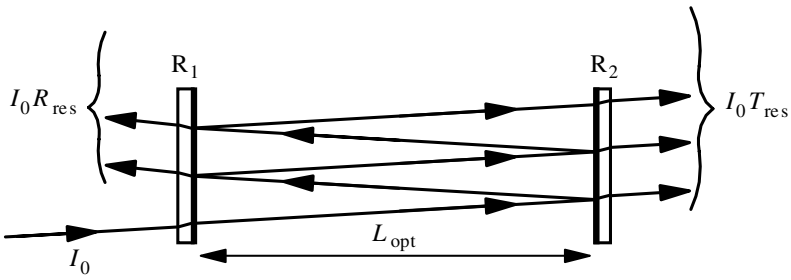

Fig. 6.56. Laser resonator as a Fabry–Perot interferometer with total transmission T_{res}

The transmitted and reflected light is a geometric series of interfering electric field contributions from the partially transmitted and reflected light traveling back and forth in the resonator with decreasing amplitude. Assuming no absorption in the two mirrors the transmittance can be written as:

$$T_{\text{res}} = \frac{(1-R_1)(1-R_2)}{(1-\sqrt{R_1R_2})^2 + 4\sqrt{R_1R_2}\,\sin^2(2\pi L_{\text{opt}}/\lambda)} \tag{6.87}$$

and the reflectance follows from:

$$R_{\text{res}} = \frac{(\sqrt{R_1}-\sqrt{R_2})^2 + 4\sqrt{R_1R_2}\,\sin^2(2\pi L_{\text{opt}}/\lambda)}{(1-\sqrt{R_1R_2})^2 + 4\sqrt{R_1R_2}\,\sin^2(2\pi L_{\text{opt}}/\lambda)} \tag{6.88}$$

with the light wavelength λ.

The maximum transmission $T_{\mathrm{res,max}}$ of this resonator is:

$$T_{\mathrm{res,max}} = \frac{(1-R_1)(1-R_2)}{(1-\sqrt{R_1R_2})^2} \tag{6.89}$$

which is 1 if $R_1 = R_2$. The spectral bandwidth of the resonator follows from:

$$\textbf{frequency bandwidth} \quad \Delta\nu_{\mathrm{FWHM}} = \frac{c}{2\pi L_{\mathrm{opt}}} \left|\ln(\sqrt{R_1R_2})\right| \tag{6.90}$$

or

$$\textbf{wavelength bandwidth} \quad \Delta\lambda_{\mathrm{FWHM}} = \frac{c^2}{2\pi\lambda^2 L_{\mathrm{opt}}} \left|\ln(\sqrt{R_1R_2})\right| \tag{6.91}$$

which is theoretically equal to 0 if both mirror reflectivities were exactly 1 and no other distortions were present. Thus the outcoupling and other losses determine the bandwidth to a large extend. The intensity at the out-coupling resonator mirror inside the resonator ($I_{\mathrm{OC,in}}$) is higher than the out-coupled intensity ($I_{\mathrm{OC,out}}$) by:

$$I_{\mathrm{OC,in}} = I_{\mathrm{OC,in}} \frac{1}{(1-R_{\mathrm{oc}})}. \tag{6.92}$$

The finesse F and the quality Q of the empty laser resonator can be calculated from the frequency bandwidth $\Delta\nu_{\mathrm{FWHM}}$ and the mode spacing $\Delta\nu_{\mathrm{res}}$ by:

$$\textbf{finesse} \quad F_{\mathrm{res}} = \frac{\Delta\nu_{\mathrm{res}}}{\Delta\nu_{\mathrm{FWHM}}} = \frac{\pi}{\left|\ln(\sqrt{R_1R_2})\right|} \tag{6.93}$$

and

$$\textbf{quality} \quad Q_{\mathrm{res}} = \frac{\nu_{\mathrm{laser}}}{\Delta\nu_{\mathrm{FWHM}}} = 2\pi\Delta\nu_{\mathrm{res}}\tau_{\mathrm{res}} \tag{6.94}$$

with the life time τ_{res} of the light in the empty resonator which is also called resonator lifetime:

$$\textbf{resonator life time} \quad \tau_{\mathrm{res}} = \frac{L_{\mathrm{opt}}}{c_0\left|\ln(\sqrt{R_1R_2})\right|} = \frac{1}{2\pi\Delta\nu_{\mathrm{FWHM}}} \tag{6.95}$$

which indicates the 1/e decay of the light or the necessary time to reach the steady state. It is usually in the range of ns.

If the resonator contains the active material and perhaps other elements, additional losses with transmission $V < 1$ and amplification with gain $G > 1$ occur.

The resonator life time $\tau_{\mathrm{res,act}}$ and the bandwidth $\Delta\nu_{\mathrm{FWHM,act}}$ of the resonator with the active material will then be:

$$\tau_{\mathrm{res,act}} = \frac{L_{\mathrm{opt}}}{c_0\left|\ln(GV\sqrt{R_1R_2})\right|} = \frac{1}{2\pi\Delta\nu_{\mathrm{FWHM,act}}} \tag{6.96}$$

and

$$\Delta\nu_{\mathrm{FWHM,act}} = \frac{c}{2\pi L_{\mathrm{opt}}} \left|\ln(GV\sqrt{R_1R_2})\right|. \tag{6.97}$$

Laser resonators with $GV > 1$ will show an increased resonator life time and a narrower spectral bandwidth. Laser threshold is reached at $GV\sqrt{R_1R_2} = 1$ (see Sect. 6.8). In this case the resonator lifetime is infinite and the bandwidth would be zero (for more details see Sect. 6.9). It is then determined by the properties of the active material. $GV\sqrt{R_1R_2} > 1$ can be achieved only for short times, and thus the analysis has to be made time dependent.

6.7.3 Spectral Broadening from the Active Material

The optical transitions of the laser materials have bandwidths from a few tens of pm or MHz up to more than 100 nm or 100 THz as shown in Table 6.11.

Table 6.11. Spectral properties of several laser materials as peak wavelength λ_{peak}, wavelength bandwidth $\Delta\lambda$, frequency bandwidth $\Delta\nu$ and number of longitudinal modes p within this bandwidth in a 10 cm long laser resonator

Active material	Type	Mechanism	λ_{peak} (nm)	$\Delta\lambda$ (nm)	$\Delta\nu$ (GHz)	p
He-Ne	gas	Doppler	632.8	0.018	1.5	1
Ar-ion	gas	Doppler	488	0.03	4.0	4
CO_2 (10 mbar)	gas	Doppler	10 600	0.20	0.06	1
CO_2 (1 bar)	gas	collisions	10 600	14	4.0	4
CO_2 (10 bar)	gas	rotation	10 600	500	150	100
KrF	excimer	vibrations	248	0.5	2500	1700
XeCl	excimer	vibrations	308	0.7	2200	1500
Ruby	solid-state	matrix	694.3	0.5	330	220
Nd:YAG	solid-state	matrix	1064	0.45	120	80
Nd:glass	solid-state	matrix	1054	20	5400	3600
Alexandrite	solid-state	matrix	760	70	36 000	24 000
Ti:Sapphire	solid-state	matrix	790	120	58 000	38 000
Rhodamin 6G	dye	vibrations	580	60	54 000	36 000
GaAs	diode	band	800	2	100	70

The possibly narrow laser lines are broadened by Doppler shifts from the motion of the particles in the gas or by collisions. Molecular laser materials are spectrally broadened by the simultaneous electronic, vibrational and rotational transitions. In solids and liquids the environment of the laser active particles (atoms or molecules) may be different and produce additional broadening. The spectral broadening can be homogeneous or inhomogeneous as a function of the characteristic time constants of the experiment, as described in Sect. 5.2.

Large spectral widths of the active material allow the generation of very short pulses as a consequence of the uncertainty relation, as described in Sect. 2.1.2 (p. 15), down to the fs range as explained in Sect. 6.10.3 (p. 460).

Lasers with very large bandwidths will have very short coherence lengths and are well suited for coherence radar measurements or for optical tomography (OCT, see Sect. 1.5).

With specially designed resonators the spectral bandwidth of the laser radiation can be decreased to much below the bandwidth of the active material. The values are in the range of Hz (see Sect. 6.7.5, p. 432). With relatively simple arrangements using etalons bandwidths of a few 100 MHz can be achieved.

6.7.4 Methods for Decreasing the Spectral Bandwidth of the Laser

The laser bandwidth can be decreased by introducing losses $V(\lambda)$ with a narrow spectral transmission width $\Delta\lambda_{\text{filter}}$ in the laser resonator [6.549–6.601]. Because of the nonlinearity of the amplification process the spectral filtering is much more effective inside the resonator compared to external filtering.

Thus all kinds of spectrally sensitive optical elements such as prisms, gratings, etalons, color filters and dielectric mirrors can be used for decreasing the bandwidth of the laser radiation. As an example a resonator using a grating for decreasing the bandwidth is shown in Fig. 6.57.

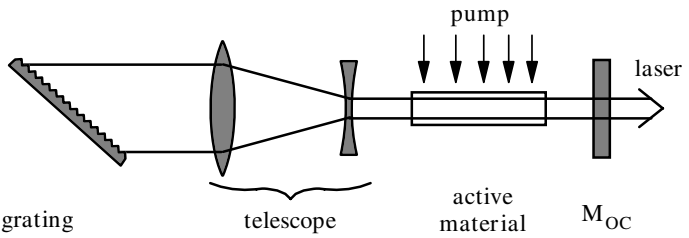

Fig. 6.57. Laser resonator with decreased bandwidth using a grating e.g. in Littrow mounting

In the shown Littrow configuration the grating grooves are blazed for maximum reflectivity at the desired wavelength reflected in the selected m_{Litt}-th grating order under the angle α_{Litt} against the grating plane. This blaze angle follows from:

$$\sin(\alpha_{\text{Litt}}) = m_{\text{Litt}}\lambda_{\text{laser}}/(2\Lambda_{\text{gr}}) \tag{6.98}$$

with the laser wavelength λ_{laser} and the grating period Λ_{gr}, usually measured in lines per mm which are equal to $1/1000\Lambda_{\text{gr}}$. The grating resolution of any grating is given by:

$$\frac{\lambda_{\text{laser}}}{\Delta\lambda_{\text{filter}}} = m_{\text{grating}} \cdot p_{\text{grating}} \tag{6.99}$$

with the resulting filter band width $\Delta\lambda_{\text{filter}}$ from the number of illuminated grating lines p_{grating} and the applied grating order m_{grating}. The larger this number p_{Litt} the higher the resolution (independent of the grating period)! Thus the telescope inside the resonator is used to enlarge the illuminated area at the grating for both increasing the selectivity by using more lines and to avoid damage in the case of pulsed lasers with high peak intensities. The grating can also be realized as a gain grating such as in distributed feedback (DFB) lasers (see, for example, [6.569–6.576] and the references in Sects. 6.7.5 and 6.10.4, p. 472).

An even narrower bandwidth can be reached by combining several spectral filters as shown in Fig. 6.58.

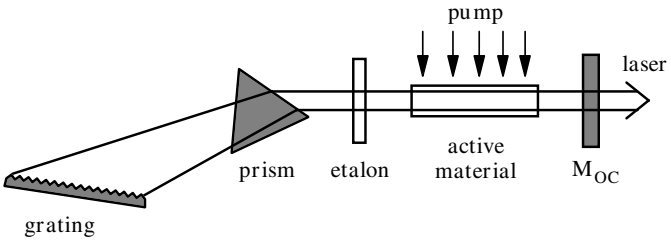

Fig. 6.58. Narrow spectral bandwidth resonator using a combination of prism, grating and etalon

The prism is used to enlarge the number of used grating lines and in addition the grating is applied at grazing incidence. Further spectral filtering is obtained from the etalon. The wavelength of the laser can be tuned [6.577–6.601] by turning the grating. In some cases the fine tuning can be achieved by changing the air pressure inside the etalon and thus tuning the optical path length of the Fabry–Perot interferometer.

For very narrow laser linewidths etalons with a finesse above 30 000 are applied in the resonator. Often the combination of two or more etalons can be necessary to combine an effective free spectral range with a small effective bandwidth of the etalons. In these lasers with very narrow bandwidth care has to be taken over spatial hole burning in the active material as described in the next chapter.

Further care has to be taken so that the high intensities in the resonator (resonance effect) do not damage the spectral filtering devices especially in pulsed lasers.

6.7.5 Single Mode Laser

As shown in Table 6.11 (p. 430) the bandwidth of the active materials is usually much larger than would be necessary for the safe operation of the laser in just one single longitudinal mode. Therefore the filtering inside the resonator has to be very narrow and is usually achieved using etalons [6.602–6.738].

If the laser operates in a single longitudinal mode in a conventional two-mirror resonator the standing light wave can cause *spatial hole burning*. At the intensity maxima of the standing wave the inversion of the active material is used up for the laser process whereas the inversion in the knots would be available. Thus the gain for the neighboring longitudinal modes can be higher than for the active mode and thus the spectral losses can be compensated. Mode hopping can occur and the laser operation is no longer stable.

Therefore several schemes have been developed to avoid spatial hole burning in the active material when the laser is operating in a single longitudinal mode. In Fig. 6.59 a ring resonator suspending spatial hole burning is shown.

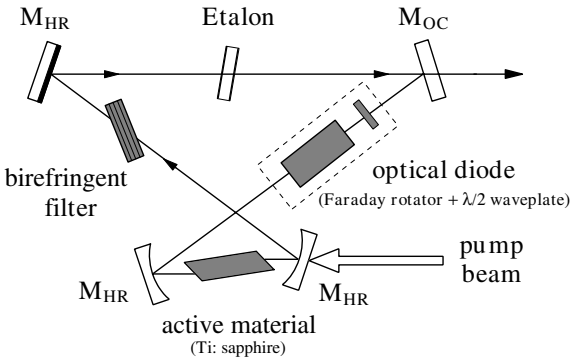

Fig. 6.59. Ring resonator for single longitudinal mode operation. The optical diode ensures the light travels in one direction, only

Spectral filtering is achieved by the etalon, which can consist of several etalons with different free spectral ranges. The optical diode guarantees that the light travels in one direction, only. Thus the laser has no standing wave and spatial hole burning cannot occur.

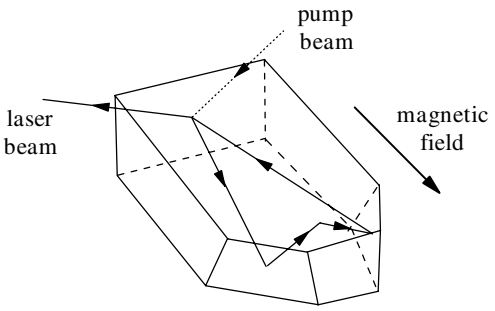

Fig. 6.60. Ring laser longitudinal mono-mode operation based on a polished laser crystal (MISER)

The very elegant and reliable concept of a ring laser emitting a longitudinal mono-mode was based on a compact laser crystal as shown in Fig. 6.60 (p. 433) [6.705–6.711].

This laser crystal is as small as a few mm and thus the mode spacing is quite large. The crystal geometry can act as the mode selector. The laser is pumped by another laser beam, e.g. a diode laser, and operates very stably in the power range of a few 10 mW to 2 W. The circulation direction is determined by the magnetic field, which guarantees the alignment for one direction, only.

Another scheme for avoiding spatial hole burning is shown in Fig. 6.61.

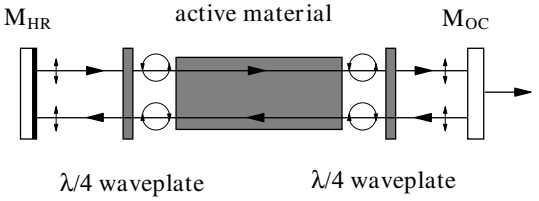

Fig. 6.61. Laser resonator for mono-mode operation using different polarizations for the back and forth traveling waves for avoiding spatial hole burning

In this resonator the back and forth travelling waves have different polarizations. Thus no intensity grating can occur and thus spatial hole burning is avoided. The elements for spectral narrowing of the laser emission are not shown in this picture.

A very simple ring resonator for avoiding spatial hole burning is shown in Fig. 6.62. This resonator is similar to the scheme of Fig. 6.59 (p. 433) but the propagation direction is determined by the high reflecting mirror M_{AUX} in a very simple way. Again the elements for mode selection are not shown.

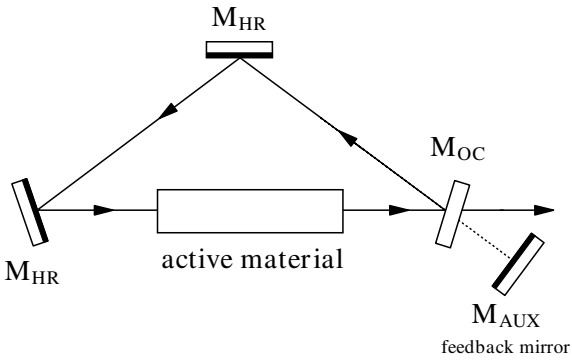

Fig. 6.62. Simple ring resonator for mono-mode operation. The propagation direction is initiated by the mirror M_{AUX}

In all schemes the pump conditions have to be carefully controlled. The laser has to be operated not too far above threshold for achieving good mode selectivity (remember Fig. 6.55, p. 427).

But stable operation in a certain single longitudinal mode with a *fixed wavelength* [6.715–6.738] usually demands further active components (piezo-driven devices) for the compensation of thermally induced changes of the optical lengths and other effects. Atomic transitions from spectral lamps are often used as a reference frequency normal for the laser. Stability in the range of Hz is then possible.

6.7.6 Longitudinal Modes of Resonators with an SBS Mirror

The phase conjugating mirror, like any other nonlinear element in the resonator, can cause complicated longitudinal mode structures [4.630, 6.739–6.765] which may vary in time. For example, the reflectivity zone of these reflectors can move and thus the resonator length is no longer constant.

Phase conjugating mirrors based on stimulated Brillouin scattering (SBS) [6.744–6.754] shift the frequency of the light towards longer wavelengths at each reflection. This shift is equal to the Brillouin frequency of the SBS material which is in the range of 100 MHz to 50 GHz depending on the used material.

Thus in such lasers a whole spectrum of longitudinal modes is generated [e.g. 6.744]. For stable operation the resonator length has to be chosen carefully. Furthermore Q-switching (see Sect. 6.10.2, p. 454) and modulation of the temporal pulse shape is obtained, as the intensity signal shows in Fig. 6.63 (p. 436).

The Brillouin shift was tuned to the roundtrip time of the resonator for resonance enhancement. The diagram of Fig. 6.63 (p. 436) shows the successive shift of the frequencies of the longitudinal modes at each roundtrip as measured time-dependently from the etalon picture.

6.8 Threshold, Gain and Power of Laser Beams

Laser operation demands light amplification based on inversion in the active material. This amplification is described by the gain factor G with the gain coefficient g. It has at least to compensate the losses of the resonator – the laser has to reach its threshold. If the laser operates above threshold then temporal oscillations in the output light may occur, and spiking is observed. Short pulses with high intensities can be produced with nonlinear elements in the resonator. Thus Q switching leads to ns or ps pulses and by mode locking ps or fs pulses can be produced which will be described in Sect. 6.10.

6.8.1 Gain from the Active Material: Parameters

Light amplification is the inverse process of light absorption but with the additional effect of "cloned" photons. Thus the theoretical description is analo-

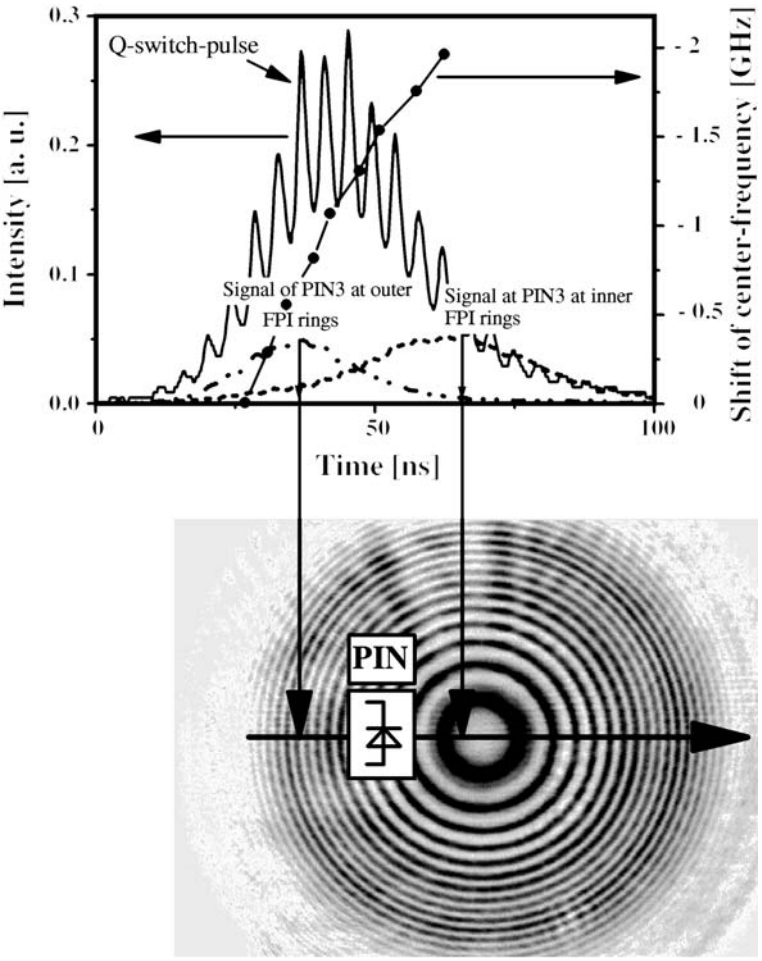

Fig. 6.63. Temporal and spectral properties of a laser with a phase conjugating mirror based on stimulated Brillouin scattering in SF_6 gas showing a Brillouin shift of about 250 MHz [6.784]. The axial mode spectrum is shifted to lower frequencies over the time of the Q-switch pulse

gous to the description of nonlinear absorption as given in Chap. 5 but with gain coefficient which corresponds to negative absorption [6.766–6.784].

The small-signal amplification follows directly from the inversion in the active material. The gain G_{ls} is given by:

small-signal gain $$G_{\mathrm{ls}} = \mathrm{e}^{g_{\mathrm{ls}} L_{\mathrm{mat}}} = \mathrm{e}^{\sigma_{\mathrm{laser}}(N_{\mathrm{upper}} - N_{\mathrm{lower}})L_{\mathrm{mat}}} \qquad (6.100)$$

with the gain coefficient g_{ls}, as given in (6.1), the cross-section of the laser transition σ_{laser} the population densities of the higher N_{upper} and lower N_{lower}

laser level and the length of the active material L_{mat}. This equation holds as long as the intensity is small enough not to disturb the population densities.

If the intensity increases, as required in lasers, the population densities of the different levels numbered with m, $N_{\mathrm{m}} = f(I_{\mathrm{laser}})$ become functions of the intensity I_{laser}, itself, and the inversion $\Delta N = (N_{\mathrm{upper}} - N_{\mathrm{lower}})$ is decreased.

$$\text{high-signal gain} \quad G_{\mathrm{hs}} = \mathrm{e}^{g_{\mathrm{hs}}(I_{\mathrm{laser}})L_{\mathrm{mat}}} = \mathrm{e}^{\sigma_{\mathrm{laser}}[N_{\mathrm{upper}}(I_{\mathrm{laser}}) - N_{\mathrm{lower}}(I_{\mathrm{laser}})]L_{\mathrm{mat}}}. \tag{6.101}$$

In this case the gain may be a complicated function of the pump process described by the pump rate W and the material parameters. It should be calculated as given in Chap. 5, whereas in many cases rate equations may be sufficient for the description.

The discussion of the general behavior is often based on the simple approximation for the gain coefficient g_{hs} similar to (5.4):

$$\textbf{gain coefficient with saturation} \quad g_{\mathrm{hs}} = g_{\mathrm{ls}} \frac{1}{\left(1 + \dfrac{I}{I_{\mathrm{nl}}}\right)^{h}} \tag{6.102}$$

with the nonlinear intensity I_{nl}, frequently called the saturation intensity. The exponent h is chosen to be 1.0 for homogeneously broadened lasers and 0.5 for inhomogeneously broadened lasers. This saturation intensity I_{nl} for the stimulated emission follows from the product of the cross-section σ_{laser} and the life time of the upper laser level τ_{upper} and measured in photon numbers as $\mathit{Ł}_{\mathrm{nl}}$ by:

$$I_{\mathrm{nl}} = \frac{hc_0/\lambda_{\mathrm{laser}}}{F_{\mathrm{lev}}\sigma_{\mathrm{laser}}\tau_{\mathrm{upper}}} \qquad \mathit{Ł}_{\mathrm{nl}} = I_{\mathrm{nl}}\frac{\lambda_{\mathrm{laser}}}{hc_0} = \frac{1}{F_{\mathrm{lev}}\sigma_{\mathrm{laser}}\tau_{\mathrm{upper}}} \tag{6.103}$$

with Planck's constant h and the velocity of light c_0. The factor F_{lev} is equal $F_{\mathrm{lev,3level}} = 2$ for three-level systems and $F_{\mathrm{lev,4level}} = 1$ for four-level systems of the active material. For a more detailed discussion see Sect. 5.3.6 (p. 277).

Typical emission cross-sections σ_{laser} of laser materials and the life times of the upper laser level τ_{upper} for the most prominent laser wavelengths λ_{laser} of these materials are given in Table 6.12 (p. 438). Further values can be found in [6.785–6.789].

The lifetime of the upper laser level is identical to the fluorescence lifetime of the laser material if no stimulated emission occurs, which will otherwise shorten it.

Using the concentration of laser atoms, ions or molecules as an order of magnitude for the inversion population density the maximum gain can be estimated. Solid-state laser can be doped by some atom% which is in the range of $10^{19}\,\mathrm{cm}^{-3}$ and thus the gain coefficient will be in the range of 0.01–$0.1\,\mathrm{cm}^{-1}$ and the maximum stored energy can reach $\mathrm{J\,cm}^{-3}$. In dye lasers the gain coefficient can reach values above $1\,\mathrm{cm}^{-1}$.

Table 6.12. Emission cross-sections σ_{laser}, and lifetimes of the upper laser level at room temperature τ_{upper} for the most prominent laser wavelengths λ_{laser} of some materials

Material	λ_{laser} (nm)	σ_{laser} (cm^2)	τ_{upper} (ns)
He-Ne	632.8	$3 \cdot 10^{-13}$	15 ± 5
Ar-ion	488.0	$2.5 \cdot 10^{-12}$	9
CO_2	10,600.0	$1 \cdot 10^{-16}$	10 000
KrF	248.0	$3 \cdot 10^{-16}$	5
XeCl	308.0	$3 \cdot 10^{-16}$	10
Ruby	694.3	$2.5 \cdot 10^{-20}$	3000
Nd:YAG	1064.1	$3.2 \cdot 10^{-19}$	230 000
Nd:YALO	1079.5	$2 \cdot 10^{-19}$	100 000
Nd:YLF	1047.0	$1.8 \cdot 10^{-19}$	480 000
Nd:YVO_4	1064.1	$2.5 \cdot 10^{-19}$	90 000
Nd:$GdVO_4$	1063	$7.6 \cdot 10^{-19}$	100 000
Nd:KGW	1067.0	$3.3 \cdot 10^{-19}$	120 000
Nd:glass	1054.0	$4 \cdot 10^{-20}$	300 000
Ho:Cr:Tm:YAG	2097	$5 \cdot 10^{-19}$	$3.6–8.5 \cdot 10^6$
Er:YAG	2940	$3 \cdot 10^{-20}$	100 000
Alexandrite	e.g. 760.0	$5 \cdot 10^{-20}$	260 000
Ti:Sapphire	e.g. 800.0	$3 \cdot 10^{-19}$	3200
Cr:LiSAF	846	$4.8 \cdot 10^{-20}$	67 000
Cr:LiCAF	763	$1.3 \cdot 10^{-20}$	170 000
Rhodamin 6G	e.g. 580.0	$4 \cdot 10^{-16}$	5
GaAs	e.g. 800.0	$1 \cdot 10^{-16}$	4

6.8.2 Laser Threshold

As mentioned above the laser is operating if the gain from the active material compensates all losses [6.790–6.795] in the resonator which for linear resonators results in:

$$\textbf{laser condition} \quad GV\sqrt{R_1 R_2} = 1 \tag{6.104}$$

with the gain in the active material G, the influence of all losses such as e.g. absorption, scattering, and diffraction in one pass through the resonator V, and the reflectivities of the two mirrors R_1 and R_2. Sometimes the average reflectivity of the resonator mirrors $R = \sqrt{R_1 R_2}$ is used and than the laser condition reads a $GVR = 1$.

Because the gain of the active material is determined by the balance of the pumping on one hand and its decrease by the back and forth traveling laser light inside the resonator $I_{\text{laser,int}}$ on the other, from the laser condition of (6.104) the laser intensity for a given resonator can be calculated as follows.

By applying the simple approximation of (6.102) the gain G is given by:

$$\textbf{gain} \quad G(I_{\text{laser,int}}) = \mathrm{e}^{g_{\text{hs}} L_{\text{mat}}} = \exp\left(\frac{g_{\text{ls}} L_{\text{mat}}}{(1 + I_{\text{laser,int}}/I_{\text{nl}})^h}\right). \tag{6.105}$$

This value has to fulfill (6.104) and thus the laser intensity for a resonator with V, R_1 and R_2 is given by:

internal laser intensity

$$I_{\text{laser,int}} = \frac{I_{\text{nl}}}{2}\left\{\left(\frac{g_{\text{ls}} L_{\text{mat}}}{\left|\ln(V\sqrt{R_1 R_2})\right|}\right)^{1/h_L} - 1\right\} \tag{6.106}$$

considering the doubling of the intensity inside the active material from the back and forth traveling of the light in the resonator and h_L has to be chosen to be 1 or 0.5 for homogeneous or inhomogeneous broadening of the laser transition.

The *laser threshold condition* follows from this equation. This is determined by the minimal value of the small-signal gain coefficient $g_{\text{threshold}}$ that satisfies (6.104) for a given resonator:

threshold gain coefficient

$$g_{\text{threshold}} = \frac{1}{L_{\text{mat}}}\left|\ln(V\sqrt{R_1 R_2})\right| \tag{6.107}$$

and thus the necessary inversion $\Delta N_{\text{threshold}}$ follows from:

threshold inversion

$$\Delta N_{\text{threshold}} = \frac{g_{\text{threshold}}}{\sigma_{\text{laser}}} = \frac{\left|\ln(V\sqrt{R_1 R_2})\right|}{L_{\text{mat}}\sigma_{\text{laser}}} \tag{6.108}$$

which determines the minimal pump rate $W_{\text{pump,threshold}}$ to reach laser operation for a given resonator. The pump rate is the density of the inverted laser particles per unit time, which will be discussed in the next chapter in more detail. At threshold the intensity of the laser is still zero. Thus in practice the threshold is determined by measuring the laser intensity as a function of the pump rate W_{pump} as sketched in Fig. 6.64.

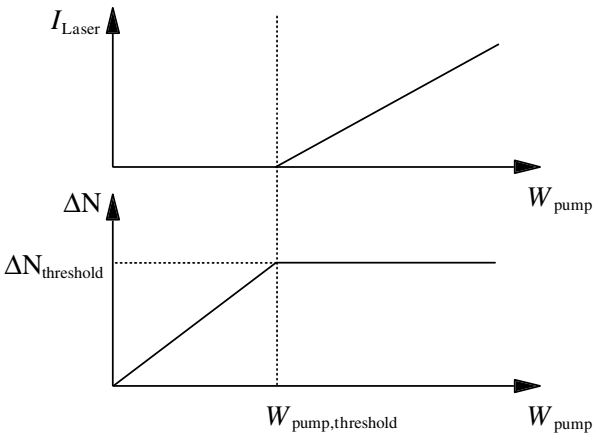

Fig. 6.64. Laser intensity and inversion as a function of the pump rate W_{pump} around the laser threshold

As an example a laser resonator with $V = 0.95$, $R_1 = 1$, $R_2 = 0.8$ and a length of the active material of $L = 0.1\,\mathrm{m}$ demands a minimal gain coefficient of $g_{\mathrm{threshold}} = 0.016\,\mathrm{cm}^{-1}$. The threshold inversion population density for Nd:YAG would be $\Delta N_{\mathrm{threshold}} = 4.1 \cdot 10^{16}\,\mathrm{cm}^{-3}$.

The minimal pump rate for reaching threshold, which is the *threshold pump rate* $W_{\mathrm{pump,threshold}}$ is a very useful measure for characterizing lasers experimentally. It is easy to measure and allows the characterization of how much the laser is pumped above threshold. Thus the output parameters can be related to this value. On the other hand the threshold pump power can be calculated via rate equations to optimize the parameters of the active material as will be shown in the next chapter.

6.8.3 Laser Intensity and Power

The laser with its linear and nonlinear interactions of light with matter, especially at the resonator mirrors and in the active material, can be described on different levels as discussed in Chap. 5. A density matrix formalism or wave equations may be necessary if detailed analysis of the temporal longitudinal mode structure or the photon statistics are important.

For the much simpler modeling of the output power characteristics and the temporal development of the laser pulses in the spiking or Q switched operation rate equations are usually sufficient [e.g. 6.796–6.803].

The photon transport equation for the intensity $\mathit{Ł} = I/h\nu_{\mathrm{Laser}}$ measured in photons/cm^{2}s has to include all losses and the stimulated and spontaneous emission of the light in the active material, and is given by:

$$\frac{\partial \mathit{Ł}}{\partial z} + \frac{1}{c}\frac{\partial \mathit{Ł}}{\partial t} = [\sigma_{\mathrm{laser}}\Delta N(\mathit{Ł}) - a]\mathit{Ł} \tag{6.109}$$

with the cross-section of the laser transition σ_{laser}, the population inversion density ΔN and possible losses in the active material described with the (absorption) coefficient a. This equation can easily be integrated, numerically. The spontaneously emitted photons are neglected in this expression because they add very low intensity in the direction of the laser light, but some starting intensity is necessary and has to be considered numerically.

To model the whole resonator, in addition the losses at the resonator mirrors and at other elements and the optical paths outside the active material also have to be taken into account during the roundtrip. The population densities as a function of the pump rate can be calculated as described in Sect. 5.3.

In addition the polarization of the light and the wavelength dependence of the intensity can be taken into account by solving this type of equation parallel for several discrete polarization directions or several discrete wavelengths (see e.g. Sect. 6.9.3.3, p. 448). The coupling will be achieved via the common inversion density in the active material (see next section).

For simple three or four level laser schemes the inversion population density can be calculated using the notation of Fig. 6.65 (p. 441).

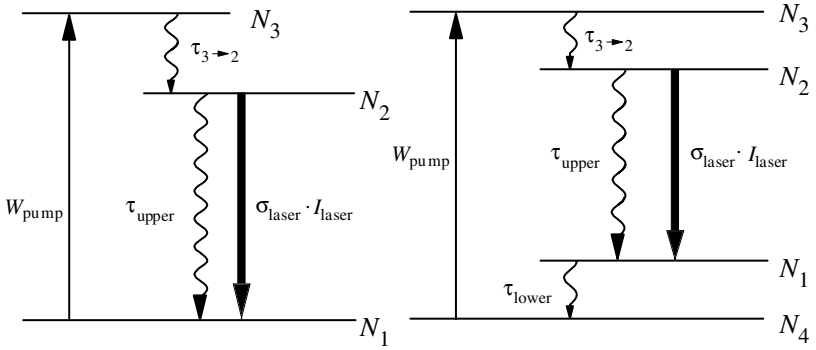

Fig. 6.65. Transitions in three- (left) and four-(right) level schemes of lasers

If the decay of level 3 in the three-level system and of levels 3 and 1 in the four-level system is fast compared to all other transitions the population density of these levels can be neglected. Under this assumption the differential equation for the inversion population densities ΔN are given by:

Three-level system:

$$\frac{\partial \Delta N}{\partial t} = \left(W_{\mathrm{pump}} - \frac{1}{\tau_{\mathrm{upper}}} \right) N_0 - \left(W_{\mathrm{pump}} + \frac{1}{\tau_{\mathrm{upper}}} + 2\sigma \mathcal{I}_{\mathrm{laser}} \right) \Delta N \tag{6.110}$$

and

Four-level system:

$$\frac{\partial \Delta N}{\partial t} = W_{\mathrm{pump}} N_0 - \left(W_{\mathrm{pump}} + \frac{1}{\tau_{\mathrm{upper}}} + \sigma_{\mathrm{laser}} \mathcal{I}_{\mathrm{laser}} \right) \Delta N \tag{6.111}$$

with the pump rate W_{pump} resulting, e.g. from the product of the pump cross-section σ_{pump} and the pump intensity I_{pump} if light of the pump wavelength is applied for pumping. N_0 describes the total population density as the sum over all population densities of all levels. These equations usually have to be solved numerically in combination with the photon transport equation, considering the losses at the mirrors and other components.

Analytical solutions are possible under steady state conditions. The cw solutions with $\partial \Delta N / \partial t = 0$ for these equations are:

Three-level system

$$\Delta N = N_0 \frac{\tau_{\mathrm{upper}} W_{\mathrm{pump}} - 1}{1 + \tau_{\mathrm{upper}} W_{\mathrm{pump}} + 2\sigma_{\mathrm{laser}} \tau_{\mathrm{upper}} \mathcal{I}_{\mathrm{laser}}} \tag{6.112}$$

indicating that $\tau_{\mathrm{upper}} W_{\mathrm{pump}}$ has to be larger 1 for inversion in the three-level scheme. For the four-level scheme:

Four-level system

$$\Delta N = N_0 \frac{\tau_{\text{upper}} W_{\text{pump}}}{1 + \tau_{\text{upper}} W_{\text{pump}} + \sigma_{\text{laser}} \tau_{\text{upper}} \text{Ł}_{\text{laser}}} \tag{6.113}$$

where all pumping leads to inversion. These steady state equations are useful for cw operation and lasers with pulse durations much larger than the lifetimes of all excited states of the laser material.

These equations have to be interpreted with $\text{Ł}_{\text{laser}} = 0$ for pump rates W_{pump} smaller than the threshold value $W_{\text{pump}} \leq W_{\text{pump,threshold}}$ and for $W_{\text{pump}} > W_{\text{pump,threshold}}$ as follows:

Below and at threshold

$$\text{Three-level system} \quad \Delta N (\leq \Delta N_{\text{threshold}}) = N_0 \frac{\tau_{\text{upper}} W_{\text{pump}} - 1}{1 + \tau_{\text{upper}} W_{\text{pump}}} \tag{6.114}$$

and

$$\text{Four-level system} \quad \Delta N (\leq \Delta N_{\text{threshold}}) = N_0 \frac{\tau_{\text{upper}} W_{\text{pump}}}{1 + \tau_{\text{upper}} W_{\text{pump}}} \tag{6.115}$$

From these equations the threshold pump rate $W_{\text{pump,threshold}}$ can be calculated for steady state operation.

Pump rate at threshold:

$$\text{Three-level system} \quad W_{\text{pump,threshold}} = \frac{1}{\tau_{\text{upper}}} \frac{N_0 + \Delta N_{\text{threshold}}}{N_0 - \Delta N_{\text{threshold}}} \tag{6.116}$$

and

$$\text{Four-level system} \quad W_{\text{pump,threshold}} = \frac{1}{\tau_{\text{upper}}} \frac{\Delta N_{\text{threshold}}}{N_0 - \Delta N_{\text{threshold}}} \tag{6.117}$$

for which the threshold population density $\Delta N_{\text{threshold}}$ has to be calculated from the threshold condition of (6.108).

For pump rates above the threshold value the internal laser intensity can be calculated from the following relations for the cw solution given above.

Above threshold:

Three-level system (6.118)

$$\text{Ł}_{\text{laser}} = \frac{1}{2\sigma_{\text{laser}} \Delta N} \left[\left(W_{\text{pump}} - \frac{1}{\tau_{\text{upper}}} \right) N_0 - \left(W_{\text{pump}} + \frac{1}{\tau_{\text{upper}}} \right) \Delta N \right]$$

and

Four-level system

$$\text{Ł}_{\text{laser}} = \frac{1}{\sigma_{\text{laser}} \Delta N} \left[W_{\text{pump}} N_0 - \left(W_{\text{pump}} + \frac{1}{\tau_{\text{upper}}} \right) \Delta N \right]. \tag{6.119}$$

Under the assumed steady state conditions the population inversion density above threshold stays constant at:

above threshold

$$\Delta N_{3/4\text{-level}}(W_{\text{pump}} > W_{\text{pump,threshold}}) = \Delta N_{\text{threshold}} \tag{6.120}$$

and thus the laser intensity can be calculated as a function of the pump rate using (6.108) for determining $\Delta N_{\text{threshold}}$:

Internal laser intensity above threshold:

Three-level system

$$I_{\text{laser}} = \frac{1}{\sigma_{\text{laser}}\tau_{\text{upper}}}\left(\frac{W_{\text{pump}} - W_{\text{pump,threshold}}}{W_{\text{pump,threshold}} - \dfrac{1}{\tau_{\text{upper}}}}\right) \tag{6.121}$$

and

Four-level system

$$I_{\text{laser}} = \frac{1}{\sigma_{\text{laser}}\tau_{\text{upper}}}\left(\frac{W_{\text{pump}} - W_{\text{pump,threshold}}}{W_{\text{pump,threshold}}}\right) \tag{6.122}$$

If the threshold pump rate and the threshold inversion are substituted in these formulas and the total loss factor $V = V_{\text{resonator}} \cdot \exp(-aL_{\text{mat}})$ is applied the following expressions for the internal laser intensity are obtained:

Three-level system

$$I_{\text{laser}} = \frac{N_0\sigma_{\text{laser}}L_{\text{mat}}(\tau_{\text{upper}}W_{\text{pump}} - 1) - (\tau_{\text{upper}}W_{\text{pump}} + 1)|\ln(V\sqrt{R_{\text{HR}}R_{\text{OC}}})}{2\sigma_{\text{laser}}\tau_{\text{upper}}|\ln(V\sqrt{R_{\text{HR}}R_{\text{OC}}})|} \tag{6.123}$$

and

Four-level system

$$I_{\text{laser}} = \frac{N_0\sigma_{\text{laser}}L_{\text{mat}}\tau_{\text{upper}}W_{\text{pump}} - (\tau_{\text{upper}}W_{\text{pump}} + 1)|\ln(V\sqrt{R_{\text{HR}}R_{\text{OC}}})|}{\sigma_{\text{laser}}\tau_{\text{upper}}|\ln(V\sqrt{R_{\text{HR}}R_{\text{OC}}})|} \tag{6.124}$$

If as a further approximation $I(L) = \text{const} = I_{\text{av}}$ is applied, assuming that the light beams in the z and $-z$ directions superimpose to an almost equal intensity distribution $2I_{\text{laser}}$ along z, from these intensities in the active material the output power $P_{\text{laser,output}}$ can be calculated. If the reflectivity of the output coupler is close to 1 the intensity in the laser material will be twice as high as the share which is propagating towards the output coupler. For lower reflectivity of the two mirrors the geometrical average may be a suitable approximation and therefore the output power is given by:

$$P_{\text{laser,output}} = I_{\text{laser}}\frac{hc_0}{\lambda_{\text{Laser}}}A_{\text{mode}}(1 - R_{\text{OC}})\frac{V\sqrt{R_{\text{HR}}R_{\text{OC}}}}{2}. \tag{6.125}$$

Using these equations the output power can be plotted as a function of the reflectivity of the output coupler as shown in Fig. 6.66.

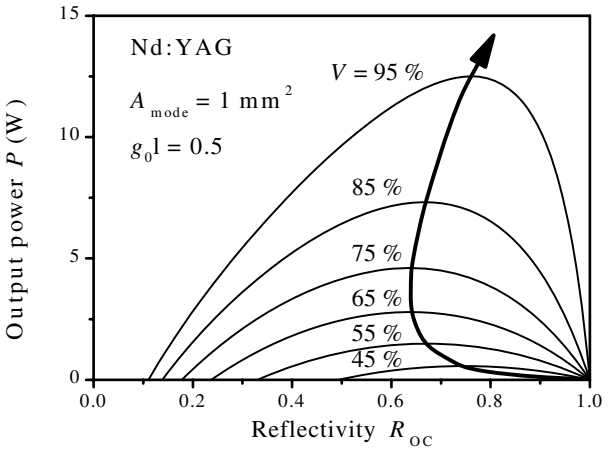

Fig. 6.66. Calculated laser output power of a Nd:YAG laser as a function of the reflectivity of the output coupler R_{OC} for different loss factors V with a pump rate resulting in $g_{\mathrm{ls}}L_{\mathrm{mat}} = 0.5$. The maxima of these curves (*arrow*) indicate the optimal reflectivity of the output coupler

As can be seen from this figure for each loss factor exists an optimal reflectivity of the output coupler which leads to the maximum output power of the laser. To avoid damage it should be noticed that the internal intensity is higher by a factor of $1/(1 - R_{\mathrm{OC}})$ than the out-coupled intensity. In cw lasers this factor can reach values of more than 100. In any case, especially for high power laser systems, the possibilities of damage should be excluded by calculating the intensities in the resonator.

For more precise modeling of the laser the calculations should be executed numerically without the used rough approximations. Nevertheless, based on this fundamental context the detailed analysis can also be carried out experimentally.

6.9 Spectral Linewidth and Position of Laser Emission

The spectral properties of the laser radiation are in general a function of the spectral resonator parameters such as the spectral reflectivity of the mirrors and the spectral curve of the spontaneous and stimulated emission of the active material (see also Sects. 6.7 especially 6.7.2, 6.7.4 and 6.7.5 and references there). In pulsed systems this will change as a function of time. Thus both the central or peak wavelength as well as the bandwidth of the laser radiation may vary in time.

Spectral and spatial hole burning may influence the final spectra and thus homogeneous or inhomogeneous broadening of the active material may be important for understanding. Thus the longitudinal laser modes may oscillate almost independently or may be coupled via the depopulation of the inversion in the active material.

A *homogeneously broadened laser transition* will show a Lorentzian shape gain profile $g_{\mathrm{ls}}(\nu_{\mathrm{laser}})$ which is proportional to the spectral curve of the emission cross-section $\sigma_{\mathrm{laser}}(\nu_{\mathrm{laser}})$:

spectral small signal gain

$$g_{\mathrm{ls}}(\nu) = \Delta N \sigma(\nu) = \Delta N \frac{\left(\frac{\Delta\nu_{\mathrm{FWHM}}}{2}\right)^2}{\left(\frac{\Delta\nu_{\mathrm{FWHM}}}{2}\right)^2 + (\nu - \nu_{\mathrm{max}})^2} \sigma_{\mathrm{max}}. \tag{6.126}$$

Potentially laser emission can occur over the whole part of the spectrum with low signal gain above threshold as discussed in Fig. 6.55 (p. 427), but because of the mode competition for inversion population density the laser will operate in the cw or long-pulse regime in a narrower range around the frequency of the gain maximum, only.

6.9.1 Minimal Spectral Bandwidth

The linewidth of a cw (continuous wave) laser can be very small as a result of the almost infinite lifetime of the radiation. The lower limit of the spectral bandwidth Δ_{min} as a result of the photon statistics was given as derived by Schalow and Townes:

minimal spectral bandwidth

$$\Delta\nu_{\mathrm{min}} = \frac{c_0^2 h \nu_{\mathrm{laser}} \sigma_{\mathrm{max}} N_{\mathrm{upper}} L_{\mathrm{mat}} |\ln(V\sqrt{R_1 R_2})|}{4\pi P_{\mathrm{out}} L_{\mathrm{res,opt}}^2} \tag{6.127}$$

with the velocity of light c_0, the population density of the upper laser level N_{upper}, the length of the active material L_{mat}, the optical length of the resonator $L_{\mathrm{res,opt}}$, the losses per transit V, the reflectivities of the two resonator mirrors $R_{1/2}$ and the output power of the laser P_{out}. Using this formula spectral bandwidths of less than 1 Hz down to 10^{-4} Hz can be calculated. Realistically all values below 1 Hz are very difficult to reach and the best values are in the mHz range [6.804, 6.673]. Several experimental precautions have to be realized for very narrow spectral laser emission (see Sect. 6.7.5, p. 432).

6.9.2 Frequency Pulling

As a consequence of the spectral bell shape of the gain profile as shown in Fig. 6.67 (p. 446) a slight frequency shift of the resonator modes occurs.

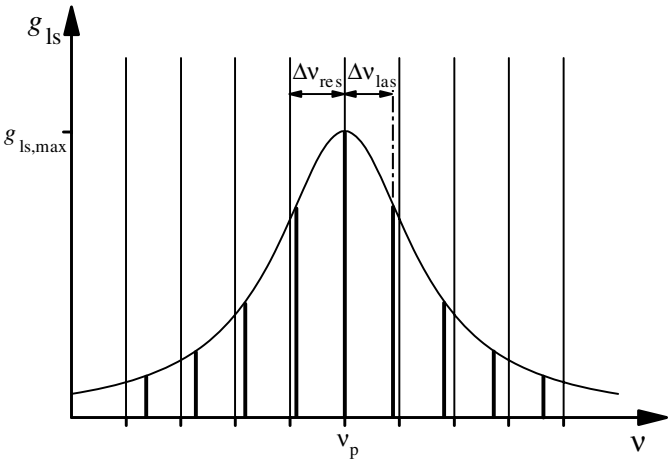

Fig. 6.67. Frequency pulling of longitudinal resonator modes towards the center of the gain curve (schematic)

Only at the frequency of the gain maximum is the derivative of the gain $\partial g_{\mathrm{ls}}/\partial\nu$ zero. At the other frequencies the gain is slightly stronger at the center-side of the resonator modes and thus the modes are pulled towards this center.

In [M24] an approximate formula was given for the shift $\Delta\nu_{\mathrm{pull}}$ of the qth resonator mode with original frequency ν_q as:

$$\text{frequency pulling} \quad \Delta\nu_{\mathrm{pull}} = \nu_q \frac{g_{\mathrm{ls}} L_{\mathrm{mat}}}{2\pi} \frac{p-q}{m} \frac{1}{1+[2(p-q)/m]^2} \qquad (6.128)$$

assuming that the pth resonator mode matches the gain maximum and containing the low-signal gain coefficient g_{ls}, the length of the active material L_{mat}, the mode numbers p, q and the number of resonator modes within the gain FWHM bandwidth m.

The relative difference of the mode spacing with pulling compared to the original resonator modes is of the order of 10^{-4}.

6.9.3 Broad Band Laser Emission

Active materials with *inhomogeneously broadened laser transitions* can emit in a wide spectral range because of the lack of any mode competition for inversion population density. For homogeneously broadened laser material special care has to be taken to get broadband laser emission, as will be described below (see, for example, [6.805–6.814]).

6.9.3.1 Broad-Band Emission from Inhomogeneously Broadening

Inhomogeneously broadened spectra in the time scale of the laser emission (see Sect. 5.2) consist of homogeneously broadened subbands with different center wavelengths and possibly different emission cross-sections. The overall gain profile usually shows a Gaussian distribution. Thus it does not matter if the peak cross-sections $\sigma_{\mathrm{peak}}(\nu_{\mathrm{p}})$ of the subbands show a Gaussian distribution as a function of their frequency ν_{p} or the associated inversion population density $\Delta N(\nu_{\mathrm{p}})$ is modulated this way. The resulting small or low signal gain g_{ls} for the frequency ν_{p} of the pth longitudinal resonator mode can be written as:

small–signal gain of inhomogeneously broadened active material

$$g_{\mathrm{ls}}(\nu_p) = \Delta N_{\mathrm{total}} \sigma_{\mathrm{total,max}} \frac{\Delta\nu_{\mathrm{homogen}}}{\Delta\nu_{\mathrm{inhomogen}}} \cdot \exp\left(-\frac{(\nu_p - \nu_{\mathrm{total,max}})^2 4\,\ln 2}{\Delta\nu^2_{\mathrm{inhomogen}}}\right) \tag{6.129}$$

with the FWHM bandwidth $\Delta\nu_{\mathrm{homogen}}$ of the sub bands which are assumed to be equal. The FWHM bandwidth $\Delta\nu_{\mathrm{inhomogen}}$ describes the whole emission band containing the homogeneous subbands. $\Delta N_{\mathrm{total}}$ is the total inversion population density of the active material independent of their distribution over the subbands and $\sigma_{\mathrm{total,max}}$ the maximum cross-section of the whole band which is obtained at frequency $\nu_{\mathrm{total,max}}$.

All longitudinal laser modes p with frequency ν_{p} which show gain above threshold can be observed in the laser:

$$V(\nu_p)\sqrt{R_{\mathrm{HR}}(\nu_p)R_{\mathrm{OC}}(\nu_p)}\,\mathrm{e}^{-g_{\mathrm{ls}}(\nu_p)L_{\mathrm{mat}}} \geq 1 \tag{6.130}$$

where the frequency dependence of the losses V and the reflectivities of the mirrors $R_{\mathrm{HR/OC}}$ have to be considered explicitly. For further evaluation it has to be noticed that the relaxation time $\tau(\nu_p)$ and the cross-section $\sigma(\nu_p)$ and thus the nonlinear (or saturation) intensity $I_{\mathrm{nl}}(\nu_p)$ may be a function of the center frequency ν_{p} of the emission of the subbands.

In many cases exchange processes take place between the inhomogeneous subspecies as known, e.g. in molecular systems from spectral hole burning measurements. The exchange rate or internal cross-relaxation has to be much slower than the pump and stimulated emission rate in the laser to conserve the inhomogeneous behavior (see Sect. 5.3).

6.9.3.2 Broad-Band Emission from Short Pulse Generation

As a consequence of the quantum mechanical uncertainty of energy and time the spectral frequency bandwidth $\Delta\nu_{\mathrm{laser}}$ of light pulses will be larger the shorter the pulse duration $\Delta t_{\mathrm{pulse}}$ if the light is bandwidth limited (see

Sect. 2.1.2, p. 15). The minimal FWHM bandwidth is given by:

$$\Delta\nu_{\text{laser,FWHM}} = \frac{1}{\pi\Delta t_{\text{pulse}}}. \tag{6.131}$$

The resulting minimal frequency bandwidth is $3.2 \cdot 10^{11}$ Hz for a pulse width of 1 ps and $3.2 \cdot 10^{13}$ Hz for a 10 fs pulse. The resulting wavelength bandwidths are 0.27 nm and 27 nm, respectively, in the visible range at a center wavelength of 500 nm (see also Table 2.3, p. 17), the factor of 2 results from the different considered times: decay vs pulse duration).

For the generation of such short pulses an active laser material with a sufficiently wide homogeneously broadened gain profile is required (see Sect. 6.10.3, p. 460). The obtained bandwidths can be much larger than there minima.

6.9.3.3 Broad-Band Emission from Gain Switching

Another possibility of broad-band emission from a homogeneously broadened laser material is the fast generation of a very large inversion, the gain switching [e.g. 6.811–6.813]. Such a laser emits a short pulse without reaching the steady state conditions. Thus the gain of the active material is switched on by fast pumping, typically with ns laser pump pulses. The output pulse usually shows a pulse duration in the ns range, too, with a delay of a few 10 ns.

This nonstationary gain switching laser can be described with time-dependent rate equations. They have to contain the spectral properties of all resonator elements and of the gain.

In the simplest case using a four-level scheme as shown in Fig. 6.65 (p. 441) the differential equation for the inversion population density $\Delta N(t)$ as a function of time t is given by:

$$\frac{\partial\Delta N}{\partial t} = -\frac{\Delta N}{\tau_{\text{upper}}} - \sum_{\lambda_m} \Delta N\sigma_{\text{laser}}(\lambda_m)\mathcal{I}(\lambda_m) + W(N_{\text{total}} - \Delta N) \tag{6.132}$$

with the approximations of the fast decay of levels 2 and 1. The intensity $\mathcal{I}$ is measured in photons $\text{cm}^{-2}\,\text{s}^{-1}$ and the wavelength λ_{m} was used as a discrete quantity with respect to the numerical calculation. τ_{upper} denotes the lifetime of the upper laser level and σ_{laser} is the emission cross-section of the active material. N_{total} is the total population density of laser active particles in the active material and is measured in particles per cm^3.

The photon transport equation for the intensity $\mathcal{I}$ as a function of time and wavelength including the resonator conditions can be written as:

$$\frac{L_{\text{res}}}{c_0}\frac{\partial\mathcal{I}}{\partial t} = \mathcal{I}(t,\lambda_m)\left\{\Delta N\sigma_{\text{laser}}(\lambda_m)L_{\text{mat}} - \ln\left(\frac{1}{V(\lambda_m)\sqrt{R_{\text{OC}}(\lambda_m)}}\right)\right\} + \mathcal{I}_{\text{sp}}(t,\lambda_m) \tag{6.133}$$

assuming a homogeneous intensity along the active material. L_{res} is the optical length of the resonator and L_{mat} the geometrical length of the pumped active material. V describes the losses in the resonator and R_{oc} is the re-

flectivity of the output coupler assuming a reflectivity of the high-reflecting mirror equal to the reciprocal of the investigated spectral range. I_{sp} gives the spontaneous emission of the laser in the direction of the laser beam. Its value usually does not influence the numerical results because of the high amplification but it is necessary to start the stimulated emission at time $t = 0$. The fluorescence spectrum of the active material can be taken as its spectral distribution. In these equations the spatial hole burning is neglected and a large number of the m resonator modes within the gain bandwidth is presupposed.

As an example the spectrum of a gain switched Ti:sapphire laser is calculated. The emission cross-section of Ti:sapphire is shown in Fig. 6.68.

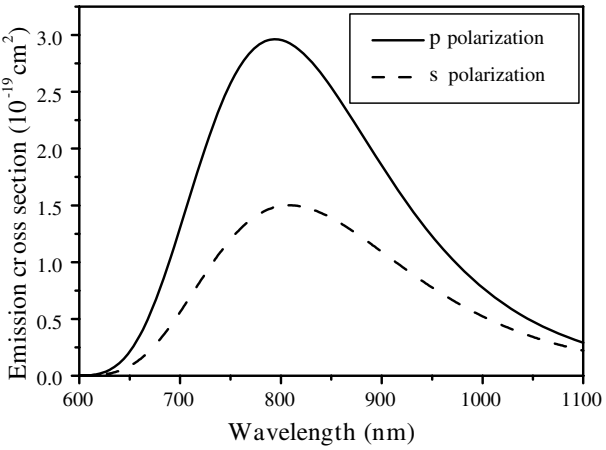

Fig. 6.68. Emission cross-section of Ti:sapphire of π and σ polarization of the light as a function of the wavelength

The reflectivity of the used commercial laser mirrors with a specified reflectivity of 0.8 as output coupler is given in Fig. 6.69 (p. 450).

The calculation of the emission spectra are obtained for a total population density of $3.3 \cdot 10^{19}\,\mathrm{cm}^{-3}$ which is equivalent to a concentration of 0.095 wt%. $V = 0.97$ follows from the reabsorption in the laser material. With these values the minimum gain factor is $G_{\mathrm{threshold}} = 1.15$. For nonstationary calculations a gain of 1.55 at 794 nm resulting in a starting inversion population density of $6 \cdot 10^{17}\,\mathrm{cm}^{-3}$ was used in a 20 mm long crystal positioned in a 0.2 m long resonator. This laser was pumped with 1.23 mJ, 17 ns pulse with a wavelength of 532 nm and a focus radius of 250 µm. With these values the delay time between pumping and the laser pulse is 50 ns.

This laser emits a ns laser pulse of 12 ns duration and the spectrum is more than 20 nm broad. The calculated results based on different model assumptions to be compared with the experimental values are given in Fig. 6.70 (p. 450).

The influence of the start intensity profile as well as the reflectivity of the mirror can be seen from this figure. The FWHM bandwidth of the laser

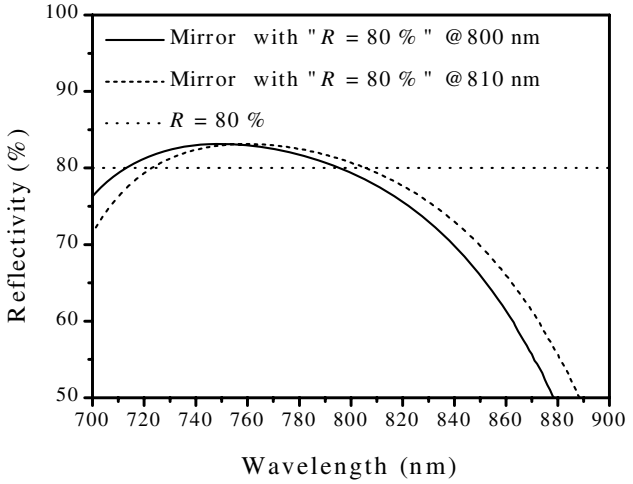

Fig. 6.69. Reflectivity of two commercial mirrors specified with a reflectivity of 0.8 at 800 nm and at 810 nm which are used as output coupler for the Ti:sapphire laser

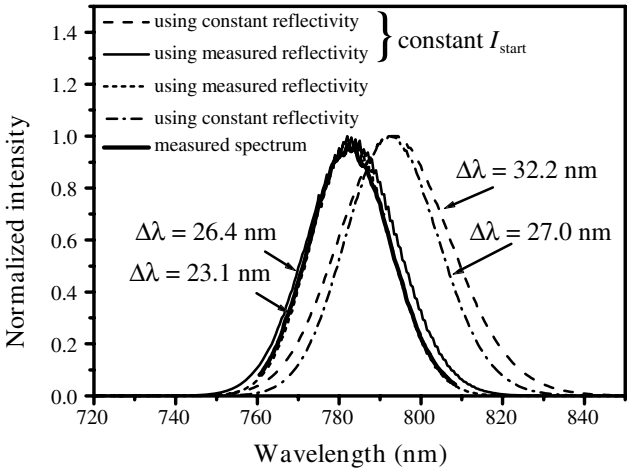

Fig. 6.70. Calculated and measured emission spectra of a Ti:sapphire laser using an artificial output mirror with a constant reflectivity of 80% or the commercial mirror I of Fig. 6.69 as output coupler while applying a spectrally constant start intensity or the spectral profile of the fluorescence

is decreased by 3 nm to 23 nm from the effect of the spectral profile of the realistic mirror compared to the flat profile mirror. Using a spectrally constant start intensity instead of the fluorescence profile the spectrum would be 9 nm wider. The theoretical results including both the spectral profile of the mirror and of the fluorescence were in good agreement with the measured spectrum.

6.10 Intensity Modulation and Short Pulse Generation

The active material in the laser resonator shows a highly nonlinear behavior resulting from the exponential dependence of the gain G as a function of the inversion density ΔN which is a function of the laser intensity $I_{\text{laser}}(t)$ and the pump rate $W(t)$. Thus all types of temporal fluctuations are possible, pulses with durations in the µs, ns, ps and fs range can be produced with different methods applying further nonlinear devices in the resonator.

6.10.1 Spiking Operation: Intensity Fluctuations

In particular, if the pump rate is switched on, such as e.g. when flash lamp or electrical discharge pulse pumping in turned on some oscillations in the laser output can be observed [e.g. 6.815–6.818]. The modeling can usually be carried out using rate equations as given in the previous sections.

For a simplified description it is assumed that pumping with rate W is switched on at time $t = 0$ and stays constant for $t > 0$. The resulting behavior is shown in Fig. 6.71.

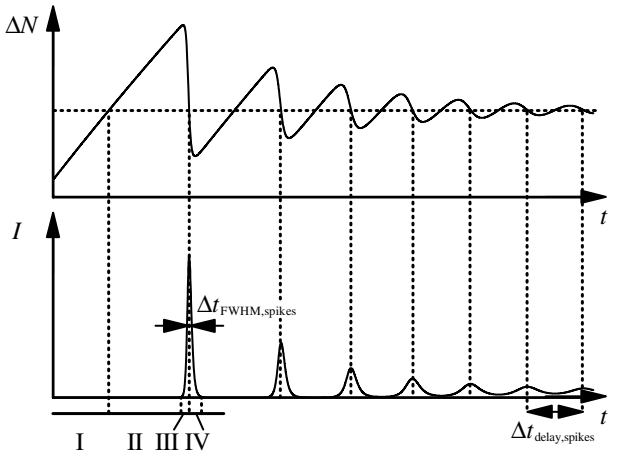

Fig. 6.71. Spiking oscillations of a laser in the laser intensity I and the population inversion density ΔN as a function of time

The following processes take place:

I pumping leads to an increase of the inversion population density (stimulated emission can be neglected);

II threshold inversion is overcome and stimulated emission takes place during the roundtrips;

III inversion population density and photon density are very high and thus the depopulation via the laser light starts up to the maximum value of the laser intensity;
IV inversion population density is strongly decreased and thus the intensity decreases to very small values with further depopulation much below threshold;
V almost no laser light is present and thus the pumping increases the inversion again for the next cycle.

Based on this simple model a series of laser pulses, the *spiking*, is obtained until steady state operation is reached. If the laser is perturbed then decaying intensity oscillations will, again occur.

The pulse widths of the spikes $\Delta t_{\mathrm{FWHM,spike}}$ are a function of the pump rate, the gain and the resonator roundtrip time. In solid-state lasers the order of magnitude is 100 ns and in dye lasers it can be as small as sub-ps. The pulse-to-pulse delay $\Delta t_{\mathrm{delay,spikes}}$ is one or two orders of magnitude larger than $\Delta t_{\mathrm{FWHM,spike}}$.

As a function of the pump rate these oscillations of the inversion decay towards the value related to the steady-state inversion population density. Assuming only small perturbations in the inversion population density and the intensity around the steady state values the solution of the differential equation for the intensity I was given in [M49] as:

$$I_{\mathrm{laser,spiking}} = I_{\mathrm{laser,spiking}}(t=0) \cdot \exp\left(-\frac{W_{\mathrm{pump}}}{W_{\mathrm{pump,threshold}}}\,\frac{t}{\tau_{\mathrm{upper}}}\,\sin(2\pi\nu_{\mathrm{spiking}}t\right) \tag{6.134}$$

with the pump power W_{pump}, the threshold pump power $W_{\mathrm{pump,threshold}}$, the fluorescence lifetime of the laser transition which is equal to the lifetime of the upper laser level τ_{upper}, and the frequency of the spiking oscillations ν_{spiking}. The initial amplitude of these oscillations $I_{\mathrm{laser,spiking}}$ can be much higher than the laser intensity in steady state operation as can be seen from Figs. 6.71 (p. 451) and 6.72 (p. 453).

The frequency of the relaxation oscillations of spiking, ν_{spiking}, is determined by the fluorescence lifetime $\tau_{\mathrm{fluore}} = \tau_{\mathrm{upper}}$, the resonator parameters described by the resonator lifetime τ_{res} as given in (6.95) and the pump rate W_{pump}:

$$\begin{aligned}\nu_{\mathrm{spiking}} &= \frac{1}{2\pi}\sqrt{\left(\frac{W_{\mathrm{pump}}}{W_{\mathrm{pump,threshold}}}-1\right)\frac{1}{\tau_{\mathrm{upper}}\tau_{\mathrm{res}}}-\left(\frac{W_{\mathrm{pump}}}{2W_{\mathrm{pump,threshold}}\tau_{\mathrm{upper}}}\right)^2} \\ &\simeq \frac{1}{2\pi}\sqrt{\left(\frac{W_{\mathrm{pump}}}{W_{\mathrm{pump,threshold}}}-1\right)\frac{1}{\tau_{\mathrm{upper}}\tau_{\mathrm{res}}}}\end{aligned} \tag{6.135}$$

Because higher losses in the resonator result in a shorter photon lifetime in the resonator τ_{res} the spiking oscillations will occur faster. Notice that

higher losses may demand higher pump rates. Stronger pumping and a shorter fluorescence lifetime will also increase the spiking frequency.

The 1/e damping time $\tau_{\text{damping,spikes}}$ of these oscillations can be given as:

$$\tau_{\text{damping,spikes}} = \frac{W_{\text{pump,threshold}}}{W_{\text{pump}}} \tau_{\text{upper}} \tag{6.136}$$

and thus stronger pumping shows faster decay.

As an example a Nd:YAG laser with fluorescence lifetime of 230 µs, an output mirror with 50% reflectivity, losses of $V = 0.95$ and a resonator length of 0.5 m which is pumped three times above threshold shows a spiking frequency of 230 kHz or a period of $1/\nu_{\text{spiking}}$ of 4.3 µs. The damping time of the oscillations is 77 µs for this laser. For comparison the resonator lifetime is 4.2 ns in this case. An experimental example from a realistic laser showing this regular pattern is given in Fig. 6.72.

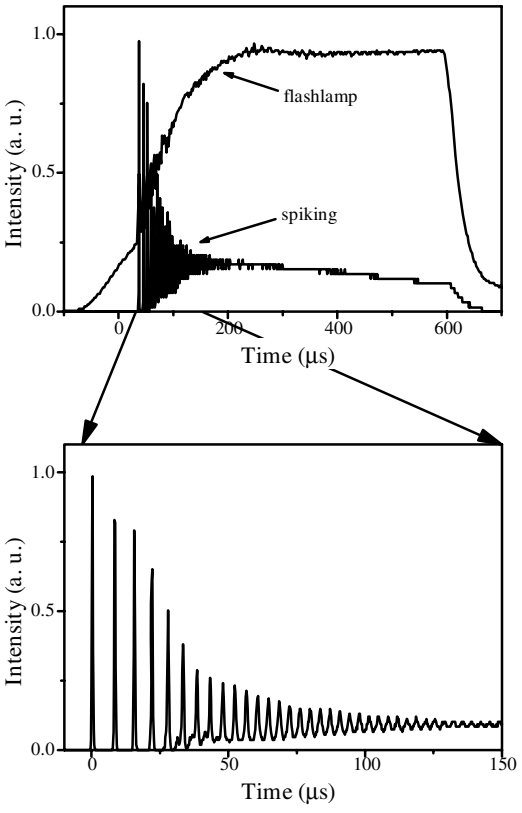

Fig. 6.72. Spiking operation of a flash lamp pumped Nd:YAG laser. In addition to the laser output the intensity of the pumping flash lamp is given

Sometimes lasers can show deviations from this regular pattern. The resulting irregular fluctuations are a consequence of the competition of longitudinal modes in the resonator. Because of the nonlinearity of the laser process

this pattern can even show chaotic behavior. If a regular oscillation pattern is required the laser should be operated in a single longitudinal mode.

In cw lasers these fluctuations can be suppressed by active stabilization of the operation by electronic controlling of the pump rate.

The fundamental limits for these fluctuations are the spontaneous emitted photons from the active material. The total noise power P_{noise} of the whole active material is given by:

$$P_{\text{noise}} = h\nu_{\text{laser}} \frac{\Delta N A_{\text{mode}} L_{\text{mat}}}{\tau_{\text{upper}}} \tag{6.137}$$

with the laser frequency ν_{laser}, the cross-section of the laser mode in the active material A_{mode}, the length of the active material L_{mat}, the inversion population density ΔN and the lifetime of the upper level.

6.10.2 Q Switching (Generation of ns Pulses)

As described above, the laser intensity and the stored inversion are a function of all the losses of the resonator and thus of the quality $\text{Q} = (\text{VR})^{-1}$ of the resonator. Q switching means the quality of the laser resonator is switched from low to high values typically in short times and thus short pulses with ns pulse width and high-powers in the kW–MW range are emitted [6.819–6.919]. These intensive pulses are useful in all kinds of nonlinear optical interactions. In many cases at least Q switched lasers (or sometimes ps or fs lasers) are necessary to achieve nonlinear optical effects.

The Q switching of the laser is achieved by rapidly decreasing of artificial losses in the resonator typically with a slope in the ns range. The stored high inversion in the active material leads to a high gain for the laser radiation and thus the positive feedback of increased intensity leads to more stimulated emission which leads to more intensity. This results in a very fast rising intensity of the laser until the inversion reaches its threshold value. Then the intensity again rapidly decreases as a result of the losses from the outcoupling.

6.10.2.1 Active Q Switching and Cavity Dumping

Active Q switching can be achieved, e.g. with electro-optical devices as shown in Fig. 6.73 (p. 455). All electro-optical effects can be used [6.819–6.850]. Using the *Pockels effect* (see Sect. 4.4.6, p. 200) the polarization of the light can be changed. In combination with polarizers the transmission of this arrangement can be varied over a wide range of more than 1:50 in ns times. Using avalanche transistor chains high voltages up to a few kV can be switched in one or a few ns.

This scheme can be extended by separating the two orthogonal polarization directions and rotating one of them by 90° before the Q switch to achieve a polarization insensitive arrangement.

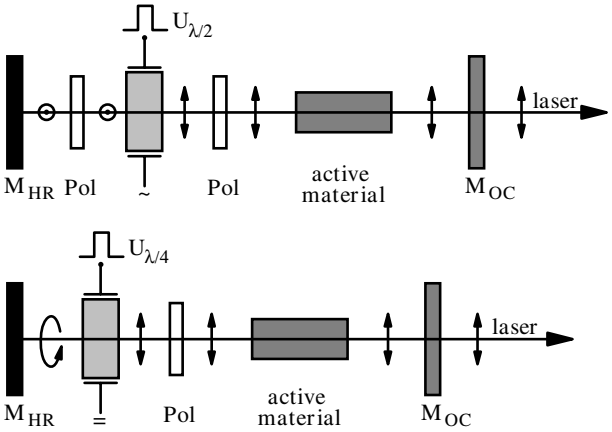

Fig. 6.73. Q switching of a laser resonator using the electro-optical Pockels effect and polarizers

Kerr cells are used for Q switching and different lasers have been synchronized by optically triggering these cell from a third laser. Today electro-optical switches allow the triggering of the Q switch laser with an accuracy better 5 ns.

For wavelengths in the IR (e.g. a Er laser) active Q switching is based on frustrated total internal reflection (*FTIR switch*) [6.822] at a very narrow slit with a thickness of some tenths of the wavelength between two glass plates. This slit width is externally decreased with a piezo-element to a width below a tenth of the wavelength. Thus the transmission is increased from a few percent to values above 50%. Another possibility is given in [6.821].

Even mechanical elements can be used for active Q switching. Rotating mirrors will be aligned only for a short time and thus allow the emission of the short pulse if they spin with about 10 000 revolutions per minute [e.g. 6.851, 6.852].

The quality of the Q-switched laser light can be improved by a prelasing configuration [e.g. 6.850]. Therefore, the losses in the cavity are tuned in the time before the Q switch pulse rises just below threshold, and, thus, almost no light will be emitted. However, during this time of typically some 10–100 μs the mode structure is formed. In the best cases a longitudinal single mode and TEM_{00} operation can be obtained. The losses can be tuned by slightly turning the polarizing elements out of the optimal position. However, very stable operation of the pump and cooling is required.

Cavity dumping works inversely to Q switching described so far. The losses of the resonator are switched on for only a short time in the ns range by out-coupling light as shown in Fig. 6.74 (p. 456).

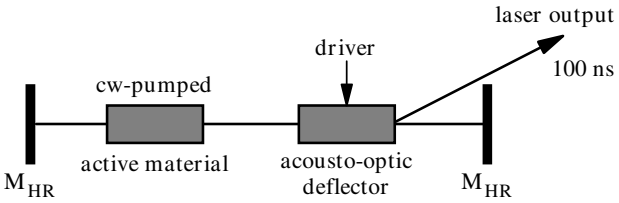

Fig. 6.74. Cavity dumping for ns pulse generation with a cw laser such as e.g. an argon laser using an acousto-optic deflector (AOM) which is switched on for a few ns. The laser light is then reflected at the sound wave grating and out-coupled

Acousto-optic switches or modulators (*AOM*s) deflect the laser light wave at an index grating which is induced by hyper-sound waves in suitable crystals such as e.g. $LiNdO_3$ or quartz. The sound wave is typically induced by a piezo-driver in the MHz range. When the sound wave generator is switched on the laser beam is deflected and the quality of the resonator drops. This method is especially useful for lasers with low gain such as argon or cw dye lasers. These lasers are continuously pumped and the acousto-optic switch is operated continuously, too. The laser output will consist of a periodical series of output pulses. The frequency of the acousto-optical modulator will occur as a side-band frequency in the laser light.

These pulses usually have a longer pulse duration in the range of 100 ns because the inversion is smaller in cw pumping. High repetition rates in the kHz range are possible and the peak power is about 100 times higher than in cw operation of the laser with an optimal out-coupling mirror.

6.10.2.2 Passive Q Switching

Applying the nonlinear absorption of a suitable material in the resonator leads to *passive Q switching* [6.853–6.901] as shown in Fig. 6.75.

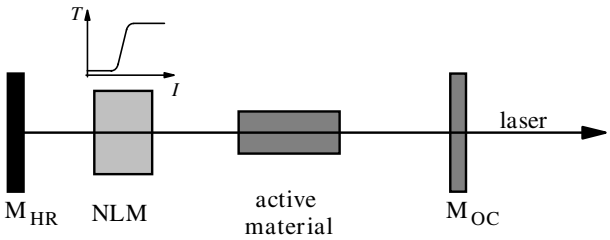

Fig. 6.75. Schematic of a laser with passive Q switching of the resonator using a nonlinear absorber material (NLM)

In this case the transmission of the absorber is progressively bleached with increasing intensity of the laser. Thus the positive feedback is amplified by

the effect that more intensity causes more transmittance which results in less losses and thus more intensity. This takes place in addition to the nonlinear effect of stimulated emission in the active material.

Dyes in solution or in polymers or other solid state materials [e.g. 6.890–6.901] are used as materials for passive Q switching. The absorption cross-section of the Q switch material has to be larger at the laser wavelength than the emission cross-section of the active material. The lifetime of the upper level of the Q switch material should not be much shorter than the pulse duration.

Cyanine dyes such as cryptocyanine and phthalocyanine are used in the red region of the visible spectrum e.g. for ruby lasers. They can be solved in alcohol. Special dyes are produced for Nd lasers, such as e.g. the numbers #9740, #9860 and #14,015 by Eastman Kodak. These dyes have to be solved in 1,2-dichlorethene. Ready-to-use polymer foils for Q switching are also offered, e.g. by Kodak. On the other hand many laser materials are useful. In particular, e.g. Cr^{4+}:YAG crystals are used as a Q switch for Nd lasers. Typical low-signal transmissions of 30–70% of the Q switch are used. This additional loss also has to be compensated by the laser gain to overcame threshold.

Optical phase conjugation, for example based on stimulated Brillouin scattering, can be used for Q switching, as described in Sect. 6.7.6 (p. 435). In this case the transparent SBS materials show a nonlinear reflectivity and are used directly as resonator mirrors.

For matching the laser intensity to the nonlinear transmission curve of the absorber the right position of the Q switch in the resonator has to be chosen. Sometimes telescopes in the resonator for providing suitable beam cross-section for the nonlinear absorber can be necessary.

6.10.2.3 Theoretical Description of Q Switching

The *theoretical description of Q switching* can be based on rate equations. The duration of the Q switch pulse is much shorter than the pump process. Thus the generation of the inversion need not be included in the rate equations and the spontaneous emission can be neglected. The differential equation for the inversion population density ΔN then reads as:

$$\frac{\partial \Delta N}{\partial t} = -\sigma_{\text{laser}} \mathcal{I} \Delta N \tag{6.138}$$

and for the intensity $\mathcal{I}$ inside the resonator as:

$$\frac{\partial \mathcal{I}}{\partial t} = \mathcal{I} \left\{ \frac{c_0 \sigma_{\text{laser}} \Delta N L_{\text{mat}}}{L_{\text{res}}} - \frac{c_0}{2L_{\text{res}}} \left| \ln(f_Q(t) V \sqrt{R_{\text{OC}}}) \right| \right\} \tag{6.139}$$

with the cross-section σ_{laser}, the geometrical length of the active material L_{mat}, the optical length of the resonator L_{res}, the resonator losses without the Q switch V, the reflectivity of the output coupler R_{OC} and a function

$f_Q(t)$ describing the Q switch. This system of two equations can be solved numerically.

If $f_Q(t)$ is a simple step function with $f_Q(t > t_Q) = 1$ these equations can be solved easily. In Fig. 6.76 the temporal structure of the inversion population density ΔN and the laser intensity I_{laser} are depicted.

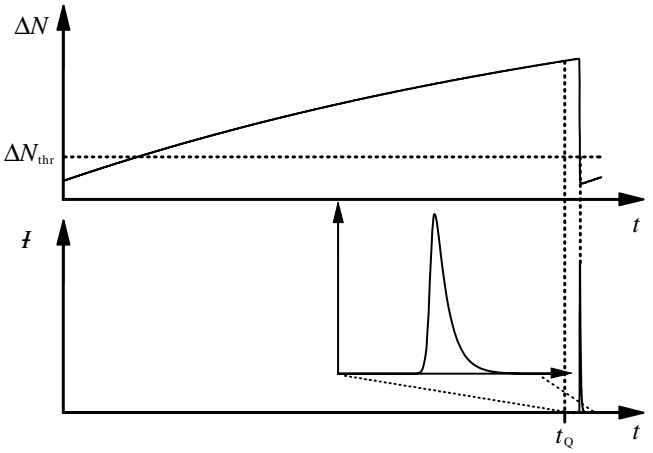

Fig. 6.76. Temporal structure of the inversion population density ΔN and the laser intensity I during Q switching the resonator at time t_Q

The quotient of these two equations results in:

$$\frac{\partial I}{\partial \Delta N} = -\frac{c_0 L_{mat}}{L_{res}} - \frac{c_0 \left|\ln(V\sqrt{R_{OC}})\right|}{2L_{res}\sigma_{laser} I \Delta N} \tag{6.140}$$

which can be solved to give

$$I(\Delta N) = I_0 + \left\{ (\Delta N_{start} - \Delta N) + \Delta N_{threshold} \ln \frac{\Delta N}{\Delta N_{start}} \right\} \frac{L_{mat}}{\tau_{round}} \tag{6.141}$$

with the population inversion density ΔN_{start} at the beginning of the Q switch process.

From this equation the maximum intensity can be calculated under the condition that at the time of the intensity maximum the inversion population density is equal to the threshold value $\Delta N_{threshold}$ which was given in (6.108). The resulting peak intensity is equal to:

$$I_{laser,max} = \frac{L_{mat}}{\tau_{round}} \left\{ \Delta N_{start} - \Delta N_{threshold} \left(1 + \ln \frac{\Delta N_{start}}{\Delta N_{threshold}} \right) \right\} \tag{6.142}$$

which is higher the shorter the resonator roundtrip time τ_{round} becomes.

The maximum output power $P_{\text{laser,max}}$ of the Q switch pulse outside the resonator is given by:

$$\textbf{peak power} \quad P_{\text{laser,max}} = \frac{1}{2} \not{I}_{\text{laser,max}} h\nu_{\text{laser}} A_{\text{mode}} (1 - R_{\text{OC}}) \tag{6.143}$$

with the photon energy $h\nu_{\text{laser}}$ and the cross-section of the transversal mode in the active material A_{mode}.

Further the stored and outcoupled pulse energy E_{pulse} of the Q switch pulse can be calculated from:

$$\textbf{pulse energy} \quad E_{\text{pulse}} = \frac{1}{2} \frac{A_{\text{mode}}}{\sigma_{\text{laser}}} h\nu_{\text{laser}} (1 - R_{\text{OC}}) \frac{\Delta N_{\text{start}} - \Delta N_{\text{end}}}{\Delta N_{\text{threshold}}} \tag{6.144}$$

with the population inversion density N_{end} at the end of the Q switch pulse, which can be calculated from the transcendental equation:

$$\Delta N_{\text{start}} - \Delta N_{\text{end}} + \Delta N_{\text{threshold}} \ln \frac{\Delta N_{\text{end}}}{\Delta N_{\text{start}}} = 0 \tag{6.145}$$

or estimated in a rough way, e.g. to zero.

Both the extracted pulse energy and the peak power are higher the higher the inversion population density at the beginning of the Q switching ΔN_{start} in relation to the threshold value $\Delta N_{\text{threshold}}$. The pulse width follows from:

pulse width

$$\Delta t_{\text{pulse,FWHM}} = \frac{2 L_{\text{res}} (\Delta N_{\text{start}} - \Delta N_{\text{end}})}{c_0 \sigma_{\text{laser}} L_{\text{mat}} \left(\frac{\Delta N_{\text{start}}}{\Delta N_{\text{threshold}}} - 1 + \ln \frac{\Delta N_{\text{start}}}{\Delta N_{\text{threshold}}} \right)}. \tag{6.146}$$

It is proportional to the optical length L_{res} of the resonator. The pulse built-up time can be estimated from:

$$\textbf{built-up time} \quad t_{\text{buildup}} = \frac{L_{\text{res}}}{c_0 \ln(G_{\text{start}} R V)} \tag{6.147}$$

which is again proportional to the resonator roundtrip time τ_{round} which is a function of the optical length L_{res} of the resonator:

$$\textbf{resonator roundtrip time} \quad \tau_{\text{round}} = \frac{2 L_{\text{res}}}{c_0} \tag{6.148}$$

and thus typical values are of the order of tens of ns. Thus the pulse durations which can be obtained with the Q switch technique are in the range of 10 ns for solid-state lasers. The output energies are in the range of mJ for high repetition rates of kHz and go up to several J for lasers with 10 Hz repetition rate. Thus 100 MW peak power are possible. Several 100 J have been produced in large devices. The Q-switch pulse shape is often very close to a Gaussian function as described in Sect. 2.7.2 (p. 54), e.g. in Eq. (2.138).

Using these formulas, as an example the results for a Nd:YAG laser with cross-section $\sigma_{\text{laser}} = 3.2 \cdot 10^{-19}\,\text{cm}^2$ and a photon energy of $h\nu_{\text{laser}} = 1.87 \cdot$

10^{-19} J at wavelength of 1064 nm will be given. For a resonator with a length of 1 m, a reflectivity of 50% for the out-coupling mirror, a loss factor $V = 0.95$ and a start gain $G_{\text{start}} = 4$ from a rod length of 80 mm and a mode diameter of 3 mm, there is a laser intensity of $2.97 \cdot 10^{26}$ photons $\text{cm}^{-2}\,\text{s}^{-1}$ or 56 MW cm^{-2}, a peak power of 1 MW and a pulse energy of 48 mJ. The inversion population density ΔN_{end} at the end of the pulse is $5.4 \cdot 10^{15}\,\text{cm}^{-3}$. The pulse width is 49 ns and the pulse built-up time 3.4 ns. These values can easily be achieved with a common laser.

6.10.3 Mode Locking and Generation of ps and fs Pulses

For the generation of pulses with pulse widths below 100 ps down to a few fs the locking of longitudinal modes can be applied using a periodically operating active or passive switch in the resonator. If the laser is operated close to threshold for a sufficiently long time or continuously the discrimination of nonlocked modes will be increased and thus a train of very short pulses with time intervals of the resonator roundtrip time τ_{round} between them will occur (see Fig. 6.77).

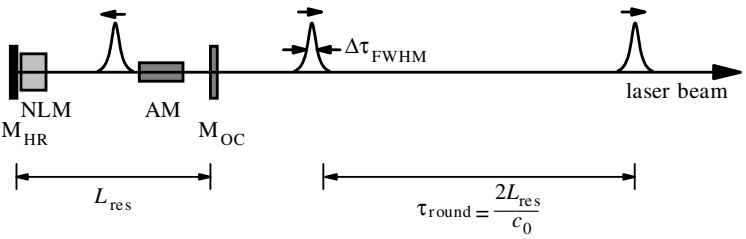

Fig. 6.77. Schematic of short pulse generation with "mode locker (NLM)" in the laser resonator built by the two mirrors M_{HR} and M_{OC} and the active material AM

Different methods have been developed for mode locking in different lasers. For an introduction see [6.920–6.923, M44, M58–M65]. Some general aspects are described in [6.924–6.942]. In any case the gain bandwidth of the active material has to be large enough for the generation of very short pulses $\Delta t_{\text{FWHM}} \geq 1/(2\pi\Delta\nu_{\text{laser}})$ (see Table 2.3, p. 17).

Pulses with durations of 10–100 ps are produced by Nd lasers, ruby lasers, gas-ion lasers and synchronously pumped dye lasers. Shorter pulses of a few fs to 100 fs are generated, e.g. from Ti:sapphire lasers, Cr lasers and dye lasers. Short pulses in the ps-range are available from diode lasers with very small resonators. The increasing demand of short pulse systems with high average output power for material processing and similar applications on one hand and small, reliable and cheap systems for measuring devices and communication technologies on the other as well as the wish for even shorter pulses in the as range and peak powers as high as possible for scientific

applications will lead to further progress in this field. Thus the different techniques for generating very short pulses as described here may be used in new systems in the future in new contexts.

In any case the pulse duration can be increased by applying narrow spectral filters (e.g. etalons) in the resonator which decrease the spectral width of the light. The measurement methods for these short pulse durations are described in Sects. 5.5 and 7.1.5.2 (p. 543), and in the references therein.

6.10.3.1 Theoretical Description: Bandwidth-Limited Pulses

Since the frequency bandwidth for short pulses of 100 ps down to 10 fs is as large as 1.6 GHz and 16 THz more than 100 and up to many 10 000 longitudinal laser modes are active in these lasers. Therefore a statistical or continuum approach can be used, not considering each resonator mode explicitly. Thus the analysis can be carried out in the frequency or the time domain which are related by a Fourier transformation.

In general the electric field vector E of all involved longitudinal laser modes numbered with p have to be summed for the resulting intensity of the laser beam:

$$E(t) = \sum_{p=p_{\min}}^{p_{\max}} E_{0,p} \cos(2\pi\nu_p t + \varphi_p) \tag{6.149}$$

with the usually unknown amplitudes $E_{0,\mathrm{p}}$ and phases φ_{p} of these axial laser modes with the frequencies ν_{p}. Many kinds of pulse shapes are possible from different amplitude distributions.

Usually bell-shaped pulses are observed and thus Gaussian or sech^2 functions were usually chosen for analysis. The Gaussian pulse can be written as a function of time t as:

$$E_{\mathrm{laser}}(t) = E_{\mathrm{laser},0}\, \mathrm{e}^{-2\,\ln 2(t/\Delta t_{\mathrm{FWHM}})^2}\, \mathrm{e}^{\mathrm{i}(2\pi\nu_p + \beta_{\mathrm{chirp}} t)t} \tag{6.150}$$

with the electric field E of the laser light, the pulse width Δt_{FWHM} and the frequency ν_p of the pth mode.

The expression $\mathrm{i}\beta_{\mathrm{chirp}} t$ causes a linear "chirp" during the pulse duration with slope β_{chirp}. This *chirp* is a linear increase of the mode frequencies during the pulse, e.g. as a result of the change of the refractive index in the active material during the pulse. This effect is similar to self-phase modulation described in Sect. 4.5.7 (p. 218).

The FWHM frequency bandwidth $\Delta\nu_{\mathrm{FWHM}}$ of this Gaussian pulse is given by:

$$\Delta\nu_{\mathrm{FWHM}} = \frac{1}{\pi}\sqrt{\left(\frac{2\,\ln 2}{\Delta t_{\mathrm{FWHM}}}\right)^2 + \beta_{\mathrm{chirp}}^2 \Delta t_{\mathrm{FWHM}}^2} \tag{6.151}$$

which leads, for chirp-free Gaussian pulses with $\beta_{\text{chirp}} = 0$, to a pulse-bandwidth product of:

$$\textbf{Gauss pulse} \quad \Delta t_{\text{FWHM}} \Delta \nu_{\text{FWHM}} = \frac{2 \ln 2}{\pi} \approx 0.44. \tag{6.152}$$

Other pulse shapes result in other values for this product. For example, sech^2 shaped pulses result in a pulse-bandwidth product of

$$\textbf{sech}^{\mathbf{2}}\textbf{ pulse} \quad \Delta t_{\text{FWHM}} \Delta \nu_{\text{FWHM}} \approx 0.31. \tag{6.153}$$

Laser pulses with experimentally determined pulse width Δt_{FWHM} and frequency bandwidth $\Delta \nu_{\text{FWHM}}$ which fulfill this condition are called *bandwidth-limited pulses* meaning they are chirp-free and in this respect of best quality at the theoretical limit. They fulfill the time–energy uncertainty relation similar to diffraction-limited beams which fulfill the space-momentum uncertainty relation.

Because of the constructive interference of all mode-locked light waves in the short pulse the peak power or intensity is m^2 times larger than these values for a single mode pulse, whereas the peak power or intensity of the nonphase-locked pulses will be only m times larger, where m is the number of interfering modes. Thus by mode locking the peak power or intensity is m times larger than in the nonlocked case. As described above the number m of locked modes can be as high as several 10 000 and thus TW and PW of peak power are possible.

Another approach to model the development of these short pulses is the numerical solution of suitable time-dependent rate equations similar to the modeling of Q switching (see Sect. 6.10.2, p. 454). In these equations the amplification and the nonlinear losses in the mode locker have to be considered. The following processes occur during the short-pulse generation:

- In an early stage one of the intensity fluctuations shows the highest peak intensity (meaning that among the large number of the random phase mixed modes some are accidentally of similar phase); in active mode locking this highest peak is produced by the lowest losses or highest gain.
- Higher intensities will be amplified more than lower intensities and thus this pulse will grow more than the other pulses and it will be narrowed (phase locking will be rewarded).
- The passive mode locker such as e.g. the nonlinear absorption in the dye, will discriminate the lower intensities especially at the rising edge and thus this pulse will be narrowed and less absorbed than the other pulses (phase locking will be rewarded a second time).
- The active mode locker such as e.g. the AOM (Sect. 6.10.2, p. 454), will show less losses at the time of this already strong pulse by the synchronization of the modulation frequency with the roundtrip time of the pulse in the resonator (phase locking is forced).

- Finally the amplification may be saturated and thus only this strongest pulse is further amplified at the expense of the rest of other pulses (phase locking is strongly forced).

Nice examples showing this process are given in [6.933]. For more details see [6.943–6.965].

6.10.3.2 Passive Mode Locking with Nonlinear Absorber

Passive mode locking is mostly used with dyes in solution or semiconductors as nonlinear absorbers which are placed directly in front of the high-reflecting mirror [6.966–6.1032] as shown in Fig. 6.78.

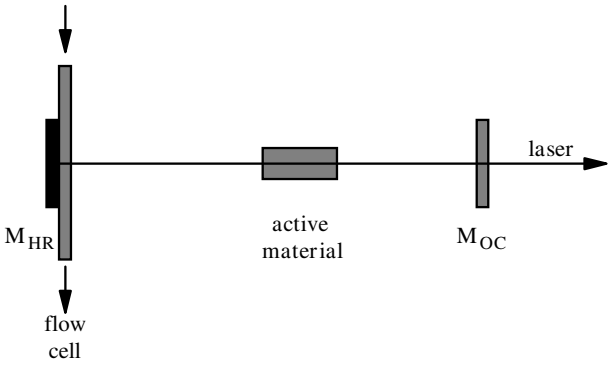

Fig. 6.78. Dye cell in front of the high-reflecting mirror as used for passive mode locking, e.g. of a Nd:YAG laser

The mechanism is described in the previous chapter. The dye has to absorb at the wavelength of the laser emission. The cross-section has to be high enough to enable bleaching with the intensities of the laser. Thus the spot size of the transversal mode has to be adapted to realize the necessary intensity. The recovery time of the dye absorption, which is often the fluorescence decay time of the dye, has to be at least shorter than the roundtrip time of the resonator. Recovery times of the size of the pulse duration are better. In any case only a negligible triplet or other long living state population should occur.

Therefore flow cells are often used for the dye. This method is typically applied in Nd or ruby lasers where the dyes have to absorb around 1060 nm or 700 nm. These dyes are often sensitive to UV radiation and thus the cells have to be shielded against daylight and the pumping flash lamps. For ruby lasers cyanine dyes are useful as in Q switch arrangements (see Sect. 6.10.2, p. 454). For Nd lasers the Eastman Kodak dyes #9740 or #9860 dissolved in 1,2-dichlorethene can be applied. This solvent is especially crucial for impurities

and should therefore be of best quality. Nevertheless, the mode locking dye has to be changed about weekly for safe operation of the lasers. Other materials as nonlinear mode lockers were also applied. For example, liquid crystals [6.978], quantum-well structures [6.982, 6.990, 6.992, 6.998, 6.1010], semiconductors and semiconductor saturable-absorber mirrors (SESAMs) [6.986, 6.988, 6.997], e.g. GaAs and PbS nanocrystals [6.983, 6.991, 6.993], Cr^{4+} and Cr^{3+} ions [6.994, 6.959] and SBS mirrors [6.967, 6.1019] are used.

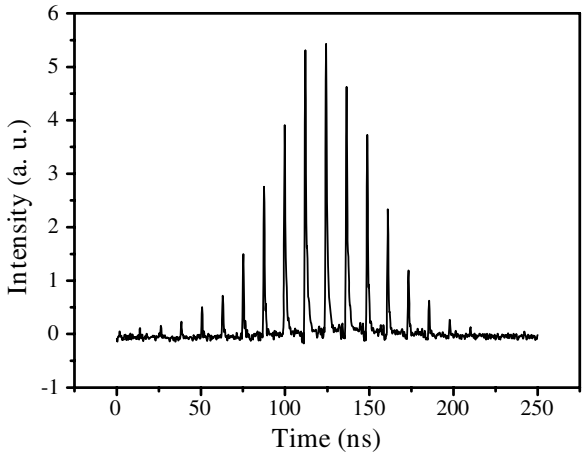

Fig. 6.79. Pulse train of ps-pulses from a Nd:YAG laser. The pulse duration is 30 ps but not resolved in this graph

If the laser is pumped with flash lamp pulses the laser will emit a limited train of ps pulses with a bell-shaped envelope as shown in Fig. 6.79.

The number of pulses can be determined by the optical density and thus the concentration of the dye cell and the pump rate. Less pulses usually show higher peak intensities. On the other hand only a sufficiently long generation time for the ps pulse guarantees a short pulse width and the suppression of satellite pulses.

Pulse widths of about 30 ps are common for flash lamp pumped Nd:YAG lasers whereas Nd glass lasers can show values below 5 ps. The energy content of a single pulse out of the pulse train can be as high as a few mJ resulting in a peak power of more than 30 MW. With laser amplifiers these single pulses can be increased to several 10 mJ resulting in GW powers. Several J are possible in large arrangements reaching the TW level.

6.10.3.3 Colliding Pulse Mode Locking (CPM Laser)

Even shorter pulses can be generated with the colliding pulse technique typically using dye solutions as active material and absorber [6.1032–6.1039] as sketched in Fig. 6.80 (p. 465).

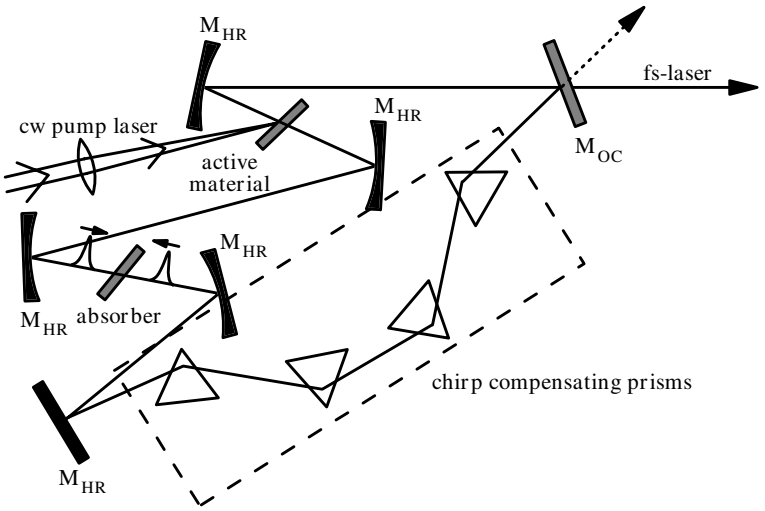

Fig. 6.80. Schematic of a colliding pulse mode locked (CPM) laser for generating fs pulses

Two counterpropagating short pulses meet in the absorber dye at the same time. By the superposition of the two intensities the dye is bleached more than in case of just one pulse. Interference between the two counterpropagating light pulse waves occurs and increases the bleaching. Thus a synchronization of these two pulses occurs in combination with pulse shortening and discrimination of all other pulses. In addition the optical path lengths are chosen for a maximum temporal distance of the two pulses in the active material for maximum amplification of both. Thus the optical path length between the absorption spot and the amplification spot has to be 1/4 of the total optical resonator length on one side and 3/4 on the other.

While the nonlinear absorber mostly increases the slope of the leading edge of pulse the saturated amplification in the active material decreases the negative slope of the trailing edge. Thus the combination of nonlinear absorption and amplification, both as a function of the intensity, shortens the pulse length during each round trip to final steady state values in the fs range.

Because of the low intensities in this type of continuously running laser the spot sizes in both the absorber and the amplifier have to be very small with diameters of a few 10 µm. The thickness of the absorber material L_{absorber} has to be not too much larger than the optical path length L_{pulse} of the short pulses. This length for the FWHM intensity part of the pulse is about:

$$\text{absorber length} \quad L_{\text{absorber}} \approx \frac{c_0}{n} \Delta t_{\text{FWHM}} \tag{6.154}$$

which is divided by the refractive index n of the absorber material to get the maximum length of the absorber. For 50 fs pulses this results in about 11 µm.

With this scheme without chirp compensation pulse durations in the range of a few 100 fs can be achieved. If in addition chirp compensation is applied, as sketched in Fig. 6.80 (p. 465), the pulse width can be smaller than 50 fs from this type of laser. This prism arrangement compensates the different optical path lengths for the different wavelengths from the dispersion in the active material and the absorber which causes the chirp of the short pulse by simulating an anomalous dispersion.

A typical combination for a CPM laser is rhodamine 6G dye solution as active material and DODCI as nonlinear absorber. Both are used in a dye jet stream. Therefore they are dissolved in ethylene-glycol for good optical quality of the jet. The gain medium is pumped by continuously operating (cw) laser emission in the green region such as e.g. by an Ar-ion laser or a diode pumped and frequency doubled Nd laser with an output power of about 5 W.

About 60 fs pulse width can easily be achieved in stable operation. The dyes allow laser wavelengths in the visible which are possible today with OPA setups. The pulse energy is in the range of a few 100 pJ which results in peak powers in the range of several kW. The average output power can be more than 30 mW at a typical repetition rate of 100 MHz. Usually these pulses are amplified with a multipath amplifier (see Sect. 6.11.3.4, p. 483).

6.10.3.4 Kerr Lens Mode Locking

Today's most common technique for generating ultra-short pulses in the fs range is the passive mode locking of Ti:sapphire lasers based on the nonlinear Kerr effect in the active material [6.1040–6.1108] (see Fig. 6.81).

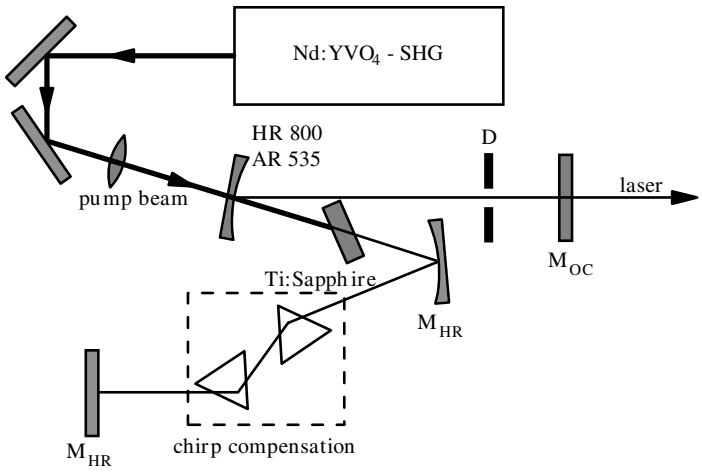

Fig. 6.81. Schematic of a fs Ti:sapphire laser with Kerr lens mode locking and chirp compensation

As described in Sect. 4.5.2 (p. 209) the refractive index of the material becomes a function of the intensity of the laser beam for sufficiently high intensities (n_2 is typically of the order of $10^{-16}\,\mathrm{cm}^2/\mathrm{W}$). Thus focusing of the laser mode occurs as a function of the laser intensity in the active material because of the transversal Gaussian intensity distribution of the fundamental mode. Shorter pulses show higher intensities. If the laser resonator is designed for fundamental mode operation based on a certain Kerr lensing in the active material the associated short pulse can be selected with a simple aperture (D in Fig. 6.81, p. 466).

All other modes with less lensing and thus longer pulses will be discriminated by this aperture. In addition the pump light beam can be focused to a small adapted spot in the active material acting as a gain aperture for the required laser mode, too. Mode locking is again forced via the lensing effect.

Besides the Kerr lensing and possible self-focusing, self-phase modulation from the longitudinal Kerr effect in the active material may occur and spectral broadening may be obtained. Thus simple chirp compensation (see previous section) in the resonator using, e.g. two prisms as shown in Fig. 6.81 (p. 466), allows further compression of the pulses.

Recently special *chirp compensating mirrors* have been used for the compensation of linear and nonlinear dispersion [6.1092–6.1102].

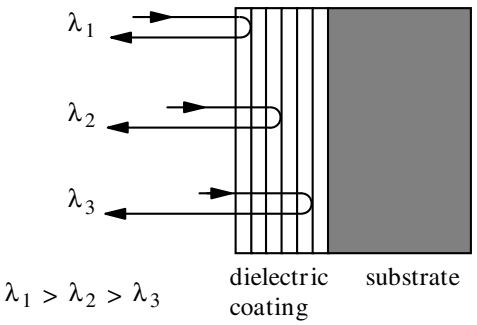

Fig. 6.82. Chirp compensating mirror with dielectric coating giving different delays for different wavelengths

In these dielectric mirrors the different wavelengths were reflected at different layers of the dielectric coating and thus different optical delays in the sub-μm range are achieved. Compact and reliable fs lasers can be built with these mirrors.

The chirp or dispersion compensation is the key task in reaching very short pulses in this simple arrangement. The dispersion can be discussed as a:

frequency-dependent propagation time

$$t_{\mathrm{disp}} = \sum_m \frac{1}{m!} \left.\frac{\partial^m t_{\mathrm{sp}}}{\partial \nu^m}\right|_{\nu_0} (\nu - \nu_0)^m \tag{6.155}$$

[6.921]. Typically, the time delay between the fastest and the slowest part of a 10-fs pulse during one round trip of a non-compensated resonator is about

100 fs. With prism chirp compensation the group delay dispersion (GDD) with $m = 1$ can be compensated, and, thus, 8.5 fs was reported [6.1063]. However, for shorter pulses, higher-order dispersion, $m > 1$, has to be compensated, too. For fused quartz a value of about 36 fs^2/mm can be obtained at 800 nm. Therefore, double-chirped mirrors were developed which allow bandwidths of 200 THz [6.1093]. In addition, good anti-reflection coating is required ($R < 10^{-4}$) over the large spectral region of the laser (690–920 nm). This demands a technical accuracy in the nm range.

The shortest pulses generated with Ti:sapphire lasers and compression showed a duration of 4.5 fs; these pulses are only 1.4 μm long (see Sect. 6.14.2, p. 523). Thus experiments with such short pulses demand very high effort to keep this extremely short timing.

As pump lasers diode pumped cw Nd lasers with frequency doubling are more convenient than Ar-ion lasers. Typically 5 W of pump power are necessary. The Ti:sapphire laser shows an average output power of up to 1 W with pulse widths of 30–100 fs. The pulse repetition rate as the inverse of the resonator roundtrip time which is a function of the optical length of the resonator, is in the range of a few 10 MHz resulting in pulse energies of some 10 nJ and peak powers of more than 100 kW.

These pulses are often amplified with lower repetition rates of 10 Hz–10 kHz and then pulse energies of up to 100 mJ have been achieved. In extreme experiments pulse energies of several J were produced approaching petawatt peak powers.

A theoretical description of the Kerr lens mode locking lasers with and without chirp compensation can be found in [6.1103–6.1108], in addition to the textbooks given above.

6.10.3.5 Additive Pulse Mode Locking

Additive pulse mode locking (APML) [6.1109–6.1125] can be obtained by the feedback of the signal from self-phase modulation in an optical fiber in an arrangement of two coupled resonators as shown schematically in Fig. 6.83.

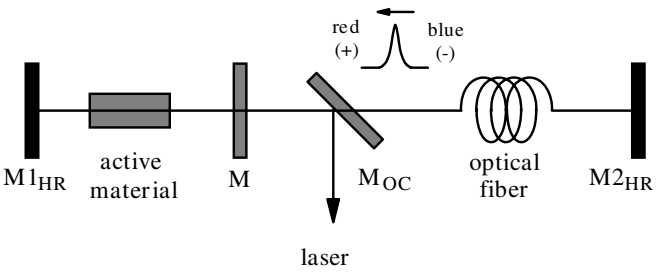

Fig. 6.83. Schematic of a laser resonator with additive pulse mode locking for generation of sub-ps pulses

Thus the main resonator between $M1_{HR}$ and M including the active material gets a feedback from the second resonator from M to $M2_{HR}$ which contains the optical fiber and the output coupler M_{OC} as a beam splitter. This feedback pulse has a red shifted trailing edge and a blue shifted leading edge from the self-phase modulation in the fiber (see Sect. 4.5.7, p. 218).

The resonator lengths have to be designed for constructive interference of the leading edge of this pulse with the main pulse in the main resonator and destructive interference for the trailing edge. Thus the pulse can be shortened to values below 0.5 ps. If the lengths are tuned well no losses in the wrong direction will occur at the beam splitter M_{OC}.

This method was applied, e.g. to color center lasers (KCl), to Ti:sapphire lasers and to Nd lasers. If these lasers are pumped with already short pulses a further shortening can be obtained to values in the range of 10 fs.

An elegant solution of this concept uses an Er-doped fiber with positive group velocity dispersion as gain medium in a ring cavity together with a standard communication fiber which shows negative group velocity dispersion at the laser wavelength of 1.55 µm. Thus the pulse is chirped inside the gain fiber and will be compressed in the standard fiber. Thus the output coupling at the end of the Er fiber shows chirped pulses in the ps range with a few 10 MHz repetition frequency. These pulses can be compressed externally to 120 fs pulse width. The Er fiber can be pumped with a diode laser at 980 nm and thus several 10 mW average power of short pulses can be achieved in a small and reliable laser. A detailed theoretical description was given in [6.1116, 6.1117].

In addition to the constructive and negative interference an amplitude modulation may occur in the fiber and thus solitons may be produced resulting in a further pulse shortening effect similar to the soliton laser.

6.10.3.6 Soliton Laser

Solitons as described in Sect. 4.5.7 (p. 218) can propagate along fibers without changing their pulse duration. A soliton generated in an optical fiber can be used for feedback into a laser seeding this laser with short pulses as shown in Fig. 6.84 (p. 470).

The scheme of the soliton laser [6.1126–6.1148] is similar to the arrangement of Fig. 6.83 (p. 468) but the feedback is tuned for the generation of a soliton in the fiber part resonator having low losses. Thus the pulse is formed as soliton in the fiber and the losses from outcoupling are compensated by the active material. The first-order solitons are a steady state pulse solution of the nonlinear Schroedinger equation including the effects of negative dispersion, self-phase modulation and the gain in the active material. In this case the fiber length has to be chosen carefully for stable operation. 170 fs were reported for this type of laser [6.1129].

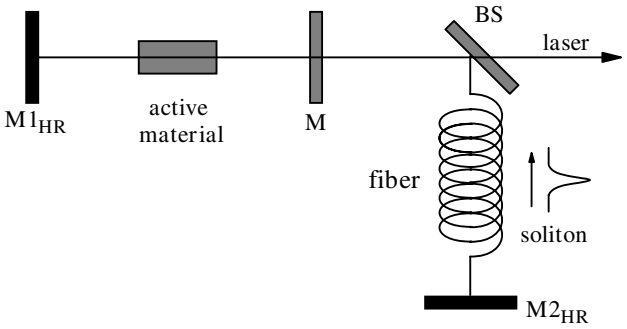

Fig. 6.84. Schematic of a soliton laser producing fs pulses

6.10.3.7 Active Mode Locking with AOM

Instead of or in addition to passive mode locking with a dye cell as shown in Fig. 6.78 (p. 463) an active mode locking device such as e.g. an acousto optical modulator (AOM) can be used for active mode locking [6.1149–6.1173]. This modulator adds oscillating losses into the resonator which are synchronized to the roundtrip time of the short pulses. Thus each pass will promote the short pulse and discriminate the nonsynchronized share of the radiation (see Fig. 6.85).

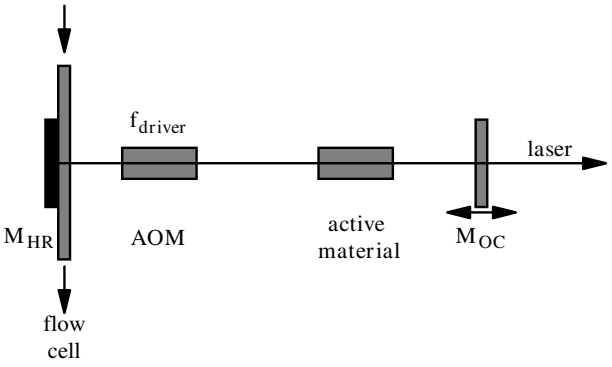

Fig. 6.85. Schematic of an active passive mode locked laser emitting ps pulses

The modulator is driven by an electrical sine generator in resonance with the modulator crystal. Each full period twice leads to minimal loss alignment and thus the driver frequency ν_{driver} has to be half of the roundtrip frequency:

$$\textbf{driver frequency} \quad \nu_{\text{driver}} = \frac{1}{2\tau_{\text{round}}} = \frac{c_0}{4L_{\text{opt}}} \tag{6.156}$$

with the optical length of the resonator L_{opt}.

The resonance of the modulator frequency has to be carefully adjusted with the laser roundtrip. Therefore, usually the optical length of the resonator is tuned to the frequency of the modulator with sub-mm accuracy. This can be achieved by shifting one of the resonator mirrors such as e.g. the output coupler in Fig. 6.85 (p. 470) or by additional variable delays using, e.g. more or less optical path through a prism arrangement. The exact alignment results in a very stable operation with ps pulses. Thus the stability of the oscillogram of the output pulses can be used as a criterion for aligning the laser.

Active mode locking is often combined with an additional passive one. The resulting pulses are usually as short as possible by the action of the passive mode locker and very stable from the active mode locker. Pulse-to-pulse fluctuations smaller than 5% are possible even for a selected single pulse out of the train in flash lamp pumped Nd:YAG lasers with pulse lengths around 30 ps and repetition rates of 30 Hz. Diode pumping allows much higher stabilities.

6.10.3.8 Active Mode Locking by Gain Modulation

Active mode locking can be achieved by synchronously pumping the laser with ps pulses of another laser [6.1174–6.1188] or of the electric pump circuit such as, e.g., in diode lasers. Thus the roundtrip time of the pumped laser has to be tuned very precisely to the repetition rate of the pump laser source or vice versa to achieve synchronization.

A typical application of this technique is the synchronous pumping of one or two dye lasers with a mode locked master oscillator such as e.g. an Ar-ion laser (see Fig. 6.86).

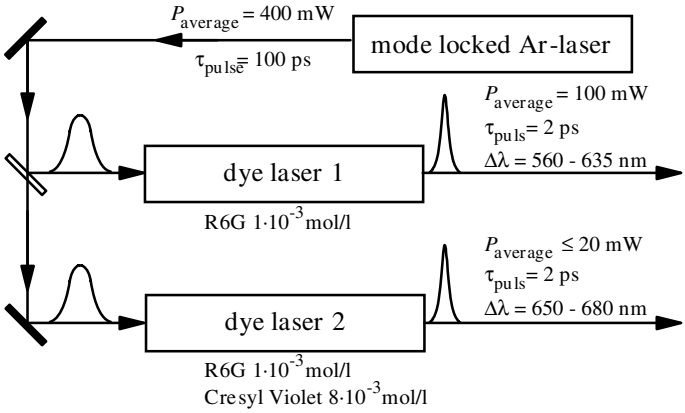

Fig. 6.86. Synchronously pumping of two dye lasers operating in the ps regime with a mode locked Ar laser

The resulting ps pulses of the dye lasers can be significantly shorter than the pump pulse duration. For example, with about 100 ps Ar laser pulses a dye laser pulse of 10 ps can be generated. A much shorter pulse duration can be achieved by the pumping of a second dye laser with the radiation of the first dye laser. In this way pulse durations of e.g. 100 ps to 55 ps to 0.6 ps were obtained for the Ar, the first and the second dye laser [6.1181].

If two dye lasers are pumped synchronously the two resulting pulses are synchronized better than the pulse width and can be tuned in wavelength. In this case the resonator lengths have to be carefully controlled using a piezo-driven mirror. This setup is useful, e.g. for pump and probe spectroscopy (see Sects. 7.7 and 7.8).

6.10.4 Other Methods of Short Pulse Generation

The spatial modulation of the gain in the active material can be used for the generation of pulses in the ps range as applied in distributed feedback lasers using e.g. dyes as active material. Other methods use a small gain area for producing short pulses.

6.10.4.1 Distributed Feedback (DFB) Laser

DFB lasers allow the generation of short pulses without mode locking [6.1189–6.1199]. With two crossed pump beams a gain grating can be excited in the active material as described in Sect. 5.3.9 (p. 296). The two beams can be produced by a holographic grating with a sine modulation reflecting the perpendicular pump beam in the +1 and −1 order, only, as depicted in Fig. 6.87.

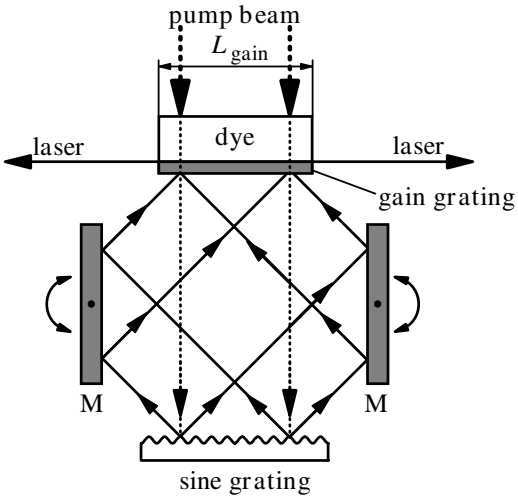

Fig. 6.87. Schematic of a distributed feedback laser pumped with ps pulses. For details about the gain grating see Fig. 5.28, p. 297

The angle of incidence and thus the emission wavelength of the laser can be varied by turning the mirrors M and synchronously moving the grating. The gain grating in the dye cell acts as a resonator by promoting these longitudinal laser modes with antinodes at the gain maxima. Thus a laser beam will be emitted towards the two opposite directions with a spectral resolution of approximately:

$$\text{spectral resolution} \quad \frac{\Delta\lambda_{\text{laser}}}{\lambda_{\text{laser}}} = \frac{\lambda_{\text{laser}}}{2L_{\text{gain}}} \tag{6.157}$$

with the optical length L_{gain} of the gain section in the material in the laser beam direction and the wavelength of the DFB laser λ_{laser}. It has to be small enough not to increase the laser pulse duration and thus L_{gain} has to be shorter than:

$$\text{gain length} \quad L_{\text{gain}} \leq \pi c_{\text{mat}} \Delta t_{\text{FWHM,pulse}} \tag{6.158}$$

with the desired pulse duration $\Delta t_{\text{FWHM,pulse}}$. E.g. a 1 ps pulse limits the maximum gain length to about 1 mm. The resulting spectral bandwidth of this laser is close to the theoretical uncertainty limit.

If this laser is pumped with short pulses it shows a spiking behavior as described in Sect. 6.10.1 (p. 451). If this laser is pumped just above threshold only one spike will be possible and the resulting DFB laser pulse will be much shorter than the exciting pulse. Ratios of about 50 have been reported [6.1194]. A typical dye laser is operated with Rhodamin 6G solution in alcohol as active material pumped by a frequency doubled Nd:YAG laser ps pulse of 25 ps. In this case the shortest observed DFB laser pulse duration is about 1 ps.

6.10.4.2 Short Resonators

If active materials with high gain are used in very short cavities a spiking operation as discussed in Sect. 6.10.1 (p. 451) can be observed but the pulse width of the resulting spikes will be much shorter as in solid-state lasers with resonator lengths of many 0.1 m.

Exciting dye solutions in cavities with lengths in the range of 1 mm, e.g. with the pump pulse of a Nitrogen laser at normal pressure with a duration of 500 ps can result in tunable dye laser pulses of a few 10 ps.

Even shorter wavelength tunable pulses can be produced with resonators of a few µm length filled with dye solution. In addition these resonators act as a Fabry–Perot system and thus by varying the resonator length the laser can be spectrally tuned. Again the bandwidth has to be large enough (see Sect. 2.9.8, p. 90) to allow for the desired short pulses. Further the gain coefficient has to be high enough to provide sufficiently high gain within the short cavity gain length. Both can be achieved in dyes or semiconductors. In diode lasers, pulse durations of a few ps are possible if the electrical pumping is fast enough.

Such a simple short cavity dye laser can be pumped by 10–30 ps pulses, e.g. with a pulsed Nd:YAG laser those radiation is frequency doubled or a trebled with nonlinear crystals to meet the excitation bands of the dyes.

6.10.4.3 Traveling Wave Excitation

In this scheme the excitation of the active material is applied by a short pulse which is moving with the same speed as the light inside the matter [6.1196, 6.1200–6.1203] as sketched in Fig. 6.88.

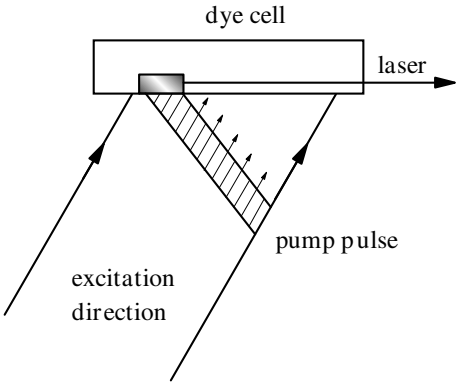

Fig. 6.88. Traveling wave excitation of a dye solution by a pump laser beam with delayed pulse across the beam for synchronized pumping of the generated laser pulse moving to the right side

Therefore the pulse has to be delayed transversely across the pump beam as shown in the figure, to be synchronized with the propagation of the laser pulse with velocity c_0/n. The laser beam is then produced by the superradiation of the excited area. Thus the transversal and longitudinal structure of the light beam is poor.

This scheme was used with discharge excitation in nitrogen lasers producing ns pulses. It can be applied for dye lasers in the near IR above 1 μm and it was considered for XUV generation [6.1200].

6.10.5 Chaotic Behavior

Laser emission can show temporal chaotic behavior of the emission [6.1204–6.1245, 6.1210–6.1239]. Theoretical investigations using the laser as a model system for chaos research are based on simple model systems based on the nonlinear wave equation as given in Sect. 4.3 and the time-dependent Schroedinger equation as given in Sect. 3.3.1 (p. 101) considering the energy levels of the active material and the interaction as a small distortion [e.g. 6.1210]. Further, using the approximations of a plane wave, slowly varying amplitudes, homogeneous transition and unidirectional ring laser operation, the three basic equations of this theory can be derived for the relevant quantities:

field

$$\frac{\partial}{\partial t}e_{\mathrm{th}}(t) = -\left(\mathrm{i}2\pi\nu_{\mathrm{res}} + \frac{1}{\tau_{\mathrm{res}}}\right)e_{\mathrm{th}}(t) + N_{\mathrm{total}}^{(V)} g_{\mathrm{th}} p_{\mathrm{th}}(t) \tag{6.159}$$

polarization

$$\frac{\partial}{\partial t}p_{\mathrm{th}}(t) = -\left(\mathrm{i}2\pi\nu_{\mathrm{mat}} + \frac{1}{\tau_{\mathrm{trans}}}\right)p_{\mathrm{th}}(t) + \Delta N^{(V)} g_{\mathrm{th}} e_{\mathrm{th}}(t) \tag{6.160}$$

inversion

$$\frac{\partial}{\partial t}\Delta N^{(V)}(t) = -\frac{1}{\tau_{\mathrm{long}}}(\Delta N^{(V)}(t) - \Delta N_0^{(V)}) - 2g_{\mathrm{th}}[e_{\mathrm{th}}(t)p_{\mathrm{th}} + \mathrm{c.c.}] \tag{6.161}$$

with the dimensionless parameters e_{th} and p_{th} which are related to the physical values of the electric field E and polarization P by:

$$E(t) = -\mathrm{i}\sqrt{\frac{2h\nu_{\mathrm{res}}}{\varepsilon_0 V_{\mathrm{mat}}}}e_{\mathrm{th}}. \tag{6.162}$$

and

$$P(t) = 2\frac{N_{\mathrm{total}}^{(V)}}{V_{\mathrm{mat}}}\mu_{\mathrm{mat}} p_{\mathrm{th}}(t) \tag{6.163}$$

The value g_{th}, which is not a gain coefficient in this case, follows from:

$$g_{\mathrm{th}} = \mu_{\mathrm{mat}}\sqrt{\frac{\nu_{\mathrm{res}}}{2h\varepsilon_0 V_{\mathrm{mat}}}} \quad \text{with} \quad [g_{\mathrm{th}}] = \mathrm{s}^{-1} \tag{6.164}$$

$N_{\mathrm{total}}^{(V)}$ describes the total number of particles in the volume V_{mat}, $\Delta N^{(V)}$ the inverted particles, $\Delta N_0^{(V)}$ the inverted particles without the laser field, ν_{res} the resonance frequency of the resonator, ν_{mat} the resonance frequency of the two-level system of the matter, τ_{res} the inverse resonator loss rate, τ_{trans} the transversal decay time which is the decay of the dipole moment, τ_{long} the longitudinal decay time which is the decay of the inversion and μ_{mat} is the dipole moment of the matter as a projection in the direction of the electric field vector. All these values are given as commonly used in these theoretical investigations.

If the corresponding relaxation rates are very fast the time derivatives of the particular differential equation can be neglected. The possible operation modes of these model lasers are determined by the relation of the resonator lifetime in comparison to the lifetimes of the inversion (in this research field, called the longitudinal relaxation time) and the polarization (transversal relaxation time) of the active material.

Thus *class A, B and C lasers* are distinguished. *Class A lasers* show a much longer resonator lifetime than the other lifetimes and thus only the derivatives of the e_{th} equation have to be considered. These lasers are therefore not chaotic. *Class B lasers* have comparable resonator and longitudinal lifetimes which are both longer than the transversal relaxation time. Thus

both differential equations for e_{th} and d_{th} have to be taken into account. These lasers can be forced into chaotic behavior by external influences such as e.g. external feedback. *Class C lasers* show comparable values of all three lifetimes and therefore all three differential equations are necessary for the description. Thus the system has three degrees of freedom and can therefore be chaotic by itself. For this purpose the laser has to be pumped about 20 times above threshold.

If further nonlinear elements are introduced in the laser resonator such as e.g. phase conjugating mirrors [6.1238] or crystals for frequency transformation, the laser emission can be chaotic in time and space. The theoretical description can be very complicated.

6.11 Laser Amplifier

Laser oscillators are limited in the brightness of their radiation especially if short pulses or very monochromatic light, very high output powers or pulse energies are required. Thus the amplification of laser light may be necessary. It allows the generation of peak powers in the PW range, average output powers of several 100 W to kW or pulse energies of several 10–100 J with diffraction-limited beam quality.

The laser amplifier contains an active material which is pumped as in oscillators but no resonator selects the light properties. Thus the properties of the amplified light are mostly determined by the properties of the incident light produced by the laser oscillator but some additional noise may occur.

The pumping of the active material of the laser amplifier is described in the same way as given for the oscillators in the previous Sects. 6.1–6.4 and 6.8.

Beam combining is applied besides or in addition to amplification for increasing the output power of laser systems. In best case this beam combining is obtained from a coherent set of sub beams which can be coherently coupled for a high power beam with very good beam quality and brilliance. These schemes can be based on special diffractive optic elements and/or optical phase conjugation. Much easier is the coupling of beams with different polarizations or different wavelengths using polarizer or e.g. gratings for the incoherent beam combining. Examples can be found in [6.1240–6.1248].

6.11.1 Gain and Saturation

Laser amplifiers show a gain or gain factor G_{amp} which is defined by the ratio of the intensities (powers or energies) of the light behind the amplifier I_{out} divided by the incident I_{inc}:

$$\textbf{gain factor} \quad G_{\mathrm{amp}} = \frac{I_{\mathrm{out}}}{I_{\mathrm{inc}}} \tag{6.165}$$

which is the same value as the transmission of the active material but shows values above 1.

The small or low signal gain $G_{\mathrm{amp,ls}}$ which can be obtained for small incident light intensities, which almost do not change the inversion population in the active material, is given by the cross-section σ_{laser} and the population inversion density in the active material ΔN_{amp} and the length of the active material L_{amp}:

$$\textbf{small signal gain} \quad G_{\mathrm{ls}} = \mathrm{e}^{\sigma_{\mathrm{laser}}\Delta N_{\mathrm{amp}} L_{\mathrm{amp}}} = \mathrm{e}^{g_{\mathrm{ls}} L_{\mathrm{amp}}} \tag{6.166}$$

with the low-signal gain coefficient g_{ls}:

$$\text{small-signal gain coefficient} \quad g_{\mathrm{ls}} = \sigma_{\mathrm{laser}}\Delta N_{\mathrm{amp}} \tag{6.167}$$

Losses in the active material are neglected. This is usually correct for modern laser materials. The losses can be introduced in these equations by an absorption coefficient a resulting in an additional expression aL_{amp} in the exponent.

The low signal gain G_{ls} can be as high as 10–100 in solid state lasers and several 1000 in dyes or semiconductors. The inversion population density can be calculated using rate equations as described in Sect. 5.3.6 (p. 277). On the other hand the gain can be measured and thus the inversion population density calculated from the known cross-section and matter length for a given setup.

If the light intensity reaches higher values in the range of the nonlinear or saturation intensity $I\!\!I_{\mathrm{nl}} = I_{\mathrm{nl}}/h\nu_{\mathrm{Laser}}$ (see Sect. 5.3) the population densities will be changed and the gain will decrease as a function of the propagation coordinate z. This can be modeled using the system of rate equations as given in Sect. 5.3.6 (p. 277). For three- and four-level schemes the equation for the inversion population density as a function of the intensity which is a function of time and space can be written as:

Three-level amplifier system:

$$\begin{aligned}\frac{\partial \Delta N(I\!\!I,t,z)}{\partial t} = &\left(W_{\mathrm{pump}}(t) - \frac{1}{\tau_{\mathrm{upper}}}\right) N_0 \\ &- \left(W_{\mathrm{pump}}(t) + \frac{1}{\tau_{\mathrm{upper}}}\right) \Delta N(I\!\!I,t,z) \\ &-2\sigma_{\mathrm{laser}}\Delta N(I\!\!I,t,z) I\!\!I(t,z)\end{aligned} \tag{6.168}$$

and

Four-level amplifier system:

$$\begin{aligned}\frac{\partial \Delta N(I\!\!I,t,z)}{\partial t} = &W_{\mathrm{pump}}(t) N_0 - \left(W_{\mathrm{pump}}(t) + \frac{1}{\tau_{\mathrm{upper}}}\right) \Delta N(I\!\!I,t,z) \\ &-\sigma_{\mathrm{laser}}\Delta N(I\!\!I,t,z) I\!\!I(t,z)\end{aligned} \tag{6.169}$$

with the pump rate W_{pump}, the lifetime of the upper laser level τ_{upper} and the total population density N_0.

Using these equations and the photon transport equation:

$$\left\{\frac{\partial}{\partial z} + \frac{1}{c}\frac{\partial}{\partial t}\right\} I\!\!I(t,z) = \sigma_{\mathrm{laser}}\Delta N(I\!\!I,t,z) I\!\!I(t,z) \tag{6.170}$$

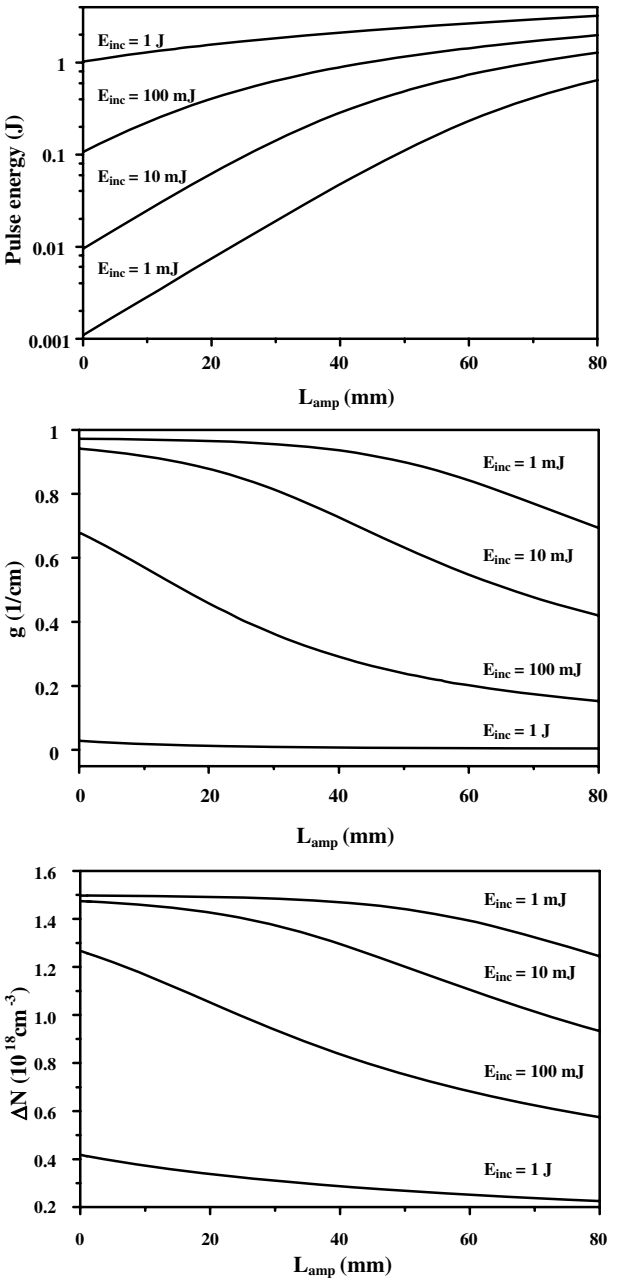

Fig. 6.89. Amplification of light from small signal value to saturation as a function of the length in the active material L_{amp}. Shown are the pulse energy E, the local gain coefficient g and the inversion population density ΔN for four different incident intensities pulse energies E_{inc} from 1 mJ to 1 J saturating the amplifier successively in this order

the resulting intensity increase and depopulation of the inversion can be calculated numerically as a function of space and time. Thus the gain is a function of time and space, too. The calculated results for the amplification of a ns pulse in a Nd:YAG laser amplifier are shown in Fig. 6.89 (p. 478).

The Nd:YAG rod was 80 mm long and 6 mm in diameter with a Nd concentration of $1.38 \cdot 10^{20}$ atoms cm^{-3}. It was assumed to be pumped with 16 J electrical power per flash lamp pulse of 140 µs duration. The electro-optical excitation efficiency was 4%.

In the saturation regime the amplification is decreased and thus the intensity increase is slowed down, the inversion population density and the gain decreased while the light is propagating through the amplifier.

In the small-signal region of the intensity $I \ll I_{\mathrm{nl}}$ the intensity increases exponentially with the length of the active material. It grows linearly in the saturation regime with $I \gg I_{\mathrm{nl}}$ [6.1249–6.1258]. The total energy extraction is higher as the incident pulse energy is larger but it saturates at high values markedly (above 100 mJ in this example).

6.11.2 Energy or Power Content: Efficiencies

The inversion population density in the amplifier material ΔN_{amp} represents a stored energy $E_{\mathrm{amp/V}}$ per amplifier volume V_{amp} which can be transformed to laser light during amplification:

$$\textbf{stored energy per volume} \quad E_{\mathrm{amp/V}} = \frac{hc_0}{\lambda_{\mathrm{laser}}} \Delta N_{\mathrm{amp}} \tag{6.171}$$

with Planck's constant h, and the laser wavelength λ_{laser}. This value can be obtained from the experimentally determined small-signal gain coefficient g_{ls} or vice versa by:

$$\textbf{stored energy per volume} \quad E_{\mathrm{amp/V}} = \frac{hc_0}{\lambda_{\mathrm{laser}} \sigma_{\mathrm{laser}}} g_{\mathrm{ls}} \tag{6.172}$$

with the emission cross-section of the laser transition σ_{laser}. Values of several J per cm^3 are possible in most laser materials (see Sect. 6.13).

The total stored energy is of course:

$$\textbf{total stored energy} \quad E_{\mathrm{amp}} = V_{\mathrm{amp}} E_{\mathrm{amp/V}} \tag{6.173}$$

and the efficiency of the amplification is the share of this energy used for amplifying the incident laser light. For pulsed lasers this energy content of the stored energy in the amplifier material can be used directly for this calculation.

For continuously operating laser amplifier systems the powers or temporally averaged powers have to be used.

The efficiencies such as quantum defect efficiency, quantum efficiency, opto-optical efficiency, electro-optical efficiency and total efficiency can be calculated as given in Sect. 6.3.6 (p. 379).

The main problems in building high-power amplifiers is damage and heating which decreases the quality of the amplified light. The limited efficiency

results in thermal loads of the active material (see Sect. 6.4). The wall-plug efficiencies are mostly below 10% and only a few active materials with low quantum defect such as e.g. Yb doped crystals or semiconductors, reach values of 20–50%.

6.11.3 Amplifier Schemes

Amplifier schemes are as diverse as laser oscillators with their properties such as low bandwidth, low noise, short pulses, high-powers and good beam quality. In the simplest case the amplifier is just a laser without a resonator in a single-pass supplied from a master oscillator in a *m*aster *o*scillator *p*ower *a*mplifier (MOPA) scheme. As a semiconductor amplifier it has a small size of, e.g., $1\,\mu m \times 10\,\mu m \times 1\,mm$. On the other hand regenerative amplifiers for ps and/or fs pulses contain, besides the multipass amplifier, also stretchers, compressors, switches, apertures and other optical components. The largest amplifier setups such as e.g. in the National Ignition Facility (NIF, USA) and the similar system in France built for fusion experiments contains more than 10 000 optical elements and many of them have an aperture of almost half a meter. The total size of these amplifier setups are in the 100 m region. Thus in each of the schemes discussed below the single amplifier can be expanded to a chain of two or many amplifiers in a row and several of these rows can be arranged parallel.

6.11.3.1 Single Pass Amplifier

This scheme is mostly useful for pulsed lasers or lasers with very high gain as diode lasers or dye lasers. The laser beam from the oscillator passes the active material once. To avoid damage in the amplifier the beam is expanded by a telescope as shown in Fig. 6.90.

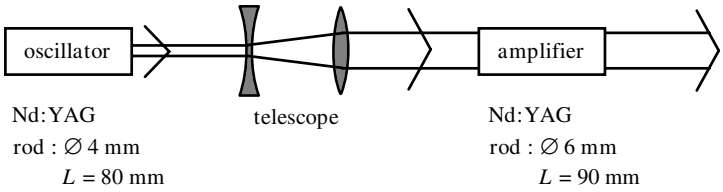

Fig. 6.90. Schematic of single-pass amplification in a Nd laser system with one amplifier

The telescope also allows the divergence of the oscillator beam to be changed. This type of amplification is often used in solid-state or dye lasers. In diode lasers mostly tapered amplifiers are used for increasing the beam cross section to avoid damage and obtain high powers. It can be necessary to avoid the back reflection of amplified light into the oscillator for stable operation

of it and also to avoid damage. Therefore high quality optical isolation may be demanded. The amplification can be as high as 10–30. In this scheme the saturation of the amplifier is often not completely reached. Therefore a second amplifier or a double-pass scheme can be applied. These single-pass amplifiers are useful for both ns and ps pulses. A typical Q switch pulse from the Nd:YAG oscillator pumped with 8 J with 25 ns pulse width and 17 mJ energy in the single and fundamental mode is, e.g. amplified to 55 mJ in the first amplifier which is also flash lamp pumped with 16 J and to 160 mJ at 1064 nm in the second amplifier which is flash lamp pumped with 16 J. A ns dye laser with two amplifiers can emit about 20 mJ with a pulse duration of 10 ns if it is pumped with about 200 mJ of a XeCl-excimer laser at 308 nm. A single 30 ps pulse from a Nd:YAG laser with an energy of 1 mJ can be amplified to about 10 mJ in a single-pass amplifier and up to 40 mJ are possible in a second amplifier. A diode laser with a cw output power of a few 10 mW can be amplified in one tapered amplifier to more than 5 W with good beam quality and narrow band width. Further examples are given in [6.1259–6.1268].

If the active material is very highly pumped superradiation or laser action between the amplifier surfaces has to be avoided, e.g. by Brewster angled arrangements or antireflection coatings.

6.11.3.2 Double Pass Amplifier

If in a single-pass of the laser light through the amplifier saturation cannot be reached a double-pass arrangement [6.1269–6.1273] may be used (see Fig. 6.91)

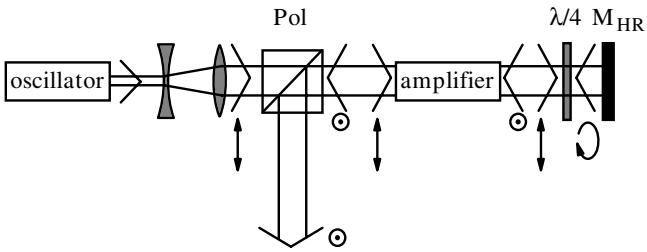

Fig. 6.91. Schematic of a double-pass amplifier setup. The polarizer in combination with the $\lambda/4$ plate achieves the out-coupling of the amplified light after the second pass

This can be necessary for longitudinal mono-mode or other special laser designs which may emit weak light powers which are below the nonlinear intensity of the amplifier material if an appropriate beam diameter is chosen.

In this scheme the incident oscillator light is linearly polarized in the plane of the paper of Fig. 6.91. Before or after the amplifier depending on the

polarization properties of the amplifier material the polarization is changed to circular by a quarter-wave plate. The high-reflecting mirror produces the second pass through the amplifier. Passing the quarter-wave plate on the way back again the polarization is changed to linear again but the direction is now perpendicular to the original one which is vertical in Fig. 6.92. Thus the polarizer reflects the light out of original path. The position of the quarter-wave plate determines the polarization of the light in the active material. If necessary a Faraday rotator can be used instead of the quarter wave plate.

Care has to be taken to not get to much light back into the oscillator. This amplified light can damage the oscillator components by the high intensity. Further it can disturb the mode selection in the resonator and thus its stable operation.

This double-pass scheme is again useful for ns or ps pulses. Typically it is applied for solid-state lasers. For example a 30 ps single pulse of a Nd:YAG laser with 1 mJ energy can be amplified with one double-pass amplifier to 25 mJ.

Double-pass amplifiers are especially useful in combination with phase conjugating mirrors as discussed in the last Subsection.

6.11.3.3 Multi Pass Amplifier

Several passes through the same zone of the active material of the multi pass amplifier [6.1274–6.1284] are useful for weak pulses as they are generated, e.g. in fs lasers. These pulses cannot saturate the gain in a single-pass. In particular in dye amplifiers very high gains can be achieved in short interaction lengths and thus the pulse broadening can be kept small.

The typical scheme of a multipass amplifier is given in Fig. 6.92.

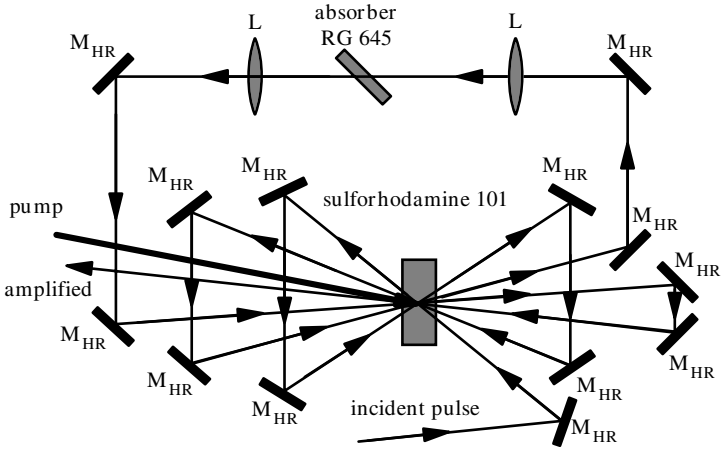

Fig. 6.92. Multipass amplifier for fs laser pulses with six transitions through the active material

In this example six passes of the laser beam are used. Even eight or twelve passes have been realized. In these cases additional lenses usually have to be applied to keep the small diameter of the laser beam in the active material. For the supression of superradiation from the amplifier a nonlinear absorber can be used as shown in Fig. 6.92 (p. 482).

For example in such a fs laser dye amplifier with six passes and sulforrhodamine 101 as active material which was pumped by frequency-doubled Nd:YAG laser light pulses with 10 ns duration and 10 mJ pulse energy, a single amplification of a factor of about 9 was reached resulting in an overall amplification of $5 \cdot 10^5$. The CPM laser pulse energy of 300 pJ at 620 nm was amplified to an output energy of 150 μJ. With a following single-pass Berthune cell dye amplifier (see Fig. 6.6, p. 366) a final output energy of 2 mJ with a pulse width of 100 fs was obtained.

6.11.3.4 Regenerative Amplifier

This type of amplifier operates as a seeded oscillator with active out-coupling after a certain number of roundtrips (see Fig. 6.93) [6.1285–6.1315]. Thus a multipass amplification with additional pulse shape regeneration is applied.

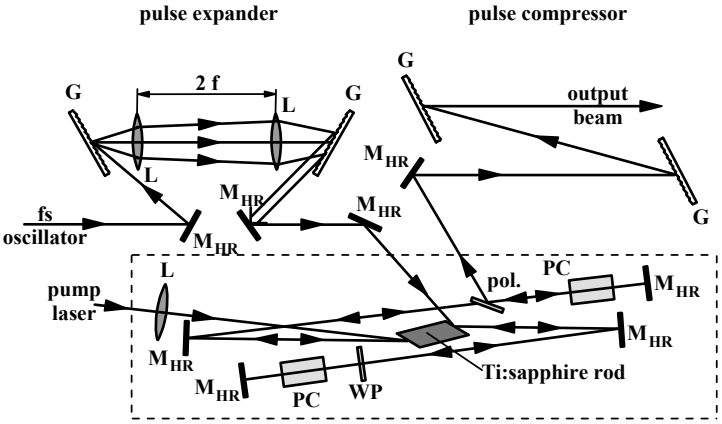

Fig. 6.93. Schematic of a regenerative amplifier

If fs pulses should be amplified the original short laser pulse is usually temporally stretched in a grating arrangement, as shown in the figure before it is fed into the amplifier. After the required number of passes through the amplifier material between the high reflecting mirrors M_{HR} it is out-coupled by switching the polarization via the Pockels cell PC. Then the pulse is recompressed to its original pulse shape or even providing a negative chirp for precompensation of further dispersion outside the laser in the experimental setup [6.1307–6.1315].

Very often this type of amplification is also used to reduce the repetition rate of the laser pulses from the MHz range to kHz or below. Therefore the regenerative amplifier is pumped with the lower repetition rate.

E.g. with a Ti:sapphire amplifier pumped by the frequency-doubled radiation of a Nd laser at 1 kHz an incident pulse of 8.5 nJ can be amplified to 1 mJ with a pulse duration of 100 fs or up to 2 ps. Thus the average output power is 1 W and the peak power 10 GW.

6.11.3.5 Double Pass Amplifier with Phase Conjugating Mirror

In the double-pass amplifier scheme phase conjugating mirrors can be applied to compensate phase distortions from the active material of the amplifier [6.1316–6.1357] (see also Sect. 4.5.14, p. 250). Thus the beam quality can be conserved although the high-power amplifier causes strong phase distortions in the single-pass. In the simplest case self-pumped phase conjugating mirrors (PCMs) based on stimulated Brillouin scattering (SBS) can be applied. The scheme is shown in Fig. 6.94.

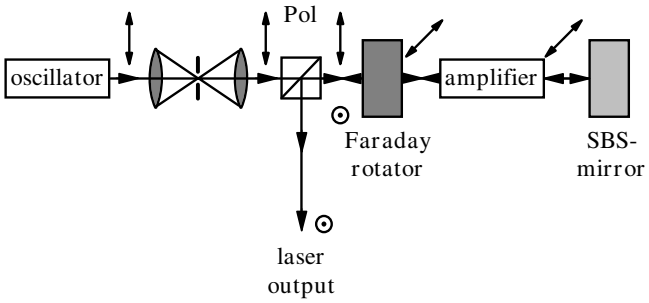

Fig. 6.94. Schematic of a double-pass amplifier with phase conjugating mirror (PCM) based on stimulated Brillouin scattering (SBS) for compensating phase distortions in the amplifier material and thus for improving the beam quality

In this double-pass scheme the temporarily constant (as long as the light is propagating back and forth), phase distortions, e.g. from the thermally induced refractive index changes in solid-state laser rods, are compensated in the second pass through the active material because the wave front is phase conjugated in the SBS mirror. More details are given in Sect. 4.5.14 (p. 250).

With solid-state double-pass MOPAs with phase conjugating mirrors average output powers of more than 100 W were obtained from a single rod amplifier [6.1324] and kW were achieved with diode pumped slab amplifier chains with diffraction-limited beam quality at TRW and LLNL. Because of the high "threshold" of the SBS mirrors up to now, pulsed radiation can usually be phase conjugated only in these systems. The highest pulse energies achieved in SBS-PCM-MOPAs were above 100 J and the smallest values are

less than 10 μJ. Waveguide geometry allow phase conjugating SBS mirrors for cw radiation, too. Phase conjugating mirrors based on the photo-refractive effect have very low thresholds below 1 W but they show very slow reaction times. They have not yet been used for high-power lasers.

6.11.4 Quality Problems

The laser amplifier usually shall amplify the laser light and conserve its properties, but the laser amplifier is itself a nonlinear optical device and thus it will change the properties of the light. Thus precautions are necessary to conserve low noise, beam quality, pulse duration, and polarization.

6.11.4.1 Noise

The laser amplifier produces additional noise in the laser radiation by spontaneous emission in the active material [6.1358–6.1376]. This can decrease the spectral, temporal, spatial and polarization quality of the laser light. Some improvements may be possible by using linear filters to conserve, e.g. the spectrum and polarization of the light. Further, the geometrical construction with small apertures for the laser beam can reduce the share of spontaneous emitted light in the beam.

If a linear polarized Gaussian beam of the spectral width $\Delta\nu_G$ around the center frequency ν_G is amplified in an amplifier with the low signal gain factor $G_{amp,0}$ an additional noise power P_G will occur in the output unavoidable from the amplified spontaneous emission [Weber]:

$$P_G = (G_{amp,0} - 1)\frac{N_{upper}}{\Delta N} h\nu_G \Delta\nu_G \tag{6.174}$$

with the inversion population density ΔN and the population density of the upper laser level N_{upper}. If the bandwidth or the spatial cross section of the amplified beam is larger than that of the incident Gaussian beam the noise power will be linearly increased. Thus spectral, spatial and polarization filtering may be necessary to realize this minimum.

As an example, a diode pumped Nd:YAG amplifier with 3.600 W optical pump power from the diodes will allow a maximum average output power of about 900 W in a Gaussian beam if its depolarization is compensated assuming excitation and extraction efficiencies of about 0.5 each. The resulting average noise power is about 10^{-7} W for the whole emission band width of about 120 GHz and only $5 \cdot 10^{-11}$ W for a bandwidth of 40 MHz.

In some cases additional nonlinear absorbers can be applied to supress the noise as, e.g. shown in Fig. 6.92 (p. 482). In any case superradiation from the amplifier should be avoided by choosing sufficiently short amplifier lengths or low gain coefficients. Parasitic resonators for the amplifier radiation have to be excluded by Brewster angles and/or careful antireflection coating of all relevant optical surfaces.

6.11.4.2 Beam Quality

The transversal shape of the beam can be changed by phase distortions, amplitude distortions and other diffraction effects, e.g. from the limited aperture of the amplifier. Geometrical conditions of pumping and the diameter of the incident light are important parameters for good beam quality.

Phase distortions can be compensated by phase conjugating mirrors or other devices, such as e.g. active controlled adaptive mirrors in double-pass arrangements. Diffraction-limited beam quality was obtained in this way (see Sect. 6.11.3, p. 480).

Amplitude distortions can not in general be compensated and thus homogeneous amplification profiles as a result of well designed pumping is a key issue for good beam quality. Thermally induced birefringence as in solid-state laser rods can be avoided using laser materials with strong natural birefringence such as e.g. Nd:YALO (see Sect. 6.4.2, p. 385). Further, the birefringence can be compensated by a double amplifier scheme with 90° rotator in between as described in Sect. 6.4.2 (p. 385). In a double-pass amplifier the scheme can be simplified by using one amplifier and a 45° rotator in front of the mirror.

Phase distortions and birefringence can be compensated in a double-pass amplifier with a phase conjugating SBS mirror and separate polarization treatment as shown in Fig. 4.53 (p. 254) in Sect. 4.5.14 (p. 250). In this scheme the two polarization directions are interchanged after reflection in the phase conjugating SBS mirror.

Diffraction losses should be avoided by choosing a sufficiently small diameter of the incident light which should be about 1.5 times smaller than the active material. The best value has to be found experimentally. This difference in pumped-to-mode volume causes a lack in efficiency. Therefore flat-top profiles for propagation through the amplifier material have been suggested.

Finally the beam quality can be improved inside the amplifier setup or after amplification with spatial filters as described in Sect. 6.6.10 (p. 413) and shown in Fig. 6.44 (p. 414). Because of the high-powers the mode apertures usually have to be used in vacuum avoiding optical breakdown in air and sometimes it may even be necessary to cool them with a water cooler.

Some other methods for conserving the quality and polarization of the beam such as, for example, self-focusing, are discussed in [6.1377–6.1382].

6.11.4.3 Pulse Duration

As a consequence of the dispersion in the amplifier material and other associated optical components the pulse duration of ps but especially fs pulses can be lengthened in the amplifier. Thus special treatment for compensation is necessary. Chirp compensating elements or nonlinear absorbers (see Fig. 6.92, p. 482) can be applied.

For high-power pulse amplification the laser pulses are often temporally stretched by more than 100 or 1000 times to decrease the peak power while

containing the pulse energy (see Sects. 6.11.3 (p. 480), 6.14.2.1 (p. 523) and [6.1383–6.1396]). Thus the intensity damage threshold of the optical components becomes noncritical even for PW-pulses. A typical scheme is given as part of Fig. 6.93 (p. 483). Sometimes ns-pulses are compressed behind the amplifier using SBS pulse compression by a factor of about 5–10 reaching about 1 ns (see Sect. 6.14.2.2, p. 523).

6.12 Laser Classification

Almost all physical and technological properties of the laser are used for classification. For practical purposes wavelength, output power and operation mode (pulsed or cw) are most prominent.

6.12.1 Classification Parameters

A list of prominent laser properties often used for classification in science and technology reads as follows:

- *Active Material*
  Lasers are often named after their active material. This is done directly as in the Nd:YAG laser, or in classes such as the excimer laser, solid-state laser and so on. All properties of the active material are used for this grouping. Details are given in Sect. 6.2.
- *Pump Mechanism*
  As described in Sect. 6.3 the active material can be pumped by other lasers, lamps or other radiation, electric discharges or chemical reactions. Pumping can be obtained continuously (cw) or pulsed. The pumping requirements are different for three- or four-level laser schemes (see Sect. 6.2).
- *Wavelength*
  The wavelength ranges can be classified as X-ray (<1 nm), XUV (1–50 nm), UV (100–300 nm), Vis (400–700 nm), NIR (800–1500 nm), IR (2–10 μm) and far IR (>10 μm) with the wavelengths as rough values.
- *Temporal Operation: Pulse Width*
  cw, quasi-cw and pulsed lasers are distinguished. Pulsed lasers can be classified for long pulses (>1 μs) or short pulses as ns, ps and fs pulses.
- *Average Output Power*
  Average output powers may be classified in the ranges <1 mW (not dangerous), <1 W, <10 W, <50 W, <100 W, <1 kW and >1 kW.
- *Bandwidth*
  Laser bandwidths can be larger than 50 nm and smaller than 10^{-12} nm (<1 Hz). Typical values are <1 nm for molecule laser without further restrictions and 10^{-3} nm (GHz) to 10^{-6} nm (MHz) for lasers with narrow bandwidth.
- *Main Application*
  The main applications are described in Sect. 1.5 and Fig. 1.4 (p. 7). Material processing, spectroscopy, communication and medicine are e.g. main fields.

These properties are given for the different types of lasers in the following Section.

For theoretical investigations using the laser as a model system the possible chaotic behavior of the temporal emission is used for classification (see Sect. 6.10.5, p. 474). Thus *class A, B and C lasers* are distinguished.

From the point of view of potential eye or skin damage, the lasers are divided into five safety classes, 1, 2, 3A, 3B and 4, as will be discussed in Sect. 6.16 in more detail.

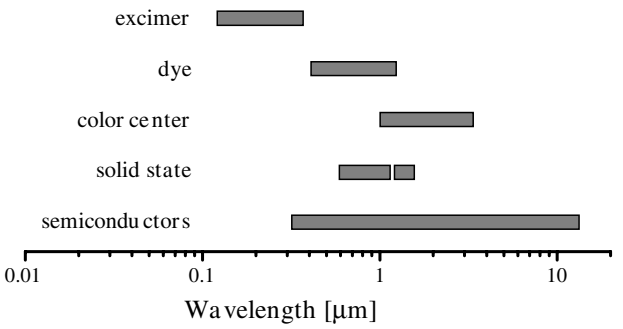

Fig. 6.95. Wavelength ranges in which tunable lasers can be achieved. The tuning range is much smaller than the total ranges shown for these lasers

6.12.2 Laser Wavelengths

From the application point of view the laser wavelength [6.1397] is often the most important parameter. In Fig. 6.95 the wavelength ranges of tunable lasers are depicted. These lasers can be grouped for semiconductor or diode lasers, solid-state lasers, color center lasers, dye lasers and excimer lasers.

The tuning ranges of the single lasers are much smaller than the given total ranges. The laser emission wavelengths can be extended by frequency conversion as second, third, fourth harmonic generation as well as sum and difference frequency generation and other techniques (see Sect. 6.15).

A general overview of typical values of laser wavelengths, tunability range per active material, the orders of magnitude of the pulse width and of the average output power, the beam quality and a rough estimate of the efficiency are given in Table 6.13 (p. 489).

Many other laser materials and their optical transitions, and e.g. free electron lasers and XUV lasers, are not considered in this table. All laser wavelengths can be converted or shifted and thus the wavelength scale is continuously filled from UV to IR with possible laser radiation.

6.12.3 Laser Data Checklist

Laser prospects and data sheets do not always contain all relevant parameters of the laser output and the installation and operation requirements. A description of such parameters is given in Sect. 6.12.1 (p. 487). The following features may be checked for a sufficient set of information. It should

be noted that, because lasers can still be quite expensive, details such as the used definition of the beam quality, background levels, jitter, power and pointing stabilities etc. and also installation, maintenance and repair costs may be important decision parameters in comparing different devices. Thus the following list may be used as a guideline for the evaluation.

Table 6.13. Wavelength, tunability range, pulse width range, average output power, beam quality and wall-plug efficiency of some lasers

Wavelength (μm)	Range (nm)	Laser	Pulse width	Average output	Beam quality M^2	Efficiency (%)
0.152		F_2-excimer	ns	10 W		
0.193		ArF-excimer	ns	10 W	multimode	<2
0.248	1	KrF-excimer	ns	10 W	multimode	<2
0.266		4xNd laser	μs,ns,ps	<1 W	1	0.005
0.308	1.5	XeCl-excimer	ns	10 W	multimode	<2
0.3-1.1	50	dye laser	μs,ns,ps	10 W	3	
0.3250		HeCd-laser	cw	200 mW	1	0.1
0.3371		N_2-laser	ns	100 mW	multimode	<0.1
0.351		XeF-excimer	ns	10 W	multimode	<2
0.355		3xNd laser	μs,ns,ps	5 W	1	0.04
0.4-1.0	20	dye laser	cw	W	1	0.2
0.41-0.415		GaN-diode	cw, ns	50 mW	<5	15
0.4416		HeCd-laser	cw	10 mW	1	0.1
0.4880		Ar^+-laser	cw	10 W	1	<0.1
0.5105		Cu-vapor laser	ns	10 W	1	1
0.532		2xNd laser	cw	100 W	5	0.5
0.532		2xNd laser	μs,ns,ps	10 W	1	<0.5
0.5435		HeNe-laser	cw	1 mW	1	0.1%
0.5782		Cu-vapor laser	μs,ns	10 W	1	1%
0.6328		HeNe-laser	cw	10 mW	1	0.1
0.6471		Kr^+-laser	cw	W	1	<0.1
0.6943		ruby-laser	μs,ns	W	5	<1
0.7–0.82		alexandrite	μs,ns,ps	50 W	1	<2
0.7–1.1	300	Ti-sapphire	cw,μs–fs	50 W, 1 W	1	<1
0.72–0.84		Cr:LiCaF	cw–fs	W	1	<10
0.75–1.0		GaAs-diode	cw,ms	1 W	300	40
0.78–1.0		Cr:LiSAF	cw–fs	1 W	1	<2
1.030		Yb-fiber	cw–ps	W–kW	1	
1.030		Yb:YAG	cw-ps	kW, 100 W	10, 1	10
1.04–1.08		Nd laser	cw–ps	kW, 100 W	30, 1	5
1.1–1.6		InGaAs-diode	cw–ms	mW	300	40
1.44		Nd laser	cw–μs	W	3	1
1.4–1.6		color center	μs,ns	100 mW	1	0.01
1.54	0.3	Er-fiber	cw	10 W	1	
1.55	50	Cr:YAG	μs–ps	W	1	0.5
2.06		Ho-laser	μs,ns	W	5	
2.6–3.0		HF-laser	cw–ms	100 W	10	
2.9		Er:YAG	μs,ns	10 W	1	1
5–6		CO-laser	cw	kW	1	20
9–11,10.6		CO_2-laser	cw–μs	kW	1	20

6.12.3.1 Output Data

- *temporal mode of operation*
  - cw, quasi-cw or pulsed operation
- *average output power*
  - maximum average output power
  - stability and fluctuations of output power and noise
  - variability of output power
- *pulse energy*
  - maximum pulse energy which may be a function of the repetition rate
  - stability and fluctuations of pulse energies
  - variability of pulse energies
- *pulse width and shape*
  - temporal structure such as e.g. single pulses or bursts
  - pulse width of single pulses (>1 µs), ns, ps or fs
  - shape of the single pulse such as e.g. Gaussian, rectangular
  - substructure of single pulses such as e.g. modulations, satellites
  - background
- *repetition rate*
  - tuning range of repetition rate
  - pulse-to-pulse jitter
- *wavelength*
  - peak wavelength(s)
  - bandwidth
  - tuning range
  - background radiation
  - short and long time stability
- *wavelength conversion possibilities*
  - availability of second, third or fourth harmonics
  - available optical parametric oscillators or amplifiers
  - Raman shifter
- *beam quality and divergence*
  - beam quality should be given as M^2 (with power content)
  - far-field divergence of the laser beam
  - dimensions of the cross-section of the laser beam
  - position of the beam waist (inside the laser) would be helpful

6.12.3.2 Installation and Connection to Other Devices

- *trigger, jitter and delay*
  - voltage, impedance and timing of trigger signal to fire the laser pulse
  - delay between triggering and laser pulse
  - jitter and drift between trigger signal and laser pulse
  - which trigger (and pre-trigger) signals are available from the laser for triggering of other devices

- *installation requirements*
  - size of laser head, power supply and cooler
  - position and direction of the laser beam(s)
  - necessary gas supply (quality of gases)
  - electrical power and voltage
  - weight
  - vibrational isolation
  - water and/or air cooling
  - air conditioning
  - dust freeness
  - ventilation, e.g. for ozone
- *possible distortions*
  - electromagnetic fields
  - distortions at power lines
  - mechanical vibrations
  - acoustic noise

6.12.3.3 Operation and Maintenance

- *operation requirements and maintenance*
  - necessary changes of gases or liquids such as dyes
  - effort required to change components such as diodes, flash lamps, laser tubes and their lifetime
  - cleaning
  - realignment cycles
  - lifetime of crystals, heating requirements
  - maintenance of vacuum and other pumps
- *handling*
  - warming-up time
  - computer controlling
  - education of operator

6.12.3.4 Prices and Safety

- *prices*
  - price and lifetime of the system
  - lifetime and price of expensive and short-lived components such as flash lamps, diodes, laser tubes, mirrors, crystals, thyratrons
  - operating price of electrical power, cooling, air conditioning, and so on
  - price of transportation, installation and maintenance
- *safety conditions*
  - laser safety classes
  - electrical safety
  - chemicals

This catalog can be used as a checklist. A clear definition of which combinations of these parameters can be obtained is important.

6.13 Common Laser Parameters

In this section some basic values for some common types of mostly commercially available lasers are collected in tables. Details, variations and new systems should be checked from the specialized literature, the large laser conferences and with the laser companies. Some perspectives may be estimated from the given references, representing mostly scientific results. Further parameters of the lasers and the active materials are given in Tables 6.2 (page 364, Quantum defect), 6.3 (page 384, thermal properties), 6.4 (page 388, shock parameter), 6.10 (page 424, stability range), 6.11 (page 430, spectral properties), 6.12 (page 438, cross sections and life times) and 6.13 (page 489, wavelength, power).

6.13.1 Semiconductor Lasers

Semiconductor laser diodes [6.1398–6.1402] are small devices with output powers of a few W. High power laser are built as quantum well structures with, e.g., up to 20 gain guided regions on the same chip as shown in Fig. 6.96.

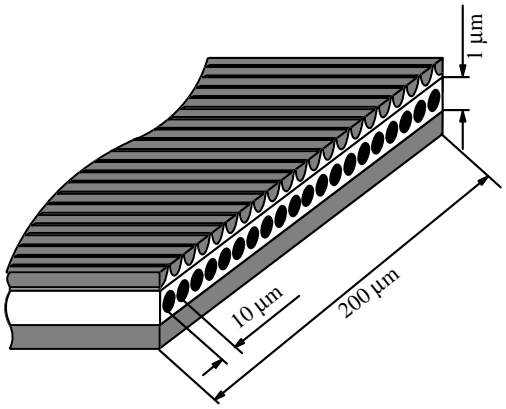

Fig. 6.96. Schematic of a power diode laser consisting of 20 separate quantum well structures on the same chip. The whole structure is about 1 mm deep

A single stripe of this figure can be packaged as a single diode laser which emits a few mW usually with good beam quality as known, e.g., from laser pointers. The incoherent coupling of their emission in power lasers as shown in Fig. 6.96 or in even larger arrangements as shown below will decrease their beam quality significantly. This can easily be calculated by considering the geometrical increase of the emitting area and constant beam divergence. Only *coherent coupling* schemes or different concepts as oscillator amplifier setups as well as tapered structures allow for higher output powers with good beam quality or even high brilliance.

Diode lasers are applied in data and communication technologies such as in CD players, in fiber communication, in bar-code readers, as well as in laser pointers. They can be coupled into fibers.

Diode bars are arrangements of about 10 to 25 of such lasers of Fig. 6.96 (p. 492) on one chip as depicted in Fig. 6.97.

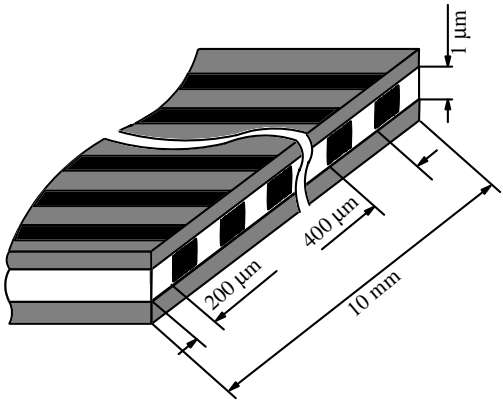

Fig. 6.97. Schematic of a diode bar emitting up to 100 W average output power. The whole structure is about 1 mm deep. Horizontally this bar is built by, e.g., 25 diode lasers as shown in Fig. 6.96 (p. 492). The vertical dimension is strongly enlarged in the drawing as the numbers show

These bars produce more than 50 W average output power but this light shows very poor beam quality. Therefore these lasers are mostly used for diode pumping of high-power solid-state lasers. The beam shape of the diode bar light with high divergence in the region of 1 rad in the fast axis (vertical in the figures) with diffraction limited beam quality from a source of 1 µm in combination with low divergence in the range of 100 mrad from a 10 mm emitter with very poor beam quality ($M^2 \approx 60$) is well suited for side pumping of solids state laser rods or slabs resulting in long lines. For end pumping of rods or pumping of fibers or disks, beam shaping optics have to be used. Crossed cylinder lenses, light ducts or other optical elements are used for this purpose and the light of the two axes can be equalized in shape, divergence and beam quality to reach the best possible average.

Bars cannot typically be air cooled as with single diodes. Peltier elements or water microcoolers have to be applied. Thermal expansion and other effect can lead to bending of these bars in the µm range, which is called smile.

For even higher powers these bars can be arranged in stacks of 3–20 or more bars. These stacks can be mounted together resulting in diode power block arrays containing 50 or more bars emitting many kW of diode laser light (see, e.g. Fig. 6.10, p. 369). The beam quality of these arrangements decreases linearly because these lasers emit not coherent with respect to each other. Thus one of the future key questions is the coherent coupling for improving the beam quality of these lasers. However, the smile and all other geometrical defects have to be much smaller than the wavelength for reproducible constructions.

Further key issues of these lasers are lifetime, cost and reproducibility, e.g. of the center wavelength and divergence. Besides the already established GaAs chip technology resulting in red and infrared emission, new structures based on GaN were developed. These devices operate in the blue region and, because of the high market demands (e.g. DVD player and laser TV), strong further progress can be expected. The emission wavelengths range from 370 to 470 nm with output powers in the range of 20 mW to more than 100 mW but lifetime is not sufficient in all cases. A 410 nm mid wavelength with 60 mW output power can be purchased today. New laser structures and new compounds may be developed in the next few years. Vertical emitting diodes (VCSELs) may serve as an example. Prices are expected to drop in the near future.

6.13.1.1 Single-Diode Lasers

Typical laser properties of today's diode lasers [6.1403–6.1440] are given in Table 6.14. These diode lasers are used as laser pointers, in CD players, for aligning purposes and for communication technologies. Laboratory setups may soon become commercial products. 1 W average output power with diffraction-limited beam quality has been reported using an external resonator [6.756]. With external resonators the band width can be decreased to 25 pm for IR lasers with 0.4 W output power and tuning ranges of 30 nm [6.1444]. Single longitudinal mode lasers with external cavity and comparable tuning ranges are available in the 100 mW region. With Bragg index gratings on the chips of the distributed feed back (DFB) diode lasers single mode emission with band widths of less than 10 MHz can be obtained with several 100 mW, good beam quality and a small tuning range of about 1 nm (e.g. 0.06 nm/K). Narrow bandwidth lasers are described and external resonators are used for improving beam quality and spectral selection [6.1441–6.1446]. Pulsed operation is reported in [6.1447–6.1458]. Frequency doubling was realized even in cw operation especially using poled SHG crystals [6.1459–6.1463]. With single amplifiers which are usually tapered these output powers can be enlarged to several W [6.1470, 6.1471].

Laser with blue emission are described in [6.1435–6.1440, 6.1464–6.1469].

Table 6.14. Some typical properties of diode lasers

	GaAs			
Active material	GaAlAs or GaAs			
wavelength	630–1800 nm 780 nm for CD player, 633–675 nm pointer around 1.3 and 1.55 µm for fiber communication			
Level scheme	similar to 4			
Emission cross-section	$1 \cdot 10^{-19}$ cm^2			
Lifetime upper laser level	4 ns			
Length of active material	0.2–2 mm			
Typical concentration	10^{17} cm^{-3}			
Refractive index	3.5			
Operation mode	cw, quasi-cw (modulation up to 5 GHz)			
Pump mechanism	electric current at a voltage of 2–3 V gain guided or index guided			
Setup	single emitter	coupled emitters	fiber coupled	external resonator
Bandwidth		4 nm		14 MHz
Average output power	1–10 mW	$\leq$ 2 W	1–100 mW	$\leq$ 1 W
Beam quality (M^2)	$\approx$ 3	60 slow axis 1 fast axis	$\approx$ 1	$\approx$ 1
Wall-plug efficiency	$\leq$ 40%		$\leq$ 20%	$\leq$ 20%
Cooling system	air	air, Peltier	air, Peltier	air
Remarks	lifetime $\leq$ 10000 h			

6.13.1.2 Diode Laser Bars, Arrays and Stacks

Diode laser grouping allows very high output powers from small laser devices with high wall-plug efficiency but poor beam quality [6.1472–6.1478]. Commercial systems are usually built with fiber output. Beam shapers are used before the diode laser light is coupled into the fiber inside the device. Today's systems deliver up to 6 kW from a fiber with 1.5 mm diameter and $NA = 0.22$ at 940 nm which is a beam propagation factor of 560. Several approaches have been reported to improve the output parameters of these laser bars, as e.g. beam shaping and beam combining. Examples are given in [6.1479–6.1484].

Table 6.15. Some typical properties of commercial diode lasers and diode laser bars

	GaAs – bars, arrays and stacks			
Active material	GaAlAs or GaAs			
Wavelength	630–1800 nm 808 nm for Nd-laser pumping 940 nm for Yb-laser pumping			
Level scheme	similar to 4			
Emission cross-section	$1 \cdot 10^{-19}$ cm^2			
Lifetime upper laser level	4 ns			
Length of active material	0.2–2 mm			
Typical concentration	10^{17} cm^{-3}			
Refractive index	3.5			
Operation mode	cw or pulsed by electrical switching with duty cycles $\leq 30\%$			
Pump mechanism	electric current with voltages of 2–3 V			
Setup	gain guided or index guided diode bar of 25 diodes	stack of e.g. 10 bars	array, e.g. 6 stacks	fiber coupled
Bandwidth	≈ 4 nm			
Average output power	30–50 W	≤ 500 W	≤ 3 kW	≤ 6 kW
Peak power (pulsed)	≤ 200 W	≤ 2 kW	≤ 10 kW	≤ 600 W
Beam quality (M^2)	2000 slow axis, 1 fast axis	2000 and 6000 (300*)	12 000 and 6000 (300*)	≈ 700
Wall-plug efficiency	$\leq 40\%$			
Cooling system	Peltier, water	water	water	Peltier, water
Remarks	lifetime ≤ 10000 h			

* With well-designed collimators for the fast axis of the emitted beam the beam quality can be improved to this value.

6.13.1.3 Vertical Cavity Surface-Emitting Lasers (VCSEL)

The short resonator length of VCSELs [6.1485–6.1501] allows narrow bandwidths of a few GHz, high-frequency stability and fast modulation of several GHz. Wavelength uniformity of less than 2 nm can be guaranteed. Arrays of 10s of single VCSELs can be produced to increase the output power. With active resonator length tuning using a small air gap between the output coupler and the active semiconductor, wavelength tuning over about 20 nm at 960 nm has been reported. Thus these lasers seem to be well suited e.g. for wavelength division multiplexing (WDM) in communication technologies. Because of their high geometrical precision these lasers may be used for coherent coupling or other related applications such as, e.g. beam steering in the future.

Table 6.16. Some typical properties of vertical cavity surface-emitting lasers (VCSEL)

	VCSEL	
Active material	InGaAs	
Wavelength	760–970 nm	
	(950 ± 20) nm, (850 ± 10) nm, (770 ± 10) nm	
Level scheme	similar to 4	
Emission cross-section	$1 \cdot 10^{-19}$ cm^2	
Lifetime upper laser level	4 ns	
Length of active material	wavelength (e.g. 0.950 µm)	
Typical concentration	10^{17} cm^{-3}	
Refractive index	3.5	
Operation mode	cw, quasi cw (modulation up to 5 GHz)	
Pump mechanism	electric current with voltages of 2–3 V	
Setup	single emitter	arrays (10×10)
Bandwidth	≤ 0.1 nm possible	
Average output power	≈ 1 mW	150 mW
Beam quality (M^2)	1	200 (8*)
Wall-plug efficiency	$\leq 57\%$	
Cooling system	air, Peltier	
Remarks	Lifetime $\leq 10\,000$ h	

* With special microlens collimators the beam quality can be improved to this value representing the number of linearly coupled lasers.

6.13.2 Solid-State Lasers

Solid-state lasers cover the whole field of photonics applications and thus a wide variety of systems is offered. Overviews can be found in [M33, 6.1502–6.1507]. Microchip lasers with output powers in the mW to W range are available as well as kW systems. PW systems are built with respect to fusion experiments. New laser and host materials may become important in the near future.

Typical laser atoms (ions) are Nd, Cr, Ti, Yb, Er, Pr. Solid-state laser host materials can be crystals, glasses, ceramics and organic matter. The crystals can be fluorides or oxides. Typical crystals are YAG ($Y_3Al_5O_{12}$), YALO or YAP ($YAlO_3$), sapphire (Al_2O_3), GGG ($Gd_3Ga_5O_{12}$), GSGG ($Gd_3Sc_2Al_3O_{12}$), LiSAF ($LiSrAlF_6$), LiCaF ($LiCaAlF_6$), fosterite (Mg_2SiO_4), YLF ($LiYF_4$), YVO (YVO_4), $GdVO_4$ and KGW (KGD (WO_4)). Glass materials are phosphate or silicate glasses. Codoping with other atoms may increase efficiency or allows for other pump sources. Examples are codoping in Nd:Ce:YAG or Ho:Cr:TM:YAG.

Many combinations have been tried in laboratory setups (see references in Subsections). The final results are crucially dependent on the quality of the investigated material. This is important for chemical impurities and for the optical quality. Therefore new combinations may become important in future and the technology for these materials will be developed to the necessary stage if the market demands it.

Other key issues for solid-state lasers in competition with other lasers are beam quality, efficiency, lifetime, reliability and price. The beam quality for high-power applications is often required to be below $M^2 < 5$ and the wall-plug efficiency should be better 10%.

6.13.2.1 Nd:YAG Lasers

Nd laser [6.1543–6.1637] are very common because of their simple construction, reliability and large variability. Besides Nd:YAG [e.g. 6.1508–6.1588], Nd:YALO (also called Nd:YAP) [e.g. 6.44, 6.204, 6.475, 6.779, 6.878, 6.1152, 6.1589–6.1597] laser rod geometries are also applied. Nd:YAG is usually diode pumped at 808 nm and Nd:YALO should be pumped at 803 nm. Frequency doubling (SHG), tripling (THG) and double doubling (FHG) is very common with these lasers, producing green and blue light (see Sect. 6.15). High powers with good beam quality are realized with slabs [6.1598–6.1605].

Similar results are obtained with Nd:YLF [6.1606–6.1615]. The better thermal conductivity, smaller thermal lensing and natural birefringence allow better beam quality of diffraction-limited pulses up to about 50 W. The last fact is also true for Nd:YALO which shows higher efficiency. The stronger thermal lens can be compensated, e.g. by phase conjugating mirrors [6.475]. Other Nd materials are investigated in [6.1616–6.1638]. Nd ceramic lasers are described in [6.1639–6.1648].

Table 6.17. Some typical properties of commercial Nd:YAG lasers

	Nd:YAG laser			
Active material	$Nd^{3+}:Y_3Al_5O_{12}$			
Wavelength	1064 nm			
Level scheme	4			
Emission cross-section	$3.2 \cdot 10^{-19}\,cm^2$			
Lifetime upper laser level	230 µs			
Length of active material	5–200 mm			
Typical concentration	$10^{19}\,cm^{-3}$			
Refractive index	1.82			
Operation mode	cw	spiking	ns	ps
Pump mechanism	arc lamp diode laser		flash lamp diode laser (808 nm) ($\sigma_{808\,nm} = 4 \cdot 10^{-20}\,cm^2$)	
Pulse width	–	60 µs–10 ms	1–100 ns	25–500 ps
Bandwidth	0.001–0.1 nm	10^{11} Hz	0.1–3 GHz	10^{11} Hz
Average output power	0.1–6 kW	0.1 W–1 kW	0.5–250 W	1–30 W
Pulse energy	–	$\leq$ 100 J	1 mJ–100 J	0.5–50 mJ
Repetition rate	–	1 Hz–50 kHz	$\leq$ 50 kHz	1–100 Hz
Beam quality (M^2)	TEM_{00} to multimode			
Wall-plug efficiency	<3%	0.5–4%	0.1–2%	$\leq$ 1%
Diode pumping	< 20%	< 20%	< 10%	< 10%
Cooling system	water	water	water	water
Remarks	multirod laser possible		amplifier systems	single pulse and amplifier

6.13.2.2 Nd:YVO Lasers

Another laser crystal with good performance is Nd:YVO [6.1649–6.1685]. It shows high efficiency in diode pumping and can thus be used to built cw lasers with probably up to 80 W average output power and very good beam quality.

This laser is typically end-pumped with diode lasers and water cooled because of the four times higher absorption ($28\,\mathrm{cm}^{-1}$ at 1.0% doping) compared to Nd:YAG and the eight times larger emission cross section. The absorption band width is about seven times larger (20 nm) and the emission bandwidth is with 0.8 nm about twice as large as from Nd.YAG with 0.45 nm. The available crystal size is currently limited to a few cm and thermally induced stress limits the maximum output power from these lasers. A similar promising material is Nd:KGW (Nd:KGd(WO_4)) [6.1051, 6.1686, 6.1687, 6.1634] which shows low threshold, natural birefringence and high efficiency. Nd:YVO can be diode pumped at 809 nm. Further Nd materials as e.g. Nd:$GdVO_4$ are described in [6.1688–6.1705].

Table 6.18. Some properties of Nd YVO lasers

	Nd YVO laser	
Active material	Nd^{3+}:YVO_4	
Wavelength	1,069 nm, 1,342 nm	
Level scheme	4	
Emission cross-section	a-cut: $2.5 \cdot 10^{-18}\,\mathrm{cm}^2$ at 1,069 nm, $7 \cdot 10^{-19}\,\mathrm{cm}^2$ at 1,342 nm	
Lifetime upper laser level	50–90 µs (3at%–1at%)	
Length of active material	5–70 mm	
Typical concentration	$1.7 \cdot 10^{19}\,\mathrm{cm}^{-3}$	
Refractive index	1.95 (a) 2.17 (c)	
Operation mode	cw	ns
Pump mechanism	diode laser ($\sigma_{808} = 1.4 \cdot 10^{-19}\,\mathrm{cm}^2$)	
Pulse width	60 µs–10 ms	10–100 ns
Bandwidth	up to $8 \cdot 10^{-12}$ Hz	
Average output power	≤ 40 W	≤ 5 W
Pulse energy		0.5 mJ
Repetition rate	≤ 30 kHz	
Beam quality (M^2)	TEM_{00} to multimode	
Wall-plug efficiency	$\leq 4\%$	
Cooling system	Water	

6.13.2.3 Nd Glass Laser

Nd glass laser material [e.g. 6.1706–6.1732] can be produced in bigger active volumes compared to Nd:YAG laser crystals and is therefore used in applications with large mode diameters as for lasers with short pulses and very high peak powers. Beam diameters of several 10 cm are used for special applications. The bad thermal conductivity of this material excludes it from applications with high average output powers in usual rod laser systems.

Table 6.19. Some typical properties of Nd glass lasers

	Nd glass laser		
Active material	Nd^{3+}:phosphate or silicate glass		
Wavelength	1054–1062 nm		
Level scheme	4		
Emission cross-section	$2.7–4 \cdot 10^{-20}\,cm^2$		
Lifetime upper laser level	290–340 µs		
Length of active material	5–500 mm		
Typical concentration	$10^{20}\,cm^{-3}$		
Refractive index	1.5–1.57		
Operation mode	spiking	ns	ps
Pump mechanism		flash lamp diode laser	
Pulse width	60 µs–10 ms	1–100 ns	10–500 ps
Bandwidth		up to $8 \cdot 10^{12}$ Hz	
Average output power		≤ 1 W	
Pulse energy	≤ 500 J	1 mJ–200 J	0.5–10 mJ
Repetition rate		≤ 10 Hz	
Beam quality (M^2)		TEM_{00} to multimode	
Wall-plug efficiency		$\leq 1\%$	
Cooling system		water	

6.13.2.4 Yb:YAG Laser

Ytterbium:YAG as an active material [e.g. 6.1718–6.1741] has a very small quantum defect if it is diode pumped at 940 nm and thus the thermal problems are strongly reduced. The laser crystal finds increasing applications in the high-power range, especially in material processing. The small thermal load allows very good beam quality even at the highest powers. Values close to $M^2 = 1$ are reported with average powers of 100–200 W. This crystal is used as rod or as a thin slices (see Sect. 6.3.1, p. 365). Other Yb materials are investigated in [6.1742–6.1785]. Short pulse results from the last years are reported in [6.1786–6.1805].

Table 6.20. Some typical properties of commercial Yb:YAG lasers

	Yb:YAG laser	
Active material	$Yb^{3+}:Y_3Al_5O_{12}$	
Wavelength	1030 nm	
Level scheme	3	
Emission cross-section	$3.3 \cdot 10^{-20}\,cm^2$	
Lifetime upper laser level	1160 µs	
Length of active material	10–80 mm	0.2–3 mm
Typical concentration	$10^{20}\,cm^{-3}$	$9 \cdot 10^{20}\,cm^{-3}$
Refractive index	1.82	
Operation mode	cw, spiking, ns, ps, fs	
Pump mechanism	diode laser ($\sigma_{940\,nm} = 7.5 \cdot 10^{-21}\,cm^2$)	
Pulse width	cw – 10 fs	
Bandwidth	monomode – nm	
Average output power	50 W	500 W
Pulse energy	0.1–8 J	0.1–1 J
Repetition rate	cw, Hz, kHz, MHz	
Beam quality (M^2)	≤ 10 (TEM_{00})	
Wall-plug efficiency	$\leq 10\%$	$\leq 20\%$
Cooling system	water	water, Peltier
Remarks		

6.13.2.5 Ti:sapphire Laser

The Ti:sapphire laser [e.g. 6.1806-6.1854] is mostly used for the generation of short pulses in the ps and fs range and for tunable lasers at the red end of the visible spectrum. It is usually pumped by frequency-doubled Nd lasers around 530 nm. The fs pulses with pulse energies of usually less than 1 μJ can be amplified in regenerative amplifiers to values in the mJ region easily and up to many J in large amplifier setups. The repetition rate goes then down from 80 MHz of the oscillator to 1 kHz of a few Hz, only. By doubling this radiation the blue spectral range can be covered. The green and yellow range in between can be generated by OPO or OPA systems which are commercially available, e.g. for fs and ps lasers (see Sect. 6.15.2, p. 527).

The Ti:sapphire laser has become a workhorse in science and may find new applications in industry using short pulses. Thus it is very useful in measuring technologies. Another advantage may be its broad emission band enabling it to be as a broad-band laser source with good beam quality and high-powers.

Table 6.21. Some typical properties of commercial Ti:sapphire lasers

	Ti:sapphire			
Active material	$Ti:Al_2O_3$			
Wavelength	700-950 nm			
Level scheme	4			
Emission cross-section	$3 \cdot 10^{-19}$ cm^2 (at 800 nm)			
Lifetime upper laser level	3.2 μs			
Length of active material	3–30 mm			
Typical concentration	10^{20} cm^{-3}			
Refractive index	1.76 (birefringent)			
Operation mode	cw	ns	ps	fs
Pump mechanism	argon laser, SHG-Nd laser pump			
	longitudinal ($\sigma_{550\,\mathrm{nm}} = 2\text{–}5 \cdot 10^{-20}$ cm^2)			
Pulse width	–	2–100 ns	1–50 ps	5–100 fs
Bandwidth	≤ 2 GHz	≤ 1 nm	≤ 1 nm	60–100 nm
Average output power	≤ 50 W	1–2 W	≤ 1 W	≤ 1 W
Pulse energy	–	≤ 100 mJ	≤ 1 mJ	≤ 1 mJ
Repetition rate	–	1 Hz–40 Hz	≤ 1 kHz	≤ 1 kHz
Beam quality (M^2)	TEM_{00} to multimode		TEM_{00}	
Wall-plug efficiency	up to 8%	0.5–1%	0.1–1%	≤ 1%
Cooling system	water, Peltier cooler			
Remarks	laser pumping	flash lamp pumping	longitudinal pumped amplified	

6.13.2.6 Cr:LiCAF and Cr:LiSAF Lasers

These laser materials [6.1855–6.1888] can be pumped directly with diode lasers e.g. around 670 nm and thus very small devices can be produced. The emission is in the red and the near IR spectral region. They provide tunable or broad-band emission in the red and IR which can be frequency converted to the visible. Thus short pulses can be generated from handy lasers. The potential of these lasers is not fully developed yet.

Table 6.22. Some properties of Cr:LiCAF and Cr:LiSAF lasers

	Cr:LiCAF	Cr:LiSAF
Active material	Cr^{3+}:$LiCaAlF_6$	Cr^{3+}:$LiSrAlF_6$
Wavelength	720–840 nm	780–1010 nm
Level scheme	4	
Emission cross-section	$1.3 \cdot 10^{-20}$ cm^2	$4.8 \cdot 10^{-20}$ cm^2
Lifetime upper laser level	170 µs	67 µs
Length of active material	$\leq$ 20 mm	$\leq$ 20 mm
Typical concentration	$7 \cdot 10^{20}$ cm^{-3}	$3 \cdot 10^{20}$ cm^{-3}
Refractive index	1.39	1.4
Operation mode	pulsed	cw, pulsed
Pump mechanism	flash lamp, laser, diode lasers (670 nm)	flash lamp, laser, diode lasers (680 nm)
Pulse width	$\geq$ 10 ns	cw, $\geq$ 10 ns
Bandwidth	$\leq$ 100 nm	$\leq$ 200 nm
Average output power	W	1 W (cw), 100 mW (ns)
Pulse energy	$\leq$ 100 mJ	$\leq$ 100 mJ
Repetition rate	$\leq$ 10 kHz	$\leq$ 10 kHz
Beam quality (M^2)	TEM_{00} to multimode	
Wall-plug efficiency	$\leq$ 10%	$\leq$ 2%
Cooling system	water, air	
Remarks	first results	

Cr:YAG [6.1889–6.1891] as active material provides laser emission in the IR around 1.5 µm. This laser can be pumped with, e.g. Nd:YAG laser radiation at 1.06 µm. The possible broad-band emission can be converted to the visible range. Besides alexandrite and ruby are other Cr lasers as Cr-fosterite [6.1892–6.1907] and as given in [6.1908, 6.1911] possible.

6.13.2.7 Alexandrite Laser

This laser crystal shows a wide spectral gain and can thus be used for tunable lasers [6.1912–6.1918]. The material can also be used in mode-locked lasers reaching 8 ps pulses. The specifications can be compared with the Ti:sapphire laser parameters.

Table 6.23. Some typical properties of alexandrite lasers

		Alexandrite laser
Active material		Cr^{3+}:$BeAl_2O_4$
Wavelength		700–818 nm
Level scheme		4
Emission cross-section		$1 \cdot 10^{-19}$ cm^2
Lifetime upper laser level		260 µs
Length of active material		30–100 mm
Typical concentration		$6 \cdot 10^{20}$ cm^{-3}
Refractive index		1.73–1.74 (birefringent)
Operation mode	spiking	ns
Pump mechanism		flash lamp
Pulse width	200 µs	20 ns
Bandwidth		≤ 100 nm, $5 \cdot 10^{-13}$ Hz
Average output power		≤ 50 W
Pulse energy		≤ 1 J
Repetition rate		≤ 100 Hz
Beam quality (M^2)		TEM_{00} (to multimode)
Wall-plug efficiency		$\leq 2\%$
Cooling system		water
Remarks		twice the thermal conductivity of YAG

6.13.2.8 Erbium (Er), Holmium (Ho), Thulium (Tm) Laser

These lasers [6.1919–6.2009] are used mainly in medical applications because of the high absorption of their radiation in water and in atmospheric research and military applications because of their IR emission. These lasers are also eye-safe. The laser setup needs special optics for the IR wavelengths and is therefore not easy to achieve. The Q switch can be carried out with a frustrated total reflection (FTIR) shutter between two glass prisms with a narrow air gap which is modulated with a piezo-driver (see Sect. 6.10.2, p. 454).

Table 6.24. Some properties of erbium and holmium lasers

	Er:YAG	CTH:YAG
Active material	$Er^{3+}:Y_3Al_5O_{12}$	$Cr^{3+}:Tm^{3+}:Ho^{3+}:Y_3Al_5O_{12}$
Wavelength	2940 nm	2080 nm
Level scheme	3	
Emission cross-section	$3 \cdot 10^{-20}\,cm^2$	$4.5 \cdot 10^{-19}\,cm^2$
Lifetime upper laser level	100 µs	3.6 ms
Length of active material	20–120 mm	50–100 mm
Typical concentration	$7 \cdot 10^{21}\,cm^{-3}$	$10^{17}\,cm^{-3}$
Refractive index	1.82	1.82
Operation mode	pulsed	pulsed
Pump mechanism	flash lamp, diode lasers (680 nm)	flash lamp
Pulse width	100–1000 µs, 20 ns	200–300 µs
Bandwidth	≤ 0.1 nm	
Average output power	≤ 50 W	≤ 40 W
Pulse energy	0.1–8 J	≤ 3.5 J
Repetition rate	1–50 Hz	20 Hz
Beam quality (M^2)	10 (TEM_{00} to multimode)	
Wall-plug efficiency	0.2–3%	$\leq 2\%$
Cooling system	water	water
Remarks	Q switch with FTIR-shutter	

6.13.2.9 Ruby Laser

The ruby laser [6.1, 6.183, 6.335, 6.702, 6.703, 6.840, 6.889, 6.965, 6.1257, 6.2442] was the first laser. It was pumped with flash lamps. Despite the quite expensive ruby crystals this laser is still used because of the wavelength in the red and the high peak powers possible in Q switch operation. Rods of 10 mm diameter are available.

Table 6.25. Some typical properties of ruby lasers

		ruby laser	
Active material		Cr^{3+}:Al_2O_3	
Wavelength		694.3 nm	
Level scheme		3	
Emission cross-section		$2.5 \cdot 10^{-20}$ cm^2	
Lifetime upper laser level		3 ms	
Length of active material		10–200 mm	
Typical concentration		$8 \cdot 10^{20}$ cm^{-3}	
Refractive index		1.76 (birefringent)	
Operation mode	spiking	ns	ps
Pump mechanism		flash lamp	
Pulse width	200 µs	10–30 ns	10 ps
Bandwidth		0.53 nm (3.3 GHz)	
Average output power		1 W	
Pulse energy		$\leq$ 100 J	
Repetition rate		$\leq$ 5 Hz	
Beam quality (M^2)		TEM_{00} (to multimode)	
Wall-plug efficiency		$\leq$ 1%	
Cooling system		water	
Remarks		long thermal relaxation time	

6.13.2.10 Er fiber Lasers

Fiber lasers [6.2010–6.2061] have good cooling conditions and thus the thermal problems are negligible. Single-mode fibers allow perfect beam quality. Short pulses are possible. The small out-coupling fiber cross-section limits the maximum peak power of such lasers. Nevertheless, fiber lasers may become more important in the future. As an example the data of Er:fiber lasers are given in Table 6.26 as it is applied, e.g. in telecom.

Table 6.26. Some properties of Er fiber lasers

	Er fiber
Active material	Er^{3+}:glass
Wavelength	550 nm, *1,550 nm*, 3,500 nm
Level scheme	3
Emission cross-section	$3 \cdot 10^{-20}\,cm^2$
Lifetime upper laser level	8 ms
Length of active material	0.3–5 m
Typical concentration	$3 \cdot 10^{20}\,cm^{-3}$
Refractive index	1.53
Operation mode	cw, pulsed, ps, fs
Pump mechanism	(Ti:sapphire) laser, diode lasers
Pulse width	cw, ≥ 100 ns
Bandwidth	≤ 0.1 nm
Average output power	≤ 1 W
Pulse energy	≤ 100 mJ
Repetition rate	≤ 2 kHz
Beam quality (M^2)	TEM_{00}
Wall-plug efficiency	depends on pump laser
Cooling system	air
Remarks	further development

6.13.2.11 High power fiber lasers

High power fiber lasers [e.g. 6.2062–6.2081] provide excellent beam quality because of the low thermal distortions from the active material. Progress in diode lasers and fiber technology allowed the setup of fiber lasers with output powers of more than 1 kW, and with coherent beam combining the multi 10 kW level is aimed for. The maximum output power is limited by the pump power delivery and damage threshold of the fiber facets on one side and the nonlinear processes on the other with stimulated Brillouin and Raman scattering (SBS and SRS) as the most important ones. Besides the cw-operation short pulses, especially with ps- and fs duration with high average output powers in the 100 W range, were generated. The growing availability and use of micro structured fibers (MSF) or sometimes called photonic crystal fibers (PCF) has led to new windows of operation and will promote further developments.

Table 6.26.1. Some typical properties of high power fiber lasers

	Yb fiber laser
active material	Yb^{3+}:glass
wavelength	1,030 nm
level scheme	3
emission cross section	$6 \cdot 10^{-21}$ cm^2
life time upper laser level	0.72–1.35 µs (function of concentration)
length of active material	several m
typical concentration	1.000–5.000 ppm
refractive index	1.45
operation mode	cw table arrangement, pulsed
pump mechanism	diode laser (980 nm)
pulse width	cw ns, ps, fs
band width	monomode - nm
average output power	kW ≈100 W
pulse energy	0.1–8 J 0.1–1 J
beam quality (M^2)	≈1 (TEM_{00})
wall-plug efficiency	≤20% ≤10%
cooling system	diode cooling
remarks	strong development

6.13.3 Gas Lasers

Gas laser are pumped via electrical discharges longitudinal or transversal to the laser beam and inelastic collisions of the electrons with the laser molecules or atoms (see Sect. 6.3.3, p. 375).

6.13.3.1 XeCl, KrF and ArF Excimer Lasers

Excimer lasers [e.g. 6.2082–6.2086] can be operated with XeCl, KrF, ArF and XeF excimer molecules. In addition, usually several buffer gases such as, e.g., argon or neon, are used to adjust the velocity and density of the accelerated electrons for best collision cross section. These lasers emit at least partly superradiation and thus the beam quality is very poor. Nevertheless the high average output powers in the UV make them attractive light sources, e.g. for pumping of pulsed dye lasers, for chemistry, for industrial applications in lithography and material processing as well as in medicine.

Table 6.27. Some typical properties of commercial XeCl and KrF lasers

	XeCl	KrF	ArF
Active material	XeCl-excimer	KrF-excimer	ArF-excimer
Gas mixture (example)	80 mbar of 5% HCL in He 60 mbar of Xe 2760 mbar of Ne 500 mbar of He	7.5 mbar of F_2 22.6 mbar of Kr 1100 mbar of He	1.3 mbar of F_2 40 mbar of Kr 1100 mbar of He
Wavelength	308 nm	248 nm	193 nm
Level scheme		4	
Emission cross-section	$4.5 \cdot 10^{-16}\,\mathrm{cm}^2$	$2.4 \cdot 10^{-16}\,\mathrm{cm}^2$	$2.9 \cdot 10^{-16}\,\mathrm{cm}^2$
Lifetime upper laser level	11 ns	7 ns	4.2
Length of active material		50–1500 mm	
Typical concentration		$10^{14}\,\mathrm{cm}^{-3}$	
Refractive index		$\simeq 1$	
Operation mode		ns	
Pump mechanism		transversal electrical discharge: 10–30 kV, kA, ns Electron temperature ≈ 5 eV	
Pulse width		5–20 ns	
Bandwidth	2 nm	0.5 nm	
Average output power		1–100 W	
Pulse energy		100 mJ–10 J	
Repetition rate		10 Hz–1 kHz	
Beam quality (M^2)		multimode: beam size $\approx 5 \times 20\,\mathrm{mm}^2$, divergence ≈ 1 mrad	
Wall-plug efficiency		$\leq 2\%$	
Cooling system		water for powers ≤ 10 W	
Remarks		gas exhaust, gas exchange weekly to monthly	

6.13.3.2 N_2 Laser

Nitrogen lasers [e.g. 6.2087–6.2089] are useful as a low-cost UV light source for direct use or for pumping of pulsed dye lasers. Because of the long lifetime of the lower laser level the maximum average output power and the pulse duration are limited and thus excimer lasers are often favored instead of N_2 lasers.

Table 6.28. Some typical properties of nitrogen lasers

	nitrogen laser	
Active material	N_2	
Wavelength	337.1 nm	
Level scheme	3	
Emission cross-section	$4 \cdot 10^{-13}\,cm^2$	
Lifetime upper laser level	40 ns	
Length of active material	100–1000 mm	
Typical concentration	$10^{11}\,cm^{-3}$	
Refractive index	$\simeq 1$	
Operation mode	ns	sub ns
Pump mechanism	transversal electrical discharge: 10–30 kV, kA, ns electron temperature 10 eV	
Gas mixture	100 mbar of N_2	1 bar of N_2
Pulse width	2–8 ns	500 ps
Bandwidth	0.1 nm	
Average output power	3 W	≤ 1 W
Pulse energy	≤ 100 mJ	≤ 5 mJ
Repetition rate	≤ 200 Hz	
Beam quality (M^2)	multimode: beam size in the range of $\leq 5 \times 20\,mm^2$, divergence in the range of 1–5 mrad	
Wall-plug efficiency	$\leq 0.1\%$	
Cooling system	air	
Remarks	N_2 flow of 2 to 30 l/min at 100 mbar necessary for high-powers	relatively compact

6.13.3.3 Home Made N_2 Laser

The principle of the nitrogen laser is so simple that it is possible to built such a laser almost completely from scratch. The scheme is given in Fig. 6.98 (p. 512).

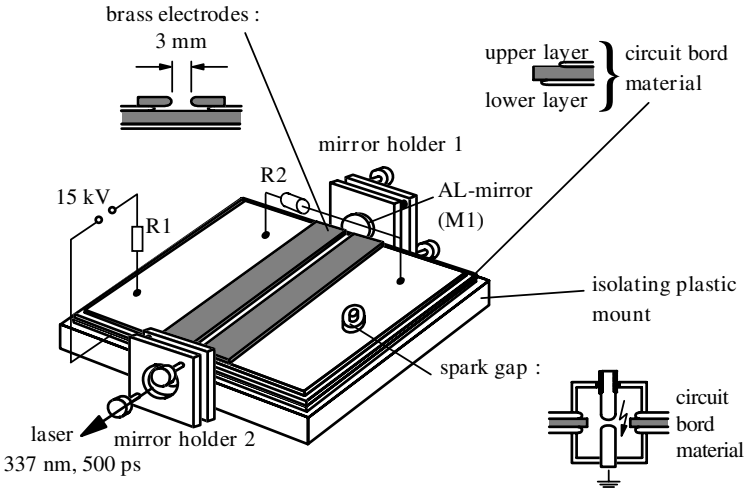

Fig. 6.98. N_2 laser with 500 ps pulse width at 337 nm as a self made construction. The foot print of this device is about 300 mm × 500 mm

Air at normal pressure can be used as the active material. A simple Al mirror can be used as mirror M1 and a quartz plate as mirror M2. M2 can even be leaved out and the laser will emit superradiation.

The only expensive device in this construction is the electric power supply providing more than $U_{\text{source}} \geq 10\,\text{kV}$. From the resistor $R_1 \geq (U_{\text{source}}/I_{\text{source}})_{\max}$ based on the maximum current I_{source} of the power supply it follows that the maximum repetition frequency of the laser with capacitance C is $f_{\text{rep}} \approx 1/2\pi(R_1 C)$. R_2 has to be somewhat smaller than R_1.

The main capacitors are made from electric circuit board material providing a capacitance of $3\,\text{pF}\,\text{cm}^{-2}$. Thus the whole capacitance is about 4 nF. Care has to be taken for avoiding sharp edges in the construction of the high-voltage elements, otherwise sparks may occur and damage the system.

Also the spark gap [6.2089] can be home-made simply from brass. Its distance has to be adjusted for breakthrough slightly below maximum voltage of the power supply.

The laser can be easily upgraded in performance and reliability by using good optics, a thyratron as switch, a sealed discharge chamber with tungsten electrodes filled with N_2 and Cu sheets of two or more mm thickness with rounded edges in the high-voltage part against unwanted discharges.

6.13.3.4 He-Ne Laser

Helium-neon lasers are used typically with red light at 633 nm for aligning or other low power applications. The good beam quality, availability of linear or circular polarization and high frequency and power stability of these lasers make them useful for calibration and aligment problems.

Table 6.29. Some typical properties of He-Ne lasers

	He-Ne laser
Active material	Ne
Wavelengths	543.3 nm (green), 594.1 nm (yellow), 611.8 nm, 632.8 nm (red), 1152.3 nm, 1523.1 nm, 2395.1 nm, 3391.3 nm
Level scheme	4
Emission cross-section	$3 \cdot 10^{-13}\,\mathrm{cm}^2$ (632 nm), $2 \cdot 10^{-14}\,\mathrm{cm}^2$ (543 nm)
Lifetime upper laser level	170 ns (633 nm)
Length of active material	100–1500 mm
Typical concentration	$3 \cdot 10^{9}\,\mathrm{cm}^{-3}$
Refractive index	$\simeq 1$
Operation mode	cw
Pump mechanism	longitudinal electrical discharge, inelastic collision He*+Ne→He+Ne* electron temperature ≈ 10 eV
Gas mixture	He:Ne as 5:1 (for 633 nm); and, e.g. as 9:1 (for 1.15 µm)
Bandwidth	1.5 GHz (633 nm), 1.75 GHz (543 nm)
Average output power	0.5–50 mW typical 5 mW at 632 nm
Beam quality (M^2)	TEM_{00}
Wall-plug efficiency	$\simeq 0.1\%$
Cooling system	air
Remarks	reliable

Mode-locked He-Ne lasers have been reported to produce ps pulses at the red line [6.2397]. The repetition rate was MHz. In cw-operation the bandwidth is limited by Doppler broadening in the active gas mixture.

6.13.3.5 He-Cd Laser

Helium-cadmium lasers are useful in low-power cw applications in the blue spectral range, (see also [6.2090]). They are in increasing competition with blue diode lasers or frequency doubled red diode lasers.

Table 6.30. Some typical properties of He-Cd lasers

	He-Cd laser
Active material	Cd^+ (300 C)
Wavelength	(325.0 nm, 353.6 nm) 441.6 nm
Level scheme	4
Emission cross-section	$9 \cdot 10^{-18}\,cm^2$
Lifetime upper laser level	810 ns
Length of active material	0.25 m–1.5 m
Typical concentration	$4 \cdot 10^{16}\,cm^{-3}$
Refractive index	$\simeq 1$
Operation mode	cw
Pump mechanism	longitudinal electrical discharge: 10–30 kV, kA, ns electron temperature ≈ 6 eV
Gas mixture	10 mbar of He, 0.1 mbar of Cd
Bandwidth	0.1 nm
Average output power	10–200 mW
Beam quality (M^2)	TEM_{00} or multimode
Wall-plug efficiency	$\leq 0.1\%$
Cooling system	air
Remarks	

6.13.3.6 Ar and Kr Ion Lasers

Argon and krypton lasers [6.2091–6.2094] are very common in science for cw applications and quasi-cw mode-locked lasers in the ps range. Thus, e.g. fs CPM dye lasers (see Sect. 6.10.3, p. 460) or Kerr lens mode-locked Ti:sapphire lasers (see Sect. 6.10.3, p. 460) are pumped with a 5 W Ar laser. The high power argon or krypton lasers have very high operating costs caused by the neccessary two-year exchange of the expensive laser tube, and the low efficiency. Nevertheless, they are still widely used because of their attractive wavelengths in the visible in the blue, green and red and comparably low prices for low power systems.

Table 6.31. Some typical properties of commercial Ar and Kr ion lasers

	Ar and Kr ion laser	
Active material	Ar^+	Kr^+
Wavelength	514.5 nm, 488.0 nm	647.1 nm
Level scheme	3	
Emission cross-section	$2.5 \cdot 10^{-12}\,cm^2$	
Lifetime upper laser level	9 ns	
Length of active material	(0.5 m–)2 m	
Typical concentration	$2 \cdot 10^9\,cm^{-3}$	
Refractive index	$\simeq 1$	
Operation mode	cw, mode-locked	
Pump mechanism	longitudinal electrical low pressure discharge: $30–150\,A\,cm^{-2}$, electron temperature ≈ 30 eV	
Gas pressure	0.01–1 mbar	
Pulse width	cw or 500 ps	
Bandwidth	4-12 GHz single line, multi line	
Average output power	1–3 W in single line, 10 W in strong lines (e.g. 488 nm), 20 W in multiline	
Pulse energy	≤ 100 mJ	≤ 5 mJ
Repetition rate	MHz in mode locking regime	
Beam quality (M^2)	TEM_{00}	
Wall-plug efficiency	$\leq 0.1\%$	
Cooling system	water (up to 60 kW)	
Remarks	magnetic field within discharge tube to increase current density, automatic gas refill system, expensive gas tubes of the high power lasers have to be replaced (2 years)	

6.13.3.7 Cu (Au, Pb) Vapor Lasers

Lasers with copper vapor as the active material [6.2095–6.2112] provide high average output powers of several 10 W in the green and yellow spectral region with high repetition rates. The beam quality can be excellent and thus these lasers find applications from spectroscopy to material processing.

Table 6.32. Some typical properties of Cu-vapor lasers

	Cu vapor laser	
Active material	Cu vapor (1480–1530°C)	
Wavelength	510.6 nm	578.2 nm
Level scheme	3	
Emission cross-section	$8.6 \cdot 10^{-14}$ cm^2	$1.25 \cdot 10^{-13}$ cm^2
Lifetime upper laser level	500 ns	610 ns
Length of active material	0.5 m–2 m	
Typical concentration	$8 \cdot 10^{13}$ cm^{-3}	
Refractive index	$\simeq 1$	
Operation mode	pulsed	
Pump mechanism	longitudinal electrical discharge tube temperature 1500°C electron temperature ≈ 5 eV	
Gas mixture	1 mbar Cu vapor, 40 mbar buffer	
Pulse width	10–50 ns	
Bandwidth	3 GHz	
Average output power	5–70 W	
Pulse energy	1 mJ–50 mJ	
Repetition rate	1–100 kHz	
Beam quality (M^2)	TEM_{00}	
Wall-plug efficiency	1%	
Cooling system	water, air	
Remarks	maintenance each 500 h	

The same laser construction operates with gold or lead. The laser wavelengths are then 627.8 nm and 722.9 nm.

6.13.3.8 CO_2 (CO) Lasers

CO_2 lasers [e.g. 6.2113–6.2120] emit in the far IR at 10.6 µm with possibly very high average output powers and pulse energies. They are very efficient. Thus material processing in machinery especially in the car industry and in medicine are the main applications.

Table 6.33. Some typical properties of CO_2 lasers

	CO_2 laser	
Active material	CO_2	
Wavelength	10 600 nm (9400 nm)	
Level scheme	4 at low temperatures → 3 at high temperatures	
Emission cross-section	$1 \cdot 10^{-16}$ cm^2	
Lifetime upper laser level	10 µs	
Length of active material	0.3 m–2 m	
Typical concentration	$3 \cdot 10^{-17}$ cm^{-3}	
Refractive index	$\simeq 1$	
Operation mode	cw	pulsed
Pump mechanism	transversal electrical discharge, DC or AC electron temperature ≈ 4 eV	
Gas mixture	rapid gas flow, CO_2:N_2 = 0.8:1 gas temperature 300°C	
	20 mbar	1 bar
Pulse width	cw	45 ns–15 µs
Bandwidth	$6 \cdot 10^7$ Hz	
Average output power	typical 5 kW, $\leq$ 100 kW	1 kW
Pulse energy		$\leq$ 10 kJ
Repetition rate		$\leq$ 1 kHz
Beam quality (M^2)	multimode or TEM_{00} (long wavelength ⇒ large beam parameter product)	
Wall-plug efficiency	10–20%	$\leq$ 30%
Cooling system	water	

This laser acts between vibrational levels of the molecule. Because of the long wavelength in the far IR the focused spot size is, for a diffraction-limited beam more than 10 times larger than for visible lasers. The CO laser is operated in a similar way. Its emission wavelength is in the range of 5–6 µm.

6.13.4 Dye Lasers

Dye lasers can in principle be built with wavelengths between 300 and 1000 nm with tuning ranges of several 10–100 nm [6.2121–6.2146]. They find themselves in strong competition with solid state laser coupled with nonlinear frequency converters. As example the tuning curves of several dyes in a commercial laser with ns pulse emission are given in Fig. 6.99.

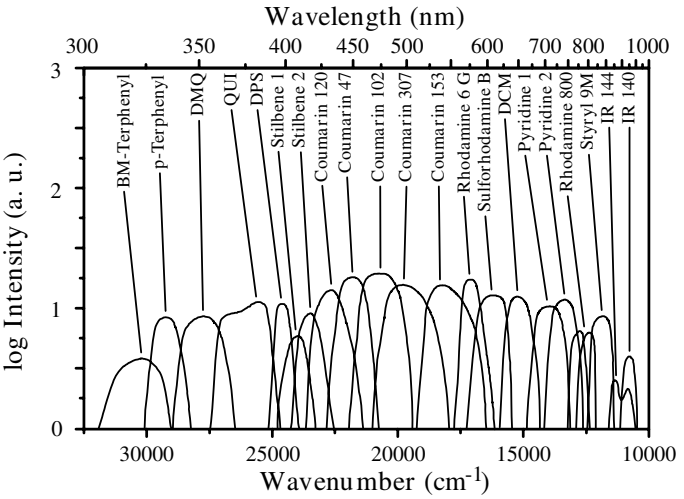

Fig. 6.99. Tuning curves of several dyes in a commercial dye laser with pulsed excitation [6.2144]

These dyes have a limited lifetime as shown for some examples in Table 6.34 and thus they are often limited to scientific applications.

Table 6.34. Life time of some laser dye solutions (after [6.2144])

Dye	Solvent	Wavelength (nm)	Excimer pumped	cw pumped
p-terphenyl	cyclohexane	340	451 Wh	
Polyphenyl 1	dioxane	380	870 Wh	
Stilbene 3	methanol	430	14 Wh	300 Wh
Coumarine 102	methanol	480	244 Wh	100 Wh
Rhodamine 6G	methanol	590	316 Wh	1000 Wh
DCM	DMSO	650	348 Wh	500 Wh
Rhodamine 700	methanol	700	80 Wh	1000 Wh
Styryl 9	DMSO	840	73 Wh	500 Wh
HITCI	DMSO	875	12 Wh	100 Wh

6.13.4.1 cw and Quasi-cw (Mode-Locked) Dye Lasers

Continuously operating dye lasers [e.g. 6.2147–6.2150] were typically pumped with ion gas lasers. They can show narrow bandwidths in cw operation. The dye laser can be mode-locked or pumped with mode-locked pulses resulting in ps or fs dye laser pulses. The dye solution is used in jets.

Table 6.35. Some typical properties of cw dye lasers

	cw-dye laser	
Active material	laser dyes	
Wavelength	410–890 nm	
Level scheme	4	
Emission cross-section	$\leq 10^{-16}$ cm^2 (maximum)	
Lifetime upper laser level	1–10 ns	
Length of active material	≤ 0.5 mm	
Typical concentration	10^{17} cm^{-3}	
Refractive index	1.4 (solvent dependent)	
Operation mode	cw	
Pump mechanism	laser pumped: Ar-ion, SHG of Nd laser dye jet, focus diameter ≈ 50 µm	
Bandwidth	broad band	1 MHz (≤ 0.5 MHz possible)
Average output power	1.2 W	≤ 0.8 W
Beam quality (M^2)	TEM_{00}	
Opto-optical efficiency	$\leq 13\%$	20%
Cooling system	water	
Remarks	dye jet with pump, dyes need to be changed (approximately weekly), frequency stabilization possible with active resonator control	

6.13.4.2 Pulsed Dye Lasers

Spiking dye lasers were built with flash lamp pumping. Mode-locked fs dye lasers are usually pumped with cw lasers. Dye lasers with ns or ps pulses are pumped by ns pump lasers such as e.g. excimer, nitrogen or frequency-converted solid-state lasers [6.2151–6.2176]. Dyes in polymers may allow new lasers [6.2153–6.2168].

Table 6.36. Some typical properties of pulsed dye lasers

	pulsed dye laser			
Active material	dyes			
Wavelength	580–650 nm	300–1200 nm	400–900 nm	570–650 nm
Level scheme	4			
Emission cross-section	$\geq 10^{-16}$ cm^2 (maximum)			
Lifetime upper laser level	1–10 ns			
Length of active material	50–200 mm	5–50 mm	0.3 mm	0.3 mm
Typical concentration	10^{20} cm^{-3}	(concentration of 10^{-2}–10^{-4} mol l^{-1})		
Refractive index	1.5 (solvent dependent)			
Operation mode	spiking	ns	ps	fs
Pump mechanism	flash lamp transversal dye cell	excimer or nitrogen laser dye cell	ps ion laser dye jet	cw laser dye jet
Pulse width	60 µs–10 ms	1–30 ns	1–50 ps	$\geq$ 50 fs
Bandwidth	up to $8 \cdot 10^{-12}$ Hz possible	6 GHz 30 MHz	sub nm	nm
Average output power	several W	1 W	100 mW	50 mW
Pulse energy	several J	$\leq$ 1 mJ	0.1 mJ	400 pJ
amplified		10 mJ	5 mJ (10 Hz)	1 mJ (10 Hz)
Repetition rate	≤ 10	1–100 Hz	$\geq$ 50 MHz	$\approx$ 100 MHz
Beam quality (M^2)	TEM_{00} to multimode	multimode	TEM_{00}	TEM_{00}
Opto-optical efficiency	10%	$\leq$ 15%	$\leq$ 5%	$\leq$ 1%
Cooling system	dye circulation, water, air			
Remarks	high-power possible	usually amplified, dye exchange weekly		

6.13.5 Other Lasers

XUV-light sources [6.2177–6.2230] can be built by laser-induced plasma generation, e.g. with metal atoms. The resulting emission shows wavelengths of a few nm up to 40 nm. In particular, laser radiation in the transmission window of water from 2 nm to 4 nm will find applications, e.g. in microscopy of biological material. Another important field is lithography for chip production. Even before laser action is obtained point source emission can be used. For

this, atoms like e.g. Al, Au and W are used. The observed light pulses have energies in the mJ range. Incoherent light sources from table-top pump lasers have average output powers of some 10 mW in the nm region. The possible availability of well-designed solid-state lasers with high average output powers in the 100 W range, perfect beam quality and pulse energies of several J during less than 10 ns may promote these light sources in the near future.

The *free electron laser* [e.g. 6.2231–6.2245] can show a wide range of emission wavelengths from the X ray (0,1 nm), XUV (1–100 nm) and in principle to radio waves. The amplification takes place in an electron beam in series bent between the Wiggler magnets of, e.g. a synchrotron. Thus average output powers of 10 W with short pulses of 100 fs can be obtained.

Color center lasers [e.g. 6.2246–6.2258] operate in the near infrared wavelength range from 0.8 to about 4 µm with up to 100 mW average output power. The active material is some mm long and is made from crystals such as e.g. NaF, built from K, Na or Li atoms at one side and F or Cl atoms at the other. These crystals are X-ray irradiated to provide defects in the crystal structure which act as a quantum well for the charges. These F centers have quantum energy levels which provide the laser transition in a four-level scheme. They are laser pumped with wavelengths between 500 nm and 1.2 µm. Unfortunately, the available laser crystals have short lifetimes of days to months.

Far-infrared lasers [e.g. 6.2259–6.2276] can be made in the wavelength range above 30 µm using vibrational transitions of molecules in the gas phase, as e.g. HCN. These lasers can be pumped by electrical discharges or with IR lasers, e.g. CO_2 lasers. The average output power can reach a few 10 mW.

New solid-state lasers [6.2263–6.2303] with wavelengths in the visible spectral range or with better thermal properties may be developed in the future. The possibilities of diode pumping allow special constructions of microchip lasers even with frequency conversion inside the resonator (see also Sect. 6.2 and references there).

New diode lasers [6.2297–6.2309] such as vertical emitting constructions or with new compounds may become important, soon. In particulary the green and blue spectral range may be filled. Therefore the technology of II–VI compounds such as e.g. ZnSe may be more developed. Several mW around 500 nm have already been reported.

Chemical lasers [e.g. 6.2310–6.2324] have already been mentioned in Sect. 6.3.5 (p. 378). They can produce very high average output powers for a short time and are therefore usually specialized for military applications.

6.14 Modification of Pulse Structure

Methods for generation of short pulses directly in lasers are described in Sect. 6.10 (see also [6.2325–6.2342]). Some further effort may be necessary to select single short pulses from a pulse train in the ps range or to com-

press Q switch pulses in the ns range or to shorten fs pulses, externally. Measurement methods for determining the pulse widths of laser pulses are discussed in Sect. 7.1.5.2 (p. 543) and the references therein. The complete characterization of fs-pulses became especially important as a consequence of shorter pulses reaching the region below 1 fs approaching values below 100 as (10^{-16} s) now. Because these pulses contain only a few cycles of the electric field vector the phase relative to the maximum of the pulse envelope can be of importance in the applications. Therefore techniques as SPIDER or FROG [7.43–7.48] were developed (see Sect. 7.1.5.5, p. 545).

6.14.1 Single Pulse Selection

Mode-locked lasers mostly produce trains of ps or fs pulses (see e.g. Fig. 6.79, p. 464). For some applications the repetition frequency of these pulses, typically of some 10 MHz can be too high and sometimes even single pulses are needed.

Single pulse selection out of a train of ps pulses as they are generated, e.g. from a ps solid-state laser, can be obtained by a fast gate using a Pockels cell and a polarizer as shown in Fig. 6.100.

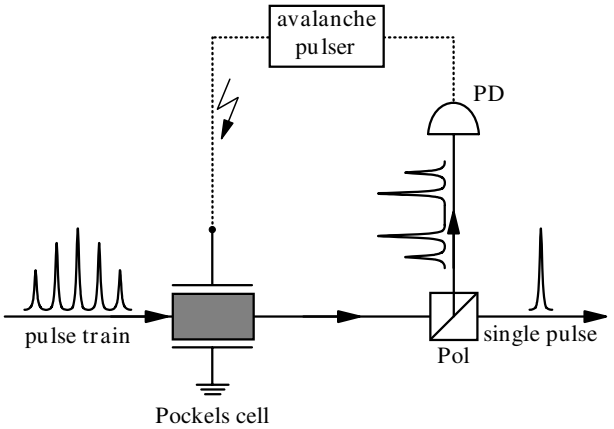

Fig. 6.100. Single pulse selection with Pockels cell and polarizer (Pol). The fast trigger is made with an avalanche transistor trigger producing ns pulses with slopes of 1 kV/ns

Another possibility is the cavity damping of a quasi-cw operated ps laser similar to that depicted for a cw-laser in Fig. 6.74 (p. 456).

Further, the repetition rate can be drastically decreased by a regenerative amplifier from MHz to kHz or some Hz. Amplifiers for short pulses in the ps or fs range can be pumped with ns pulses and if the lifetime of the upper laser level is in the ns range these amplifiers will amplify with their own repetition rate, only. This principle can be applied, e.g. in dye or Ti:sapphire amplifiers.

6.14.2 Pulse Compression and Optical Gates

The duration of short pulses can be decreased externally using gates or nonlinear effects for ns pulses and compressors for ns, ps or fs pulses. Synchronization of laser pulses can be realized with very high occuracy [6.2343–6.2348].

6.14.2.1 Pulse Compression of fs Pulses

Compression of pulses [6.2349–6.2398] down to fs widths can be applied if these pulses show a frequency chirp. This chirp can be generated by self-phase modulation in an external device, e.g. a fiber, see Sect. 4.5.7 (p. 218). Frequency chirp may also be obtained from dispersion of the involved optical matter in laser oscillators. This chirp can be compensated inside the resonator or externally.

The combination of an optical fiber with a grating compressor allows the shortening of pulses down to some fs. The principle is depicted in Fig. 6.101.

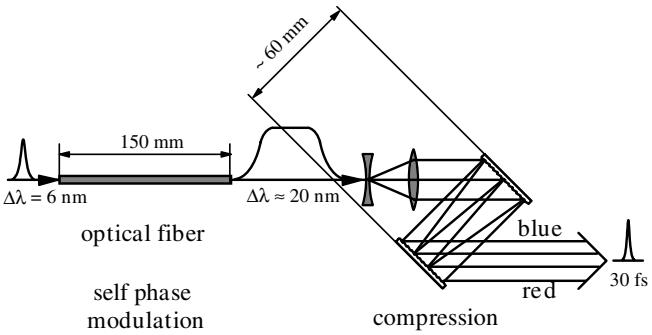

Fig. 6.101. Pulse compression using self-phase modulation in a single-mode polarization-conserving optical fiber and a grating compressor

The original laser pulse had a duration of about 90 fs and a pulse energy of 0.6 nJ at 619 nm. The fiber was 3.3 μm in diameter and thus the pulse peak power was about $5\,\mathrm{GW\,cm^{-2}}$. Shortest pulses generated with this scheme were 4.5 fs long [6.2382, 6.2389]. Pulses with durations below 1 fs (attosecond pulses) are reported in [6.2399–6.2429].

6.14.2.2 Pulse compression of ns Pulses

Pulses of about 10 ns pulse duration can be compressed by a factor of about 10 using stimulated Brillouin or Raman scattering with good energy conservation [6.2430–6.2449]. The scheme is shown in Fig. 6.102 (p. 524).

In this scheme the zone of large SBS reflectivity is moving towards the entrance window of the cell. Thus the incident beam is reflected at different positions of the counter propagating sound wave and finally a compression

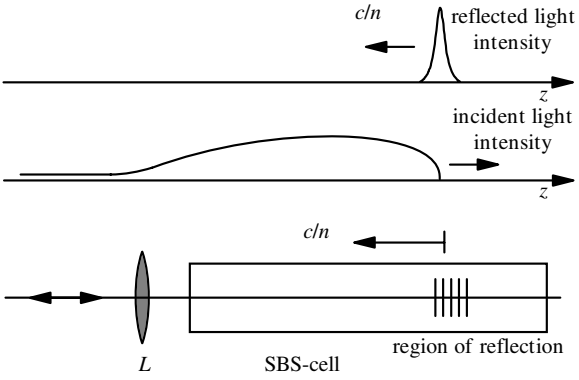

Fig. 6.102. Compression of ns pulses using stimulated Brillouin scattering in a long-focusing geometry

similar to snow-shoving takes place. If the nonlinear conditions are suitable chosen, which is not simple, perfect compression occurs with good energy conservation in the pulse of much more than 50%. It turned out that acoustic and thermal distortions of the SBS material which is several m long can disturb this process. Therefore it may be thermally isolated.

6.14.2.3 Pulse Shortening by Nonlinear Effects

Each nonlinear effect such as harmonic generation or nonlinear absorption will change the pulse duration of short pulses [e.g. 6.2450–6.2453]. If the nonlinear effect is not saturated the exponent of the nonlinear effect temporally shortens Gaussian-shaped pulses by the square root of the exponent.

However, in addition nonlinear absorption causes losses of the pulse energy and is therefore rarely used. Nevertheless, it keeps the original wavelength of the light and thus is useful in the low-power section of the laser system before power amplification.

6.14.2.4 Pulse Shortening with Gates

Slices of pulses can be obtained using optical shutters such as Pockels cells or Kerr cells (see Sect. 4.5.2 (p. 209) and 6.14.1, p. 522) or via other effects [6.2454–6.2459]. Electro-optic shutters are usually limited to widths larger than 1 ns. If optically driven Kerr cells are used, very fast shutters can be made and thus pulse durations of ps or even fs are possible. This method can be used to observe the dynamics of processes such as e.g. fluorescence, or to take photographs of the short pulses. efficiency decreases of course proportional to the shortening or slicing ratio.

6.14.2.5 Optical Gating with Up-Conversion

Optical gating can also be achieved by up-conversion of the original light via a nonlinear frequency transformation [e.g. 6.2460–6.2462]. The scheme is given in Fig. 6.103 (p. 525).

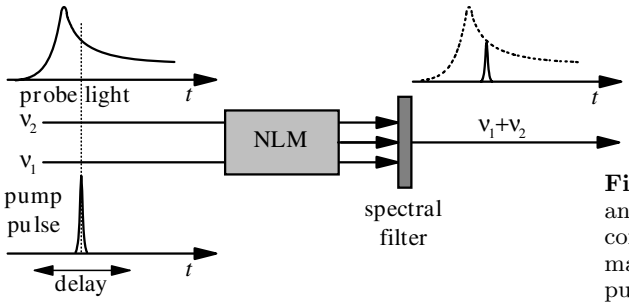

Fig. 6.103. Schematic of an optical gate using up-conversion in a nonlinear material for spectroscopic purposes

The sum frequency generation occurs during the presence of the short pump pulse, only. Thus the decay of the probe signal can be obtained by delaying the pump pulse. This method can be used for the investigation of fast fluorescence decay times, e.g. of organic molecules. It has the additional advantage of the possible amplification and wavelength transformation of the probe light to be better adapted to the detector parameters (see Sects. 4.4.3, p. 192 and 4.4.4, p. 193).

6.15 Frequency Transformation

Laser radiation can be transformed into the harmonic frequencies by doubling and mixing processes and to other frequencies by parametric devices. Further, Raman media can be used to shift the laser frequency. Nonlinear processes in liquids, in bulk or fiber materials especially in micro structured fibers can be applied for the generation of spectrally very broad light emission.

Physical details are described in Chap. 4 and technical details should be extracted from catalogues. In all cases the beam quality plays a key role for the efficiency of the transformation. High values of above 50% are possible. Typical values are above 10% but in special cases, such as reaching the far UV, efficiencies below 10^{-3} are possible.

Further crucial points are the long-term stability of the nonlinear materials especially for radiation below 300 nm and temperature control of the crystals can be demanding. Moreover the design of these devices and the spot sizes have to optimized for high efficiency on one hand and no damage on the other. For material parameters see [6.2463–6.2483] and the references of Sect. 4.4.1 (p. 181).

6.15.1 Harmonic Generation (SHG, THG, FHG, XHG)

The generation of the second (SHG) [6.2484–6.2629], third (THG) [6.2630–6.2641] and fourth (FHG) [6.2642–6.2657] harmonics producing laser light with $\lambda_{\text{laser}}/2$, $\lambda_{\text{laser}}/3$ and $\lambda_{\text{laser}}/4$ is quite common for pulsed solid-state

and dye lasers. SHG is also applied for high-power cw lasers. It is also used increasingly for diode laser with a few W average output power. Further harmonics (see [6.2658] and references in Sect. 4.6) show poor efficiency.

Materials and schemes for harmonic generation are discussed in Sects. 4.4.1 (p. 181)–4.4.3 (p. 192) and 4.5.1 (p. 208). As an example the frequency transformation of the light from a Q switched Nd:YAG laser with a transverse fundamental mode and longitudinal single mode is shown in Fig. 6.104–6.106 (p. 527). Figure 6.104 shows a typical parameter set for SHG. An efficiency of to 50% was observed for this laser for stable operation. The crystal was 7 mm long and 7 mm in wide.

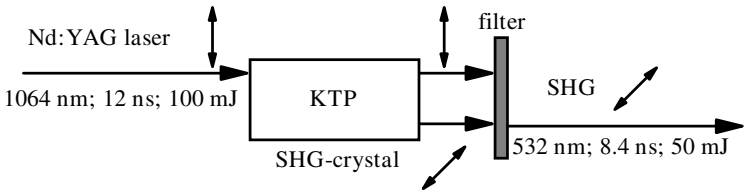

Fig. 6.104. Frequency doubling (SHG generation) of Q switched Nd:YAG laser light. The fundamental wave can be blocked with, e.g. a dielectric mirror as filter

For frequency conversion of low power laser light periodically poled crystals typically Li:NbO_3 (PPLN) with some codoping can be applied (see Fig. 4.9, p. 191). Thus cw diode laser light at 976 nm with a power of 4 W could be transformed to 0.6 W of 488 nm radiation [6.1460]. At smaller power levels 30 mW of SHG at 488 nm with diffraction limited beam quality could be obtained from 1 W pump with a tuning range of 1.5 nm and a band width of 20 pm [6.1459]. PPLN crystals in waveguide geometry may allow about 100 mW of SHG or other parametric radiation in the visible with more than 30% efficiency without damage.

The configuration of Fig. 6.104 can be used for further third-harmonic generation (THG) but with different optimization. The scheme is shown in Fig. 6.105.

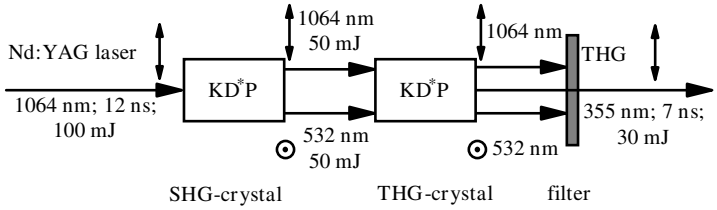

Fig. 6.105. Frequency tripling (THG generation) of Q switched Nd:YAG laser light by SHG and mixing of the second harmonics with the fundamental

As mentioned in Sect. 4.5.1 (p. 208), stepwise transformation with SHG and then mixing of the fundamental with the SHG light is much more efficient than direct tripling. The second crystal was KD*P and the overall efficiency for the third harmonics was 30%. Care has to be taken for the polarization demands of the crystal. In the case shown the polarization of the fundamental and the SHG are perpendicular. For example BBO crystals which are, e.g. used for the tripling of Ti:sapphire laser radiation, demand parallel polarization of these lights. In this case an optical arrangement is necessary for the rotation of tunable short light pulses from a fs laser.

Fourth-harmonic generation (FHG) is just twice the second harmonic generation as shown in Fig. 6.106.

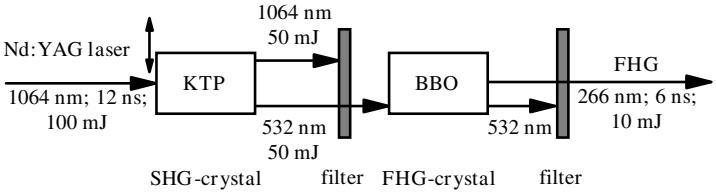

Fig. 6.106. Fourth-harmonic generation (FHG) as a series of two SHGs of Q switched Nd:YAG laser light

The overall efficiency is 10% in this case. The efficiencies of the two SHGs are different because the crystals for the different wavelength ranges have different coefficients. The lifetime of the FHG crystal is crucial for average output powers in the range of 1 W and above.

Higher harmonics can be produced, e.g. in atom vapors (see Sect. 4.6 and [6.2659–6.2674]). The efficiency of these conversions is usually small. Other methods of frequency conversion including mixing and upconversion are reported in [6.2675–6.2695].

6.15.2 OPOs and OPAs

Optical parametric oscillators (OPO) and amplifiers (OPA) were described in Sect. 4.4.4 (p. 193) and in references [6.2696–6.2777]. Commercial devices are available for use with pulsed lasers from ns to fs.

The achievement of good frequency stability can be difficult with these devices. Further, narrow bandwidth and good beam quality are difficult to obtain. Therefore different schemes have been developed to combine the OPO with other sources such as e.g. with a dye laser (ns) or a broad band white light source with narrow band width selection (ps-fs) as a seeder for the required radiation.

The whole spectrum from UV to IR is covered continuously by OPOs or OPAs in combination with SHG, THG and FHG. For a commercial

Ti:sapphire laser the OPA is specified with following pulse energies in the fs range covering the range from 300 nm to 3 μm (see Table 6.37, p. 528).

Table 6.37. Pulse energies of a commercial OPA in the fs range pumped by a 1 kHz Ti:sapphire laser of 80 fs pulse duration and 750 μJ pulse energy

Method	Wavelength (nm)	Pulse energy (μJ)	Pulse width (fs)	Stability (%)
Idler	2080	≥ 25	≤ 100	≤ 3
Signal	1300	≥ 55	≤ 100	≤ 3
SHG-idler	900	≥ 7	≤ 100	≤ 5
SHG-signal	650	≥ 10	≤ 100	≤ 5
FHG-idler	450	≥ 2	≤ 170	≤ 7.5
FHG-signal	330	≥ 2	≤ 170	≤ 7.5

This OPA is pumped with a fs laser pulse of 80 fs duration with a pulse energy of 0.75 mJ at a repetition rate of 1 kHz. Similar results are reached with the same device in the ps range. Pumping with a 1 mJ pulse of 1 ps duration at a repetition rate of 1 kHz again results in the values given in Table 6.38.

Table 6.38. Pulse energies of a commercial OPA in the ps range pumped by a 1 kHz Ti:sapphire laser of 1 ps pulse duration and 1 mJ pulse energy

Method	Wavelength (nm)	Pulse energy (μJ)	Pulse width (ps)	Stability (%)
Idler	2080	≥ 25	≤ 1.25	≤ 3
Signal	1300	≥ 60	≤ 1.25	≤ 3
SHG-idler	900	≥ 7	≤ 1.25	≤ 5
SHG-signal	650	≥ 10	≤ 1.25	≤ 5
FHG-idler	450	≥ 3	≤ 1.25	≤ 7
FHG-signal	330	≥ 3	≤ 1.25	≤ 7.5

Similar good results are obtained with ns or longer ps pulses as reported. Thus from a single Nd:YVO_4 laser with 40 W average output power, a pulse width of 7 ps, a repetition rate of 80 MHz and a beam quality of $M^2 < 1.2$ three light beams with wavelengths of 446 nm, 532 nm and 639 nm could be generated, simultaneously. The total power of all three beams together resulting in white light as usable in laser television application was 19 W.

6.15.3 Raman Shifter

Raman scattering in gases, liquids or solids can shift the laser spectrum [6.2778–6.2807] by the Raman frequency of the material (see Sects. 3.11.4

(p. 165) and 4.5.12, p. 238) which is of the order of magnitude of $1000\,\mathrm{cm}^{-1}$ or $3 \cdot 10^{13}$ Hz, resulting in a few nm shift in the visible. The beam quality is usually decreased by these Raman shifters.

For high efficiencies gas cells with high pressures of about 50 bar have been applied. The light has to be strongly focused for sufficiently high intensities in the material.

Solid-state materials, such as e.g. $Ba(NO_3)_2$, allow for larger shifts with still good efficiency. Thus with intracavity Raman conversion with this material in a Q switched Nd:YAG laser the original wavelength of 1,064 nm was shifted in the region between 1160 nm and 1198 nm with an efficiency of about 25%. Frequency doubling of this radiation leads to a wavelength range from 580 to 599 nm with an output energy of 0.6 mJ of the 5 ns pulse [6.2790].

With heavy hydrogen D2 a large shift of $2991\,\mathrm{cm}^{-1}$ is possible resulting in shifted wavelengths from a Nd:YAG laser with 1064 nm emission to 1561 nm for the Stokes and 807 nm for the anti-Stokes first lines. The second harmonic with a wavelength of 532 nm would result in 632.7 nm and 459 nm. Another material with good efficiency is KGdWO4 with the Raman shifts of $767.3\,\mathrm{cm}^{-1}$ and $901.5\,\mathrm{cm}^{-1}$.

For high efficiencies in the solid Raman materials the light can be "focused" with axicons which produce a beam filament of up to a few cm with a thin and almost constant diameter.

Raman lasers are reported in [6.2808–6.2857]

6.16 Laser Safety

There are laws about the correct use of laser radiation to avoid any damage [e.g. 6.2858–6.2862]. They are slightly different in different countries and should be seriously recognized.

In addition some simple rules while using laser radiation can help to avoid any eye or skin injury or damage. First, all laser radiation should stay in restricted areas. Usually all optical beams should be on the optical table at a certain height, the beam height. All unused laser reflexes have to be dumped with beam catchers. Special care has to be taken for beams leaving the plane of the optical axes as produced, e.g. by polarizers. It has to be noticed that reflection from one glass surface contains about 4 W radiation of a 100 W laser! Therefore, it helps if the operator does not wear rings or watches. Take special care of visitors in the laser lab if high-power systems are working. All beams which are not needed for direct access in the experiments should be covered. This also increases the signal-to-noise ratio.

But the main rule is:

Never look into a laser beam!

As obvious as this may appear the violation of this simple rule is still one of the main reasons for eye injury.

In many cases a pair of glasses with suitable filters can be used to avoid injury. Most dangerous are IR and UV laser radiation. IR laser radiation is not visible and UV radiation is mostly underestimated by its weak fluorescence appearance.

UV radiation can dull the eye lens after sufficient exposure. The damage will accumulate over time even over years. Light with wavelengths between 400 and 1400 nm will reach the retina focused to a diameter of about 10 µm resulting in a 100 000 times increased intensity.

The rules about laser safety are similar in Europe and the USA and can be found in [6.2859, 6.2860]. The problem is difficult to describe in simple rules because the different wavelengths, pulse durations, powers and pulse energies, as well as mode structure, have different influences and thus many kinds of combinations have to be considered. Lasers can be classified by the possible damage to the eyes or the skin and for fire danger.

Fire danger is possible for lasers with average output powers of 500 mW or more. Thus no papers should be placed at the beam height in the lab.

Skin damage can occur above average output powers of $10\,\mathrm{mW\,cm^{-2}}$ or above pulse energies of $10\,\mathrm{mJ\,cm^{-2}}$.

Eye damage can occur even from laser pointers with output powers of 1 mW and if the eye does not blink, with even much lower powers. As rough rules the values in Table 6.39 for the maximum permissible exposure (*MPE*) of the eye may be used for choosing the optical density of protection goggles at the laser wavelengths (without any guaranty).

Table 6.39. Maximum permissible exposure (MPE) power or pulse energy of the eye as function of the pulse length and the wavelength of the laser radiation (without guaranty)

pulse length	200–620 nm	620–1050 nm	1050–1400 nm	1400 nm–1000 µm
$\geq 0.5\,\mathrm{s}$	$1\,\mu\mathrm{W\,cm^{-2}}$	$10\,\mu\mathrm{W\,cm^{-2}}$	$1\,\mathrm{mW\,cm^{-2}}$	$100\,\mathrm{mW\,cm^{-2}}$
$\geq 1\,\mathrm{ns}$	$0.5\,\mu\mathrm{J\,cm^{-2}}$	$0.5\,\mu\mathrm{J\,cm^{-2}}$	$5\,\mu\mathrm{J\,cm^{-2}}$	$1\,\mathrm{mJ\,cm^{-2}}$
$< 1\,\mathrm{ns}$	$0.5\,\mathrm{kW\,cm^{-2}}$	$0.5\,\mathrm{kW\,cm^{-2}}$	$5\,\mathrm{kW\,cm^{-2}}$	$1\,\mathrm{MW\,cm^{-2}}$

For comparison sunlight [6.2862] has a power density of about $0.12\,\mathrm{W\,cm^{-2}}$ in central Europe and would definitely damage the eye if someone looked directly into the sun. The spot diameter of the sun is about 160 µm at the retina.

The necessary optical density $\mathrm{OD}_{\mathrm{goggles}}$ or transmission T_{goggles} of goggles at the laser wavelength λ_{laser} can be calculated from the MPE values of Table 6.39 and the maximum laser power $P_{\mathrm{laser,maximum}}$ or pulse energy $E_{\mathrm{laser,maximum}}$ as a function of the wavelength λ_{laser}, pulse duration Δt_{FWHM} and cross section of the beam A_{beam} by:

$$T_{\mathrm{toggles}}(\lambda_{\mathrm{laser}}) = \frac{\mathrm{MPE}(\lambda_{\mathrm{laser}}, \Delta t_{\mathrm{FWHM}}) \cdot A_{\mathrm{beam}}}{P_{\mathrm{laser,maximum}} \text{ or } E_{\mathrm{laser,maxmimum}}} \tag{6.175}$$

and

$$\mathrm{OD}_{\mathrm{goggles}}(\lambda_{\mathrm{laser}}) = -\lg_{10}\{T_{\mathrm{goggles}}(\lambda_{\mathrm{laser}})\}. \tag{6.176}$$

The lasers are officially categorized into five safety classes, 1, 2, 3A, 3B and 4, starting from nondangerous lasers in class 1 to most dangerous lasers for eye, skin and fire danger in class 4. The laser classes can be characterized as in the following description but all details have to be checked for legal consequences.

Class 1 (safe) are safe devices under foreseeable conditions of operation, including the use of optical instruments for intrabeam viewing. The device may contain high power laser with higher classification, e.g. compact disc player, laser printers, CD ROM players but it has to be in a closed box.

Class 2 (low power) has a maximum output below 1 mW and is declared only for visible light from 400 nm to 700 nm. Because of the blink response of the eye the resulting protection is realized even for use with optical instruments. It is applied, e.g., in supermarket scanners, HeNe lasers in teaching labs, laser diodes in teaching labs, laser pointers.

Class 3R (former 3A, low power) allows a maximum output power below 5 mW and an irradiance smaller 25 Wm^{-2} again in the visible range 302 nm to 700 nm, only. The blink response of the eye protects to some degree but direct intrabeam viewing using optical aids (binoculars, telescopes, microscopes) is hazardous. Lasers in the non-visible IR-range above 4 μm are treat as class 1.

Class 3B (moderate power) have maximum output powers of 0.5 W in the visible and non-visible spectral region. Direct intrabeam viewing is always hazardous. Viewing diffuse reflections is normally safe if the eye is not closer than 13 cm to the diffusing surface and exposure duration is less than 10 s.

Class 4 (high power) is for higher output powers than 0.5 W. It is declared as always hazardous. Viewing direct or reflected beams as well as diffuse reflections results in injury. Environmental damage (fire), skin burns as well as eye injuries are possible.